MODELING OF EWASO NAROK FLOODPLAIN

A STUDY OF THE HYDROCHEMISTRY AND HYDROGEOLOGY IN A DATA SCARCE ENVIRONMENT

Dissertation

zur

Erlangung des Doktorgrades (Dr. rer. nat.)

der

Mathematisch-Naturwissenschaftlichen Fakultät

der

Rheinischen Friedrich-Wilhelms-Universität Bonn

vorgelegt von

Layla Hashweh

aus

Jerusalem, Palästina

Bonn 2022

Angefertigt mit der Genehmigung der Mathematisch-Naturwissenschaftlichen Fakultät der
Rheinischen Friedrich-Wilhelms-Universität Bonn

1. Gutachterin: Prof. Dr. Barbara Reichert

2. Gutachter: Prof. Dr. Christian Borgemeister

Tag der Promotion: 13.12.2022

Erscheinungsjahr: 2023

Table of Contents

Acknowledgments

This study was funded by the DAAD, for which I am grateful.

I wish to express my deepest gratitude to Prof. Dr. Barbara Reichert for her valuable support and guidance throughout the last few years. My greatest appreciation also goes to Prof. Eilon Adar, whose continuous feedback and support have been a blessing. I want to extend my appreciation to Massoth Silvi and her assistance in the MCM model.

I am beyond thankful to ZEF, its enriching courses, and the good colleagues I encountered there. I am thankful to Steinmann-Institut für Geologie, Mineralogie und Paläontologie (University of Bonn), the students in the AG, the lab assistants, and the workers, mainly Dr. Sven-Oliver Franz, Dr. Sonja Burghof and the laboratory team, Bettina Schultevan Berkum, Camilla Kurth, and Beate Dahlhausen. A lot of gratitude to Jana Schneider and Kim Hußmann.

I thank Dr. Christine Stumpp and the Helmholtz Zentrum laboratory team in Munich for their support regarding stable water isotopes and evaluation.

I want to thank WRMA and the private well-owners in Kenya for the shared data.

GlobE people have been a second family. Thank you for allowing me to correspond with other members, exchange data, and attend workshops.

On more personal notes:

I dedicate my work to my supportive and loving parents, who always believe in me and ensure I get the best education and life. To my sisters, Hind, for motivating, editing, and helping me always! You are an amazing role model with your dedication. Nada, you make me smile every day. Thank you for talking me through my fears and life, reminding me of my capabilities, and waking me up. I am blessed with loving, strong, successful, and supportive sisters!

To Konrad, thank you for everything you do, from editing to making sure I am happy to being patient and believing in me in the most challenging times. To my dear friends and support system, particularly Clara, Sid, Maysa, Viviane, Gohar, and Julius, thank you for everything!

Abstract

The Ewaso Narok wetland, a floodplain intensively used for grazing, drinking, and agriculture, is part of Kenya's largest drainage basin. This study lies within the water and food security scope, in affiliation with the 'GlobE project' of reconciling future food production with environmental protection. The primary objective is to quantitatively evaluate the surface water-groundwater interactions in the Ewaso Narok wetland in terms of water recharge/discharge and water flux. This is done by developing a comprehensive interdisciplinary approach to understanding the aquifer's structure, water dynamics, and water composition and modeling this scarce data wetland.

The field data were collected using surveys, water, soil, and rock measurements. It was processed and analyzed while combined with secondary data. The survey results show that people rely on the wetland for most of their daily livelihoods, including drinking. However, there is a lack of responsibility and awareness of the wetland's pollution and well-being, seen in the direct conscious disposal of fertilizers, manure, and plastic containers in the Ewaso Narok wetland. The survey further provided potential input points of water and pollution into the wetland for sampling and then modeling the Ewaso Narok wetland.

The field and laboratory results show that the dominant process controlling groundwater chemistry is silicate weathering expressed in low electric conductivity and high content of HCO_3^- and SiO_2, with the topsoil layers experiencing more weathering. The chemical index of alteration ranges between 65 and 91 %, depending on soil type, depth, and use of the area. The western part of the wetland is more weathered compared to the eastern side. The weathered profile consists of illite/muscovite, kaolinite, goethite, and small proportions of quartz and calcite. Two aquifer systems exist. The regional confined aquifer is recharged from high altitudes reaching the Ewaso Narok wetland by the lateral flow of groundwater and the local semi-confined aquifer that occurs in the weathered basement rock system. Recharge is small in the Ewaso Narok area and occurs by direct infiltration of rainwater along with fractures within the rocks and in the weathered zones of the metamorphic rocks and by indirect infiltration of the run-off along the river courses. The surface water is a mixture of rainwater and groundwater. There are perched aquifers underneath both the wetland and the river. Additionally, the weathering profile acts as storage for groundwater. The groundwater is discharged to the ephemeral streams, the main river, and the wetland. In addition, flash floods contribute to the water balance of this wetland. These results provide the hydrogeological and hydrochemical database for characterizing the Ewaso Narok wetland. They further set a conceptual framework building a base for the mathematical model to run. As data and information regarding the physical hydrogeology of the basin and the wetland are rare, the Mixing Cell Model (MCM) is used to identify and quantify the active sources of recharge and their contribution to the total water balance at the wetland and catchment scale.

The results of the statistical cluster analysis and the subsequent single and multi-cell modeling, indicate clear hydraulic connectivity between the wetland's surface water and groundwater, with 17 to 84 % of the inflow originating from groundwater. The groundwater feeding the wetland is evident upstream of the wetland and even more vivid downstream. The downstream part of the Ewaso Narok wetland is the main contributor to the total amount of water in the whole system. However, the middle part of the wetland does not show any contribution from

groundwater. In this middle part, the impermeable clay layer separates the wetland from groundwater, and faults and fractures act as hydraulic barriers. The river courses show advanced weathering profiles, allowing groundwater discharge and thus suggesting permeability. The model results show a high negative error indicating one or several additional missing sources contributing to the calculated mass balance. Regardless, the MCM provides meaningful results with the limited information available. These results are used to develop a conceptualized model summarizing the Ewaso Narok aquifer system.

The study also compares the water quality to human drinking standards and irrigation guidelines. Regarding surface water quality, levels of iron, aluminum, and copper exceeded those recommended in the guidelines. Nitrate values of surface water samples were higher during the flash floods than during dry periods. Regarding groundwater values of fluoride and arsenic, higher amounts were observed than recommended in the guidelines. The results did not clearly distinguish between the groundwater in the confined and semi-confined aquifers in terms of quality and isotopes.

Regarding surface water, the recommended guidelines for irrigation were exceeded for manganese, fluoride, ammonium ion, potassium, and bicarbonate. The groundwater sampled exceeded recommended irrigation limits for chlorine, calcium, potassium, sulfate, manganese, nitrate, ammonium ion, fluoride, and bicarbonate.

As the groundwater is a feeding source to the Ewaso Narok wetland, precaution is required regarding any exceeded measurement values for any polluting element or compounds. Determining the source of these pollutants and possibly finding other drinking water sources is vital. Furthermore, awareness campaigns are important and should focus on proper sanitation practices, hygiene, and good agricultural practices. Applying fewer fertilizers would be more cost-effective and easier to realize than wetland restoration measures. In addition, there is a need to construct sewage infrastructure, car wash, and toilets.

Ewaso Narok wetland is the backbone of people's local livelihoods; however, it is a diminishing resource. More attention is needed for it to maintain this role. A holistic approach is recommended to manage the basin and the Ewaso Narok wetland in particular. The study's unique results of quantitatively assessing the groundwater and surface-water interactions, despite scarce hydrological information, can be used to develop such an approach. They clearly demonstrate the need for management approaches that consider both surface water and groundwater alike to ensure the wetland's long-term sustainability of the wetland.

Zusammenfassung

Das Feuchtgebiet Ewaso Narok, ein als Weideland, für die Trinkwasserversorgung und Landwirtschaft intensiv genutztes Überschwemmungsgebiet, ist Teil des größten Flusseinzugsgebietes in Kenia. Die vorliegende Arbeit hat die Wasser- und Ernährungssicherheit zum Gegenstand und wurde im Rahmen des "GlobE" Projektes verfasst, welches zukünftige Nahrungsmittelproduktion und Umweltschutz in Einklang bringen soll. Ihr vorrangiges Ziel ist die quantitative Bewertung der Interaktion zwischen Oberflächen- und Grundwasser im Feuchtgebiet Ewaso Narok in Bezug auf Grundwasserneubildung und -abfluss sowie Oberflächenabfluss. Diese Bewertung wird durch die Entwicklung eines umfassenden, interdisziplinären Ansatzes vorgenommen, der hilft die Struktur des Grundwasserleiters, die Wasserdynamik und die Wasserzusammensetzung zu verstehen und das Feuchtgebiet trotz Datenknappheit zu modellieren.

Die vor Ort gesammelten Daten wurden aus Umfragen in der Bevölkerung, sowie Wasser-, Boden- und Festgesteinsmessungen gewonnen. Diese wurden verarbeitet und analysiert und anschließend mit Sekundärdaten kombiniert. Die Umfrageergebnisse zeigen, dass die Menschen für den größten Teil ihres täglichen Lebensunterhalts, einschließlich der Gewinnung von Trinkwasser, auf das Feuchtgebiet angewiesen sind. Es mangelt jedoch an Verantwortung und Bewusstsein für die Verschmutzung und Intaktheit des Feuchtgebiets, was sich in der direkten und bewussten Entsorgung von Düngemitteln, Gülle und Plastikbehältern im Ewaso-Narok-Feuchtgebiet zeigt. Die Umfrage ermittelte Eintragsquellen von Wasser und Verschmutzung in das Feuchtgebiet, welche in der folgenden Probennahme und der Modellierung des Ewaso-Narok-Feuchtgebietes berücksichtigt werden sollten.

Die Feld- und Laborergebnisse zeigen, dass Silikatverwitterungsprozesse die Grundwasserchemie hauptsächlich steuern. Dies drückt sich in niedrigen EC-Werten und hohem HCO_3^- sowie SiO_2 Gehalt im Boden aus, wobei die Oberböden stärker verwittern. Der chemische Verwitterungsindex liegt zwischen 65 und 91 % in Abhängigkeit von Bodentyp, Tiefe und Nutzung. Der westliche Teil des Feuchtgebietes ist im Vergleich zum östlichen Teil stärker verwittert. Das Verwitterungsprofil besteht aus Illit/Moskuvit, Kaolinit, Goethit und geringen Anteilen von Quarz und Kalzit. Es gibt zwei Aquifersysteme: Den regional begrenzten Aquifer, der sich vom Gebirge aus bis zum Ewaso Narok Feuchtgebiet durch laterale Grundwasserströmung speist, und den lokalen, halbbegrenzten Aquifer, der im verwitterten Grundgebirge liegt. Die Grundwasserneubildung im Ewaso Narok Feuchtgebiet ist gering und erfolgt durch direkte Infiltration von Regenwasser entlang von Klüften, Rissen und verwitterten Zonen metamorphe Gesteine, oder durch indirekte Infiltration des Abflusses entlang der Flussläufe. Das Oberflächenwasser ist eine Mischung aus Niederschlags- und Grundwasser. Sowohl unter dem Feuchtgebiet, als auch unter dem Fluss befinden sich schwebende Grundwasserleiter, ebenfalls dient das Verwitterungsprofil als Grundwasserspeicher. Grundwasser wird in die ephemeren Flüsse, in den Hauptfluss und in das Feuchtgebiet entwässert, Sturzfluten tragen zusätzlich zum Wasserhaushalt des Feuchtgebietes bei.

Diese Ergebnisse bilden die hydrogeologische und hydrochemische "Datenbank" für das Ewaso Narok Feuchtgebiet, und stellen den konzeptionellen Rahmen für die Anwendung eines mathematischen Bilanzmodells dar. Da Daten und Informationen über die physikalische Hydrogeologie des Einzugsgebiets und des Feuchtgebietes kaum verfügbar sind, wird das Mixing

Cell Model (MCM) verwendet, um aktive Quellen der Grundwasserneubildung und ihren Beitrag zur Gesamtwasserbilanz des Feuchtgebietes und des Einzugsgebietes zu identifizieren und zu quantifizieren.

Die Ergebnisse der statistischen Clusteranalyse und der darauf folgenden Einzel- und Multizellmodellen, zeigen eine klare hydraulische Verbindung zwischen dem Oberflächenwasser des Feuchtgebietes und dem darunter liegenden Grundwasser, aus dem 17 bis 84 % des Zuflusses stammen. Das speisende Grundwasser ist im stromaufwärts gelegenen Teil des Feuchtgebietes klar erkennbar, im stromabwärts gelegenen Bereich des Ewaso Narok Feuchtgebiets jedoch, wird der größte Teil der Gesamtwassermenge generiert. Der mittlere Teil des Feuchtgebietes weist hingegen keine Interaktion zwischen Grundwasser und dem Oberflächenwasser auf. Hier trennt eine undurchlässige Tonschicht das Feuchtgebiet vom Grundwasserkörper, zusätzlich zu den Verwerfungen, die als hydraulische Barrieren wirken. Die Flussläufe weisen fortgeschrittene Verwitterungsprofile auf, was einen Grundwasserabfluss ermöglicht und auf höhere hydraulische Durchlässigkeit schließen lässt. Die Modellergebnisse zeigen einen stark negativen Fehler, der auf eine oder mehrere zusätzliche Wasserquellen hindeutet, die zur Massenbilanz beitragen und in den Berechnungen fehlen. Unabhängig davon liefert das MCM mit den begrenzten verfügbaren Informationen gute Ergebnisse. Diese wurden verwendet, um ein konzeptionelles Modell zu entwickeln, welches das Aquifersystem von Ewaso Narok zusammenfasst.

Ebenfalls wurde in der Untersuchung die Wasserqualität mit Trinkwasserstandards und Bewässerungsrichtlinien verglichen. Die im Oberflächenwasser gemessene Werte für Eisen, Aluminium und Kupfer lagen über den empfohlenen Richtwerten. Nitratwerte in Oberflächenwasserproben waren während Sturzfluten höher als in Trockenzeiten. Die im Grundwasser gemessenen Werte für Fluorid und Arsen, waren ebenfalls höher als in den Richtlinien empfohlen. Die Ergebnisse für Isotopenwerte und Wasserqualität lassen keine klare Unterscheidung zwischen dem Grundwasser aus begrenzten und halbbegrenzten Grundwasserleitern zu.

Beim Oberflächenwasser wurden die empfohlenen Richtwerte für Bewässerung für Mangan, Fluorid, Ammoniumionen, Kalium und Bikarbonat überschritten. Das beprobte Grundwasser überschritt die empfohlenen Grenzwerte für Chlor, Kalzium, Kalium, Sulfat, Mangan, Nitrat, Ammonium-Ion, Fluorid und Bikarbonat.

Da das Grundwasser eine Quelle für das Ewaso-Narok-Feuchtgebiet darstellt, ist Vorsicht in Bezug auf die erhöhten Messwerte aller belastenden Elemente oder Verbindungen geboten. Die Ermittlung der Schadstoffquellen und die Suche nach anderen Trinkwasserquellen ist hierbei unerlässlich. Darüber hinaus sind Aufklärungskampagnen wichtig und sollten sich auf angemessene sanitäre Praktiken, Hygiene sowie nachhaltige landwirtschaftliche Praktiken konzentrieren. Weniger Düngereintrag wäre kosteneffizienter und einfacher durchführbar als Ökosystemrestauration. Es besteht darüber hinaus die Notwendigkeit für den Bau von Abwasserkanälen, Autowaschanlagen und Toiletten.

Das Ewaso Narok Feuchtgebiet bildet das Rückgrat der Daseinsfürsorger der lokalen Bevölkerung, ist aber eine schwindende Ressource. Mehr Aufmerksamkeit ist notwendig, dass es diese wichtige Rolle weiterhin ausführen kann. Ein holistischer Ansatz wird empfohlen um das Einzugsgebiet, und das Feuchtgebiet im Besonderen, zu managen. Die Ergebnisse der Studie

mit ihrer quantitativen Bestimmung der Grund- und Oberflächenwasserverbindung sind trotz der Knappheit hydrologischer Daten und können die Grundlage für einen solchen Ansatz bilden. Sie zeigen deutlich, dass Managementansätze notwendig sind, die sowohl Oberflächenwasser, als auch Grundwasser berücksichtigen um die langfristige Nachhaltigkeit des Feuchtgebietes zu sichern.

List of Figures

List of Tables

List of Appendix

List of Units

cm	centimeter
°C	degree Celsius
b.g.l.	below ground level
d	day
g	gram
Ga	10^9 years
kg	kilogram
km	kilometer
km^2	square kilometer
L	liter
m	meter
m^2	square meter
m.a.s.	meter above surface
m.a.s.l.	meter above sea level
m.b.s.	meter below surface
m.b.s.l.	meter below sea level
mg	milligram
mL	milliliter
mm	millimeter
mmol	millimole
mmol (eq)	millimole equivalent
mol	mole
mV	millivolt
µS	microsiemens
ppm	parts per million
s	second
v	volume

List of Abbreviations

ASAL	Arid and Semi-Arid Land
CAI	Chloro-alkaline indices
CETRAD	Centre for Training and Integrated Research in ASAL Development
CIA	Chemical Index of Alteration
CIPW	Cross, Iddings, Pirsson, and Washington
CNS	Carbon, nitrogen, sulfur
DAP	Diammonium phosphate
DHWQ	Degree of Health-related Water Quality
DRU	Degree of Restriction on Use
ET	Evapotranspiration
FAO	Food and Agriculture Organization
GoK	Government of Kenya
GW	Groundwater
HCA	Hierarchical Cluster Analysis
ITCZ	Intertropical convergence zone
KEBS	Kenya Bureau of Statistics
KNBS	Kenya National Bureau of Statistics
LOD	Limit of Detection
LOQ	Limit of Quantification
MCM	Mixing cell model
MCMsf	Mixing Cell Model for Steady Flow system
MEMR	Ministry of Energy and Mineral Resources
Ma	Million years
Mio	Million
NPK	Nitrogen, phosphorus, and potassium
NW	North West
PC	Principal component
PCA	Principal Component Analysis
R	Regolith
S	Sediment
SE	South East
SF	Surface water
SSA	Sub-Saharan Africa
SWL	Static Water Level
WHO	Water Health Organization
TC	Total carbon
TN	Total nitrogen
TS	Total sulfur
WRAP	Water Resources and Planning Project
WUA	Water User Association

1. Introduction

In the last ten years, the agriculture industry has seen advancements in efficient irrigation technologies, weed management, crop variety, genetic modification, and post-harvest practices, to name a few (Saiz-Rubio & Rovira-Más, 2020). Despite this, more than 820 million people do not have enough to eat (FAO, 2019a).

Kenya, as part of East Africa, is no exception: 46 % of the population live on less than 1 USD a day, 36.5 % of the people are food insecure (FAO, 2019b), and only 57 % of its population have sustainable access to improved drinking water sources (WHO, 2015). 35 % of children under five are stunted and chronically malnourished (FAO, 2019b).

Over-exploitation of water resources continues to be the most significant constraint on sustainable agricultural development (Mutiga et al., 2010). Populations and economies heavily depend on natural resources, including freshwater. Water is key to food security, as 70 % of all water withdrawals globally are for agriculture (FAO, 2017; WB, 2017). The agricultural sector in Kenya accounts for 65 % of the export earnings and provides livelihoods (employment, income, and food security) for more than 80 % of the population (FAO, 2019b).

Kenya‘s Arid and Semi-Arid Lands (ASALs) constitute 89 % of the country, making it a water-scarce country (UNDP, 2018). People living in arid and semi-arid areas rely heavily on groundwater (Paron et al., 2013). This is the case for Kenya, besides its freshwater being supplied from surface water and wetlands (Paron et al., 2013). Droughts are becoming endemic in some areas of Kenya, especially in the poor, vulnerable ASALs, and the coping mechanisms are becoming ineffective (UNESCO-WWAP, 2006).

The “water towers” in Kenya, “a term for a mountain area that supplies disproportional runoff as compared to the adjacent lowland area” (Viviroli et al., 2007), are under serious threat from population increase, poor agricultural deforestation, and lack of implementation of policy decisions (Paron et al., 2013). Kenya currently has an estimated 52.21 Mio population, which ranks 27th globally (KNBS, 2019; UN, 2019). Based on the United Nations (UN) World Population estimates and projections (UN, 2019), Kenya’s population is expected to double by 2065 to 107.17 Mio, which would bring it to the 19th rank in population.

Wetlands play a significant role in conserving biological diversity, supporting human life, and economic activities in Africa drylands (Finlayson et al., 2001). Amongst other functions, wetlands provide a solution to food security by delivering fertile land, groundwater recharge, and discharge, and absorbing large quantities of rainwater, water purification, pollutant removal, removal of aquatic pathogens, sediment trapping, nutrient cycling, and adsorption of heavy metals (Paron et al., 2013; Sakané et al., 2011). Besides, wetlands act as water storage and assist in flood reduction, maintenance of aquifers, and storm protection (MEMR, 2012). Wetlands also provide socio-economic value in that they provide papyrus for collection, trees for building, and sand and soil for making pottery and building bricks (Paron et al., 2013).

In Kenya, wetlands occur in small but distributed patches, covering 2.5 % of the country’s total surface area of 583,645 km^2 (Finlayson et al., 2001). However, their area has declined by approximately 7 % per annum due to drainage for agriculture (Finlayson et al., 2001; Gichuki et al., 2001). The use of wetlands has also changed over the past years from having a very low impact to incidents of fire hazards, clearing and draining the wetlands, and building settlements

and agricultural areas. Achieving food security is of utmost importance for Kenya, especially in the ASALs. Technical and infrastructural developments during the 20th century enabled the intensification of agriculture in wetlands, among other places, and fertilizers applications. Excessive water abstractions and consumption influence and put pressure on wetlands (Gleick, 1994; Maltby & Barker, 2009; Ward, 2003). Wetlands are further at risk from industrial, municipal, and local disposals of waste material (Sciortino et al., 1999). Furthermore, migrants, international agribusiness companies, and export companies scramble for valuable resources (Dixon & Wood, 2003) in wetlands.

In the scope of these problems, the Ewaso Narok wetland, the study area of this study, is similar to many other wetlands, threatened by human encroachment, excessive de-vegetation, collection of construction material, a heavy abstraction of water (MoEF, 2019; Thenya et al., 2011), and disposal of waste material and dumping (Gichuki, 2002; Paron et al., 2013). Ewaso Narok wetland, a floodplain within a weathered basement aquifer and part of the largest drainage basin in Kenya (Ewaso Ngiro) is an example that applies to many other wetlands in Kenya. It is a wetland that was intensively used for grazing and agricultural use to meet the growing increase in demand for food and water (Adams, 1993; Richards, 1985; Wood, 1985). The wetland, a significant source of people's livelihoods (Boy, 2011), does not only guarantee agricultural production and food security, but local communities depend on it for domestic water, livestock grazing, and other diverse uses. Natural wetlands are threatened by intensive development initiatives that include intensification and drainage as they have available soil moisture even in dry times (Dixon & Wood, 2003; Wood et al., 2013). According to the Ministry of Environment and Forestry (MoEF) (2019), human activities recently threatened the Ewaso Narok wetland with extinction (MoEF, 2019).

Further challenges associated with relying on the Ewaso Narok river for livelihood - other than the fluctuation in the flow and the unreliable rainfall - include significant water quality concerns and the necessity to co-manage the resource with all the different users (Ransom et al., 2012).

The water quality concerns in the Ewaso Narok wetland arise from the fact that 80 % of the households in the area live inside the wetland, in addition to car washing, domestic laundry, bathing in water sources, chemically spraying livestock close to water sources, poor disposal of chemical discharge from agricultural activities, and the lack of sewage facilities in highly populated urban areas upstream namely Nyahururu, and Rumuruti (Gichuki, 2002; Kibson Consult, n.d.; Wachira, 2014; WRMA & LWF, 2013). However, little effort has been made to protect water quality and quantity (WRMA & LWF, 2013). Given these quality concerns, boreholes and groundwater pans are the most reliable water sources. Groundwater is thus filled in tanks and used for pipe systems (ESGHS, 2012). Wells's abstraction of water is high inside the wetland and around it.

Coupled with the factors mentioned above, water resources' vulnerability is increased by poverty, lack of water control, law enforcement, and inadequate maintenance that ends in conflicts over land and water. Food producers experience greater competition for land, water, and energy. The need to curb the many adverse effects of food production on the environment is becoming increasingly clear (e.g., Godfray et al., 2010).

1.1. GlobE project – Wetlands in East Africa

Within the water and food security scope, the BMBF funded the GlobE project – Wetlands in East Africa, with the overall aim of reconciling future food production with environmental protection by providing science-based guidelines and tools to facilitate this process.

Wetlands have year-round water availability with generally high resource base quality and present potential production hotspots. Wetlands in Sub-Saharan Africa (SSA) consist mainly of inland valleys and alluvial floodplains that make up more than 80 % of East Africa's total wetland area and cover some 18 Mio hectares in Kenya, Rwanda, Uganda, and Tanzania (GlobE-Wetlands, 2014; Leemhuis et al., 2016). Their accelerated conversion into production sites has been largely responsible for the recent increases in per-capita food production and the decline in the number of undernourished people in the region (GlobE- Wetlands, 2014). It has further generated food for urban communities and income for thousands of families (FAO, 2012). On the other hand, this land conversion is also responsible for a loss in biodiversity, and a severe reduction in the provision of diverse ecosystem services, particularly when associated with large-scale drainage measures (Dixon & Wood, 2003; Russi et al., 2013; Verhoeven et al., 2006; Wood et al., 2013; WRI, 2005).

The GlobE's agreed definition of wetlands is land areas that are permanently or occasionally water-logged with fresh, saline, brackish, or marine waters, including both natural and human-made areas that support characteristic plants and animals (MEMR, 2012).

With the GlobE-Project Wetlands in East Africa, four wetlands were selected in Kenya, Rwanda, Tanzania, and Uganda. Two study sites, Ifakara (Tanzania) and Namulonge (Uganda), were declared as super test sites. The wetlands selected represent the two main wetlands types of East Africa in terms of national priority, floodplains and inland valley wetlands (Leemhuis et al., 2016). The approaches used in this project involve cross-scale interdisciplinary research, combining field experiments and surveys with modeling approaches, and assessing regional and global change scenarios.

The research activities are divided into five clusters (Fig. 1.1). The scope of this thesis falls within two clusters, first A5 Water and matter fluxes (functioning of wetland with the aims of quantitatively assessing: (i) the dynamics of resource availability, (ii) the dynamics of groundwater, (iii) water quality, and public health, and (iv) water balance on wetland and catchment scale), and to B2B Effect of management options on water quality and public health.

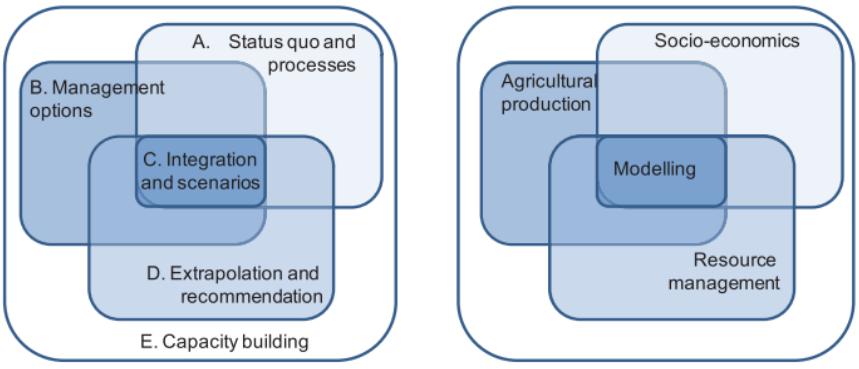

Fig. 1.1: Conceptual linkages between the work clusters and the different discipline areas of the GlobE project (Source: www.wetlands-africa.de).

1.2. Work of other GlobE students in Ewaso Narok

This section presents the work of different GlobE students in Ewaso Narok (Tab. 1.1) who sampled and worked before the political instability of 2016, with the most relevant findings.

Tab. 1.1: Work of GlobE students in Ewaso Narok.

Name	Topic/ paper/ thesis	Important related findings
Heinichen (2015)	"Water use-related conflicts and resource management around a small wetland in Ewaso Narok". Understanding the social and economic backgrounds of wetland users, exploring their management systems, and investigating possible water use-related conflicts and challenges.	Problems related to water included: 1. Lack of water harvesting. 2. Water scarcity. 3. Poor irrigation methods. 4. Water pollution. 5. Weak management. 6. Wetland degradation.
Ngolo (2018)	Application of pesticides by small-scale farmers for vegetable management in Ewaso Narok wetland.	The practices among farmers are poor and might impact humans and the environment negatively. Leaching of pesticides into the groundwater and surface runoffs is evident.
Muriuki (2016)	Evaluating the effects of agricultural activities on the groundwater-surface water interactions in the wetland during the dry and wet seasons.	Need to investigate the relationship between the wetland's unconfined aquifer and the confined aquifer in the surrounding areas.
Bours (2016)	Estimate crop and irrigation water requirements of agricultural sites along the Ewaso Narok wetland and their impact on available water resources.	There is not much water generated in the Ewaso Narok area itself, so water users have to rely on the few perennial streams entering the wetland area from the south.
Kyalo Willy (personal communication, 2016)	The socio-economic group organized a survey in March 2015 with 350 respondents (households).	The types of fertilizers used.
Anthonj et al. (2016)	"Water, sanitation, and hygiene in wetlands. A case study from the Ewaso Narok Wetland, Kenya".	The wetland is the most important water source for many people living around Ewaso Narok Wetland. Unsafe water sources and limited water hygiene were perceived to be associated with several diseases.

1.3. Problem statement

Floodplain wetlands are among the world's most endangered ecosystems due to the impacts of river regulation and its impact on hydrological regimes (Tockner & Stanford, 2002). The Ewaso Narok wetland, a 20 km in length floodplain along the Ewaso Narok river, is the study site for this research. Located in the Ewaso Narok's subbasin in the semi-arid highlands of the Laikipia plateau (1,645 – 1,900 m.a.s.l. (meters above sea level)), it drains the Aberdares mountain ranges and the western part of the Laikipia Plateau (Notter, 2003). Laikipia's crystalline basement is dominated by Precambrian metamorphic rocks (gneisses, schists, quartzites, and patches of granite) that are covered by Miocene volcanic rocks (basalts and phonolites). The Ewaso Narok wetland's water supply is critical, causing conflicts between various land users, wildlife, and intensive irrigation (Ashley et al., 2004; Mungai et al., 2004). In general, and compared to other countries, Kenya lacks an adequate base of data on its natural resources and easy access to them (Paron et al., 2013). Management, even in protected areas like Mount Kenya and Aberdares mountain ranges, is lacking and has led to conflicts over land and water (Paron et al., 2013). The study site is data-scarce in terms of geology, hydrology, and water quality. The lack of data for most East African regions impedes general conclusions about wetland hydrogeology and management (e.g., Burghof, 2017). No attempts have been made to assess the surface water-groundwater interactions in the Ewaso Narok wetland in terms of

water recharge and discharge and water flux or to manage this scarce water resource. As for any effective and integrated management of a water resource, there is a need for proper aquifer characterization, as well as for an understanding of groundwater flow direction, recharge, and discharge mechanisms, water flux, and chemicals from and to groundwater, and the water chemistry processes.

Groundwater plays a significant role in the water balance of wetlands, yet it is hard to estimate the groundwater's water contribution. It is, therefore, often omitted from calculations (e.g., Gilvear et al., 1993). Also, little information exists on the vulnerability of weathered basement aquifers to contamination from agricultural cultivation practices. Basement aquifers may be more vulnerable to pollution from anthropogenic activities as the vadose zone is often thin, and preferential flow through regolith fracturing can occur (Chilton & Foster, 1994). According to UNESCO-WWAP (2006), nitrate contamination has been detected in the Laikipia plateau, located on the Equator in the former Rift Valley Province, Kenya, due to livestock waste accumulation at watering points. In addition, fluoride levels in the Ewaso Narok wetland are quite high, as seen in well drilling records (ESGHS, 2012; Geolink Associates, 2010; Groundwater Survey, 1988). A comprehensive water quality analysis in Laikipia country is nonexistent, except for a few specific investigations or projects (Ministry of Agriculture, 1983).

Regarding the surface water quality in Laikipia, sampling is usually done at irregular intervals when an appointee from the Ministry's Water Quality and Pollution Control division visits or requests a quality investigation (Republic of Kenya, 1987). Groundwater quality is only checked upon drilling a new well and remains in possession of the owner. No record of checks is carried out during the wells' subsequent history (Republic of Kenya, 1987).

This research gap motivated the current interest and assessment of the aquifer, its suitability, its water quantity, and quality within a scarce data environment. The factors contributing to data scarcity include but are not only limited to political instability and lack of security. Security is a major threat to development in the Ewaso Narok area and is brought about by cattle rustling activities and highway robberies (WRMA & LWF, 2013).

1.4. Aim and research approach

The study aims to quantitatively assess the surface water-groundwater interactions in the Ewaso Narok wetland in terms of water recharge and discharge and water flux. As the area is data-scarce, an interdisciplinary approach to studying the wetland is developed, and a survey is prepared. Scientifically, the hydrogeological investigation approach (Kovalevsky et al., 2004) is used to understand the aquifer structure, water dynamics, and water composition.

The main aim is accomplished by setting specific objectives related to water and matter fluxes and quantitatively assessing the dynamics of resource availability (surface water and groundwater) and water balance on a wetland scale.

1. To develop a hydrogeological and hydrochemical database to characterize the wetland, its setting, and processes. This is performed and used to delineate possible groundwater flow paths and understand the aquifer system. Furthermore, this helps improve the knowledge basis for decisions in an area where water is naturally scarce.

2. To define possible chemical indicators for groundwater admixture. Surface water and groundwater are interlinked; water carrying contaminants and materials is interchanged, and the development or contamination of one affects the other. Thus, a proper understanding of the interactions is essential for managing water resources (Winter, 1999). The environmental impacts of intensification and diversification on resource base quality (surface water and groundwater) in terms of hydrological and hydrogeological processes and water quality were thus investigated.
3. To identify and quantify the active sources of recharge or pollution in this data-scarce environment and its contribution to the total "water balance" of the wetland and catchment scale through modeling (Adar, 1996; Adar & Neuman, 1988; Adar et al., 1992). A quantitative assessment of groundwater dynamics and its availability versus the tributaries' contribution to the surface water in the wetland and the running stream using the mathematical Mixing Cell Model (MCM) model is performed. The MCM that incorporates the spatial distribution of hydrochemistry and environmental isotopes is adopted to account for the hydrological deficiencies.
4. To evaluate the status quo of water compared to human drinking standards and irrigation and to give recommendations to sustain the wetland's short- and long-term functioning. The water quality along its flow paths and along the used gradient is determined, and the water quality with respect to both human consumption and food production is evaluated. Hydrological recommendations on how to sustain the wetland are developed and addressed to policymakers, local inhabitants, and researchers to sustain the wetland's short and long-term functioning.

2. Study area

The selected site, Ewaso Narok wetland, is a floodplain located in Rumuruti Division in the Ewaso Narok subbasin in Laikipia County, Kenya (Fig. 2.1) between latitudes 0° 15 and 0° 17 N and between 36° 34 and 36° 41 E along the Ewaso Narok river, which is a major tributary of Ewaso Ngiro. Ewaso Narok wetland area ranges between 14 km^2 and 20 km^2 depending on the season (Thenya, 2001). The following chapter describes in detail the geographic setting of the study area, the geology of East Africa in general, and the Laikipia plateau and Ewaso Narok wetland in specific.

The area considered for this hydrogeological study is the Ewaso Narok subbasin in general and the Ewaso Narok wetland (floodplain) in specific (Fig. 2.1).

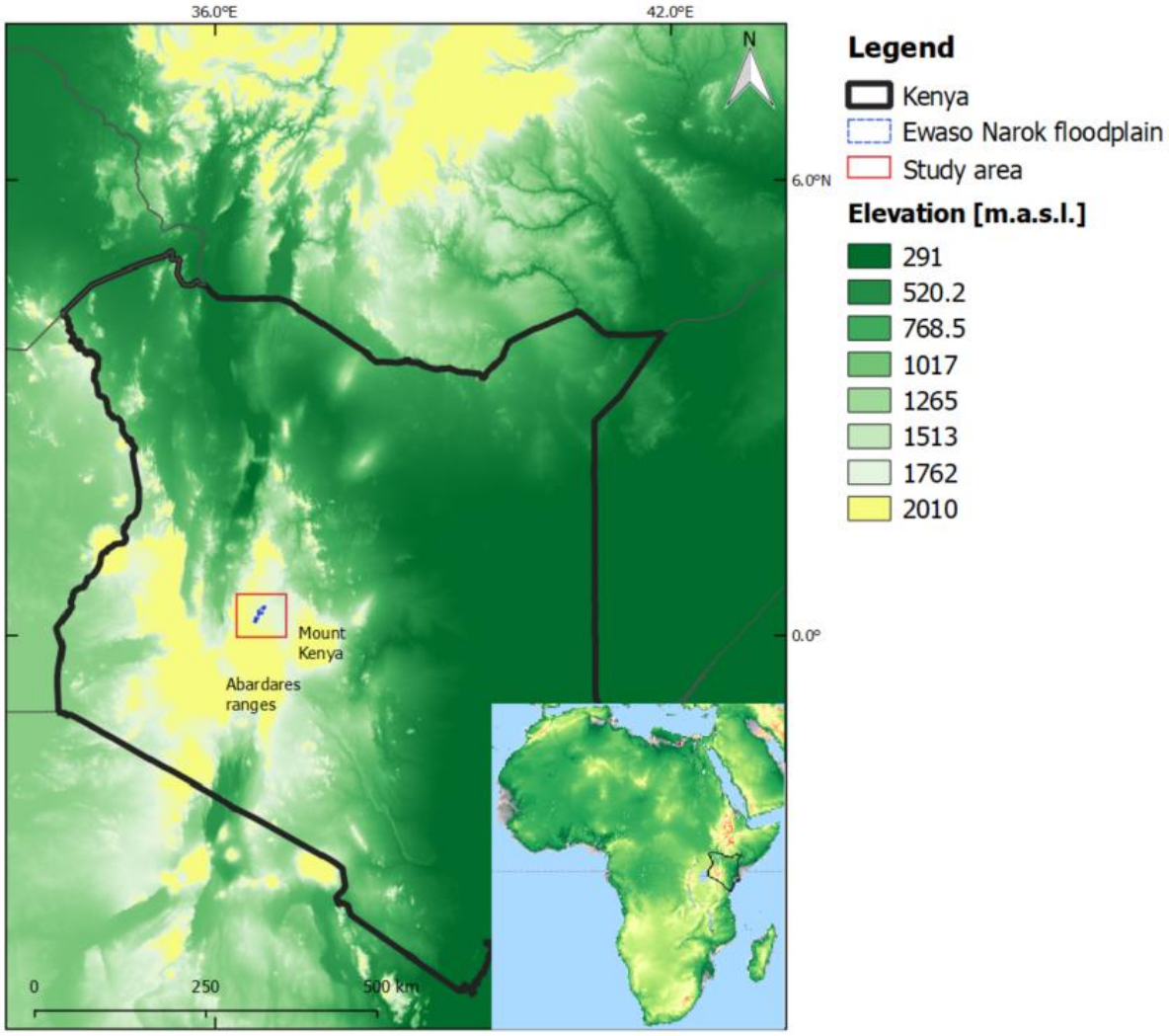

Fig. 2.1: Topographic map of East Africa, showing the location of the study area and Ewaso Narok floodplain. Data sources: earthexplorer.usgs.gov (STRM, digital elevation), subbasin (WRMA).

2.1. Geographic setting

The area is characterized by three major physiographic zones; the Gregory Rift Valley, the Laikipia Plateau, and the Basement Upland. The Laikipia Plateau corresponds essentially with a broad outcrop of Miocene phonolitic extrusive, bounded to the West by a series of faulted escarpments overlooking the Rift valley (Hackman, 1988).

The plateau surface is found on Miocene flood "Phonolites" and is monotonous with a slope of about 2 to 4 degrees for over 50 km to the north (Hackman, 1988). The Rift valley to the West is complex (Groundwater Survey, 1988). The escarpment complex's echelon reflects the interference of two sets of normal high-angle faults trending NNE and NW (Hackman, 1988). The faulting on the West controls the troughs on the plateau (Groundwater Survey, 1988). The Laikipia plateau is bounded by the volcanic edifices of the Aberdares mountains ranges and Mount Kenya to the SE and SW (Republic of Kenya, 1987) (Fig. 2.2).

The Laikipia plateau has a very diverse topography resulting from tectonic and volcanic events (cp. Section 2.2). Altitudes range between 1,780 and 1,900 m.a.s.l. (Aqua Well, 2013; Groundwater Survey, 1988; Hackman, 1988) (Fig. 2.2). The main area is characterized by wide-open valleys, slopes, and wetland depressions (Hackman, 1988; Kibson Consult, 2014).

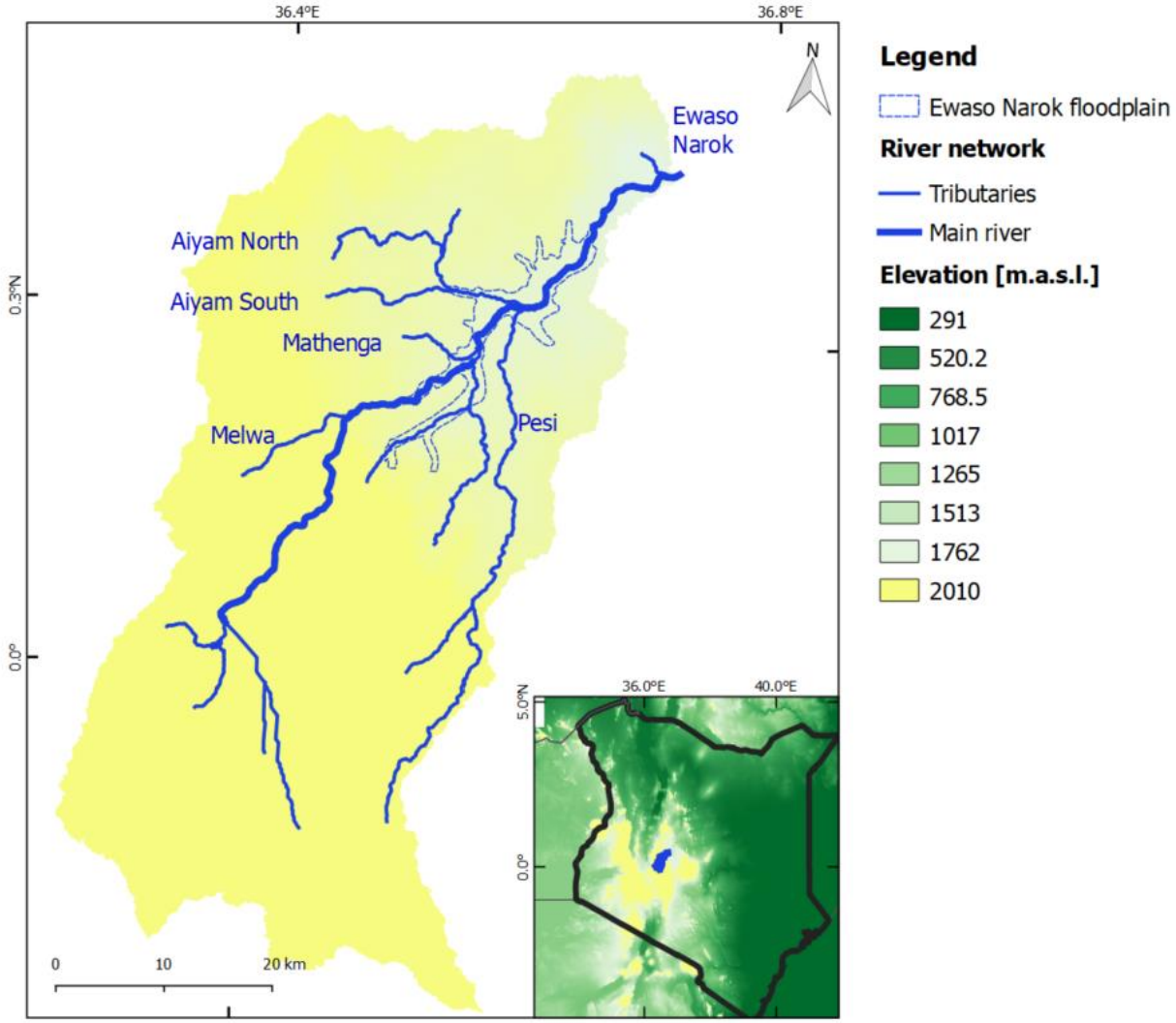

Fig. 2.2: Topographic map of the Ewaso Narok subbasin and river network. Data sources: earthexplorer.usgs.gov (STRM, digital elevation), CETRAD, and WRI (streams), wetland delineation (Beuel et al., 2016, personal communication E. Amler (2016)), subbasin (WRMA).

The Laikipia plateau is bounded to the West by faulted escarpments overlooking the Rift Valley (Groundwater Survey, 1988; Hackman, 1988). The West's boundary is called Laikipia Escarpment and is made of two sets of normal high-angle faults trending NNE and NW. To the east, the Laikipia Plateau drops gradually down to an elevation of 1,645 m a.s.l. (Hackman, 1988).

The Laikipia plateau covers an area of 10,000 km^2 (Rovero & Jones, 2012), and is divided into three subbasins (Fig. 2.3), the Ewaso Narok subbasin, the Ewaso Ngiro-Mt. Kenya subbasin, and the Ewaso Ngiro Lowland Subbasin (Gichuki, 2002). The work's focus is mainly on the Ewaso Narok subbasin (1,840 km^2), which drains the Aberdares mountain ranges and the Western part of the Laikipia Plateau (Evanson et al., 2014; Notter, 2003). The upper part of the catchment is characterized by relatively steep terrain. The lower reaches are ridge to gently undulating and level topography (Kibson Consult, n.d.). The altitude of the Aberdare Forest and Lake Ol Bolossat, the main sources of the perennial rivers of Ewaso Narok, are 3,300 and 2,349 m.a.s.l. consecutively.

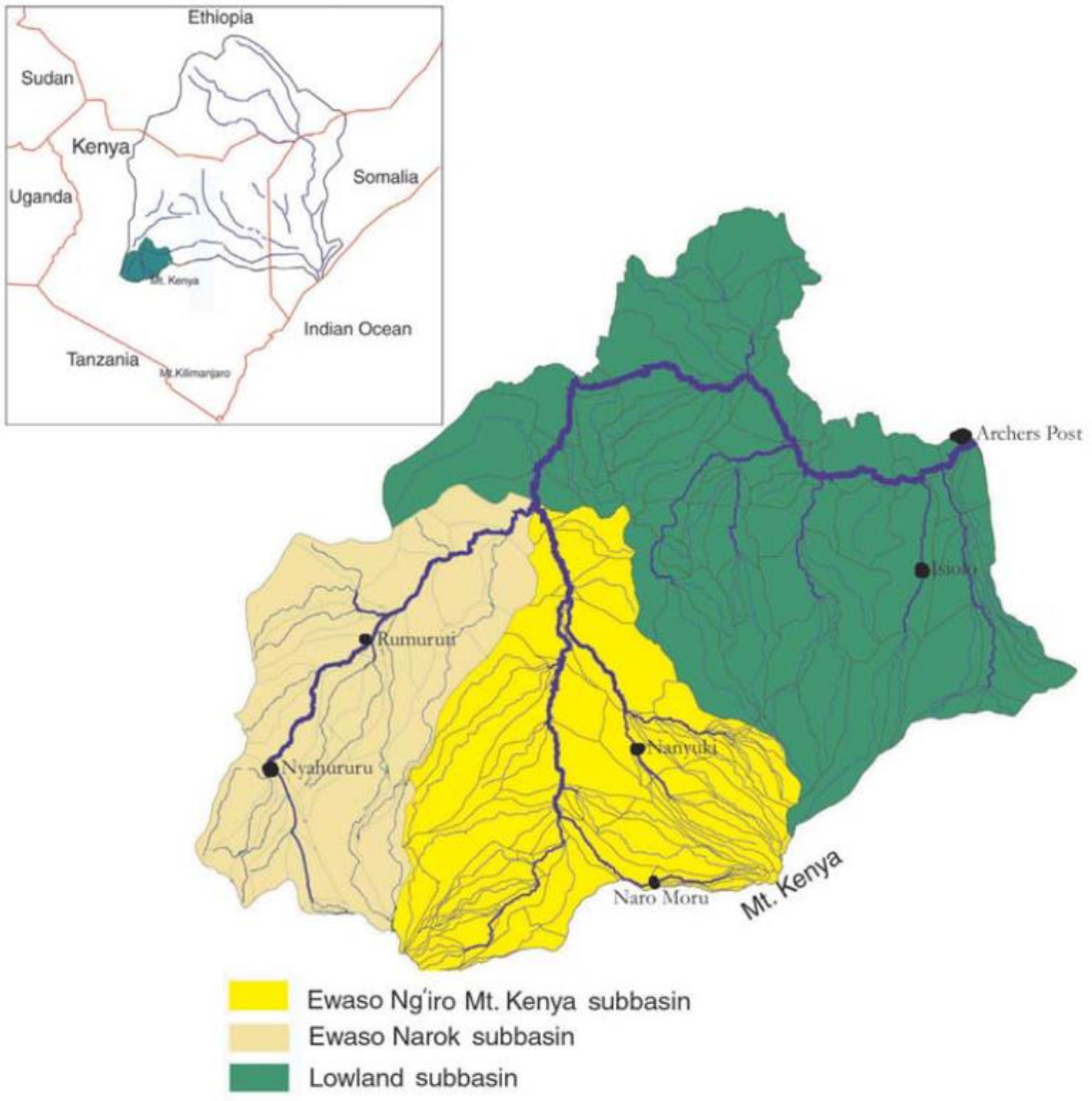

Fig. 2.3: Map depicting towns and the three subbasins in the Laikipia plateau (Gichuki, 2002).

The wetland map was delineated as the borders of the wetland ecosystem (Beuel et al., 2016). The criteria used for delineation are according to the occurrence of depressions in the landscape (Bwangoy et al., 2010) and vegetation that differs from the surrounding uplands (Beuel et al., 2016; Semeniuk & Semeniuk, 1995). The delineation of the Ewaso Narok wetland was improved using high-resolution satellite image composites provided on Google Earth® (Beuel et al., 2016) (personal communication E. Amler, 2016).

2.2. Climate

The climate of Laikipia's semi-arid plateau is affected by the inter-tropical convergence zone (ITCZ) (Kibson Consult, 2014). Additionally, Mount Kenya (5,199 m.a.s.l.) and the Aberdare mountain ranges (4,403 m.a.s.l.) cause orographic effects as the humid air is lifted and falls as rainfall.

There are four seasons in the Laikipia plateau (Berger, 1989; Gichuki et al., 2001). The season of "long rains" is from March to June, when ITCZ is crossing the Equator resulting in high reaching convection that causes heavy rains. The second wet season (November to December) is the "short rains" that penetrate the plateau from the dryer northern region and contribute to 50 – 60 % of the annual precipitation of the arid areas (Gichuki, 2002). The "continental rains" are from July to September when the ITCZ is located north of the Equator, pulling winds from the Indian Ocean (Berger, 1989; Gichuki et al., 2001; Groundwater Survey, 1988). This precipitation is mainly restricted to the western part of the plateau (Gichuki, 2002). The mean annual rainfall ranges between 600 and 800 mm (Groundwater Survey, 1988). The last season is the dry season. The annual precipitation in the Ewaso Narok wetland is around 500 mm, and the mean monthly temperature range between 16 and 20 °C (Thenya, 2001). Temperatures and evapotranspiration (ET) rates in the basin decrease with increasing altitude. For the Ewaso Narok wetland, two automated meteorological climate stations exist, one at the Rumuruti Water Resource Management Authority (WRMA, 2016) office and the other at Evans farm (part of the GlobE-Project) (Fig. 2.4).

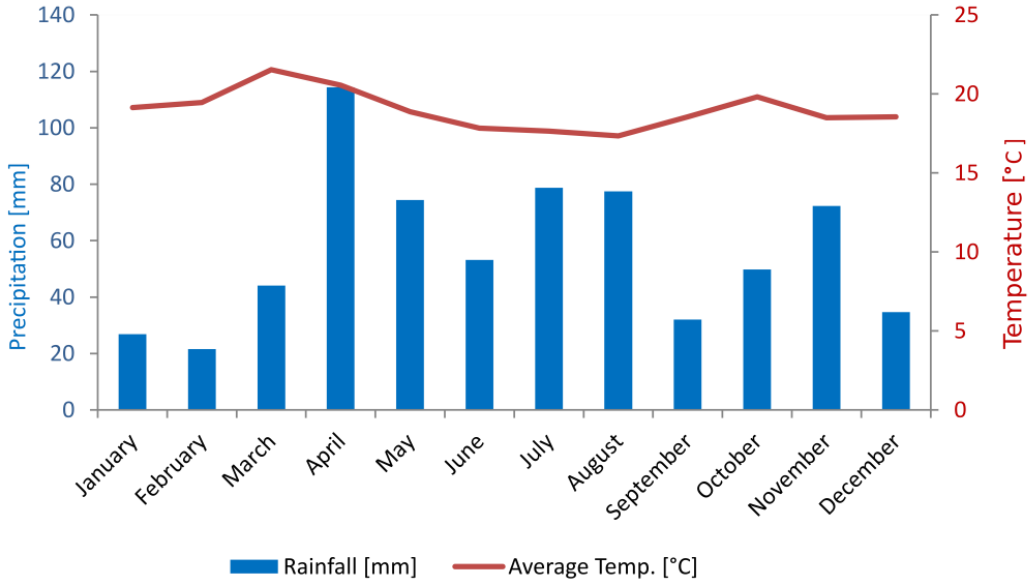

Fig. 2.4: Precipitation [mm] and temperature [°C] per month (average values for 1965 to 2016 of two stations) in Ewaso Narok wetland.

From a larger perspective, four different rainfall stations exist in the Ewaso Narok area; Ol Maisor Farm, north of the wetland, Rumuruti, south of Ewaso Narok, Ndaragwa Forest station, south of the wetland, and Nyahruru, south of the wetland (Fig. 2.5 and App. 4 for the values).

High ET characterizes the subbasin with a maximum of ca. 3.300 mm in the northern lowlands. Rainfall exceeds annual ET, causing water excess to occur only in areas above 2,200 m.a.s.l. (approx. 1 % of the basin) does rainfall exceed annual ET (Gichuki, 2002). In the Ewaso Narok

wetland, there is a water deficit as ET rates are 1,600 - 1,800 mm annually, outstripping precipitation amounts. Particularly, December to March represents a prolonged dry period with maximum evapotranspiration values and minimum rainfall (Fig. 2.4 and Fig. 2.5). These values were taken from the Climate Forecast System Reanalysis (CFSR) GP3 (Bours, 2016).

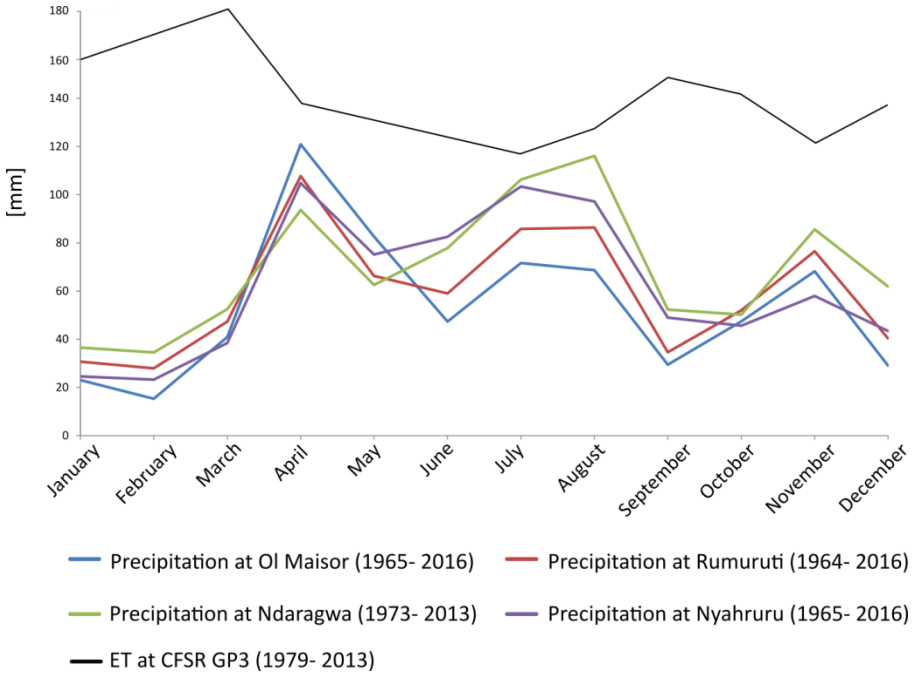

Fig. 2.5: Monthly average precipitation measured at four stations across Ewaso Narok wetland. Source: WRMA and average monthly evapotranspiration at CFSR GP3 (1979-2013).

2.3. Geological framework

2.3.1. Africa's crystalline basement

Evidence for major crust-forming events that date to 3.8 Ga is preserved in the African continent. The main orogenic episodes that occurred in Africa are summarized in Table 2.1 (Choubert and Faure-Muret, 1990; Dirks et al., 2009).

Africa's crystalline basement is composed of metasedimentary, meta-igneous, and igneous rocks ranging in age from Archaean to Cenozoic (Gubanov & Mooney, 2009; Hinsbergen et al., 2011; Key, 1992; Schlüter, 1997) (Fig. 2.6). This heterogeneous basement is concealed beneath un-metamorphosed sedimentary and extrusive rocks of variable thickness and weathering products (Key, 1992). Archaean cratons and the mobile belts developed during orogenic Precambrian cycles are the main and oldest parts of East Africa's crystalline basement (Key, 1992; Schlüter, 1997). They are composed of granitic-gneissic greenstone belts and are generated in two sequences (Key, 1992; Schlüter, 1997). They hold the key to the evolutionary history of the early Earth (Anhaeusser, 2014), making the use of the term "greenstone belt" wide. The Archaean granite-greenstone has a distinctive geotectonic style that introduced the idea of "gregarious batholiths" (Anhaeusser, 2014), explaining the structure of the craton and the greenstone belts occurring as elongate slivers of sedimentary volcano rocks as given in the Tanzanian Craton (Westerhof et al. 2014) or in the northeast cratons (Borg & Shackleton, 1997). The greenstone belts of the Tanzanian Craton can be subdivided into granitoid terrains and the

schist belts of the Dodoman, Nyanyian, and Kavirondian System (Key, 1992). Mobile belts, and a new crust, were formed around the Tanzanian Craton during the Proterozoic times (Condie, 1998). This mobile belts can be subdivided into two belts: the ENE-striking Usagaran Belt to the east and the NW-trending Ubendian Belt to the S and SW (Fritz et al., 2013).

Tab. 2.1: Main orogenic episodes in Africa (after Choubert and Faure-Muret, 1990).

Orogeny	Age (Ga)	Main outcome
Alpine	0.12 – 0	Subduction of African plate under Eurasia and formation of the Atlas mountains
Hercynian	0.45 - 0.25	Limited collision and tectonic activity along the NW and S margins of the African plate
Pan-African	0.85 - 0.50	Merging of all cratonic fragments to form the Gondwana supercontinent to which Africa is central
Kibaran	1.40 - 0.85	Merging of Southern and Central Africa cratons as part of the Rodinia supercontinent
Eburnian	2.20 - 1.80	Growth of the West Africa Craton along an active accretionary margin (Birrimian). Merging of the Congo and Tanzania cratons in the Central Africa Craton. Passive margin development and orogenesis along the W margin of Central and Southern Africa cratons
Neoarchean	2.75 - 2.55	Stabilization of Kaapvaal, Zimbabwe, Congo, Tanzania cratons and the Man and Reguibat shields; merging of Kaapvaal and Zimbabwe cratons as Southern Africa Craton
Mesoarchean	3.15 - 2.75	Accretionary growth of Kaapvaal, Zimbabwe, Congo, Tanzania cratons and the Man and Reguibat shields
Paleoarchean	3.55 - 3.15	Formation of early Archean cratonic cores (Kaapvaal, Tokwe)

During the Paleoproterozoic, the Eburnean orogenic cycle happened (Westerhof et al., 2014), laying down the Ubendian and Usagaran belts in Tanzania and the Buganda-Toro System in Uganda (Schlüter, 1997); both are lithologically similar to the Archaean greenstone belts (Key, 1992). In the Mesoproterozoic, the second supercontinent cycle occurred, resulting in the Rodinia Supercontinent (Westerhof et al., 2014). Orogenic activities in East Africa were less pronounced during the Paleoproterozoic (Key, 1992). The last orogeny of the Proterozoic age influencing Central and East Africa is the Pan-African Orogeny (650 - 400 Ma) that brought together old continental kernels (Hinsbergen et al., 2011; Thorpe & Smith, 1974). This resulted in the formation of the Bukoban System and the Mozambique Belt (Kroner, 1977; Petters, 1991; Schlüter & Trauth, 2006). Mobile belts generally bear the imprint of the Pan-African tectonothermal event (Thorpe & Smith, 1974).

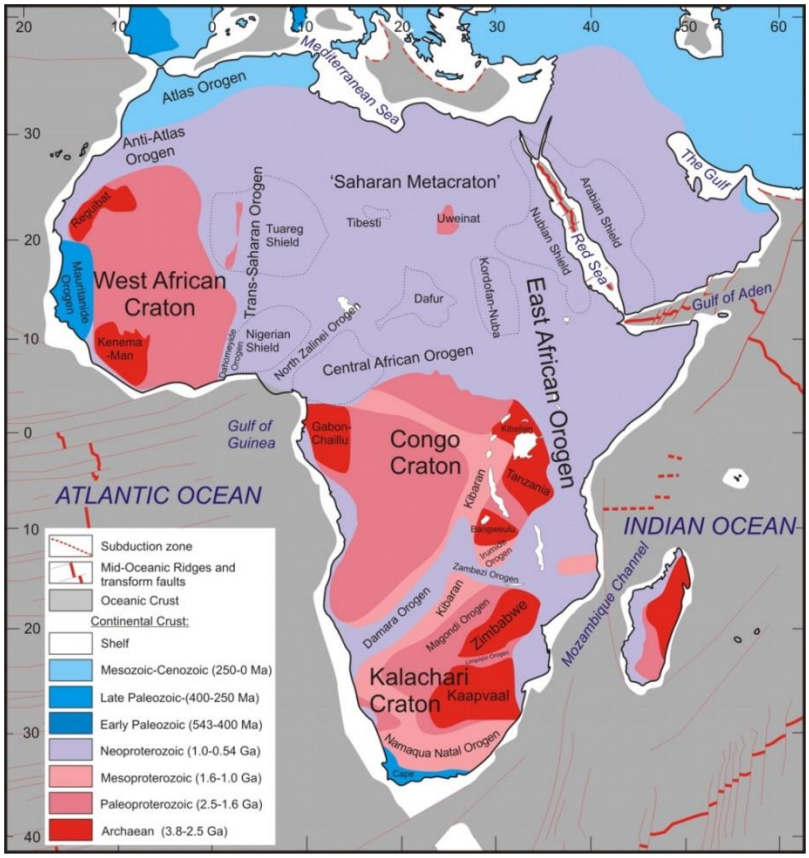

Fig. 2.6: Age of African crustal basement (Hinsbergen et al., 2011 after Gubanov and Mooney, 2009).

2.3.2. The evolution of Kenya's Rift

Since its development in the early Miocene till today, the East African Rift System (EARS) (Fig. 2.7) has had a very important role in East Africa's geodynamical evolution. As a succession of rift valleys, its eastern branch, the Gregory Rift, compromises the Ethiopian and Kenyan Rifts, whereas its western branch runs from northern Uganda along the western borders of Uganda and Tanzania. The eastern branch developed in the Early Miocene (Omenda, 2007; Rooney, 2017). It is characterized by Cenozoic volcanism, faulting, and eruption of large volumes of mafic and silicic lavas and pyroclastics (Omenda, 2007). The eastern branch is a continental extension of the world's rift system (Baker & Wohlenberg, 1971) and is dominated by basalt, trachyte, and rhyolite. Cenozoic volcanism is mainly restricted to intracratonic areas (Thorpe & Smith, 1974). The eastern branch The western branch, dominated by potassium alkaline, represents a typical rift structure developed in the Late Miocene, which is deprived of its cratonic character (Thorpe & Smith, 1974). It is dominated by faulting that has created deep basins currently filled with lakes and sediments (Omenda, 2007). There has been some work on the association between volcanism and penecontemporaneous domal uplift (Le Bas, 1971; Thorpe & Smith, 1974; WoldeGabriel et al., 2016).

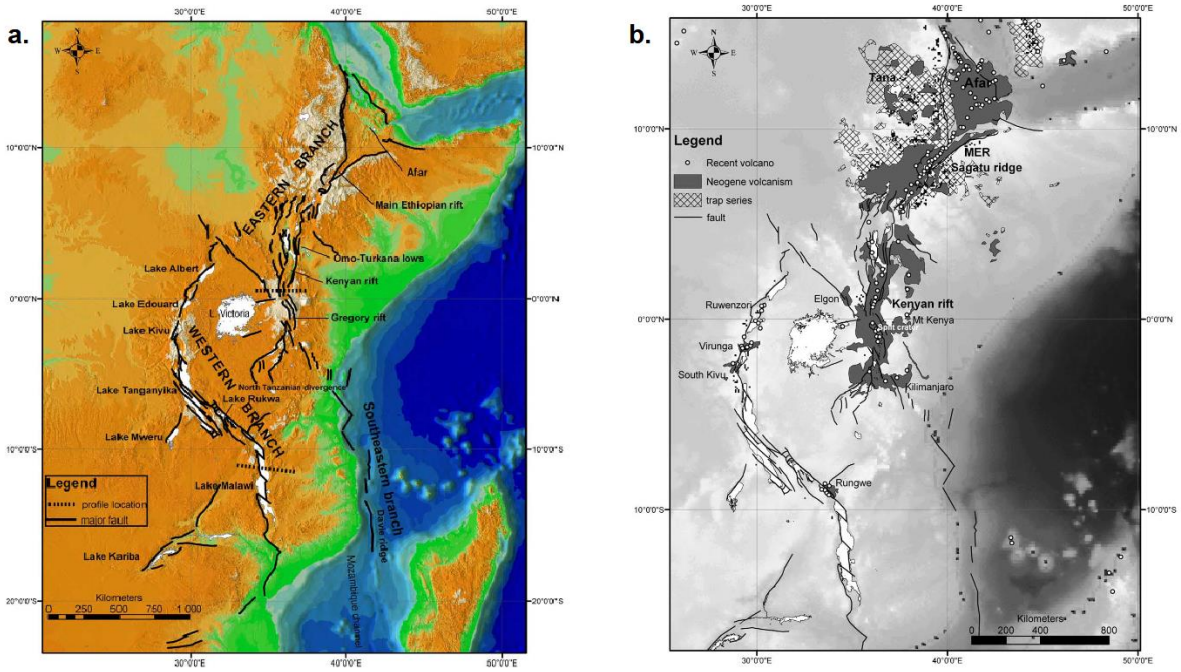

Fig. 2.7: The East African Rift System (EARS): a. The Eastern and Western Branch, b. The volcanic provinces within the EARS (Chorowicz 2005).

The EARS evolution has been a debate among geologists and geophysicists. The most recent and popular theory is mantle plumes (Macdonald, 2002; O'Connor et al., 2019; WoldeGabriel et al., 2016). These mantle plumes heat the overlying crust, causing it to expand, fracture, and become emplaced (Thorpe & Smith, 1974). The mantle sources underlying the mobile belt comprise four-phase peridotite with small amounts of amphibole (Macdonald, 2002).

Three important phases of epeirogenic and crustal flexure happened in Kenya; periodic up-arching of central Kenya and local down-warping of the coastal zone. The early Miocene monoclonal up-warping of the Kenya-Uganda border area is known as the nephelinitic central volcanism (Baker & Wohlenberg, 1971). It was accompanied by down-flexing of the Turkana depression, which is filled with basalt, local faulting, and a crustal unwarping or a dynamic uplift of central Kenya (Baker & Wohlenberg, 1971). This uplift is referred to as the Kenya Dome, massive fissured phonolite eruption of about 300 m thickness in the late Miocene. The fault pattern suggests progressive confinement to a narrow "Rift Valley" zone towards the Quaternary (Hackman, 1988). The chemistry in the Miocene suggests that the extrusive ranged from nepheline normative basalts to the voluminous plateau phonolites (Hackman, 1988).

The Miocene Samburu basalts (Tab. 2.2) were affected by the earliest Cenozoic faults (Carney, 1972). An unconformity exists between the Samburu basalts and the overlying Rumuruti group (McCall, 1967). Carney (1972) observed minor faulting within the Rumuruti group. Golden (1978) related Miocene phonolite dykes to tensional stress with an axis of mild down-warping. The high dips in the Samburu basalts result from the post-eruptive phase of the median up-warping (Hackman, 1988).

An uplift of 1,400 m succeeded the Kenyan Dome during the late Pliocene to mid-Pleistocene times (Baker & Wohlenberg, 1971; Macdonald, 2002). It was in isostatic equilibrium and supported by anomalous mantle loading within the underlying lithosphere (Macdonald, 2002). It further coincided with the zone of volcanism, rifting, and anomalous mantle within the Rift

Valley (Macdonald, 2002). To the west, there was evidence of regional monoclonal down warping (Hackman, 1988). Continued plume uprise raised geothermal gradients, thus permitted dehydration and melting of the metasomatized lithospheric mantle (Macdonald, 2002). Partial melting occurred, and the magmas ranged in composition from nephelinitic to hy-normative basaltic, with silica undersaturated at greater depths (Baker & Wohlenberg, 1971; Macdonald, 2002). Eruptions of the voluminous flood phonolite (Tab. 2.2) took place in the Miocene (Baker & Wohlenberg, 1971). The primary magma underwent polybasic fractionation and contributed to the basal crustal layer. This layer of basaltic magma could have been the source of phonolites and trachyte through partial melting (Macdonald, 2002). The extrusives in the Pliocene and Quaternary ranged from alkali basalts with some tholeiitic affinities to trachyphonolites, phonolitic trachyte, and sodatrachytes (Hackman, 1988). Along the Rift, all the strongly under-saturated phonolites are older than 7 Ma, apart from the phonolitic nephelinites. The mafic and felsic rocks show a general decrease in silica undersaturation with time (Hackman, 1988).

The Kenyan Rift valley, where tertiary magmatism was initiated 35 Ma (Macdonald, 2002), is part of the EARS. Its formation started early Miocene in the Turkana area (Macdonald, 2002). Its development occurred within the Late Proterozoic basement of the Mozambique mobile belt (400 – 800 Ma) and close to the eastern margin of the Tanzania Craton (Macdonald, 2002). The formation of the Rift started with up doming, volcanism and was followed by faulting to form a half-graben and extension/expansion (Omenda, 2007). The Rift's basement geology is divided into three domains that strike approximately NW-SE (Smith & Mosley, 1993). The Rift's major fault pattern defines a complex graben (the Gregory Rift), which trends along the uplift's major axis (Baker & Wohlenberg, 1971). The faults are antithetic and downthrown eastwards (Baker & Wohlenberg, 1971). The marginal plateau's major uplift began after, accompanied by several phases of graben faulting, creating the Gregory Rift (Baker & Wohlenberg, 1971). The developing graben was partly filled by lower to middle Pleistocene flood trachyte (Baker & Wohlenberg, 1971). Baker (1987) stressed the complexity of magmatic associations in the Kenyan Rift, ranging from nephelinites through basanites and alkali olivine basalts to hypersthene normative basalts. Macdonald (2002) found in the craton nephalinites in 80 % of the samples, and alkali olivine basalts and hy-normative basalts in only 20 %.

When the first faults developed, relatively minor phonolite and trachyte volcanism existed (Baker & Wohlenberg, 1971). In the mid-Pliocene, voluminous basalt eruptions along the trough and the formation of the dominantly basaltic Aberdare central volcanic range happened (Baker & Wohlenberg, 1971). In the late Pliocene times, massive eruptions of trachytic and phonolitic ignimbrites began in the Rift's floor (Naivasha sector) (King et al., 1972).

2.3.3. Laikipia's basement - tectonic history and metamorphism

The geological history of Laikipia's basement (Tab. 2.2) describes the different tectonic episodes from the early Paleozoic until recent years. Accompanying the Samburu episode, complete recrystallization occurred, forming the following minerals: quartz, plagioclase, biotite, hornblende, garnet, carbonate, ore, microcline, diopside, and sillimanite (Republic of Kenya, 1987). K-Feldspar and muscovite were occasionally formed.

Both the Laikipia Plateau and the Eastern Rift Shoulder were established by faulting in a tectonic episode around 13 - 14 Ma. Regional tectonic deformation leads to the structural history of the Laikipia basement rock of the Kirimun area. The interaction of the different episodes has

disrupted the metamorphic rocks on all scales to produce the following features (Hackman, 1988): 1. slicing of original lithological units, 2. several ages of bounding structures, 3. several fold styles are related to different events, 4. regional and small scale interferences of fold structures, 5. interlaying of migmatites and banded gneisses, 6. transported fabrics and all planar fabrics tend to be composite, and 7. minor intrusives of several ages are emplaced along brittle and plastic shear zones.

Evidence of folds with axes trending NW and NNW from the Baringo episode is noticed left in the Upper Ewaso Ewaso Ng'iro subbasin (Key, 1987). Charsley (1984) recorded a synformal structure-oriented NNW beside the Ewaso Narok river with a tendency to trend NNW. Baker and Wohlenberg (1971), McCall (1967), and Shackleton (1978) describe in detail the evolution of the Gregory Rift, including the history of the Baringo-Laikipia from the Miocene to the present day. In the area of Baringo-Bagoria and the Laikipia Plateau, major trends of planar fractures have been documented by Hackman (1988):

1. Faults trending NW: They appear on the eastern part of the Laikipia plateau, either went through faults that caused a belt of discontinuous fractures or are probably a result of tension features.
2. Faults trending NNE: The Laikipia Monocline area has faults defined by dip variations and the Loroki Escarpment (Carney, 1972).
3. Faults trending N-S.
4. Lineaments trending WNW.
5. Lineaments trending ENE: They are mostly tension features of the late orogenic phase. They manifest in the basement as well-defined, rectilinear joint swarms locally with evidence of minor strike-slip shear. This trend transects the northern Laikipia Plateau.

Additionally, the disposition of lineaments on the Laikipia Plateau suggests that the Miocene phonolites have been faulted (Hackman, 1988) (Fig. 2.8).

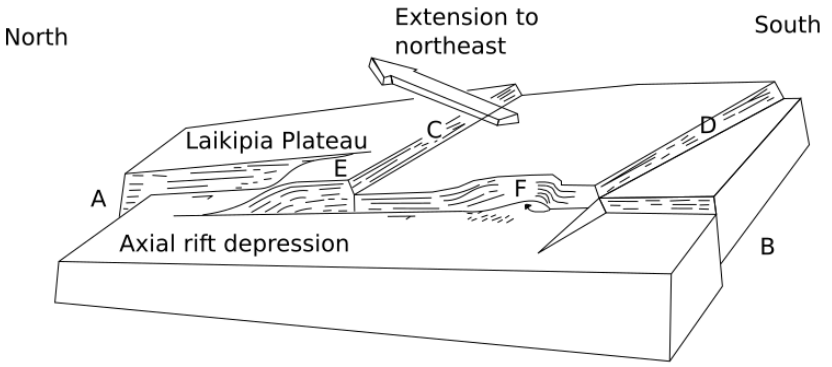

A-B Ngelesha Lobolus Changmasa fault zone
C Waseges fault
D 'Ol Legisianan Sapuko fault'
E Site of Kinsoget box-faults
F Hanington fault & depression

Fig. 2.8 Vertical and strike-slip faulting in the eastern Rift Valley shoulder. Modified after Griffiths (1977).

The geological history of the Laikipia plateau includes metamorphism, volcanism, glaciations, and peneplanation (ESGHS, 2012). The basement rocks are of Precambrian time and range from differentiated gneisses to undifferentiated intrusive types, including migmatites, late granites,

and foliated biotite leucogranite (Groundwater Survey, 1988). They are believed to belong to the Mozambique orogenic belt (Republic of Kenya, 1987). They are composed of various sediments that were transformed by regional metamorphism into gneisses, schists, and quartzites, thus being compact and impervious (Republic of Kenya, 1987). Migmatites are formed through partial melting of pre-existing rocks, which are assemblages of quartz, brown biotite, micro-perthites, with or without modal amounts of diopside and apatile (ESGHS, 2012). The gneisses are derived from marine deposits of more than 4,000 Mio years that were pushed underground and exposed to heat, pressure, and chemical actions (Boy, 2011). These processes formed hard, crystalline rocks resembling granite but containing a high proportion of quartz (Boy, 2011).

Above the Precambrian basement, rocks are formed from extrusive ranging from alkali-basalts to trachytes with voluminous Miocene phonolites with a thick deposit of sedimentary formation of poorly consolidated to weakly indurated gravels and silts (Tab. 2.2) (ESGHS, 2012; Hackman, 1988). Rumuruti phonolites (discussed in detail in Section 2.3.4) form a uniform series of flows characterized by twisted flow structure of parallel aligned feldspar with a glittering appearance or fresh fracture. However, the finer lava is showing a matt surface (Aqua Well, 2013).

In some areas, the Rumuruti phonolites intercalate with basalts. They are overlaid by calcrete deposits above, which are tuffs, and above it superficial deposits. The tuffs are yellow or welded or ignimbrites porous or lapilli with gravel and sand or impermeable ignimbrites of decomposed clayey pumice (Aqua Well, 2013; ESGHS, 2012). Recent deposits, quaternary volcanic, and sediments further overly the basement system rocks (Geolink Associates, 2010). Sediments cover the top area. After sedimentation, orogenic movements set in folding the sediments and formating large mountain masses. Sediments accordingly were metamorphosed into quartz and feldspar rich with biotite, hornblende, and garnet. Afterward, the denudation process wore down the mountain masses to the level of peneplain (ESGHS, 2012). The area has alluvium and colluviums compromising of a crudely stratified mixture of clay, rock fragments. This is a hill slope deposit derived from weathered rock by sheet wash (ESGHS, 2012).

The different tectonic and volcanic disturbances of the Rift Valley and, more specifically, the down-warped basin of the Precambrian basement, which was initially a plain, at different periods, explain the topography of Laikipia plateau (Hackman, 1988; Kibson Consult, 2014). The disturbances lead to the dislocation of the peneplain surfaces forming separated ridges and troughs and piling of volcanic rocks and eruptions (Aqua Well, 2013; Groundwater Survey, 1988; Hackman, 1988).

Ewaso Narok wetland, as part of the Laikipia Plateau, has resulted from a combination of impermeable warping of lava at the surface and centripetal groundwater drainage, perhaps conditioned by broad warping (Hackman, 1988). It is described as a monotonous phonolite shallow pan (dambo) that got flooded with black cotton soil (Earth Scope, 2012; Hackman, 1988). The superficial parts in the area are of alluvium and fluvial-lacustrine deposits.

Tab. 2.2: Geological History of Laikipia basement (after Republic of Kenya, 1987).

Age	Formation	Sedimentation/Vulcanicity/ Metamorphism	Igneous intrusives	Year (Ma)	Tectonic/ Thermo-tectonic episodes
Recent	-	Alluvium, colluvium	-	-	Marigat lineament - continued seismicity
	-	Fluviolacustrine sediments	-	-	-
Pleistocene	-	Korosi-Paka trachyte/basalt central volcanoes	-	-	-
	-	Fluviolacustrine and glaciofluvial sediments	-	-	Grid faulting
	Gregory Rift	Hannington Group Trachy-phonolites	-	-	-
Pliocene	-	Trachyte shield volcanoes and basalts	-	5- 6	Graben faulting
Miocene	-	Late Miocene phonolites and trachytes	-	9	Box-fault's systems-ramps, monoclonal down-warping
	Laikipian Plateau and Eastern Rift Shoulder	Rumuruti Group plateau phonolites and Inner Rift Shoulder volcanics	Enkare Nairoua microsyenite	13- 14	Faulting
		Samburu Basalts	Mugomul syenite, Cherelgat phonolites- dyke complexes	-	-
		Fluvial, terrigenous sediments (Kirimun Formation)	-	-	-
Early Paleozoic	-	-	-	450	Late Mozambiquian
	Mozambique Orogenic Belt	Amphibolite Facies	Local melting-vein phases Ol Doinyo Ngiro Gabbro	580	Barsaloian
		Amphibolite Facies	Local melting-vein phases	630	Baragoian
		Amphibolite Facies	G2 granites	830	Sabachian
		Upper Amphoibolite Facies	G1 granites: migmatites	-	Samburuan
	-	Sedimentation of Son Sol, Ol Doinyo Ngiro, and Loroki sequences	-	-	-
	-	-	Older migmatites	-	Pre-Samburuan

2.3.4. Lithostratigraphy and stratigraphy of Laikipia Plateau

The rock formation can be divided into three groups in terms of stratigraphy (Republic of Kenya, 1987) (Tab. 2.3): Metamorphic rocks of the Basement System (Precambrium), Tertiary volcanics, and Quaternary volcanics (Fig. 2.9).

Another way of grouping includes two main groups: Late Precambrian-Early Paleozoic Mozambique Orogenic Belt, and the Cenozoic volcanics of the Rift Valley with the adjacent shoulder plateau (Hackman, 1988). In addition, there is sedimentation from the Late Cambrian to the Miocene (**Miocene sedimentary rocks**).

The Mozambique orogenic belt's metamorphic rocks are divided into five types: Loroki Gneisses, Ol Doinyo Ng'iro Gneisses, Don Dol Gneisses, Undifferentiated migmatites, and Ndura Complex.

In the Ewaso Narok wetland, only the **Ndura Complex**, and the **Don Dol Gneisses** are exposed (MEMR, 1987) (Fig. 2.9). The **Ndura Complex** has different rock types (flaggy gneiss, almandine permeation gneiss, mafic permeation gneiss). The flaggy gneisses, exposed in the middle part of the Ewaso Narok wetland, are foliated metamorphic rocks. They are massive pale, grey to white leucocratic rocks, weathering to shades of brown (Hackman, 1988).

Tab. 2.3: Lithostratigraphy of Laikipia Plateau (Republic of Kenya, 1987).

Period	Epoch	Formation		Lithology	Maximum thickness [m]
Quaternary	Recent	Alluvium		Loam, silt, clay, gravel	
		Mount Kenya Volcanic Series	Upper (parasitic vents)	Basaltic pumice	60 - 100
			Middle (parasitic fissure eruptions)	Trachytes, olivine basalts, mugearites, olivine trachytes	500
	Pleistocene		Lower (main eruptive episode)	Nepheline syenite of the plug	
				Kenytes, phonolites, pyroclasts	> 600
				Phonolites and trachytes	> 530
				Porphyritic phonolites	130
				Unexposed volcanics	3000
Tertiary	Pliocene	Ol Arabel Tuffs		Tuffs	120
		Laikipian Basalts		Olivine basalts	130
	Miocene	Sipili Trachytes		Trachytes	150
		Tasiokwank and Igumiti phonolitic trachytes		Phonolitic trachytes	40
		Thomsan's Falls Phonolites		Phonolites	85
		Rumuruti Forest Basalt		Basalts	
		Rumuruti Group	Upper Ewaso Narok Phonolites	Phonolites	750
			Marmanet Phonolites		
			Lower Ewaso Narok Phonolites		
			Ngelesha Phonolites		
			Simbara Basalt Series	Basalts and agglomerates	> 300
			Sub Volcanic	Conglomerates	10
			Sediments		
Precambrium		Basement system		Granite, gneisses, schists, quarzites	

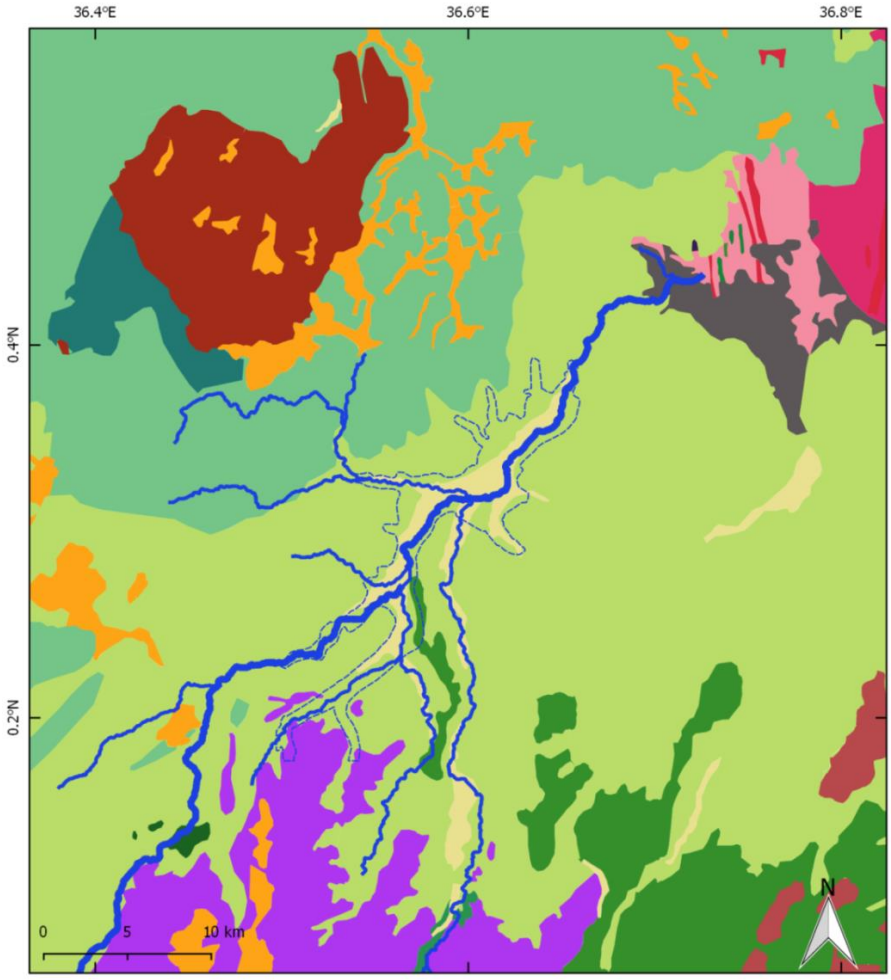

Legend

Ewaso Narok floodplain

River network

Tributaries

Ewaso Narok

Geological formation

Alluvium minor calcrete & lacustrine sediments/ Recent superficial deposits

Residual regur & gravel (pan deposit)/ Recent/ Superficial

Upper mixed Nanyuki Formation/ Recent sediments

Laikipia Forest (Sirrima Basalats)/ Pilocene

Pesi River Basalts/ Miocene

Spili Trachystes/ Miocene

Thomson's Falls Phonolites/ Miocene

Rumuruti Forest Basalts/ Miocene

Upper Phonolites (cf Uaso Narok)/ Miocene Rumuruti Phonolites

Upper Phonolites (cf Marmanet)/ Miocene Rumuruti Phonolites

Middle Phonolites (cf Uaso Narok)/ Miocene Rumuruti Phonolites

Lower Phonolites (cf Ngelesha)/ Miocene Rumuruti Phonolites

Don Dol Gneisses/ Precambrian

Amphibolites/ Don Dol Gneisses/ Precambrian

Metamafic-ultramatic intrusives/ Don Dol Gneisses/ Precambrian

Foliated biotite leucogranite/ Intrusive Rocks/ Precambrian

Massive & flaggy veined grey Gneisses/ Ndura Complex/ Precambrian

Fig. 2.9: Geological map of Laikipia plateau. Georeferenced and modified after MEMR (1987).

The Don Dol Gneisses (Fig. 2.9) occupy most of the southeastern part of the Precambrian outcrop (Degree Sheet 35) and in the West, where Ewaso Narok river discloses a re-entrant in the escarpment of the overlying Miocene phonolites. These gneisses weather more readily than the granitic-magmatic intrusive, giving rise to the low ground (Hackman, 1988). The Don Dol Gneisses are divided into graphitic gneiss, marbles, sillimanite gneiss, amphibolites, metamafic-ultramafic intrusives, and chert breccia (MEMR, 1987). In the Ewaso Narok valleys, amphibolite or mafic gneiss were mapped by Charsley (1984), consisting of biotite-gneiss hornblende-biotite-gneiss and true amphibolite. The latter are discordant bodies indicating dykes or dislocated tectonically. Massive quartz feldspathic gneisses, graphitic gneisses, marble, and amphibolites are further present in the area (Hackman, 1988).

The Precambrian Intrusives include the foliated biotite leucogranite**.** These make-up thin sections in the Ewaso Narok wetland and are composed of about 50 % quartz, 25 % microcline, 20 % microperthite, and 5 % oligoclase, with small amounts of magnetite (Hackman, 1988). Bands that are internally xenomorphic granular have sharp margins, indicating catalysis with a proportion of fine-grained feldspar and quartz (Hackman, 1988).

The Miocene sedimentary rocks are situated north of the Ewaso Narok river. Small pockets of sediment and volcanic interactions have been exposed. These rocks are exposed below the phonolite escarpment, particularly in gallies, by runoff from the volcanic plateau. The Kirimun sediment is 30 cm to a few meters thick and is sandwiched between the basement and phonolites of the Rumuruti Group north of Ewaso Narok (Hackman, 1988). The lithology includes sepiolite, white clays, marls, shales, vesicular tuffs, striped yellowish chert, laminated grey-green siltstones, graded grits, and grey calcareous gravels.

The **Cenozoic volcanic** can be divided into the Samburu basalts, the Miocene Volcanic of the inner eastern Rift shoulder, the Miocene Plateau Phonolites (The Rumuruti Group), the late Miocene Phonolitic Trachytes and Basalts, the Pliocene basalts, the Pliocene Trachyte shield volcanoes, Flood Trachyphonolites and Trachytes and Trachyte/Basalt Central Volcanoes (Hackman, 1988). Each of these groups occupies a certain area. For example, the Rumuruti Group dominates the north and central parts of the Laikipia Plateau (MEMR, 1987).

The **Tertiary volcanics** are overlying the metamorphic rocks of the basement system. Subvolcanic deposits of the Lower Miocene are underneath the Phonolites. They can be erosion products of the basement rocks and are rounded pebbles (Republic of Kenya, 1987). The volcanic rocks in this area are products of eruptions. The lower layers are basaltic, while the upper ones are phonolitic and trachytic with interbedded tuffs and sediments (Republic of Kenya, 1987).

The Phonolites

The Miocene Plateau Phonolites of the Rumuruti group are named after the township of Rumuruti and make up the faulted Phonolite plateau surface. They include Miocene plateau phonolites, younger extrusive formations, the Thomson Falls Phonolites, and Sipili trachytes (Groundwater Survey, 1988). The phonolites are of homogenous composition and thickness in the Laikipian Plateau (Groundwater Survey, 1988), impermeable, and massively unjointed (Aqua Well, 2013; ESGHS, 2012). Phonolites have an intermediate silica feldspar and quartz content (Hem, 1985). According to Baker (1963), four geological units exist in the area; the sub-volcanic

sediments, porphyritic basalts and tuffs, phonolites of the Rumuruti Phonolites, and porphyritic olivine and augite basalts (Geolink Associates, 2010; Kibson Consult, n.d.).

The **Ewaso Narok phonolite flows** form the most common type of the Rumuruti phonolites and is characterized by a dark green porcellaneous matrix and can be observed in roadside cuttings (Kibson Consult, n.d.). Carney (1972) recognized three major sequences of Rumuruti Phonolites (**Upper, Middle, and Lower** (Hackman, 1988), each separated by an unconformity associated with a period of faulting (Groundwater Survey, 1988). The upper consists of **Upper Ewaso Narok phonolites** and **Marmanet Phonolites**. The middle is the **Lower Ewaso Narok Phonolites,** and the lower is the **Ngelesha Phonolites** (Hackman, 1988). The Rumuruti Phonolites rest in conformity on the Samburu basalts. The variation in their thickness is a result of the distance from the eruptive source and the irregularity of the substratum on which the flows consolidated.

Lower Rumuruti Phonolites: Ngelesha phonolites

Ngelesha phonolites are the lowest lava in the Rumuruti phonolite sequence (Hackman, 1988). They are exposed in different areas and overlay the Samburu basalt. They are dark greenish, compact, and fine-textured, showing only sparse feldspar phenocrysts. They are described as fine-grained black fissile phonolites, distinctive due to abundant vugs infilled by a white or yellow powder in the northeast. The flow is covered by bright red soil. Alkali feldspar phenocrysts' alignment suggests flow in the EW direction (Geolink Associates, 2010; Groundwater Survey, 1988; Hackman, 1988). Their average thickness is around 460 m, thinning to the West against the Samburu basalt (125 m thick at the eastern edge of the Laikipia Plateau). Vesicles are often filled with white zeolites and are characterized by spheroidical further north along the Ngelesh- Aruru Escarpment, and covering the plateau as the Ngelesha Formation composed of dominantly sparsely phyric types: 1. Lower dark phonolite with tare nepheline phenocrysts. 2. Middle biotite Phonolite. 3. Bedded yellow lapilli's tuffs. 4. Upper mottled arphyic Phonolites (Groundwater Survey, 1988).

Middle Rumuruti Phonolites: Lower Ewaso Narok phonolites

The Lower Ewaso Narok phonolites are mainly around the Ewaso Narok river and close to Rumuruti road covering an extensive area of Southern Laikipia and northeast of the plateau. They form much of the faulted eastern Rift (Groundwater Survey, 1988) and show considerable petrographic uniformity; anorthoclase-phyric phonolite in a blue or green matrix with less obvious biotite flakes. Phenocrysts of aegirine and nepheline are occasionally observed. They were divided into three units: lower tuffs, middle dark biotite phonolites, and upper mottled biotite phonolites. The lower tuffs (thickness from 15 to 180 m) are mostly friable, fine-grained yellow tuffs, probably air fall in origin, with calcareous concentrations and mud cracks suggesting lacustrine conditions. Carney (1972) suggests a thickness of up to 150 m for the Lower Ewaso Narok Phonolites, a thickness of 300 m in the south Rumuruti area (according to Charsley (1984) around 250 m), and between 100 to 150 m in the eastern extremities of the Laikipia Plateau (Hackman, 1988).

The dark biotite phonolites are widely distributed in the outcrop, with uniform textures; black and compact with phenocrysts of alkali feldspar, nepheline, and flakes of yellow-brown biotite. An age determination Ewaso Narok formation's lava is of 10.3 ± 0.3 Ma (Hackman, 1988). Other studies show rocks medium to dark grey or greenish-grey in color with a local mottling. They are

either blocky with a sharp subconchoidal fracture or fissile in the field, an indication of internal fluxional texture. Phenocrysts consist of ubiquitous nepheline, alkali feldspar, less common biotite, and rare pyroxene. There is an indication of E-W motion (Hackman, 1988).

Upper Rumuruti Phonolites (Hackman, 1988)

The Upper Rumuruti Phonolites (Fig. 2.9) are characterized by unusual white and dark, patchy textures. Carney (1972) described them as highly porphyritic mottled phonolites, with biotite and age between 10.6 ± 0.3 and 11.6 ≥ 0.3 Ma. Their maximum thickness reaches 245 m as infilling a graben-like depression east of the Ngelesha fault scarp. East of the plateau, they are 100 to 150 m thick. The rocks were further divided into members assuming each represented an eruptive phase: upper biotite phonolites, Garoua phonolite (has less abundant phenocrysts), Ol Doinyo Oiroua phonolites (contains occasional biotite), and Nygyipe Phonolites. These sub-units are all mottled porphyritic types but contain biotite and have less abundant phenocrysts. In the Rumuruti area, the Marmanet flows are distinguished from the underlying Lower Ewaso Narok by having a greater abundance of large phenocrysts (Hackman, 1988).

Hackman (1986) mapped **Ewaso Narok phonolites** (brownish-grey mottled sparsely feldspar phyric types) as overlying the Marmanet phonolites. The Upper Ewaso Narok phonolites intercalated between Marmanet and Losiolo phonolites in the regional stratigraphic sequence. Carney (1972) reported a localized flow underlying the Marmanet phonolites of Ol Doinyo Oiroua Carney's isopach map suggests a thickness of 100 to 150 m. The thickest part of the sequence is a faulted complex trending NNE that corresponds with the extrusive dome or tholoid sources. This concept is supported by the occurrence of pyroclastics, and glassy lavas in the same area and by anomalously high easterly dips of flow boundaries. Hackman (1986) mapped a cluster of four small domes, aligned NW, below the low escarpment of Upper Ewaos Narok phonolites. It is suggested that they are small tholoids developed in the vents from which the neighboring phonolites were extruded (Hackman, 1988). In the hand specimen, the phonolites are green, and very fine-grained, with a conspicuous polka dot mottling occasioned by kataphorite and aegirine aggregates. Phenocrysts of anorthoclase, nepheline, and biotite may be abundant: the molted lavas may alternate with flow-banded and glassy phonolites with well-developed stratification (Hackman, 1988).

The alluvium is part of the **recent Quaternary sediments**. Alluvial deposits are present in the study area, varying in thickness and lithology according to the nature of the underlying solid geology. On the phonolite plateau, the valleys are floored with silt or clay. Boulders are much less abundant than in the basement gorges to the east: on the flat interfluves, an elaborate network of ill-drained pans (dambos) is plugged by volcanoclastic silts and clays, with pebbly gravels and impervious black cotton soil (associated with nodular calcrete) (MEMR, 1987). Between the pans, the higher parts of the plateau are covered with lava rubble and thin dusty soils of aeolian origin, according to Wilkinson (1983). The alluvium is only a few meters thick at the Ewaso Narok river, where it forms a well-drained platform for a citrus plantation. The constituent material in the area is brownish and grey clay-silt soil strewn with fragments of basalt, trachyte, and phonolite derived from the fan's coalescence (Hackman, 1988).

2.3.5. Soil

Plateau depressions are characterized by dark grey to black vertisols and planosols soil, which are unsuitable for crop production (GoK, 1994). The Laikipia Plateau parent material is granite, gneisses, and tertiary igneous rocks, forming Lithosols and Xerosols in the uplands and Fluvisols from alluvial deposits in floodplains (Mwita et al., 2013). The parent material around Mount Kenya is of volcanic origin, forming Andosols and Nitisols (Mwita et al., 2013). According to the CETRAD map (Evanson et al., 2014) and Dijkshoorn (2007) (Fig. 2.10), the upstream area of the wetland is characterized by moderately deep and well-drained clayey luvic Phaeozems, whereas the downstream wetland lies in gleyic Solonchaks with extremely slow and poor drainage. Phaezems are slightly acid soils with a thick, dark-coloured surface layer that is rich in organic matter and well-supplied with nutrients. They are highly productive soils, provided they are not inhibited by continuous hard rock (Jones et al., 2013).

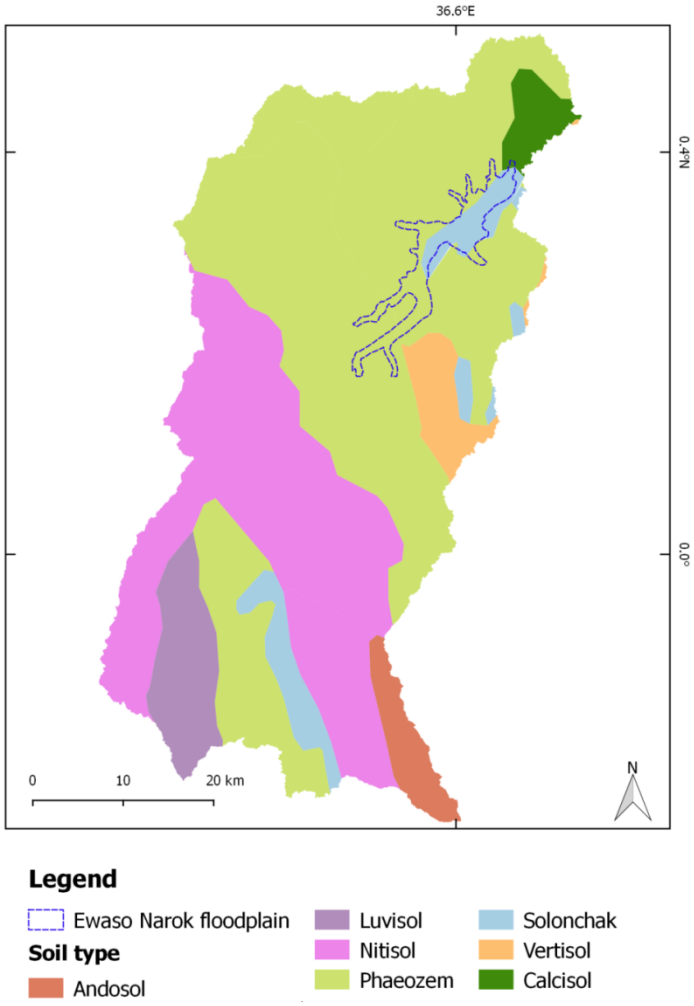

Fig. 2.10: Soil types in the Ewaso Narok subbasin. Modified after Evanson et al. (2014), and Dijkshoorn (2007).

Solonchaks are strongly saline with high concentrations of soluble salts. They are associated with arid regions where saline groundwater comes close to the surface or where evapotranspiration rates are considerably higher than precipitation, at least during a large part of the year. Salts dissolved in soil moisture remain behind after the evaporation of the water. They are good for grazing (Jones et al., 2013).

Further soil types surrounding the Ewaso Narok wetland are Calcisol and Vertisol. Calcisol is common where the climate is dry, allowing the accumulation of calcium carbonate in the soil. Caalcisol forms through the leaching of carbonates from the upper part of the soil, which precipitates when the subsoil becomes oversaturated from carbonate-rich water moving through the soil or by the evaporation of water leaching behind dissolved carbonates (Jones et al., 2013). Precipitated calcium carbonate precipitates fill the pores, causing calcrete that is impermeable to plant roots.

Vertisols are clay-rich soil that develops deep, wide cracks upon drilling. They exhibit cracks that open and close periodically upon drying and wetting. This is caused by the presence of the clay mineral montmorillonite (Jones et al., 2013).

The upper described soil types show that the Laikipia Plateau, including Ewaso Narok wetland, is characterized by different kinds of soils ranging from black cotton soils of poor drainage (Lind et al., 1974), dark brown humic soils, fine alluvial clay, grey volcanic loams, and murram soil. Murram, or what is known as laterite soil, is formed from the parent rock's leaching after intensive and long-lasting weathering in dry and wet conditions. They are rich in iron and aluminum, giving them their red color (Aqua Well, 2013). The soil cover generally consists of shallow yellow-brown to lateritic sandy soils (ESGHS, 2012). This yellow color is typical of weathered terrains and has a variable thickness ranging from 8 to 15 m below the ground level. Water-lain fluvial and lacustrine deposits are present in the top layer up to 35 mm thick in some parts of the Ewaso Narok floodplain (Aqua Well, 2013; ESGHS, 2012; Geolink Associates, 2010). They include conglomerates, sandstones, shales, calcareous rocks and fossiliferous limestones, and laminated clay rocks (Aqua Well, 2013; ESGHS, 2012).

2.3.6. Hydrology

The wetland is part of a semi-arid grassland plateau with frequent drought and unreliable rainfall (GOK, 1994; Thenya, 2001). Similar to other meanders and floodplains in the Laikipia plateau, water in the Ewaso Narok floodplain is not transported rapidly and tends to pile up, making the low-lying zones more liable to flooding (Paron et al., 2013). Ewaso Narok river (Fig. 2.11), a major tributary of Ewaso Ng'iro, runs in a north-by-east direction and is joined by other tributaries before discharging into Ewaso Ng'iro North River beyond the wetland (Kibson Consult, n.d.). Seasonal tributaries include Pesi and Melwa, Methenga, Aiyam South, Aiyam Noth, and Mutara (Fig. 2.2) (LWF et al., 2013; Thenya, 2001; Thenya et al., 2011). The Ewaso Narok catchment originating in Nyandarua ranges and Ol Bolossat catchment (Thenya, 2001; Thenya et al., 2011) drains the southeast (SE) side of the Plateau, the northwest (NW) flows to the northeast (NE) in conformity to the direction of the fracture system (ESGHS, 2012; Groundwater Survey, 1988; Wachira, 2014) draining towards the Indian Ocean (Hackman, 1988). The Ol Bolossat forest and the lake provide Ewaso Narok headwaters' source, as the river is located on both extreme northern fringes. Lake Ol Bolossat is under threat of extinction due to degradation through encroachment by the local communities (Kibson Consult, n.d.). The Plateau's western part drains the Rift valley (ESGHS, 2012; Wachira, 2014).

The total length of the Ewaso Narok river is 95 km. Some parts of the Ewaso Narok river have been structured. The river channel is highly linear and trends SE/NW. The Ewaso Narok and the associated tributaries will tend to follow the main fracture system (Groundwater Survey, 1988).

The discharge of the Ewaso Narok river has been continuously declining, particularly during the dry season, but flash floods have increased (Thenya et al., 2011). It dries up during severe droughts and leaves only a few large pools in the lower catchment (WRMA & LWF, 2013). This stream seasonality, coupled with high evaporation rates, causes a major water deficit in this area. The fact that it is affected by climatic patterns makes it unreliable, especially during dry spells (Groundwater Survey, 1988). The water demand is supplied by boreholes, roof harvesting, and dams.

Fig. 2.11: The Ewaso Ng'iro Basin in Kenya, its main rivers, and the flow of the Ewaso Ng'iro river. Data sources: CDE, University of Bern, Switzerland.

2.3.7. Hydrogeology of Ewaso Narok catchment

Kenya's hydrogeology is categorized as unconsolidated sedimentary aquifers, consolidated sedimentary aquifers, basement aquifers, and igneous aquifers (Tab. 2.4), with yields ranging from very low to very high (Tab. 2.5) (BGS, 2019; Ó Dochartajgh & Brighid, 2019).

The Ewaso Narok subbasin aquifer is igneous with moderate yields (Fig. 2.12) (BGS, 2019; Ó Dochartajgh & Brighid, 2019).

Tab. 2.4: Hydrogeology and aquifer systems of Kenya (BGS, 2019; Ó Dochartajgh & Brighid, 2019).

Aquifer category	Subcategory	Definition
Unconsolidated Sedimentary		Unconsolidated sedimentary aquifers with dominantly intergranular flow
Consolidated Sedimentary	Consolidated sedimentary intergranular / fracture	Aquifers with significant intergranular and fracture flow
	Consolidated sedimentary intergranular	Aquifers with dominantly intergranular flow
Igneous	Igneous intrusive	Intrusive igneous aquifers, often granitic
Basement		Crystalline basement aquifers with typical weathered/ fractured aquifer properties

Tab. 2.5: Categories of aquifers and yield (BGS, 2019).

Category	Attribute Code	Approximate range in yield (L/s)
Very High	VH	> 20
High	H	5 - 20
Moderate	M	2 - 5
Low to Moderate	LM	0.5 - 2
Low	L	0.1 - 0.5
Very Low	VL	< 0.1

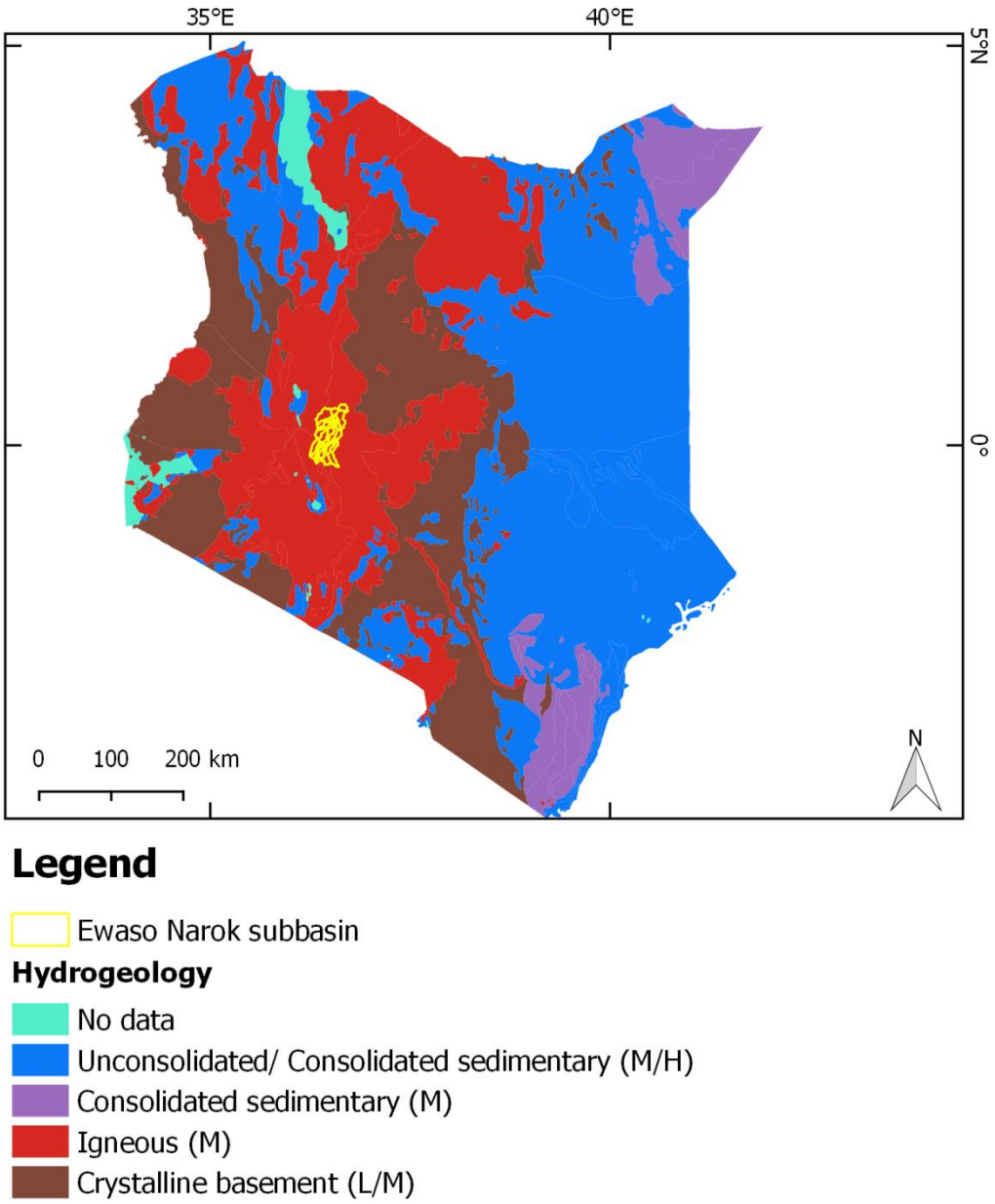

Fig. 2.12: Aquifer systems of Kenya with their approximate yield (cp. Tab. 2.4 and 2.5). Data sources: BGS (2019), Ó Dochartajgh & Brighid (2019), subbasin (WRMA).

The whole Laikipia plateau is mainly a recharge area with a deep groundwater table though locally shallow groundwater and wetlands occur, associated with a perched aquifer (Republic of Kenya, 1987).

Two aquifers discharge the area:

1. The **regional confined** aquifer system is composed of fractured and weathered volcanic with interbedded old land surface deposits. This aquifer system is recharged in the high areas with high rainfall. Part of the infiltrated water rises in springs, for example, in the Ewaso Narok floodplain (Republic of Kenya, 1987). The springs are a permanent source for human consumption. The regional aquifer occurs in the Miocene Rumuruti group (Ngelesha Phonolites, Lower and Upper Ewaso Narok Phonolites) up to the Pleistocene

Mount Kenya Volcanic Series. Due to the lack of data, the depth of the water-bearing layers and aquifers is unknown in the Ngelesha Phonolites and the Rumuruti Forest Basalts. Its water is tapped multiple times in drilling profiles. However, they are very deep and accordingly cause disappointments at times as some wells rarely tap the water level. The depth of this aquifer in the Lower Ewaso Narok Phonolites varies between 55 and 214 m, and within the Marmanet Phonolites, between 66 to 237 m. Boreholes drilled within the Upper Ewaso Narok Phonolites will encounter water between 122 and 183 m, in the Lower Ewaso Narok Phonolites between 7 to 69 m, in the Marmanet Phonolites between 23 to 76 m, and in the Upper Ewaso Narok Phonolites between 46 to 123 m (Republic of Kenya, 1987).

2. The **local aquifer** is composed of fissured and weathered **basement rocks**. Recharge is either by direct infiltration of rainwater along the fissures and fractures, diffuse infiltration in weathered zones, or indirect infiltration of the runoff along with the river courses (Republic of Kenya, 1987). The depth of the local aquifer ranges from 20 to 142 m. The piezometric water levels vary between 20 and 142 m.b.s.l.

2.3.8. Land Use

Ewaso Narok wetland was under pristine vegetation until the early 1980s (Heinichen, 2015) and covered an area of 44.8 km^2 by 2013 (GoK, 1983). Part of the wetland was drained for farming through a government ASALs program (Mathuva et al., 1997; Thenya, 2001). With time, land use shifted mainly to extensive cattle ranching, carried out by European settlers (Heinichen, 2015; Kohler, 1987), and from large-scale ranching to small-scale farming, thus, altering the natural vegetation (Kibson Consult, n.d.; Thenya, 2001). Around 25 % of the Ewaso Narok subbasin is under crops and settlements, 59 % under grass and a mixture of woodlands, 15 % under forest, and the remaining 1 % underwater and moorland (Fig. 2.13) (Evanson et al., 2014).

The main land use in the Ewaso Narok wetland is pastoralism, horticulture, subsistence farming, commercial cattle ranches, tourism, and fish ponds inside the wetland (WRMA & LWF, 2013). Today, the Ewaso Narok wetland is settled by people who crop, cultivate, weave, and live off the wetland, including herders, pastoralists, and cattle ranchers, due to its fertility and water availability. Due to human activity, the land has been cleared for agriculture, thus reducing the vegetation cover (WRMA & LWF, 2013). This led to a reduction in water quantity and higher soil erosion (WRMA & LWF, 2013). Part of the wetland is still covered with semi-natural vegetation making the wetland an important habitat for wildlife. The wetland area is dominated by *Cyperus papyrus L*., wetland grass, and reed flourish (Groundwater Survey, 1988; Hackman, 1988). On the one hand, the papyrus vegetation decreased from 37.5 to 8.25 % from 2006 to 2010, possibly due to conversion to grazing land. On the other hand, cultivated land increased from 12 to 33 % (Muriuki, 2016). The main crops grown are maize, tomatoes, kale, onions, beans, watermelon, and cut flowers (WRMA & LWF, 2013).

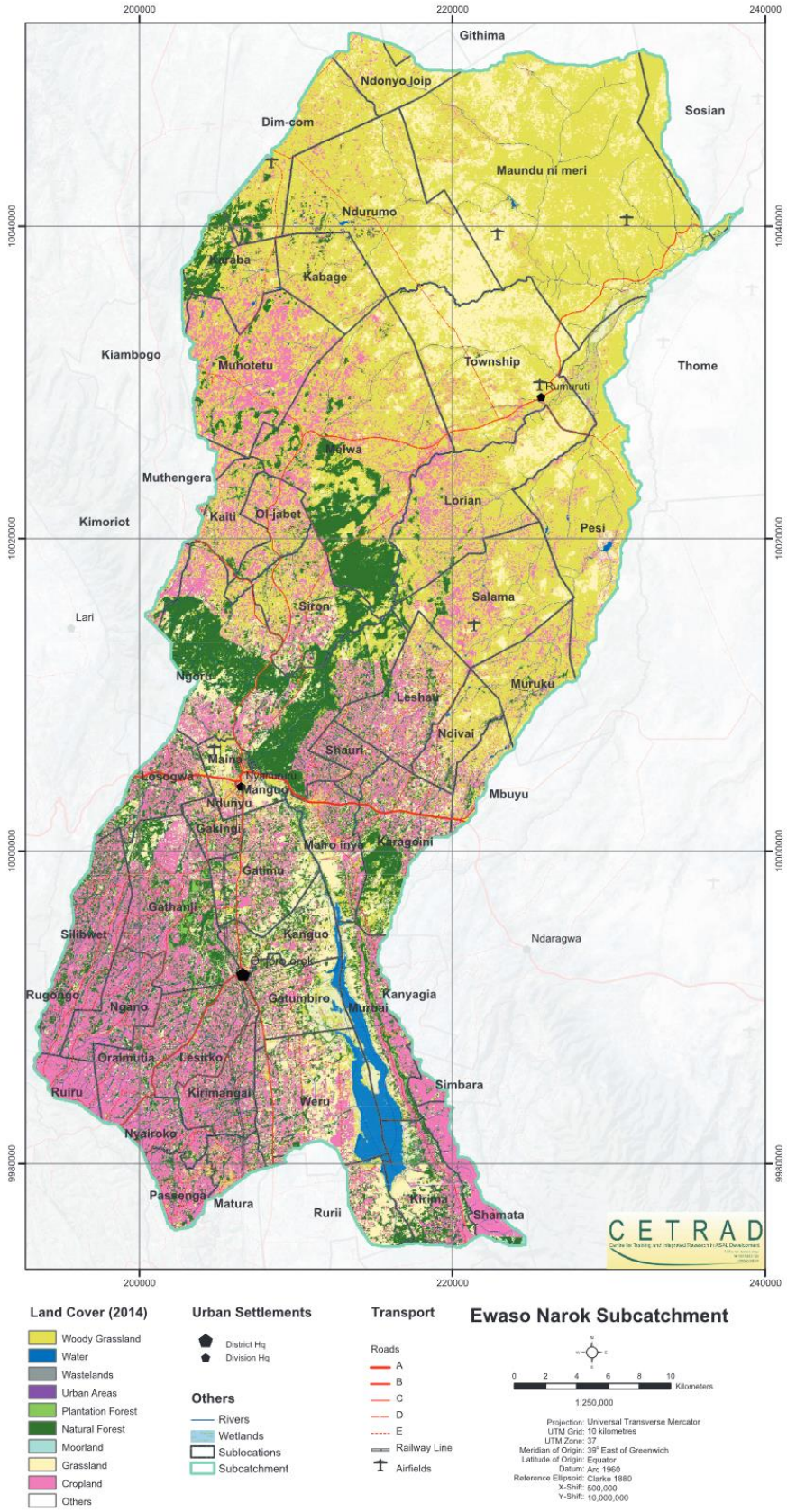

Fig. 2.13: Landcover of the Ewaso Narok subbasin (Evanson et al., 2014).

3. The current state of research

This section gives an overview of the current state of research. The first section is about wetlands and floodplains. Next, the hydrogeology of weathered basement aquifers and the chemical weathering of rocks are described. The last two sections address the stable water isotopes and water quality in wetlands.

3.1. Wetlands

Wetlands tend to form where surface and groundwater accumulate within topographic depressions, such as along floodplains (EPA, 2008). Wetlands can be classified based on their unique hydrologic, geomorphic, and hydrodynamic characteristics (Brinson, 1993; EPA, 2008). To understand and manage a wetland, identifying the wetland hydrological inflow and outflow is vital. The direction and rate of water movement into and out of wetlands are controlled by the spatial and temporal variability of energy or a change in pressure (from zones of high pressure to low pressure). Like any hydrological system, the water budget of wetlands is used to account for the inputs and outputs to the wetland and helps to characterize the behavior of the wetland system (EPA, 2008). The inputs into wetlands include precipitation, overland flow, surface water inputs from rivers, streams, overbank flow, and groundwater sources, including subsurface, lateral unsaturated, and saturated flow from uplands to toe-slope and flat landscapes (EPA, 2008). Wetlands can be recharge wetlands, flowthrough wetlands, and discharge wetlands depending on the groundwater flow (Fig. 3.1).

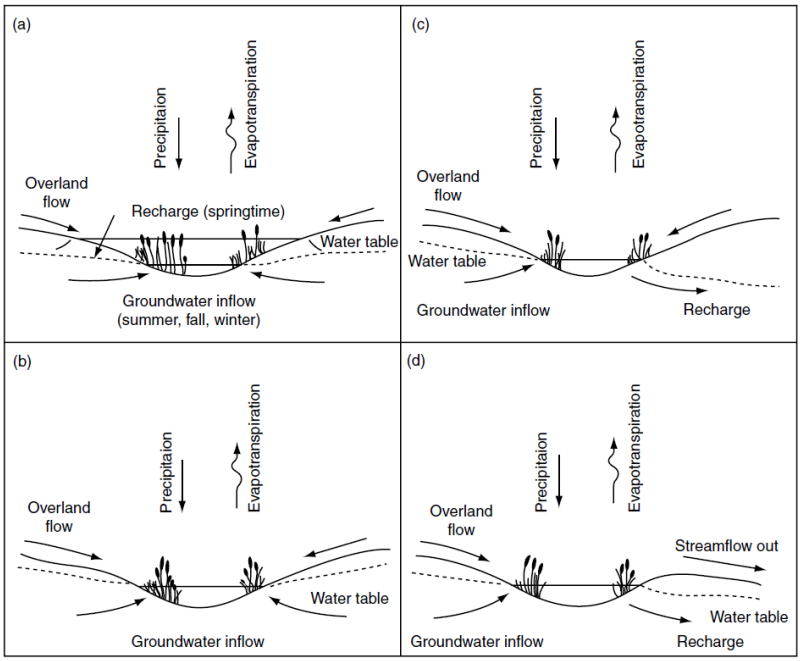

Fig. 3.1: Possible flow components of wetlands fed by groundwater and surface water: a. Inflow or outflow, b. Inflow, c. Through-flow, d. Through-flow with occasional streamflow out (Larson, 2009).

Floodplains definition ranges from “areas of low-lying land that are subject to inundation by lateral overflow water from rivers or lakes with which they are associated” (Junk & Welcomme, 1990) to “riverine marsh or high water-tables are usually recharged from faults or springs, even

when the land surface undergoes aridification during dry periods" (Renaut & Jones, 1997) after Ashley et al. (2004).

Floodplains are zones of important geomorphological and hydrological processes (Jung et al., 2004) and are among the most biologically productive and diverse ecosystems on earth (Tockner & Stanford, 2002). Like wetlands in general, they redistribute, store, and release water (Jung et al., 2004). Accordingly, their formation and maintenance are closely tied to fluvial dynamics (Hughes, 1997; Ward et al., 1999).

Floodplains develop in all geographic regions and at different locations along river corridors (Tockner & Stanford, 2002). They are sensitive to changes in river hydrology, increased alterations of the land-water interface, and inputs of nutrients and toxicants (EPA, 2008; Naiman & Décamps, 1997; Nilsson & Berggren, 2000; Ward et al., 1999).

3.1.1. Flow conditions in floodplain

As areas that support interaction processes between groundwater and surface water (Butturini et al., 2002; Hayashi & Rosenberry, 2002; Stanford & Ward, 1993), floodplain aquifers receive water from direct precipitation, upland sources, hillslope seepage, and channels during floods or lateral overflow and rising groundwater (Mertes, 1997; Tockner & Stanford, 2002). The interaction between groundwater and surface water ranges from flow to transport to water and nutrients exchange. This interaction depends in floodplains on the pressure head gradient and the connectivity between the water bodies, such as the channel and alluvial plain (Krause et al., 2007; Woessner, 2000). The permeability of the stream bed, its position, the permeability of the aquifer, and the size and geometry of the contact area, further control this connectivity (Krause et al., 2007; Woessner, 2000). The interactions between groundwater and surface water vary in space and time (Krause et al., 2007; McCartney, 2000; Nyarko et al., 2010). These interactions happen in the hyporheic zone (Hinkle et al., 2001; Woessner, 2000). In general, groundwater recharge and discharges happen beneath floodplains (Maltby & Barker, 2009). The groundwater exchange with the stream water of floodplains occurs by recharge, discharge, flow-through, and parallel flow (Fig. 3.1) (Larson, 2009; Woessner, 2000).

The inundation of floodplains is a complex phenomenon caused by different water sources via multiple pathways (Tockner & Stanford, 2002). Most floodplains experience large seasonal and interannual fluctuations (Tockner & Stanford, 2002). Even small decreases in flood volumes can result in large reductions in an area flooded, particularly in semi-arid and arid areas (Tockner & Stanford, 2002). In arid and semi-arid regions, wetlands are likely to be recharge zones. However, at high groundwater levels, these zones are subject to reversal, thus becoming discharge sites (Maltby & Barker, 2009). Floodplains are usually groundwater discharge sites and are characterized by unconfined aquifers (Maltby & Barker, 2009), particularly in arid countries. However, some arid-floodplains become recharge sites during floods (Harrington et al., 2002), but others do not (Akeroyd et al., 1998).

Under base flow conditions, groundwater is discharged into the river from the floodplain (Jung et al., 2004) and downwards (Woessner, 2000). Thus, baseflow is that portion of the streamflow that is the result of groundwater discharge (Richardson & Vepraskas, 2001). During low flow conditions, hillslope groundwater discharges to the stream and flows into the floodplain. Groundwater movement is accordingly lateral and, in some reaches, perpendicular to the river

(Bates et al., 2000; Grannemann & Sharp, 1979). At the beginning and end of a flood event, the hydraulic gradient is down-valley and cross-floodplain within the alluvial sediments.

During floods (Fig. 3.1), the domination of cross-floodplain fluxes perpendicular to the river is common (Bates et al., 2000; Woessner, 2000), but eventually, water ends up flowing towards the river only. This takes place when the water level in the channel rises above the water table in the floodplain, and the hydraulic gradient is reversed, inducing flow from the channel into the floodplain; it is referred to as over-bank flow. A groundwater ridge is formed below the floodplain, hampering groundwater's inflow (Jung et al., 2004). After the flood, the river level falls, causing a stream-ward hydraulic gradient. Throughout flood times, the water table gradient is effectively zero across most of the floodplain, with the back of the flood being an exception (Jung et al., 2004). The hydraulic gradient change was also demonstrated by Krause et al. (2007), who attributed it to fluctuations in surface water levels and higher water retention capacity in some floodplain parts.

Numerous models for wetlands are available. However, few explicitly simulate the hydrological pathways and processes occurring in wetlands (Maltby & Barker, 2009). Research on floodplains has focused on measuring and evaluating water levels to assess interactions in floodplains (Cook and Herczeg, 2000; Jung et al., 2004; Kaplan et al., 2010; King et al., 2014). Models are increasingly being linked to chemistry and isotopes to better understand the hydrochemical processes within wetlands (Koeniger & Leibundgut, 2001; Lambs, 2004; Nyarko et al., 2010). Numerical modeling has been used to understand flow processes between streams, flooding water, and groundwater in floodplains (Bates et al., 2000; Krause et al., 2007; Rassam et al., 2009).

3.1.2. Sediments in Wetlands and Floodplains

Depending on the soil layer's infiltration potential, vertical recharge might happen during floods. Low infiltration potential limits vertical recharge (Burt et al., 2002; Lamontagne et al., 2005), and a low conductive soil layer facilitates the lateral transmission of flood pulses in alluvial aquifers. In general, most floodplains have low infiltration potential (Lamontagne et al., 2005). The floodplain's carried sediment is suspended load, compromised of clay- and silt-sized debris and occasionally fine sand. A general trend is common, where more deposition of overbank sediment occurs downstream (Nichols, 2009). The fluvial and alluvial deposits in the floodplain are affected by the nature, type, and abundance of vegetation, by the subsidence rate, and by the quantity of sediment. Describing the channel and overbank depositions in fluvial succession depends on the shape and size of the sand and gravel deposited relative to finer overbank facies. The thickness and expansion of the deposited channel lens depend on the river's depth and width and are governed by avulsion and lateral migration processes (Fig. 3.2).

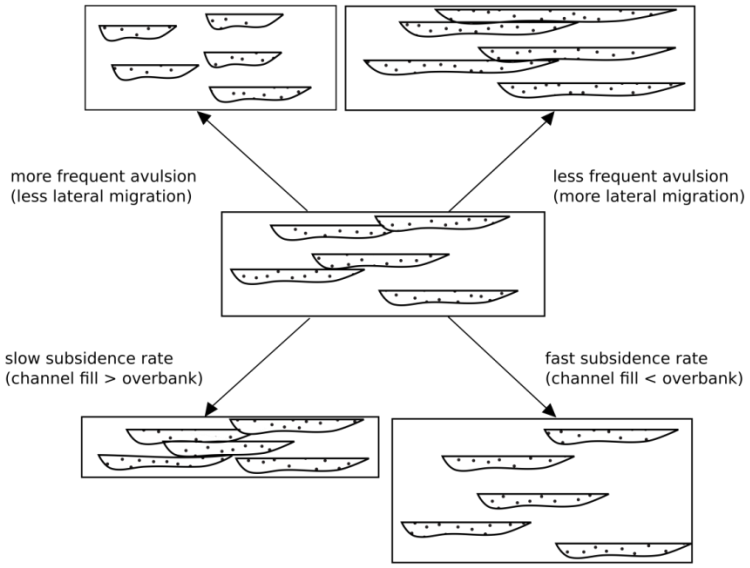

Fig. 3.2: The architecture of fluvial deposits determined by the rates of subsidence and frequency of avulsion (Woessner, 2000).

3.2. Weathering profiles above crystalline rocks

3.2.1. Hydrogeology of weathered basement aquifers

Basement aquifers are distinctive in their occurrence and characteristics and are mostly a consequence of weathering interaction processes related to recharge and groundwater throughflow (Wright, 1992). The lithological sequence above crystalline basements depends on the physical, chemical, and mineralogical features. As East Africa has long-term tectonic stability and a tropical climate, large parts of its crystalline basement rocks developed deep weathering profiles (Chilton & Foster, 1995). A general structure is observed and used in this study following similar works (Burghof, 2017; Heiss, 2016), which adopts the zonal grouping suggested by Chilton and Foster (1995) from bottom to top (Fig. 3.3):

1. Saprock is the weathered bedrock on top of the fresh bedrock etc. (Hebert et al., 1992; McFarlane, 1992; Middelburg et al., 1988; Wright, 1992).
2. Saprolite (derived from in-situ weathering and has become disaggregated). Saprolite with the collapsed zone makes the regolith.
3. Collapsed zone (stone line) or the residual zone is developed from the underlying saprolite by further dissolution and leaching, combined with other chemicals, physical and biological processes.

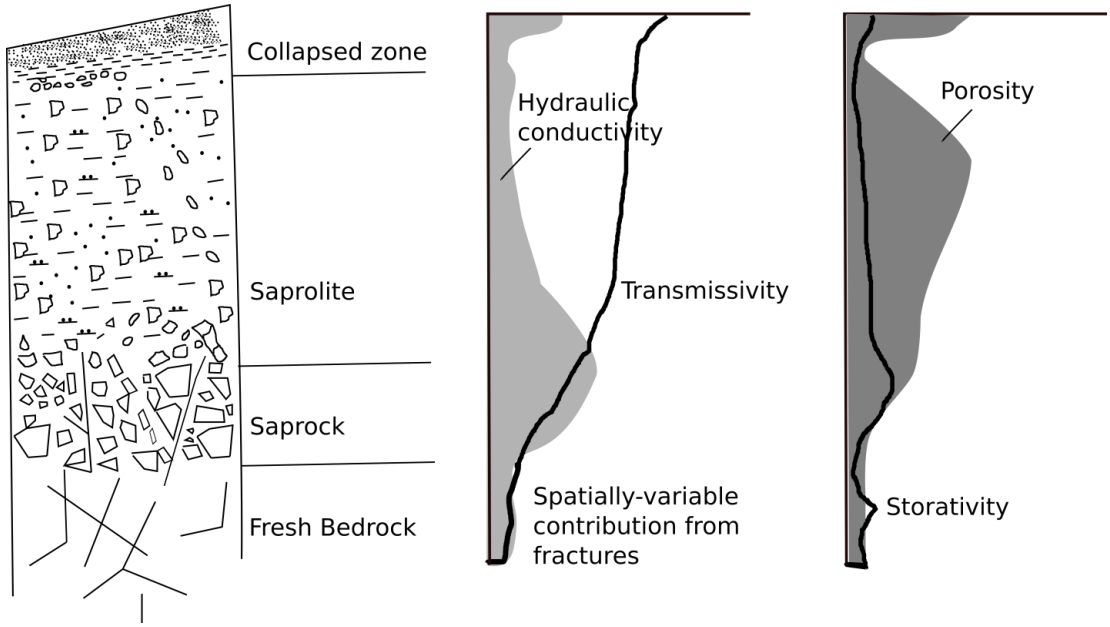

Fig. 3.3: Hydrogeological properties of weathering profiles above crystalline rocks in tropical Africa. Modified after Chilton and Foster (1995).

The collapsed zone on watershed areas is generally sandy with illuviated clay, where colluvial material with secondary clay minerals and laterites gathers there, leading to perched water tables. At slopes, colluvial material accumulates (Wright, 1992).

Residual soil is formed by the collapse of underlying saprolite due to intensive leaching and bioturbation (Chilton & Foster, 1995). It is sandy in general on watershed areas with illuviated clay near the base (Wright, 1992). Colluvial material, secondary clay, and laterites may be present, too, resulting in perched water tables (Wright, 1992). Saprolite is made of two parts, upper and lower. In saprolite weathering, the upper part is characterized by kaolinization, quartz, and iron minerals oxidation as it is associated with vadose zone conditions. The lower is abundant with primary minerals (Na^+, K^+, Mg^{2+}, and Ca^{2+}) that are mobile and are leached from the residual soil. Intermediate weathering products (McFarlane, 1992; Middelburg et al., 1988) are also abundant, in addition to Mn-Fe mottles, which are associated with phreatic conditions (McFarlane, 1992; Wright, 1992). The less mobile elements, such as Ti accumulate in the residual soil (McFarlane, 1992). Saprolite is caused to collapse by kaolinite dissolution in advanced weathering stages, forming a residuum dominated by silica in the form of quartz and iron as goethite (McFarlane, 1992). Within the weathered residual overburden (the regolith) and the fractured bedrock, the basement aquifer occurs. The thickness and lithology of the regolith depend upon bedrock type, amount of fracturing, subsequent erosion, and climate (Hazell et al., 1992). The bedrock includes the weathered saprock and freshly fractured rock (a result of surface decompression, producing subhorizontal joints, or a result of tectonic forces generating subvertical fractures) (Chilton & Foster, 1995; Wright, 1992). The fracture usually increases because of weathering in saprock unless filled with clay minerals.

Weathering in crystalline rocks leads to changes in their hydraulic properties; hydraulic conductivity, porosity, and specific yield (Chilton & Foster, 1995). Weathering of primary minerals increases hydraulic conductivity and specific yield, whereas the formation of secondary clay minerals reduces hydraulic conductivity and specific yield as they seal fractures and pores (Wright, 1992). Weathering can further dissociate kaolinite, leading to an increase in hydraulic

properties (Chilton & Foster, 1995). The weathered crystalline rock aquifers are usually porous (Fass, 2004) and represent good aquifer systems.

In terms of hydraulic properties, a differentiation can be made with the upper and lower saprolite (Fig. 3.3). The upper part is richer in secondary clay minerals compared to the lower part and, accordingly, has a lower hydraulic conductivity (Chilton & Foster, 1995). The underlying saprock combined with the lower saprolite make up the most permeable part of the weathering profile. This is the most important aquifer for drinking water supply for rural populations (Wright, 1992). Further aquifers present are in the fractured crystalline rocks. Permeability development in crystalline rocks depends on their type. For example, coarse, grained, quartz-rich, crystalline rocks develop weathering profiles with the highest permeabilities. Metamorphic rocks and tectonic disturbed zones, on the other hand, have thicker regoliths and lower permeabilities (Chilton & Foster, 1995).

3.2.2. Chemical weathering on crystalline rocks

The main processes of chemical weathering are hydrolysis, oxidation, and dissolution**.** Chemical weathering is locally and temporally limited by high temperatures and water scarcity and is less intense than in humid areas (Tardy et al., 1973). The weathering thickness and lithology depend on complex combinations of bedrock characteristics, climate, age of the land surface, relief, and other factors (Wright, 1992).

The weathering of silicate minerals is a slow process (Sigg & Stumm, 1996), and its mechanisms on a catchment scale are less understood than carbonate weathering (Drever & Clow, 1995). Silicate weathering causes the dissolution of primary minerals and precipitation of secondary minerals (clay minerals and iron hydroxides). The most common secondary clay minerals forming during silicate weathering are kaolinite, illite, montmorillonite, and gibbsite (Appelo & Postma, 2005). The weathering of silicate minerals usually results in increased concentrations of major cations (Na^+, K^+, Mg^{2+}, Ca^{2+}), along with silica (SiO_2), and bicarbonate (HCO_3^-) in the solution (Appelo & Postma, 2005), making the proportion of alumina to alkalis higher in the weathered product (Middelburg et al., 1988). In addition, iron and aluminum, the more insoluble ions, accumulate in the weathering profile. In fresh volcanic rocks, iron is in the reduced state of Fe^{2+}. It is, however, usually oxidized by dissolved oxygen and precipitates as Fe^{3+} oxides and hydroxides.

Silicate minerals weather at different rates due to their susceptibility to chemical weathering; quartz, muscovite, and k-feldspar are resistant to chemical weathering, whereas anorthite, albite, and biotite show a higher weatherability (Fig. 3.4) (Appelo & Postma, 2005; Goldich, 1983). The aquifers in siliciclastic rocks are susceptible to acidification. Thus, silicate weathering strongly influences the pH buffering system (Appelo & Postma, 2005).

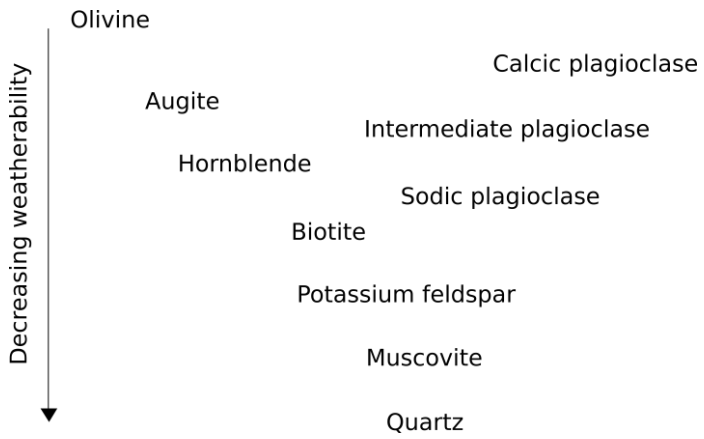

Fig. 3.4: The Goldich weathering sequence based on observations of disappearance in soils (Goldich, 1938).

The hydrolysis of feldspar to clay minerals can be described after Appelo and Postma (2005) in equations 3.1, 3.2, 3.3, and 3.4. From these silicate minerals' weathering equations, specific ion ratios can be deduced. If pure albite weathers to kaolinite, 1 mol Na^+, 1 mol HCO_3^-, and 2 mols SiO_2 will be released into the solution (Appelo and Postma, 2005) (Eq. 3.1). Thus, specific ion ratios in solution are 1 for HCO_3^-/Na^+ and 2 for SiO_2/Na^+ and SiO_2/HCO_3^-.

Albite: $2Na(AlSi_3)O_8 + 11H_2O + 2CO_2 \rightarrow Al_2Si_2O_5(OH_4) + 2Na^+ + 4H_4SiO_4 + 2HCO_3^-$ (Eq. 3.1)

During weathering of pure anorthite, 0.5 mol Ca^{2+} and 1 mol HCO_3^- get into the solution, leading to a specific ion ratio of 2 for HCO_3^-/Ca^{2+} (Eq. 3.2).

Anorthite: $Ca(Al_2Si_2)O_8 + 3H_2O + 2CO_2 \rightarrow Al_2Si_2O_5(OH)_4 + Ca^{2+} + 2HCO_3^-$ (Eq. 3.2)

Pure end members of plagioclase are usually not present in nature, but solid solutions occur. The reaction equation of plagioclase, composed of anorthite (x) and albite (1-x), that weathers to kaolinite show that the ratio of SiO_2/Na^+ in the solution is 2, while the ratio of $HCO_3^-/(Na^+ + 2Ca^{2+})$ is 1 regardless of the exact plagioclase composition (Van der Weijden & Pacheco, 2007) (Eq. 3.3).

$(1-x)Na(AlSi_3)O_8 x Ca(Al_2Si_2)O_8 + (1+x)CO_2 + (5.5 - 2.5x)\,H_2O \rightarrow$
$0{,}5(1+x)Al_2Si_2O_5(OH)_4 + (1-x)Na^+ + xCa^{2+} + (1+x)HCO_3^- + 2(1-x)H_4SiO_4$ (Eq. 3.3)

Alkali-feldspars' weathering, being solid solutions of albite and orthoclase (k-feldspar), leads to specific ion ratios of 1 for $HCO_3^-/(Na^+ + K^+)$ and 2 for $SiO_2/(Na^+ + K^+)$ (Eq. 3.1, 3.4) (Appelo and Postma, 2005).

K-feldspar: $2K(AlSi_3)O_8 + 11H_2O + 2CO_2 \rightarrow Al_2Si_2O_5(OH)_4 + 2K^+ + 4H_4SiO_4 + 2HCO_3^-$ (Eq. 3.4)

Carbonate weathering (Hem, 1985; Krauskopf, 1967; Krauskopf & Bird, 1995):

Calcite is one of the two common minerals, in addition to aragonite where calcium carbonate occurs in nature. It is more stable and abundant. At strong acid concentration, calcite dissolves as follows (Krauskopf, 1967; Krauskopf & Bird, 1995) (Eq. 3.5):

$$CaCO_3 + 2H^+ \rightarrow Ca^{2+} + H_2O + CO_2 \quad \text{(Eq. 3.5)}$$

At low acid concentrations, the calcite dissolves (Eq. 3.6), where H^+ takes CO_3^{2-} away from Ca^{2+} to form the very weak acid HCO_3^-. These reactions take place in nature, for example, where acid solutions from the weathering of pyrite encounter limestone. The reactions can be reversed by any process that uses H^+. For example, if a base is added (Eq. 3.7), presented in the reaction of calcite with aqueous H^+ (Hem, 1985).

$$CaCO_3 + H^+ \rightarrow Ca^{2+} + HCO_3^- \quad \text{(Eq. 3.6)}$$

$$Ca^{2+} + HCO_3^- + OH^- \rightarrow CaCO_3 + H_2O \quad \text{(Eq. 3.7)}$$

An equilibrium can be attained, with the H^+ derived from water or other source attacking the solid to give calcium and biocarbonate (Eq. 3.6). In mass-law form, the equation for the equilibrium constant (K) is presented (Eq. 3.8) (Hem, 1985), where the quantities in brackets represent activities in moles per liter.

$$K = \frac{[Ca^{2+}][HCO_3^-]}{[CaCO_3(c)][H^+]} \quad \text{(Eq. 3.8)}$$

Under natural conditions, the dissolving of calcium carbonate is somewhat more complicated because the acids involved are usually weak. An example is when limestone dissolves in carbonic acid (Eq.3.9) (Krauskopf, 1967; Krauskopf & Bird, 1995).

$$CaCO_3 + H_2CO_3 \rightarrow Ca^{2+} + 2HCO_3^- \quad \text{(Eq. 3.9)}$$

The solubility depends on the partial pressure of CO_2, (donated as P_{CO_2}) above the solution since this pressure helps to determine the concentration of dissolved H_2CO_3 by the reaction (Eq. 3.10). The equilibrium value of H^+ (i.e., pH) also varies strongly with P_{CO_2}.

$$H_2O\ (l) + CO_2(g) \leftrightarrow H_2CO_3(aq) \quad \text{(Eq. 3.10)}$$

The ion ratio Ca^{2+}: HCO_3^- is an indicator for weathering of the calcite-rich carbonate rocks (Kovalevsky et al., 2012) and is controlled primarily by equilibrium in the reaction. The concept of chemical equilibrium establishes boundary conditions towards which chemical processes will proceed and can be discussed from either a kinetic or an energetic viewpoint. Any process that increases the amount of CO_2 available to the solution makes more $CaCO_3$ dissolve; anything that decreases the amount of CO_2 causes $CaCO_3$ to precipitate (Krauskopf, 1967; Krauskopf & Bird, 1995).

The solubility of calcite in pure water decrease as the temperature rises because CO_2 is less soluble at higher temperatures. Carbonates are more influenced by the change in solubility of CO_2 than by the temperature dependency of the solubility itself. Calcite is soluble even in water that does not contain CO_2 (eq. 3.11).

$$CaCO_3 + H_2O \leftrightarrow Ca^{2+} + HCO_3^- + OH^- \quad \text{(Eq. 3.11)}$$

This is a hydrolysis reaction, as HCO_3^- is a weak acid. Even the small amount of CO_3^{2-} produced by dissolving calcite can take a little H^+ away from the OH^- of water. The solubility of calcite in

nature is controlled by equilibria involving $H_2CO_3^-$, CO_3^{2-}, and water. This equilibrium is sensitive to changes in the amount of dissolved CO_2. Surface water and groundwater are often saturated with calcite and as such, can either dissolve or precipitate the carbonate depending on external conditions. Hydrolysis of insoluble carbonate is sufficient to make solution in contact with them slightly basic (Krauskopf, 1967; Krauskopf & Bird, 1995).

Geochemical weathering indices have been used widely to describe weathering profiles and to assess the degree of bedrock weathering (Chittleborough, 1991; Nesbitt & Young, 1982; Parker, 1970; Price & Velbel, 2003; Wilford, 2012). The Chemical Index of Alteration (CIA) (Nesbitt & Young, 1982) is used as a quantitative indicator to estimate the degree of silicate weathering. It measures the extent of conversion of feldspars to clays (Fedo et al., 1995; Kautz & Martin, 2007; Maynard, 1992; Nesbitt & Young, 1989).

Higher CIA values indicate stronger chemical weathering and more leaching of Na^+, K^+, and Ca^{2+} bound minerals from parent rocks relative to stable residual constituents (Al^{3+}, Ti^{4+}) during weathering. CIA optimum weathered value is 100, whereas the optimum fresh value is less or equal to 50 (Nesbitt and Young (1982). As weathering intensity increases, changes occur in the regolith's hydrological, geochemical, and geophysical characteristics (Wilford, 2012).

Chemical weathering of the floodplain sediments may significantly change the composition of river-borne particulate matter (Heller et al., 2001; Johnsson & Meade, 1990), causing enhanced CIA values. As weathering increases, clays such as illite and smectite change to more stable clays such as kaolinite. With extreme leaching, iron and silicon can be removed, leaving aluminum, which is immobile as aluminum hydroxide (gibbsite) residuum (Eggleton, 2001; Summerfield, 1991; Wilford, 2012).

Kaolinite is the dominant secondary mineral phase in highly weathered soils (Dixon & Weed, 1989; Tardy et al., 1973). It is a stable phyllosilicate species in extreme hydrolytic weathering environments (Meunier et al., 2013). It is often associated with goethite and/or hematite in lateritic crusts (Meunier et al., 2013; Tardy et al., 1973). Over long periods, the infiltrated acidic rainfall interacts with the alkaline minerals, leaching soluble and mobile components and re-precipitating less mobile minerals to form kaolinite and Fe-Al oxides (Chilton & Foster, 1995). In extreme cases, kaolinite dissolution occurs, leaving only quartz sand (Chilton & Foster, 1995).

3.3. Stable water isotopes

Environmental isotope hydrology allows the characterization of groundwater recharge processes, especially when hydrogeologic information is scarce (Sklash & Mwangi, 1991).

When examining atmospheric and hydrological science, ^{18}O for oxygen, corresponding to the most abundant isotope ^{16}O, and ^{2}H (Deuterium) for hydrogen, corresponding to the most abundant isotope ^{1}H, are the most relevant isotopes (Gat, 1971; Kazimierz et al., 2000). Accordingly, isotope ratios are defined as the ratio of the two most abundant isotopes, i.e., $^{18}O/^{16}O$ for oxygen and $^{2}H/^{1}H$ for hydrogen (Clark & Fritz, 1997).

The stable water isotopes ^{18}O and ^{2}H express the differences between the measured isotope ratios of the sample and an international standard reference called the Vienna Standard Mean Ocean Water (Eq. 3.12) (Clark & Fritz, 1997). Positive $\delta^{18}O$ and $\delta^{2}H$ values signify enrichment in

heavy isotopes of the sample compared to the standard, while negative values signify depletion (Clark & Fritz, 1997).

$$\delta^{18}O_{sample} = \left(\frac{\left(\frac{^{18}O}{^{16}O}\right)_{sample}}{\left(\frac{^{18}O}{^{16}O}\right)_{reference}} - 1 \right) \times 1000‰ \text{ VSMOW} \qquad \text{(Eq. 3.12)}$$

$\delta^{18}O$ and $\delta^{2}H$ of rainwater from sampling sites worldwide are correlated and described by the Global Meteoric Water Line (GMWL): $\delta^{2}H = 8 * \delta^{18}O + 10$ (Craig, 1961). In general, groundwater recharged at cooler and higher elevations is usually relatively depleted in ^{18}O and ^{2}H, whereas groundwater recharged at warmer and lower elevations is relatively enriched in ^{18}O and ^{2}H (Clark & Fritz, 1997; Sklash & Mwangi, 1991). This dependency produces seasonal variations of precipitation, where heavier isotope depletion occurs during winter precipitation compared to summer precipitation. Isotopes in precipitation are further influenced by the latitude effect, where high-latitude precipitation has been depleted more than low-latitude precipitation. The altitude effect is another influencer as the heavy isotope content of precipitation decreases with increasing altitude (Friedman et al., 1964; Moser & Stichler, 1970; Rozanski et al., 1993). Evaporation of water leads to an enrichment of heavy isotopes in the residual water, while the vapor becomes depleted (Clark & Fritz, 1997). Thus, the evaporated waters plot below the GMWL and have gradients below 8 (Moser, 1998).

Isotopic fractionation is a function of reaction progress, where the relative abundance of heavy isotopes is affected. It occurs because of different reasons that include biological activity and exchange with other materials (Dansgaard, 1964). However, preliminary indications of the water's origin and flow path can be provided from the natural abundance of stable heavy hydrogen (deuterium, ^{2}H) and oxygen-18 (^{18}O) isotopes.

In arid environments, groundwater is recharged most times from ephemeral streams; thus, groundwater will take on the evaporated signature rather than the precipitation signature. Craig (1961) noted that East African precipitation is already isotopically enriched, probably owing to evaporation of the precipitation as it falls through the dry atmosphere (Sklash & Mwangi, 1991). However, deep groundwaters are expected to retain much of the isotopic signature of precipitation unless the recharge from evaporation is the main contributor to the hydrological cycle (Gibson et al., 2008).

Groundwater recharge in arid environments, as suggested by Darling et al. (1987), can be through (1) direct recharge from rainfall, (2) recharge from surface runoff via ephemeral streams, (3) recharge from perennial streams, (4) lateral recharge from higher areas, (5) palaeo-recharge during more humid climatic times (Sklash & Mwangi, 1991).

Surface waters, such as almost stagnant rivers and lakes, undergo significant evaporation and develop ^{18}O and ^{2}H signatures that plot below the global meteoric water line (Sklash & Mwangi, 1991).

The local meteoric water line (LMWL) is used in various hydrological applications, commonly to determine the relationship of surface or groundwater to a potential precipitation source or to determine the degree of evaporative enrichment of the water (Clark & Fritz, 1997; Crawford et al., 2014). LMWLs in arid environments will exhibit the same slope of 8 but plot higher in

relation to d^2H because of increased evaporation (SAHRA, 2005). The LMWL is produced by fitting a linear regression to precipitation data.

3.4. Water quality in wetlands

Much research has been done on the purification functions of wetlands on industrial, municipal, and agricultural wastewaters (Hammer, 1989; Whigham et al., 1988). Wetlands have been widely used for water quality improvement, as they act as sinks for constituents or rather like short- and long-term storage systems that purify water (Hemond & Benoit, 1988; Maltby & Barker, 2009). Wetlands are mainly associated with the reduction of nutrient loads (Fisher & Acreman, 2004), specifically nitrate and phosphorus from surface water (Nahlik & Mitsch, 2006; Spieles & Mitsch, 2000). Wetland soils further serve as sink sources and transformers of nutrients and other chemical contaminants, enabling biogeochemical processes to occur, thus improving the water chemistry and ecosystem productivity (Hemond & Benoit, 1988; Mitsch & Gosselink, 2000; Reddy & DeLaune, 2008). High sedimentation rates, biodegradation of organic compounds, filtration, elemental cycling, atmospheric exchange, processing capacity, microbial interaction, plant nutrients' uptake, and reducing eutrophication in adjacent water bodies are further important processes being controlled by the unique conditions found in the wetland environment (Fisher & Acreman, 2004; Hemond & Benoit, 1988; Johnston, 1991; Reddy & DeLaune, 2008).

Wetlands maintain the widest range of oxidation-reductio reactions of any ecosystem on the landscape, allowing them to transform nutrients and metals (Guntenspergen et al., 2002). Flooding, lasting from several hours to a few days, is frequent in wetlands and results in isolation of the soil system from oxygen, thus activating biological and chemical processes and changing the system from aerobic and oxidizing to anaerobic and reducing (Guntenspergen et al., 2002; Mitsch & Gosselink, 2000). Accordingly, several elements become reduced with lower redox potentials.

As water quality deteriorated in streams, combined with the population increase and intensively farmed regions, interest in wetlands' functions as water purification increased. Accordingly, the restoration of wetlands and the creation of wetlands for water quality enhancement became popular, especially in intensively agriculturally used wetlands (Verhoeven et al., 2006). A lot of research and books (for example, Constructed Wetlands for Water Quality Improvements, 1993) exist on constructed wetlands, how they emulate and replicate the properties of natural wetlands in water purification, and their higher removal efficiencies of metals compared to natural wetlands (Mays & Edwards, 2001). Further research focuses on plants' ability to remove trace elements (Collins et al., 2004; Williams, 2002) and heavy metals (Du Laing et al., 2009; Sheoran & Sheoran, 2006) from wetlands.

Though often the positive aspects of water quality improvement are emphasized, research shows that the function of wetlands in water quality has counter functions (Fisher & Acreman, 2004). If the reduction of nitrate to N_2 is incomplete, N_2O (Machefert & Dise, 2004), a greenhouse gas, is produced, which might happen especially in conditions of low pH or soil moisture (Verhoeven et al., 2006).

Besides, wetlands that reduce nutrient loading may become degraded (Fisher & Acreman, 2004), and drastic changes to the ecosystem functions and biodiversity may occur if a certain nutrient inflow threshold is surpassed (Verhoeven et al., 2006).

Water quality in wetlands is additionally influenced by factors other than water purification, which include the type of soil, permeability of the soil, water quality of the inflow, position in the landscape, groundwater quality, and water and rock interactions (Hollands, 1987; Mitsch & Gosselink, 2000; Whigham et al., 1988).

Wetlands can remove various pollutants, including heavy metals, nutrients, and organic material (Greenway, 2005; Kadlec et al., 2008; Yeh, 2008). Furthermore, they can create reactive substances that chemically bind incoming pollutants. For example, sulfide formation in the wetland's anaerobic zones can precipitate divalent metal cations and drive autotrophic denitrification (Maltby & Barker, 2009).

The most important elements, their cycle, and their removal from the wetland are discussed below to assess the water purification functions in the wetland (Tab. 3.1).

Nitrogen is an essential nutrient for plants and animals. The N cycle in wetlands plays a significant role in the transport, storage, and biological availability of N in the surrounding watershed (DeBusk, 1999). The removal of particulates is through burial and settling, whereas that of the dissolved forms is through biogeochemical reactions (Reddy & DeLaune, 2008). In denitrification, the nitrate is converted to N_2O and then to N_2, which is emitted by the wetland (Hemond & Benoit, 1988; Verhoeven et al., 2006). Nitrogen transformation in wetlands is by microbially-mediated processes (Hammer, 1989) and at redox conditions below 250 mV (Mitsch & Gosselink, 2000) (Tab. 3.1). Nutrient uptake by the vegetation may be returned to the solution upon plant decomposition (Hemond & Benoit, 1988) unless harvesting happens, thus removing the nitrogen. Wetland sediments have a significant sorption capacity for ammonium nitrogen (Maltby & Barker, 2009). The basic nitrogen transformations in terrestrial, wetland and aquatic ecosystems are similar, yet the relative rates and storages differ in each of these ecosystems (Reddy & DeLaune, 2008).

Tab. 3.1: Oxidized and reduced forms of elements and their approximate redox potentials (Mitsch and Gosselink, 2007). The numbers are approximate because they are pH and temperature-dependent (Maltby & Barker, 2009)

Element	Oxidized form	Reduced form	Redox potential [mV]
Oxygen	O_2	H_2O	+400
Nitrogen	NO_3^-	N_2O, N_2, NH_4^+	+250
Manganese	Mn^{4+}	Mn^{2+}	+225
Iron	Fe^{3+}	Fe^{2+}	+100 -100
Sulphur	SO_4^{2-}	S^{2-}	-100 -200
Carbon	CO_2	CH_4	-200

Phosphorus is released into the environment mainly from the weathering of minerals and inputs from fertilizers. The phosphorus cycle is dynamic and involves interaction or exchange between biotic and abiotic pools. As wetlands are converted to agricultural use, their capacity to retain phosphorus decreases (Reddy & DeLaune, 2008). Phosphorous is removed from the system by sedimentation, soil adsorption, plant uptake, and microbial immobilization (Havens et al., 2004; Hogan et al., 2004; Uusi-Kämppä et al., 2000; Verhoeven et al., 2006). In P's retention,

the sediment's oxygen content is important to Al and Fe binding's capacity to P (Fisher & Acreman, 2004). This means that P can precipitate as iron-, aluminum- or calcium-phosphate (Hemond & Benoit, 1988). However, the solid Fe and Al compounds' stability is contingent upon the maintenance of high redox potential and high pH (Patrick & Khalid, 1974). Dissolved phosphate is adsorbed by hybrid iron- and aluminum-oxides or clays by ion exchange (Hemond & Benoit, 1988).

Sulfate is a common constituent of many wastewaters. It is highly reactive, redox-sensitive, and microbially active (Sturman et al., 2008), which governs its transformation processes within wetlands, and makes them interconnected to other products. Under oxidizing conditions, assimilatory SO_4^{2-} reduction, inorganic S^{2-} and S oxidation, and organic S's mineralization to inorganic SO_4^{2-} occurs. Assimilate sulfate reduction (SO_4^{2-}) is reduced by plants, fungi, and various prokaryotes to S^{2-}, which is needed for the biosynthesis of sulfur-containing amino acids (Schiff & Fankhauser, 1981). This can happen under aerobic and anaerobic conditions. Evidence shows that iron minerals and redox-active organic matter play a role in sulfide oxidation to elemental sulfur or thiosulfate (Pester et al., 2012). The recycling of reduced sulfur compounds to sulfate is the main mechanism of sulfate reduction in wetlands (Wieder & Lang, 1988). The dissimilatory reduction on SO_4^{2-} requires conditions with redox potentials below -100 mV (Mitsch & Gosselink, 2000). It occurs mainly in the reduced lower soil horizons and in saturated, flooded subsoils (Faulkner & Richardson, 1989). However, redox conditions of wetlands' soils vary from aerobic to anaerobic (Faulkner & Richardson, 1989). It can also be stored in the wetland soil matrix and then oxidized to sulfate or sulfide. Furthermore, the identity of the SO_4^{2-} reducing bacteria in wetlands is largely unknown (Pester et al., 2012). Wetlands can function as sulfate sinks, as the sulfate reduction process occurs over long periods (Pester et al., 2012).

Iron and **manganese** are two essential trace elements for living organisms and are key elements involved in oxidation-reduction reactions in soils (Reddy & DeLaune, 2008). Under oxidizing conditions, the dissolved iron and manganese precipitate as iron and manganese hydroxide (Appelo & Postma, 2005), and under reducing conditions, they will precipitate or become a major process for organic matter decomposition by microorganisms. Ferrous iron is far less soluble than Mn^{2+} and forms insoluble phases such as pyrite or siderite and iron monosulfides (Burdige, 1993). The biogeochemistry of iron and manganese is complex but similar and is regulated by various biotic and abiotic processes (Reddy & DeLaune, 2008). As aeration is not sufficient for Mn-reoxidation in confined aquifers, Mn remains reduced and migrates to wells (Gounot, 1994). On the other hand, wetland water is aerated, and aerobic bacteria may precipitate and oxidize soluble Mn^{2+} (Gounot, 1994). High concentrations of dissolved Fe^{2+} and Mn^{4+} are common features of aquifers contaminated with organic compounds (Gounot, 1994; Lovley, 1991).

Heavy metals

In a wetland, heavy metals are accumulated and uptaken directly by the aquatic macrophytes and plants (Khan et al., 2009). The rhizosphere is of high importance as well. Wetlands act as sinks by adsorption on organic matter and sorption of heavy metals (Hemond & Benoit, 1988), and the biogeochemical cycling provides storage and conversions for heavy metals (Yeh, 2008). Furthermore, wetlands soil, with its high organic content and reduced conditions, accumulates heavy metals (Yeh, 2008). Metal retention processes also happen in wetland soils and include

cation exchange, complex building with organics, and precipitation as oxides, carbonates, and sulfides. Mechanisms that are active in wetlands include sedimentation, filtration, chemical precipitation, adsorption, and microbial interactions (Yeh, 2008). Wetland plant species differ in their abilities to accumulate and translocate metals (Yeh, 2008). Numerous factors affect the remediation processes of the contaminated sites, including the physiochemical water and sediment parameters (e.g., pH), uptake from the soil, sequestration within the root, plant growing, transpiration rates (Khan et al., 2009), the inflow water quality, the metal removal mechanism, speciation of inflow metals, and the type of wetland system (Yeh, 2008). For example, higher pH values and oxidizing conditions increase the sorption of heavy metals (Hemond & Benoit, 1988). In constructed wetlands, heavy metal removal is done through physicochemical treatment technologies such as ion exchange, precipitation, and electrochemical and membrane processes (Khan et al., 2009).

3.5. Hydrochemical and isotopes modeling using Mixing Cell Model (MCM)

3.5.1. Introduction to MCM

Flow and transport models describe the physical groundwater-streamflow interaction processes observed in many hydrological basins worldwide and are all based on the flow and transport equations. Examples of widely used flow and transport models include MODFLOW-SURFACT, SWAP, and HYDRUS. Analytical solutions are available only for straightforward flow patterns, while, for most cases, the only solution method relies on a finite difference or a finite element numerical solution (Bear & Verruijt, 1987; Pinder & Gray, 1977). For the latter, basic hydrological information, such as piezometric levels, fluxes across the boundaries, or precise hydraulic heads over the boundaries, must be determined. The process of infiltration and percolation through heterogeneous anisotropic formations is a complex physical phenomenon. It is even more so when studying the transport of organic pollutants. Chemical evolution across the vadose zone involves either aerobic or anaerobic biodegradation processes, which are difficult to assess in a quantitative manner. Neither analytical nor numerical modeling of such processes is easy due to the scarcity of hydrological, geological, and hydrochemical information. In such situations where it is impossible to implement any of the conventional flow and transport modeling methods for basins, the Mixing Cell Model (MCM) approach (Adar & Long, 1987; Adar, 1995; Adar et al., 1988; Adar & Neuman, 1988) is used. Hydrochemical data and stable water isotopes are used accordingly to account for the abovementioned hydrological deficiencies. The MCM has been applied in several hydrological basins worldwide, from the Kalahari Desert (Namibia), Jezreel, Bessor basins (Israel), Arava Basin (Jordan-Israel) to the Ili basin in Kazakhstan (Margolis & Chaouni, 2014).

3.5.1.1. MCM theoretical explanation

The Mixing Cell Model for Steady Flow system (MCMsf) has been developed specifically for basins with complex hydrogeological structures where information about environmental hydrochemistry and the stable distribution of stable isotopes is more easily accessible than information about the aquifer's physical hydrological parameters (Adar & Long, 1987; Adar, 1995; Adar et al., 1988; Adar & Neuman, 1988).

3.5.1.2. Mathematical description of the MCM for steady-state flow system

The aquifer is divided into n discrete cells. A set of balance equations for the water flux and the associated flux solute flux is written for each n cell over a given time period dt (Adar & Massoth, 2017; Adar & Sorek, 1990).

The mass balance for cell n for a simplified flow model of water with a constant density is calculated (Eq. 3.13). Q_{rn} denotes R different unknown sources into cell n and q_{in} denotes the unknown flux (average volumetric flow rate) from the ith upstream compartment or cell into the nth cell. Q_{nj} stands for the outflow from the nth cell into the jth cell. W_n accounts for the withdrawal of water from cell n, i.e., pumping. S_n represents the storage capacity within cell n, and h_n denotes the hydraulic head within cell n during dt. The inflows and outflows from different sources are iterated over the number of inflows, I, and the number of outflows, J, into each cell (Adar & Massoth, 2017; Adar & Sorek, 1990).

$$\sum_{r=1}^{R_n} Q_{rn} + \sum_{i=1}^{I_n} q_{in} - \sum_{j=1}^{J_n} q_{nj} - W_n = S_n \frac{dh_n}{dt} \qquad \text{(Eq. 3.13)}$$

For a steady flow system or for quasi-steady flow (Eq. 3.14) over a sufficiently long time interval, an average water balance expression is obtained. The top bars (Eq. 3.14) above each term represent the average flux for the specific time interval.
ε_n is the error term and accounts for errors with the measurements or assessment of the flow and deviations from the flux balance in cell n (Adar et al., 1988).

$$\sum_{r=1}^{R_n} \overline{Q}_{rn} + \sum_{i=1}^{I_n} \overline{q}_{in} - \sum_{j=1}^{J_n} \overline{q}_{nj} - \overline{W}_n = \varepsilon_n \qquad \text{(Eq. 3.14)}$$

Due to the assumption of complete mixing within each cell, the mixing cell concept is applied, for a quasi-steady state variation of the dissolved constituents, based on mass balance expressions for each tracer k (k=1,2,…,K) in cell n (Eq. 3.15) (Adar & Neuman, 1988).

$$\sum_{r=1}^{R} \overline{C_{rk} Q_{rn}} + \sum_{i=1}^{I} \overline{C}_{ink}\, \overline{q_{in}} - \overline{C}_{nk} \left[\sum_{j=1}^{J} \overline{q}_{nj} + \overline{W}_n \right] = \varepsilon_{nk} \qquad \text{(Eq. 3.15)}$$

$\overline{C_{rk} Q_{rn}}$ denotes the average flux of the k^{th} constituent from source r into cell n. $\overline{q_{in}}$ represents the average flux from the i^{th} cell into the n^{th} cell, having an average concentration $\overline{C_{ink}}$ of solute k. $\overline{C_{nk}}$ denotes the concentration of the k^{th} constituent within cell n, and $\overline{q_{nj}}$ stands for the average outflow from the n^{th} cell into the j^{th} one. The average pumping from the n^{th} cell during a specific time interval

is expressed by $\overline{W}_n$, and ε_{nk} is the error associated with the mass balance of the k^{th} constituent or the deviation from the solute balance in cell n.

For every cell n, there are $K+1$ equations: one for the water balance and K more for every k species (k= 1,2,.....,K) (Eq. 3.16).

$$
\begin{aligned}
&\sum_{r=1}^{R_n}\overline{Q}_{rn} + \sum_{i=1}^{I_n}\overline{q}_{in} - \sum_{j=1}^{J_n}\overline{q}_{nj} - \overline{W}_n = \varepsilon_n \\
&\sum_{r=1}^{R}\overline{C_{rk_1}Q_{rn}} + \sum_{i=1}^{I}\overline{C}_{ink_1}\,\overline{q_{in}} - \overline{C}_{nk_1}\left[\sum_{j=1}^{J}\overline{q}_{nj} + \overline{W}_n\right] = \varepsilon_{nk_1} \\
&\sum_{r=1}^{R}\overline{C_{rk_2}Q_{rn}} + \sum_{i=1}^{I}\overline{C}_{ink_2}\,\overline{q_{in}} - \overline{C}_{nk_2}\left[\sum_{j=1}^{J}\overline{q}_{nj} + \overline{W}_n\right] = \varepsilon_{nk_2} \\
&\sum_{r=1}^{R}\overline{C_{rk_3}Q_{rn}} + \sum_{i=1}^{I}\overline{C}_{ink_3}\,\overline{q_{in}} - \overline{C}_{nk_3}\left[\sum_{j=1}^{J}\overline{q}_{nj} + \overline{W}_n\right] = \varepsilon_{nk_3} \\
&\quad\vdots \qquad\qquad \vdots \qquad\qquad \vdots \qquad\quad \vdots \\
&\sum_{r=1}^{R}\overline{C_{rK}Q_{rn}} + \sum_{i=1}^{I}\overline{C}_{inK}\,\overline{q_{in}} - \overline{C}_{nK}\left[\sum_{j=1}^{J}\overline{q}_{nj} + \overline{W}_n\right] = \varepsilon_{nK}
\end{aligned}
\qquad \text{(Eq. 3.16)}
$$

Equations (3.13) and (3.14) are combined into a matrix form for each cell *n* (Eq. 3.17).

$$\underline{\underline{C}}_n \underline{X}_n + \underline{P}_n = \underline{E}_n \qquad \text{(Eq. 3.17)}$$

X_n is a vector of unknowns (Adar et al., 1988). $\underline{\underline{C}}_n$ (3.18) is a matrix with known concentrations in cell *n*, having $k+1$ rows (for *k* species and one water balance equation) and as many columns as there are unknown X terms (Adar et al., 1988), presented in Equations (3.19), (3.20) and (3.21), respectively (Adar & Sorek, 1989). P_n is a vector of known terms that are measured and known quantitavily of the length $k+1$. E_n is an unknown vector of error having a similar length.

$$\underline{\underline{C}}_n = \begin{bmatrix}
1, & 1, & \Lambda, 1, & 1, & 1, & \Lambda, 1, & -1, & \Lambda, -1 \\
\overline{C}_{r_1nk_1}, & \overline{C}_{r_2nk_1}, & \Lambda, \overline{C}_{Rnk_1}, & \overline{C}_{i_1nk_1}, & \overline{C}_{i_2nk_1}, & \Lambda, \overline{C}_{Ink_1}, & -\overline{C}_{nk_1}, & \Lambda, -\overline{C}_{nk_1} \\
\overline{C}_{r_1nk_2}, & \overline{C}_{r_2nk_2}, & \Lambda, \overline{C}_{Rnk_2}, & \overline{C}_{i_1nk_2}, & \overline{C}_{i_2nk_2}, & \Lambda, \overline{C}_{Ink_2}, & -\overline{C}_{nk_2}, & \Lambda, -\overline{C}_{nk_2} \\
\mathrm{M} & \mathrm{M} & \mathrm{M} & \mathrm{M} & \mathrm{M} & \mathrm{M} & \mathrm{M} & \mathrm{M} \\
\overline{C}_{r_1nK}, & \overline{C}_{r_2nK}, & \Lambda, \overline{C}_{RnK}, & \overline{C}_{i_1nK}, & \overline{C}_{i_2nK}, & \Lambda, \overline{C}_{InK}, & -\overline{C}_{nK}, & \Lambda, -\overline{C}_{nK}
\end{bmatrix}_{[(K+1)\bullet(R_n+I_n+J_n)]} \qquad \text{(Eq. 3.18)}$$

$$\underline{X}_n = \begin{bmatrix}
\overline{Q}_{r_1} \\ \overline{Q}_{r_2} \\ \mathrm{M} \\ \overline{Q}_{R_n} \\ \overline{q}_{i_1} \\ \overline{q}_{i_2} \\ \mathrm{M} \\ \overline{q}_{I_n} \\ \overline{q}_{nj_1} \\ \overline{q}_{nj_2} \\ \mathrm{M} \\ q_{nJ_n}
\end{bmatrix}_{[(R_n+I_n+J_n)\bullet 1]} \qquad \text{(Eq. 3.19)}$$

$$P_n = \begin{bmatrix} \overline{W}_n \\ \overline{C}_{nk_1}\overline{W}_n \\ \overline{C}_{nk_2}\overline{W}_n \\ \overline{C}_{nk_3}\overline{W}_n \\ \mathrm{M} \\ \overline{C}_{nK}\overline{W}_n \end{bmatrix}_{[(K+1)\bullet 1]} \qquad \text{(Eq. 3.20)}$$

$$\underline{E_n} = \begin{Vmatrix} \varepsilon_n \\ \varepsilon_{nk_1} \\ \varepsilon_{nk_2} \\ \varepsilon_{nk_3} \\ \mathrm{M} \\ \varepsilon_{nK} \end{Vmatrix}_{[(K+1)\bullet 1]} \qquad \text{(Eq. 3.21)}$$

Based on Equation (Eq. 3.17) and by assembling the square error terms over all cells, a quadratic objective function is obtained (Eq. 3.22).

$$J = \sum_{n=1}^{N} \left[\underline{E}^T \underline{\underline{\Phi}} \underline{E}_n\right] = \sum_{n=1}^{N} \left[(\underline{\underline{C}}_n \underline{X}_n + \underline{P_n})\Phi(\underline{\underline{C}}_n \underline{X}_n + \underline{P_n})\right] \qquad \text{(Eq. 3.22)}$$

^{T} denotes transpose and $\underline{\underline{\Phi}}$ represents a diagonal matrix comprised of weighting values associated with expected estimated errors (independent of each other) for each of the terms building the mass balance for the fluid and the constituents (Adar & Neumann, 1986; Adar & Sorek, 1989). These compose the mass balance for the fluid and the dissolved constituents. With a quadratic objective function, only positive values will be assigned for the calculated fluxes for the unknown flow components. The weighting matrix $\underline{\underline{\Phi}}$ also reflects the degree of confidence to which the tracers are assumed conservative and/or the degree of accuracy of the chemical and isotope analyses (Adar & Neumann, 1986; Adar & Sorek, 1990).

All identified flux components in the aquifer are then estimated by minimizing the sum of square errors, J using the simplex method with the Wolf Mathematical Algorithm (Wolf, 1967). As a result of the mathematical optimization, a flow rate is attributed to each active flow component. Depending on the results obtained from the mathematical optimization, the flow model might be changed by a modification of the proposed flow pattern and the potential sources (Adar & Massoth, 2017; Adar & Sorek, 1990).

3.5.1.3. The MCM concept

The MCMsf enables the calculation of groundwater fluxes in a complex, steady, hydrogeological system in which the piezometric heads and the spatial distribution of dissolved minerals do not vary with time (Adar & Massoth, 2017). In a complex hydrogeological system, the precise locations of boundaries and hydrological conditions along the boundaries are not sufficiently clear or distinct, and there is a lack of hydrogeological and hydrochemical information (Adar,

1995, 1996; Adar et al., 1992). Thus, it is difficult to construct, solve, and calibrate a hydrological model based on the continuity approach. Therefore, the algorithm proposed in this study is based on a more simplistic approach. The flow domain is subdivided into pseudo-homogeneous flow cells forming a multi-compartmental flow model (Adar & Massoth, 2017). The creation of the multi-compartmental structure is based on the spatial and temporal distributions of dissolved ions and isotopes in a transient hydrological system (Adar & Neuman, 1988).

The MCMsf software is associated with the development of a numerical model for a steady-flow hydrological system. The model relies on the so-called mixing cell or compartmental approach that utilizes environmental tracers, hydrochemistry, and environmental isotopes, to elaborate and quantify groundwater fluxes in complex basins with obscured hydrological information (Adar & Sorek, 1989; Adar et al., 1988). The concept is based on the incorporation of environmental isotopes and hydrochemistry in a numerical algorithm of a steady hydrological scheme to solve for groundwater fluxes and assess the sources of groundwater recharge (Adar & Neuman, 1988). The model is aimed at hydrological basins with vague hydrogeological systems where common numerical models cannot be adopted due to a lack of essential data, such as the location and hydrological properties along the boundaries (Adar, 1995; Adar et al., 1988). Spatial variations in hydraulic heads and the hydrochemistry of groundwater are used to assemble a set of water and mass balance equations in which fluxes, groundwater storage, and the saturated volume of the compartment are the unknowns (Adar & Neuman, 1988).

Similar to other models, the MCM is based on assumptions. The basic assumptions for the MCM are after Adar et al. (1992):

1. The spatial structure, geometry, size, and volume of cells remain constant throughout the entire duration of the model run.
2. The isotopes and the dissolved minerals are inert and do not undertake any chemical reactions within the aquifer.
3. The dissolved ions are in pseudo-equilibrium with the rocks and soil minerals. All potential unknown fluxes (groundwater fluxes between compartments of the system and discharge of external contributors to the compartments) have been identified in terms of their hydrochemical and isotopic compositions.
4. Spatial variations in chemical and isotopic compositions within the aquifer are exclusively due to a) variable mixing ratios among the recharge components and b) dilution and mixing along the groundwater flow paths.
5. There is a complete mixing of all dissolved constituents within the designated cells.
6. No gradients of hydraulic heads or isotopic or chemical compositions are allowed within the cells, only across the cell's boundaries.

The solver for the MCMsf model is based on a quadratic optimization scheme of water balance and mass balance expressions of each parameter (Adar, 1996; Adar & Neuman, 1988; Adar et al., 1992). It is solved with the Wolf algorithm, which is based on the simplex optimization method. The MCM illuminates the active pollution sources and quantifies the relative flux of water from each source, replenishing the water body aquifer (Adar & Sorek, 1989).

3.5.2. MCM technical explanation

The modeled flow system is discretized or subdivided into homogenous compartments within which all the considered parameters (e.g., hydraulic heads, isotopic compositions, and ionic concentrations) are assumed to be constant for a specific time period (Adar and Massoth, 2017). Mixing of various sources or contributors, such as from upstream compartments and external sources, and dilution with water already existing in the cell controls the concentration of the characteristic parameter of each compartment. Therefore, every well-mixed or homogenous aquifer section referred to as a cell or compartment is characterized by a unique representative chemical parameter (Adar & Massoth, 2017).

A cell must have input fluxes, either from output flux from one source or from several sources. Each cell must have an output flux, either into a downstream cell or cells or via withdrawal of water (e.g., pumping or springs, or evapotranspiration). Every cell can have several sources and contribute water as output flux to several downward cells (Adar & Massoth, 2017) (Fig. 3.5).

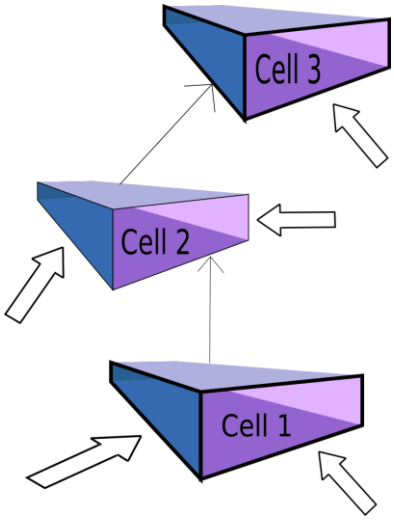

Fig. 3.5: A schematic flow pattern of MCM with three cells, with various input fluxes (open arrows) and one output flow from one cell into the next cell.

4. Data and Methods

As the area is scarce in data, a comprehensive interdisciplinary approach (Fig. 4.1) to understand the aquifer‘s structure, the water dynamics, and the water composition, and to model the wetland was developed.

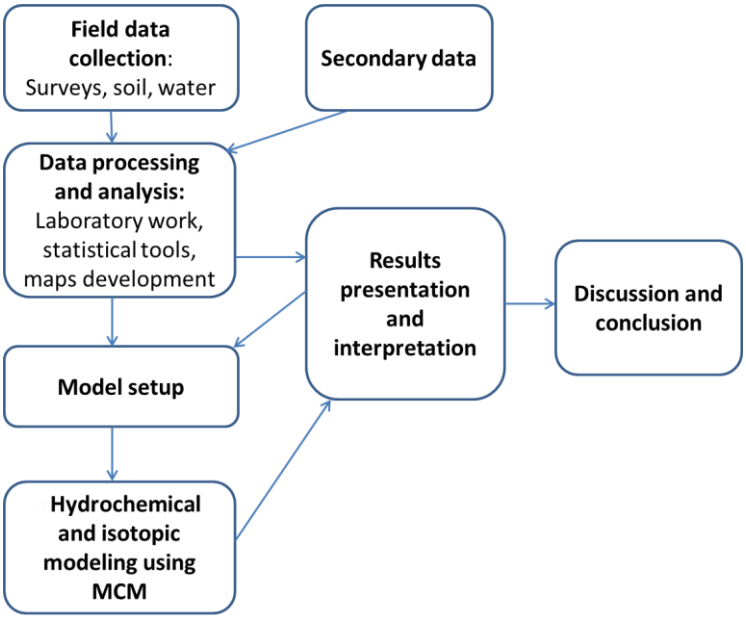

Fig. 4.1: Flowchart of the overall conducted approach

This integrated approach using water level measurements, hydrogeological and hydrochemical data, water isotopes, in addition to numerical modeling, leads to the optimum use of these techniques and a logical interpretation. This is discussed in detail in this chapter. The chapter is divided into surveys, analysis of aquifer structure and properties, water dynamics, water composition, statistical analysis, hydrochemical and isotopic modeling, and the database for Ewaso Narok.

The sampled points were registered using **GPS Venturex (GARMIN)**. The determination of the geographic coordinates is based on the reference system WGS 84. Maps were developed with the software **Quantum GIS version (QGIS-Dufour).**

4.1. Surveys

In the Ewaso Narok floodplain, a survey addressing 114 people about the wetland use, what is disposed of in it, and the access to groundwater was done in July and August 2016. Furthermore, the change in people’s behaviour with floods was understood. These people belonged to one of the following groups: Farmers, pastoralists, agropastoralists, shop owners, and business owners in Rumuruti town and the catchment area. The questions were asked in both English and Swahili, and an interpreter was present to translate. The interviewed people refused to sign or allow fingerprints as they requested payment in exchange. However, general consent for questioning and reading the ethical form was accepted.

The survey was intended to better identify the wetland’s resource use (surface water and groundwater), the policies regarding its use, the inlet of fertilizers, sewage, and their type. It

further provided potential points of pollution input into the wetland for sampling and then modeling of Ewaso Narok.

More particularly, the questions were:

- What do you use the wetland for (washing, cars, cattle, agriculture, drinking)?
- What do you dispose of in the wetland (fertilizers/ sewage or cleaning material)/ their composition and temporal and spatial distribution of these activities)? What are the alternatives?
- Where are the inlet points?
- Do you have access to the groundwater? Wells?
- Do you dispose of anything directly in the groundwater/ wells?
- Do you plant inside the wetland? Or around it?
- What kinds of fertilizers are applied? Where do you dispose of the fertilizer cans?
- What kind of sewage is flowing into the wetland? Is there any other kind of waste disposal?
- Do your activities change with floods? If yes, how?
- Are floods good or bad? Is the water cleaner or dirtier?

The survey results were exported, and some statistical analyses, and graphs, were used to demonstrate the results.

Raw data collected by Kyalo Willy, 2015 (direct contact Kyalo) as part of the GlobE study, where 350 households were surveyed in 2015, was used as secondary data. Some questions were not answered, making the sample number smaller, and are indicated in the results.

4.2. Analysis of aquifer structure and properties

Chemical, mineralogical, and lithological data about the aquifer is of great help during the interpretation of groundwater quality data (Kovalevsky et al., 2004).

4.2.1. In-situ soil and rock sampling

Soil samples are taken at different points and depths using a 2m length soil hand auger. Different soil types were recognized as they were used for various purposes, and accordingly, a sample was selected from them. More soil was collected but not analyzed. The purpose was to see the consistency and make-up of the soil and measure the water table's depth. The soil samples were transferred to the laboratory of the Institute of Geoscience in Bonn to be analyzed.

4.2.2. Geological records – geometrical parameters of the aquifer

The geometrical parameters are derived from the study of the area's geology and borehole drilling reports collected from private owners in the field. At times there is a mention of a well and its distance from a source, then it is drawn and combined with other reports trying to conclude the name and information. In addition, WRMA provided some quality data information and the names of wells. Other sources were the Republic of Kenya (1987), chemical data collected by WRAP, and water quality provided by wells owners from privately paid quality checks.

Field observations were used to add on and improve the existing collected geological records. Digital maps were developed that correspond with the lithology and geological drillings.

4.3. Mineralogical and geochemical analysis of soil and rocks

Representative soil samples were weighed and afterward dried in an oven at 105 °C for 24 hours and again weighed to calculate the water content. The soil samples were crushed into small pieces using a mallet hammer to become fine and homogenous. Afterward, the samples were ground using a vibratory disk mill (T250 Siebtechnik GmbH) and filled in bottles for the following investigations (Fig. 4.2).

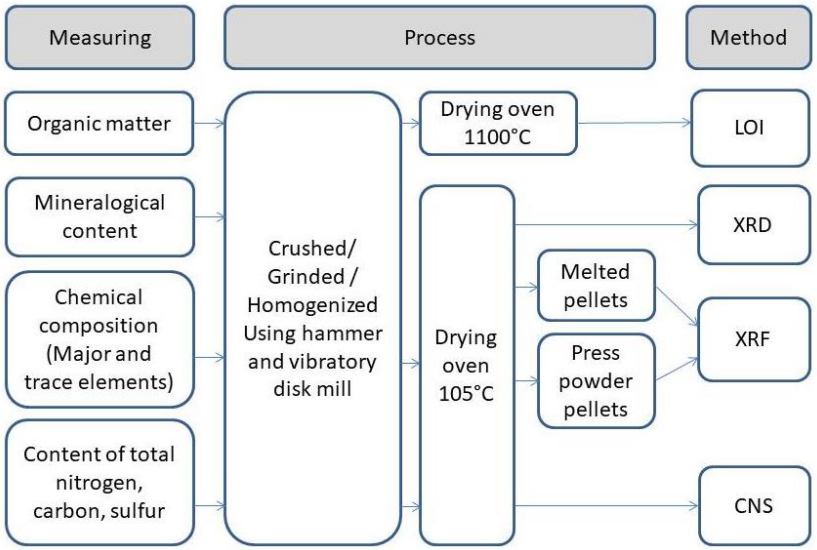

Fig. 4.2: Flowchart of different preparation steps of mineralogical and geochemical analyzes.

The **Loss on Ignition** (LOI) (Eq. 4.1) was used to determine the organic matter content by comparing the weight of a sample before and after the soil had been ignited. The LOI further determines the captured water, Cl, CO_2, F, and S (Heiri et al., 2001) and is measured to calculate the **total inorganic carbon** (TIC). The measurement was calculated in double determination, where a 5 mg sample was ignited for 2 hours at 1100°C. The **organic matter (OM)** is then calculated (Eq. 4.2).

$$\mathrm{LOI}\ (\%) = \frac{(m_{\mathrm{Sample+crucible}} - m_{\mathrm{Sample+crucible\ after\ annealing}})}{m_{\mathrm{Sample+crucible}} - m_{\mathrm{crucible}}} * 100 \qquad \text{(Eq. 4.1)}$$

$$\mathrm{OM}\ (\%) = \frac{(m_{\mathrm{Pre-ignition}} - m_{\mathrm{Post-ignition}})}{m_{\mathrm{Pre-ignition}}} * 100 \qquad \text{(Eq. 4.2)}$$

Carbon, nitrogen, sulfur (CNS) analysis is then performed in double determination. The soil samples were analyzed for the CNS to exclude geogenic nitrogen sources. For the CNS measurements, samples are dried at 105 °C. 20 mg of tungsten oxide (WO_3) and 20 mg of each sample are weighed in tin silver boats. The boats are folded tightly to avoid the material drop and ensure proper functioning of the ball valve. Then total carbon (TC), Total nitrogen (TN), and total sulfur (TS) are measured and assessed using Vario El cube from the company “Elementar Analysensysteme GmbH”. This method is based on a purge and trap principle.

To measure the **total organic carbon** (TOC), the indirect Muffle-Furnace method is used. The samples are first dried at 105 °C. The samples are then annealed at 450 °C for 16 hours. Accordingly, the organic substance in the sample is thermally decomposed, but carbonates remain in the sample.

Finally, TOC (Eq. 4.3) is determined as follows:

$$\mathrm{TC} - \mathrm{TIC} = \mathrm{TOC} \qquad \text{(Eq. 4.3)}$$

The samples were then analyzed for their mineralogical and chemical compositions using X-Ray Diffraction Analysis (XRD) and X-Ray Fluorescence Analysis (XRF). Samples are dried for 24 hours at 105 °C as the first preparation for both methods.

XRF is measured using PANalytical Axios 3KW. This method is quantitative and analyzes the amount of major and trace elements of a bulk sample (in mg/kg). Press powder pellets with a ratio of 5.0 g sample and 1.0 g $C_{38}H_{76}N_2O_2$ (wax) were used to identify trace element concentrations. The limits of detection are 100 ppm for Na, Mg, Al, Si, and P, 10 ppm for S, K, Ca, Ti, Mn, Fe, and Cl, and 1 ppm for Sc, V, Cr, Co, Ni, Cu, Zn, Ga, Ge, As, Rb, and Sr (Hahn-Weinheimer et al., 1995).

XRF results, in addition to LOI, CNS, and TOC data, are used to decide which samples can be used to produce melt tabs to avoid destroying platinum crucibles upon melting. Melted pellets were prepared to measure major oxide concentrations. These pellets have a portion of 0.4 g sample and 4.0 g of $Li_2B_4O_7$ (spectroflux). For some of the main elements, melt tabs were not used, and instead, they were measured by the program IQ+, which identifies the elements in the rock/soil samples. If it is not possible to produce a melt tab of a sample, the major elements were determined by the press powder Tab. However, these results are not as reliable as the data of the melted pellets.

XRD was carried out using a Bruker AXS D8 Advance device. The minerals are identified by their atomic and molecular structure. As some minerals show similar structures and, therefore, highly similar diffraction patterns, they are identified in minerals groups (e.g., micas, plagioclases, and k-feldspars) (Cook et al., 1975). The evaluations of the diffractograms are processed using the software MacDIFF 4.2.5. Each mineral has its distinct characteristic spectrum of interferences with specific peak intensity and angular range of 2θ (Moore & Reynolds, 1997). The method used is qualitative, and the range of 2θ angle is used for identification. To avoid quartz's overestimation, the 20 % quartz peak (20.88 θ) is multiplied by 5. Factorization of the results is done according to Cook (1975). With the background noise, peaks above 100 count were only identified with a mineral characteristic's peak. The clay minerals are listed together. Quantification is done with the Rietveld method (Program Profex 3.14.0).

4.3.1. Evaluation tests for soil and rocks

The chemical index of alteration (CIA) (Nesbitt & Young, 1982) is used as a quantitative indicator to estimate the degree of silicate weathering using molecular proportions (Eq. 4.4). According to McLennan (1993), CaO*, which represents Ca^{2+} in the silicate fraction, can be estimated assuming reasonable Ca^{2+}/Na^{+} ratios in silicate material. If the CaO molar content is less than that of Na_2O, the measured CaO content equals CaO*; if the CaO molar content is greater than that of Na_2O, CaO* it is assumed to be equivalent to Na_2O (McLennan, 1993).

$$\mathrm{CIA} = \frac{\mathrm{Al_2O_3}}{\mathrm{Al_2O_3(Al_2O_3 + CaO^* + Na_2O + K_2O)}} \times 100 \qquad \text{(Eq. 4.4)}$$

To determine the origin of the soil and rock samples, the volcanic rocks' geochemical characteristics were made using the total alkali-silica (TAS) diagram (Bas et al., 1986). The classification requires the values of $Na_2O + K_2O$ and SiO_2, and if the analysis fell in certain fields, additional calculations such as Cross, Iddings, Pirsson, and Washington (CIPW) norms were performed (Bas et al., 1986; Maitre et al., 2002). Care has to be taken when classifying rocks that are weathered and altered (Sabine et al., 1986). The results provided the root name for the different classifications, as will be seen in section 6.2.2.

4.3.2. Water dynamics

4.3.2.1. Installation of piezometers and calculation of water flow direction

According to EPA (2008), multiple piezometers can be placed at different depths at each location to evaluate the magnitude of vertical flow. Ten piezometers (twenty pairs) were installed in the field (Fig. 4.3). Each pair was installed following the directions of (Sprecher, 2008; WRAP, 2000) (App. 5), one of a length longer and one of a shorter length (e.g., 215 cm and 87 cm) using PVC pipes and a hand auger. The bentonite prevents the infiltration of surface or precipitation water along the pipes and hydraulic connections between different aquifers. Both pipes were 34 cm above the ground. They were left for two days, and then the water level in both rose and was measured.

Fig. 4.3: Piezometers installed in the field.

The piezometers were left covered, and the water level was measured and recorded after a day and again after a week. The piezometers were used to assist in determining the water flow in the area (Fig. 4.4).

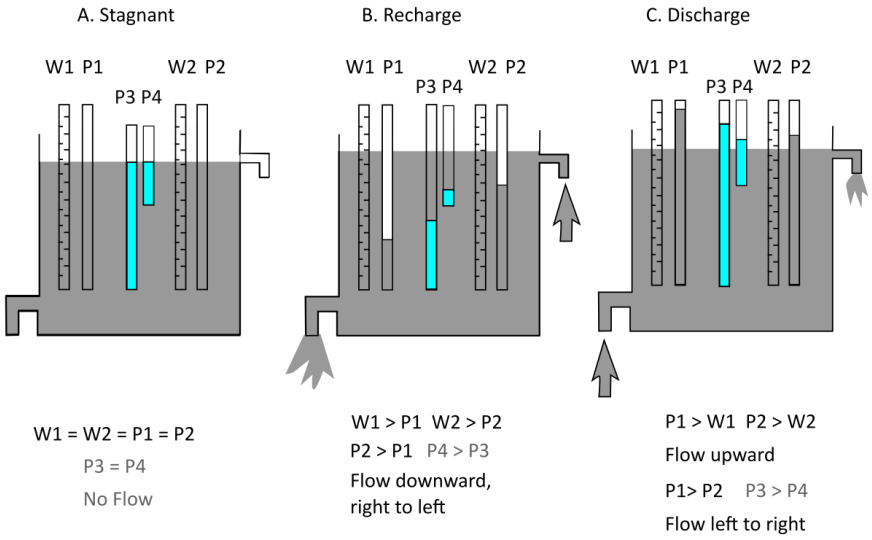

Fig. 4.4: Determining water flow from the installation of two piezometers, modified after Sprecher (2008). P stands for piezometer and W for water level. A. stagnant, no flow. B. Recharge, flow downward from right to left. C. Discharge, flow upward from left to right.

4.3.2.2. Creation of piezometric maps

Piezometric maps were created based on groundwater level measurements to know the groundwater flow direction. Hydraulic heads (piezometric levels) were calculated by subtracting the measured groundwater levels below the surface from elevation values derived from digital elevation models (DEMs). The maps generated show isolines of hydraulic heads above sea level reference level.

Water table levels were measured for the period of June 2015 and January 2016 by Muriuki Karugi (2016). Further groundwater level measurements were collected from WRMA and the installed piezometers. Additionally, secondary data on water levels are used as supplementary data and are taken from borehole records. This might lead to error as the span of data collected is over a long period of years (Allen et al., 1989).

4.4. Water composition

The chemical components' overall distribution provides information about the current flow processes and the long-term conditions in the aquifer system (Kovalevsky et al., 2004).

4.4.1. In-situ water measurements and sampling

Water samples were taken for surface water from the wetland and its ephemeral streams. Throughout the sampling, flash floods occurred, and thus some samples were before it, through it, and after it. In regards to groundwater, piezometers were installed, deep wells were accessed, shallow wells, and one spring. The groundwater samples were pumped (Tauchpumpe ECO-PLUS 12V) (Fig. 4.5). Measurement and sampling took place after a sufficient time (pumping threefold the volume of the well) to ensure fresh groundwater.

Fig. 4.5: Sampling of groundwater from wells and piezometers with a hand pump linked with a battery.

In addition to recording the name of the sampling place, its coordinates, and elevation, in-situ measurements of water using multi-meter (WTW Multi 342) were made for: specific electrical conductivity (EC), the temperature of water (T_w), and air (T_a), pH value, redox potential (Eh), and dissolved oxygen (DO). The sampled points were registered using GPS Venturex (GARMIN).

According to TrinkwV 2011 (Borchers, 2013), titration was conducted directly in the sampling location with hydrochloric acid (HCl) to reach a pH of 4.3, and with sodium hydroxide solution (NaOH) to reach a pH of 8.2. Assuming a pH value between 4.3 and 8.2, concentrations of bicarbonate (HCO_3^-) and carbon dioxide (CO_2) were calculated (Eq. 4.5 and Eq. 4.6) (Hütter, 1994):

$$c_{HCO_3^-} = V * c * f * M_{HCO_3^-} \quad \text{(Eq. 4.5)}$$

C_{HCO3}^-	Concentration of HCO_3^- [mg/l]
V	Volumetric amount of acid used to reach pH of 4.3 [ml]
c	HCl concentration [0.02 mol/l]
f	Conversion factor (for 100 ml sample f= 10) [10 mmol/mol mL]
M_{HCO3}^-	Molar mass of HCO_3^- [61.02 g/mol]

$$c_{CO_2} = V * c * f * M_{CO_2} \quad \text{(Eq. 4.6)}$$

C_{CO2}	Concentration of CO_2 [mg/l]
V	Volumetric amount of base used to reach pH of 8.2 [ml]
c	NaOH concentration [0.02 mol/l]
f	Conversion factor (for 100 ml sample f= 10) [10 mmol/mol mL]
C_{CO2}	Molar mass of CO_2 [44.01 g/mol]

On-site water samples were filtered using filters with a pore size of 0.45 µm and placed in bottles. A total of 4 bottles from each site were taken; in one bottle, nitric acid (HNO_3) was added, and in another, sulfuric acid (H_2SO_4) was added (Tab. 4.1). The samples were stored in a fridge and transported to Germany to the Institute of Geoscience laboratory, the University of Bonn.

4.4.2. Hydrochemical water analysis

The concentrations of phosphate (PO_4^{3-}), borate (BO_3^{3-}), and silica (SiO_2) were determined using photometry (Analytik Jena Specord 50 plus) (Welz, 1976). Ion-Chromatography (IC) (Shimadzu HIC-A6) was used to measure the major, minor, and trace anions (Weiss, 1995). The Atomic-Absorption-Spectrometry (AAS) (Perkin Elmer AAnalyit 700) was used to measure the concentrations of major, minor, and trace cations (Isaac & Kerber, 2015). A summary of the different analytes, how they were preserved, their amount, and the method of determination is given in Table 4.1.

Tab. 4.1: Methods of determination, analytes, conservation methods, necessary volume, the limit of detection (LOD), and limit of quantification (LOQ).

Method	Analyte	Conservation	Volume [ml]	LOD [mg/l]	LOQ [mg/l]
Ion-Chromatography (IC)	Chloride [Cl^-]	None	20	0.075	0.245
	Sulfate [SO_4^{2-}]			0.103	0.326
	Nitrate [NO_3^-]			0.093	0.292
	Nitrite [NO_2^-]			0.109	0.341
	Fluoride [F^-]			0.059	0.196
	Bromide [Br^-]			0.179	0.531
Photometry	Silica [SiO_2]	H_2SO_4 (3 drops)	100	0.644	2.102
	Phosphate [PO_4^{3-}]			0.04	0.139
	Borate [BO_3^{-3}]			0.039	0.136
Atomic Absorption Spectrometry (AAS)	Sodium [Na^+]	HNO_3 (3 drops)	100	-	1
	Potassium [K^+]			-	0.5
	Calcium [Ca^{2+}]			-	0.5
	Magnesium [Mg^{2+}]			-	0.5
	Iron [Fe^{2+}]			-	0.005
	Manganese [Mn^{2+}]			-	0.005
	Aluminum [Al^{3+}]			-	0.005
	Arsenic [As^{3+}]			-	0.005
	Cadmium [Cd^{2+}]			-	0.001
	Chromium [Cr^{3+}]			-	0.005
	Copper [Cu^{2+}]			-	0.005
	Nickel [Ni^{2+}]			-	0.005
	Lead [Pb^{2+}]			-	0.005
	Zinc [Zn^{2+}]			-	0.001
	Strontium [Sr^{2+}]			-	0.5

4.4.3. Water quality assessment for drinking and irrigation

Groundwater is the major drinking source for the local population, in addition to the wetland surface water in the study site. Surface water is further used for domestic and irrigation purposes.

To check the quality of surface water and groundwater, the guidelines for drinking water quality and acceptability aspects according to WHO (2011), the Kenyan standards (KEBS, 2015), and the irrigation limit (FAO, 1985) were used (Tab. 4.2, Tab. 4.3, and Tab. 4.4). Furthermore, the groundwater and surface water quality data is used to independently validate and explain the system's physical function and the flow paths (Kovalevsky et al., 2004).

Tab. 4.2: Health and irrigation guideline values and acceptability threshold for selected heavy metals (KEBS, 2015; WHO, 2011; FAO, 1985).

Constituent	Unit	Guideline value (WHO, 2011)	Kenyan standards (KEBS, 2015)	Irrigation limit (FAO, 1985)	Acceptability threshold and remarks
Arsenic [As^{3+}; As^{3-}; As^{5+}]	mg/l	0.01	0.01	<0.1	Carcinogenicity in humans. Intake over long periods causes arsenic poisoning
Cadmium [Cd^{2+}]	mg/l	0.003	0.003	<0.01	
Chromium [Cr^{2+} / Cr^{3+}]	mg/l	0.05	0.05	<0.1	Risks to health above the threshold. Health effects are determined by oxidation state
Copper [Cu^{2+}]	mg/l	2	1	<0.2	Laundry and sanitary wary stain above 1. Bitter taste and color above 5
Lead [Pb^{2+}; Pb^{4+}]	mg/l	0.01	0.01	<5	Designated as provisional on basis of treatment performance & analytical achievability. Lead is classified as a possible human carcinogen. Inorganic lead compounds are probably human carcinogen
Mercury [Hg^{2+}]	mg/l	0.006	0.001		Intake of organic mercury compounds is not of direct risk. Methylmercury converted into inorganic mercury is of concern, and thus the threshold
Nickel [Ni^{2+}]	mg/l	0.07	0.02	<0.2	Toxicity value from drinking water on an empty stomach above the threshold
Zinc [Zn^{2+}]	mg/l	3	5	<2	Taste threshold of 4

Tab. 4.3: Health and irrigation guideline values and acceptability threshold for selected water elements and compounds (KEBS, 2015; WHO, 2011; FAO, 1985).

Constituent	Unit	Guideline value (WHO, 2011)	Kenyan standards (KEBS, 2015)	Irrigation limit (FAO, 1985)	Acceptability threshold and remarks
Aluminum [Al^{3+}]	mg/l	0.9	0.2	<5	Deposition of aluminum hydroxide floc and exacerbation of discoloration of water by iron above 0.2
Ammonia [NH_3]	mg/l		0.5		Taste threshold of 35 and odor threshold of 1.5
Ammonium [NH_4^+]	mg/l			<5	Catalytic action leading to drinking water containing nitrite
Barium [Ba^{2+}]	mg/l	0.7	0.7		
Bicarbonates [HCO_3^-]	mg/l			<91	
Boron [boric acid]	mg/l	0.5	2.4		
Calcium [Ca^{2+}]	mg/l		150	<60	Acceptability depends on individual's taste
Chloride [Cl^-]	mg/l		250	<140	Taste threshold of 250
Fluoride [F^-]	mg/l	1.5	1.5	<1	Skeletal fluorosis and increased bone fracture risk. Dental fluorosis if ingestion amongst young kids
Iron [Fe^{2+}/Fe^{3+}]	mg/l	0.3	0.3	<5	Laundry stains and deposits in pipes above the threshold. Color and turbidity may develop above the threshold
Magnesium [Mg^{2+}]	mg/l	50	100	<25	Acceptability depends on individual's taste
Sodium [Na^+]	mg/l	50	200	<60	Average taste threshold of 200 at room temperature
Nitrite [NO_2^-]	mg/l	3	0.003		Methaemoglobinaemia in infants above the threshold
Nitrate [NO_3^-]	mg/l	50	45	<66	Recommendation of below 100 for bottle-fed infants
Manganese [Mn^{2+}]	mg/l	0.4	0.1	<0.2	Undesirable taste, laundry, and sanitary ware stain above 0.1. Coating on pipes above 0.2
Postassium [K^+]	mg/l		50	<20	
Phosphate [PO_4^{3-}]	mg/l		2.2		
Phosphorus [P^{5+}/ P^{3+}/P^{3-}]	mg/l			<0.4	
Sulfate [SO_4^{2-}]	mg/l	500	400	<81	Taste threshold of 250
Sulfur [S]	mg/l			<27	

Tab. 4.4: Health and irrigation guideline values and acceptability threshold for selected water parameters (KEBS, 2015; WHO, 2011; FAO, 1985).

Constituent	Unit	Guideline value (WHO, 2011)	Kenyan standards (KEBS, 2015)	Irrigation limit (FAO, 1985)	Acceptability threshold and remarks
Electric conductivity [EC]	S/m			<1.5	
Hardness [$CaCO_3$]	mg/l		600	<60	Hard water can increase soap consumption and scale deposition in water distribution systems and reduces the efficiency of heat exchangers. Excessively hard water has corrosion tendencies
pH [25°C]	log H^+		6.5 - 8.5	8.4	Recommended range of 6.5 - 8.5 to avoid corrosion of water mains and pipes
Specific absorption rate [SAR]	mg/l			<10	
Total Dissolved Solids [TDS]	mg/l		1500		Unpalatable drinking water at TDS above 1000. Excessive scaling in water pipes, heaters, boilers, and household appliances in high TDS
Turbidity	NTU	<1	<5	<10	Interferes with efficiency of disinfection above the threshold and negatively impacts consumers' acceptability of water. It is an indicator of the possible presence of contaminants

In regards to the water quality in terms of irrigation, the modified guideline of Ayers and Westcot (1985) is used. The guideline helps to determine the water results suitable for irrigation based on the Degree of Restriction on Use (DRU) in terms of salinity and infiltration and was given a value of 0, 1, 2 for none, slight to moderate, and severe (Tab. 4.5).

Tab. 4.5: Guidelines for the interpretation of water quality for irrigation based on the Degree of Restriction on Use (DRU) in terms of salinity and infiltration modified after UCCC (1974) and Ayers and Westcot (1985).

Potential Irrigation Problem		Degree of Restriction on Use (DRU)		
		None (0)	Slight to Moderate (1)	Severe (2)
Salinity (affects crop water availability) Using EC or TDS		**EC [µS/cm]**	**EC [µS/cm]**	**EC [µS/cm]**
		< 700	700 – 3,000	> 3,000
		TDS [mg/l]	TDS [mg/l]	TDS [mg/l]
		< 450	450 – 2,000	> 2,000
Infiltration (affects infiltration rate of water into the soil) Using EC and SAR together	**SAR**	**EC [µS/cm]**	**EC [µS/cm]**	**EC [µS/cm]**
	0 – 3	> 700	200 – 700	< 200
	3 – 6	> 1,200	300 – 1,200	< 300
	6 – 12	> 1,900	500 – 1,900	< 500
	12 – 20	> 2,900	1,300 – 2,900	< 1,300
	20 - 40	> 5,000	2,900 – 5,000	< 2,900

Additionally, water quality for irrigation can be evaluated in terms of salinity, expressed by EC or TDS, and infiltration, expressed by salinity and sodium adsorption rate (SAR) (Eq. 4.7), (Tab. 4.5) (Ayers and Westcot, 1985).

$$SAR = \frac{Na^+}{\sqrt{\frac{Ca^{2+} + Mg^{2+}}{2}}} \qquad \text{(Eq. 4.7)}$$

SAR Sodium adsorption ratio
Na^+ Concentration of sodium [mmmol(eq)/l]
Ca^{2+} Concentration of calcium [mmmol(eq)/l]
Mg^{2+} Concentration of magnesium [mmmol(eq)/l]

4.4.4. Stable water isotopes

The analyses of the stable water isotopes ^{18}O and ^{2}H were performed at the Institute for Groundwater Ecology at the Helmholtz Zentrum in Munich using a cavity ring-down spectrometer (Picarro Isotopic Analyzer L2120-i). Every sample is measured up to nine times. The average value and the standard deviation are taken from the latter six injections. The values of hydrogen and oxygen isotope ratios are expressed per mil [‰] based on the international delta scale as defined by Gonfiantini (1978). They will be referred to as $\delta^{2}H$ and $\delta^{18}O$, respectively, with an accuracy of 0.1 ‰ for $\delta^{18}O$ and 0.5 ‰ for $\delta^{2}H$.

There have been no studies showing the LMWL of the Ewaso Narok area. Thus Kericho's station, Kenya was chosen for the local meteoric water line (IAEA, 1971, 1973, 1975; Sklash & Mwangi, 1991, Rietti-Shati et al., 2000). After Rozanski et al. (1996) the LMWL can be expressed as $\delta^{2}H = (7.96 \pm 0.35)\ \delta^{18}O + (11.35 \pm 0.96)$ (with $r^{2}= 0.912$). Darling et al. (1990) proposed for precipitation samples in the Kenya Rift valley a different relationship ($\delta^{2}H = 5.56\ \delta^{18}O + 2.04$ ($r^{2}=0.88$)).

General assumptions and theories used in the analysis of the stable water isotopes $\delta^{2}H$ and $\delta^{18}O$:

- Comparison is made against the GMWL and LMWL.
- As precipitation samples did not exist, the LMWL used in this study is taken from Rozanski et al. (1996) as follows: **$\delta^{2}H = (7.96\pm 0.35)\ \delta^{18}O + (11.35 \pm 0.96)$** $r^{2}= 0.912$.
- Evaporation of water results in an enrichment of heavy isotopes in the residual water, while the vapor becomes depleted (Clark & Fritz, 1997).
- Signatures close to the global meteoric water line indicate minimal evaporation; signatures below the global meteoric water line indicate significant evaporation (Sklash & Mwangi, 1991).
- Evaporated waters plot below the GMWL with slopes below 8 (Moser, 1998).
- Groundwater has signs of depleted isotopes as it does not go through evaporation or attenuation.
- Although the isotopic content of water samples may represent mixtures of water from different sources (e.g., different aquifers), the assumption here is that the water samples are generally representative of the available water at that site (Sklash & Mwangi, 1991).

4.4.5. Precipitation and temperature data measurements

Precipitation measurements, both daily and hourly resolution, were obtained from a GlobE weather station located in two places within the study site (Fig. 4.6), Evan's Station (8/5/2015 31/10/2016) and Rumuruti's Station (14/4/2016 to 20/10/2016). The modeling team of GlobE "Wetlands" filled data gaps in precipitation records. Temperature data was as well collected from the same stations. Further data was acquired from WRMA (2016) for long-term analysis and trends for four different stations (cp. App. 4).

Fig. 4.6: The Evan's weather station installed as part of the GlobE project.

4.4.6. Plausibility tests and data processing

Most of the data was processed and assessed for plausibility before interpreting the results.

A plausibility test was done to verify the water calculations results, the ion charge balance error, and the difference between measured and calculated total dissolved solids (Freeze & Cherry, 1979; Moya et al., 2015). Samples with ion charge balance errors higher than 10 % (Eq. 4.8) were discarded from further analyses (Güler et al., 2002; Moya et al., 2015).

$$\text{Ion charge balance error } [\%] = \frac{\sum(\text{cations}) - \sum(\text{anions})}{\sum(\text{cations}) + \sum(\text{anions})} * 100 \qquad \text{(Eq. 4.8)}$$

$\sum(\text{cations})$ Sum of cations [mmol(eq)/L]
$\sum(\text{anions})$ Sum of anions [mmol(eq)/L]

Redox potentials were measured with an ORP Sentix probe were referenced (Eq. 4.9) to a normal hydrogen probe by adding (U_{ref}) 214, 210, 207, 203 mV simultaneously to the redox measured on the field (U_{Mess}) depending on the temperatures 15 C°, 20 C°, 25 C°, and 30 C° (WTW, 2009).

$$U_H = U_{Mess} + U_{Ref} \qquad \text{(Eq. 4.9)}$$

Regarding the limit of detection (LOD) and limit of quantification (LOQ), numerical values were applied when numerical calculations were performed. Half LOD values replaced LOD in the IC and photometry results (Farnham et al., 2002). Values below the LOQ were replaced by the actual measured value. In regards to LOQ, values below the LOQ were replaced by half LOQ, whereas those above the LOQ were quantified (Farnham et al., 2002).

4.4.7. Hydro-geochemical and hydrochemical processes evaluation and presentation

The chemical composition of water is related to the soil and rock, which are being weathered. To identify the main hydro-geochemical processes occurring in this system, the stoichiometric relations of the dissolved ions are calculated and evaluated. Molar ratios or equivalent-concentration ratios are used to identify hydrochemical ratios, and graphs are used to present the results.

In regards to the hydrochemistry of water, several methods were applied to the hydrochemical data to gain information about the groundwater system and related processes. These methods included calculations of characteristic values, graphical tools, and statistical analyses. The presentation of data and information was done in graphs, statistical tables, maps, and cross-sections following Kovalevsky et al. (2004). Piper (1944), Schoeller (1955), and Udluft (Carlé, 1975) were selected to present the hydrochemical composition of the different water sampling points (Güler et al. 2002, Kovalevsky et al. 2004). The classification by dominant cation and anion was used. The most abundant cation and the most abundant anion comparing mmol(eq)/L values represent the respective water type.

More specifically, the Udluft diagram of the different sampled points is drawn with a scale of the radii where the area of the circle represents the total ionic concentration, and the subdivisions represent proportions of the different ions (half of the circle is the ions and the rest cations). This means that the overall graph's size is related to the overall mineralization of the sample (Langguth & Voigt, 2004). In the middle of the diagram, the proportion of carbon dioxide is given.

4.5. Statistical Analysis

Multivariable Statistical Analysis (MSA) allows for samples to be grouped by similar chemical properties but does not immediately identify the trends and processes important in controlling groundwater (Blake et al., 2016; Güler et al., 2002). MSA includes the Principal Component Analysis (PCA) and Hierarchical Cluster Analysis (HCA).

4.5.1. Principal Component Analysis (PCA)

PCA is a technique that attempts to explain an underlying structure to a dataset by reducing the number of variables in the dataset. It tries to reveal patterns by calculating principal components (PC). It has been used to elucidate physical processes responsible for water geochemical characteristics (Farnham et al., 2003; Guan et al., 2013; Güler et al., 2002). Two approaches are usually considered when running the PCA; either running it on raw hydrochemical data or on log-transformed data (Blake et al., 2016; Engle et al., 2014). The components represent the eigenvectors of the covariance-variance matrix of the data. Each PC represents one or more hydrogeochemical processes affecting the variation of the dataset (e.g., Burghof, 2017). To identify the major processing controlling and affecting the water sampled hydrochemistry, the statistical package SPSS® factor analysis was used to run PCA on selected hydrochemical parameters of the sampled water. Kaiser-Meyer-Olkin (KMO) and Bartlett's Test are performed, and the number of components is decided upon based on the eigenvalues and the scree plot.

4.5.2. Hierarchical Cluster Analysis (HCA)

Mixing and diluting the stream and wetland water by runoff from tributaries and upward or downward side seeping of groundwater affects the evolution of chemical and isotopic composition in the downstream flows. The statistical package SPSS® cluster analysis was used to run the hierarchical cluster on the water chemistry data and isotopes to understand the water flow and mixing. It helped in classifying the water-groups based on their hydrochemical and isotopic characteristics.

Statistical analysis is a powerful tool for analyzing water chemistry and testing water quality as samples can be grouped into distinct sub-groups of significant geological, statistical (Judd, 1980; Nadew & Tefera, 2013), or hydrochemical significance. The system is complex, with many options, and the contribution and make-up are not known. Accordingly, cluster analysis helps to identify and classify 'water bodies' or sub-aquifers units based on the similarity and hierarchy among all water samples. This depends on the hydrochemical characteristics and isotopes of the dissolved minerals. It suggests possible linkages to potential sources of recharge. Later on, geographical and geological aspects are taken into account.

There are no prior constraints about which water samples belong to which cluster in the cluster analysis. The grouping or clustering into groups or sub-groups is defined through a systematic analysis of each of the parameters, such as ions and trace elements of the hydrochemical and isotopes database. Ward's method (Ward, 1963) is applied as it is distinct from all other methods because it uses an analysis of variance (ANOVA) approach to evaluate the distances between clusters. Ward's method calculates the error sum of squares, which is the sum of the distances from each individual to the center of its parent group (Judd, 1980), and forms smaller distinct clusters than those created by other methods (StatSoft, Inc. 1995). The Euclidean distance, the straight line distance between two points in c-dimensional space defined by c variables, is used as similarity measurement, together with Ward's method for linkage. This produced the most distinctive groups where each member within the group is more similar to its fellow members than to any member from outside the group (Güler et al., 2002).

This approach is commonly applied to water chemistry investigations to define groups of samples with similar chemical and physical characteristics because rarely is a single parameter sufficient to distinguish between different water types (Güler et al., 2002).

A hydrochemical file in Excel format is prearranged for the cluster analysis since cluster analysis cannot be performed unless values are available for all the used parameters in every cell (no zero values allowed). If a particular parameter's value was missing, this parameter was omitted from the entire water samples or replaced by another parameter by adopting this parameter from an earlier sampling campaign if it was available.

4.6. MCM

Due to the hydrogeological complexity of the Ewaso Narok wetland and the limited hydrological information, hydrological modeling based on the conventional flow and transport modeling concept could not be used to elaborate or quantify the hydraulic connectivity between the surface water and the aquifer. As an alternative assessment, the MCM approach (Adar & Long, 1987; Adar, 1995; Adar et al., 1988; Adar & Neuman, 1988), which incorporates a spatial distribution of hydrochemistry and environmental isotopes, was adopted and performed to identify and quantify the hydraulic connectivity and fluxes among water bodies (wells, streams, springs, effluents, etc.).

The MCMsf mathematical model developed for complex hydrogeological basins (Adar & Neuman, 1988) was used for assessing natural recharge and the flow pattern and for quantifying the relative contribution of the different sources. The flow domain was subdivided into pseudo-homogeneous flow cells forming a multi-compartmental flow model (Adar & Massoth, 2017).

An input file of the hydrochemical and isotopic compositions was first generated, as elaborated in the respective sections. A conceptual schematic diagram of the modeled aquifer was then drawn. Based on the cluster analysis, an optimum number of cells or compartments was decided upon for modeling. Possible contributors were determined and assigned. In the beginning phase, the single-cell version of the MCMsf was applied, followed by the multiple cell (multicell) versions. Different scenarios were performed for every cell, where certain wells and surface water points were designated as potential recharge sources. It was verified that all the chosen potential inflows have a hydrologic potential to flow into a specific cell-based on piezometric potential and geological feasibility.

Single-cell MCM modeling was used to illuminate the potential contributors and the hydraulic connectivity for every proposed compartment in the modeled system. It also aimed at confirming possible water flow movement from groundwater into the wetland. In addition, it provided the ability to assess both the active sources of recharge and the active sources of pollution, if existing.

Multi-cell MCM modeling was used to establish the hydraulic connectivity and confirm the water flow movement from groundwater to the wetland. It provided the ability to assess and quantify the active water fluxes and recharge sources.

5. Database for Ewaso Narok

The data used in this study is divided into primary data and secondary sources (Tab. 5.1). Throughout the scope of this work, surface water is abbreviated and donated to SF and groundwater to GW. Own data (sampled in 2016) is mainly used, and the sampled points are indicated with SF or GW and a number. External data is shortened to E. and is written before SF or GW. For proper identification of names of wells or locations (App. 11).

Tab. 5.1: Database for the Ewaso Narok wetland used in this study.

Data description	Used in	Primary / Secondary	Source
Survey data		Primary / Secondary	Own survey / Kyalo Willy (personal communication, 2016)
Altitude/Topography	Maps	Secondary	earthexplorer.usgs.gov (STRM, digital elevation)
Drilling logs		Secondary	Private well-owners and reports (Aqua Well, 2013); database of WRMA (2007, 2013a, 2013b)
Groundwater level	Maps	Primary / Secondary	Installed piezometers / Muriuki Karugi (2016) piezometers installed between June 2015 till January 2016, drillings logs (WRMA, 2007, 2013a, 2013b, 2013c, 2016; WRA reports, 2016; Aqua Well, 2013, Groundwater Survey, 1988, ESGHS, 2012)
Hydrochemical data	Statistical analysis; model	Primary / Secondary	Measured data in field and Laboratory / Private drilling wells reports, names of wells, and quality data information (Aqua Well (2013), Groundwater Survey (1988), WRMA (2007), WRMA (2013a, 2013b, 2013c), ESGHS (2012), Report book (WRA) (WRMA, 2016 / Republic of Kenya, 1987)
Local Meteoric Water Line	Isotopes analysis	Secondary	International Atomic Energy Agency (IAEA) / Rozanski et al., 1996; Rietti-Shati et al., 2000; Darling et al. 1990
Stable water isotopes	Isotopes Analysis	Primary	
Precipitation, temperature	Climate description	Primary / Secondary	Automated metrological GlobE weather stations installed at the study (WRMA, 2016)/ (WRMA, 2013a)
Wetland delineation	Maps	Secondary	(Beuel et al., 2016) (personal communication E- Amler, 2016)
Mineralogical, geochemical data of regolith and sediment samples	Soil analysis/ Hydrogeology	Primary	
Soil	Maps	Primary / Secondary	Sampled soils / drilling logs (private landowners); Georeferencing CETRAD soil map (Evanson et al., 2014)
Geological and lithological data	Maps	Secondary	Georeferencing the Geological map of Kenya 1:250,000 Baringo-Laikipia; geological map: Africa Kartenwerk 1:1,000 000 - (2001); georeferencing the Groundwater Modelling System (GMS) software results of Muriuki's Karugi (2016) thesis; description of deep drilling logs provided by private landowners, WRMA and CETRAD Kenya for some shapefiles
Discharge and precipitation data of river gauging stations		Secondary	Discharge and precipitation data series of river gauging stations and rainfall stations: WRMA office (WRMA, 2016), Kenya Meteorological Service (KMS)
Hydrogeological maps		Secondary	Georeferencing the Hydrogeological map of Ewaso Ng'iro North Basin Area (WRA, 2020); Hydrogeology and aquifer systems in Kenya (BGS, 2019).
Streams and wetland sub-catchment maps		Secondary	CETRAD (2016), WRI (2016), WRMA data (2013a).

5.1. Data for the aquifer structure and properties

Five soil samples were taken from the alluvial year-rounded flooded wetland and referred to as S (sediments). Fourteen soil samples and three rock samples, both taken from the regolith

profile, are labeled as R (regolith) (Fig. 5.1, Tab. 5.2). The areas where the samples were taken were categorized according to their land use: seasonally cultivated, grazing, papyrus, and continuously cultivated.

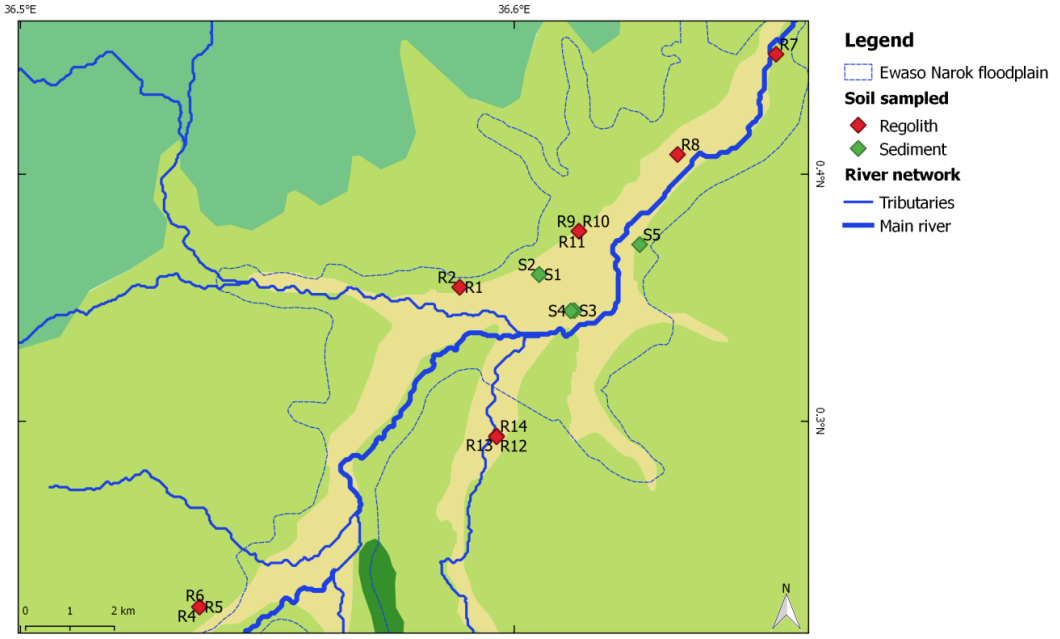

Fig. 5.1: Sampling points for soil and rock, drawn on the geological map (cp. Fig. 2.9, p.19).

Tab. 5.2: Soil and rock sampling points (R = Regolith, S = Soil) with depth, setting, and land use.

ID	Depth [cm]	Setting	Land use	Additional notes
R1	70 - 80	Regolith	Continously cultivated	Agricultural land
R2	100 - 110	Regolith	Continously cultivated	Agricultural land
R3	30 - 65	Regolith	Grazing	Next to fish ponds
R4	100 - 116	Regolith	Grazing	Next to fish ponds
R5	140	Regolith	Grazing	Next to fish ponds
R6	170 - 178	Regolith	Grazing	Next to fish ponds
R7	120	Regolith	Grazing	Outlet of the swamp, phonolite
R8	76	Regolith	Grazing	River course
R9	31	Regolith	Seasonally cultivated	River course
R10	60	Regolith	Seasonally cultivated	River course
R11	90	Regolith	Seasonally cultivated	River course
S1	89	Flooded wetland	Papyrus	Slash and burn area
S2	128	Flooded wetland	Papyrus	Slash and burn area
R12	130	Regolith	Grazing	River course
S3	40	Flooded wetland	Papyrus	Flooded fields
S4	120	Flooded wetland	Papyrus	Flooded fields
S5	50	Flooded wetland	Papyrus	Flooded fields
R13	100	Regolith	Grazing	River course
R14	160	Regolith	Grazing	River course
R15	0	Hard rock	Road cutting	Murram rock samples
R16	0	Hard rock	Road cutting	Rocks
R17	0	Hard rock	Road cutting	Rocks

5.2. Hydrochemical and isotopic data

The sampled surface and groundwater points are shown in Figure 5.2.

The surface water points were divided into groups as follows:

- Main River: SF43, SF42, SF29, SF20, SF22, SF16, SF13, SF 48
- Tributary river (Melwa): SF2, SF3
- Tributary river (Pesi): SF6, SF25, SF26
- Dam: SF51, SF53
- Wetland dry: SF36, SF28, SF12, SF8, SF33, SF34
- Wetland flooded: SF35, SF40, SF39, SF37, SF38, SF15
- Effluent (from the stone cutting): SF21

The groundwater points were divided into four different clusters:

- Installed Piezometers: GW14, GW31
- Shallow hand-dug wells: GW32 and GW5
- Deep wells: GW19, GW30, GW9, GW10, GW27, GW7, GW45, GW49, GW50, GW44, GW52, GW47, GW46, GW18, GW17, GW23, GW24, GW41, GW1, GW4
- Spring: GW11

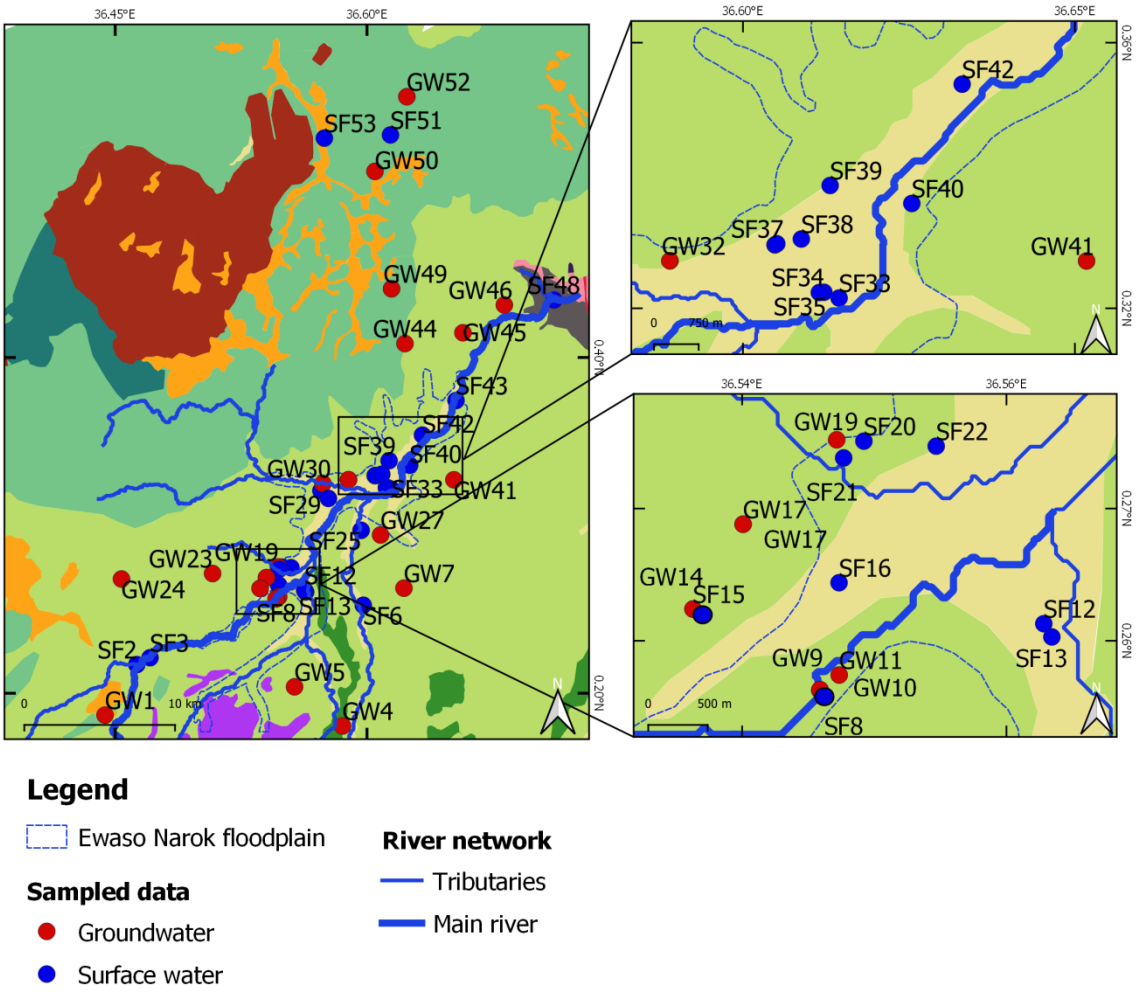

Fig. 5.2: Sampling points for water (GW = groundwater, SF = surface water) in Ewaso Narok, drawn on the geological map (cp. Fig. 2.9, p.19).

6. Results and Discussion

6.1. Survey results

The survey was intended to better identify the wetland's resource use, surface water, and groundwater. It further provided potential points of pollution input, from fertilizers to sewage, into the wetland for sampling and then modeling of the Ewaso Narok wetland. The results of the 114 random persons selected for this study are presented. Secondary raw data results collected by Kyalo Willy (personal communication, 2016), when used, are specifically labeled with KW results.

Ewaso Narok wetland is the primary source for people with water supply for drinking, washing clothes, domestic use, agriculture (irrigation and cropping), livestock drinking, and dipping (Fig. 6.1). The questioned people could mark more than one category of their use of the wetland. 85 % of the sampled people use the wetland for agriculture, and 83 % drink from the wetland directly. 75 % of the sampled people use the wetland to wash their clothes and dishes or shower, whereas 57 % use the wetland to provide their cattle with drinking water and 56 % to dip their cattle.

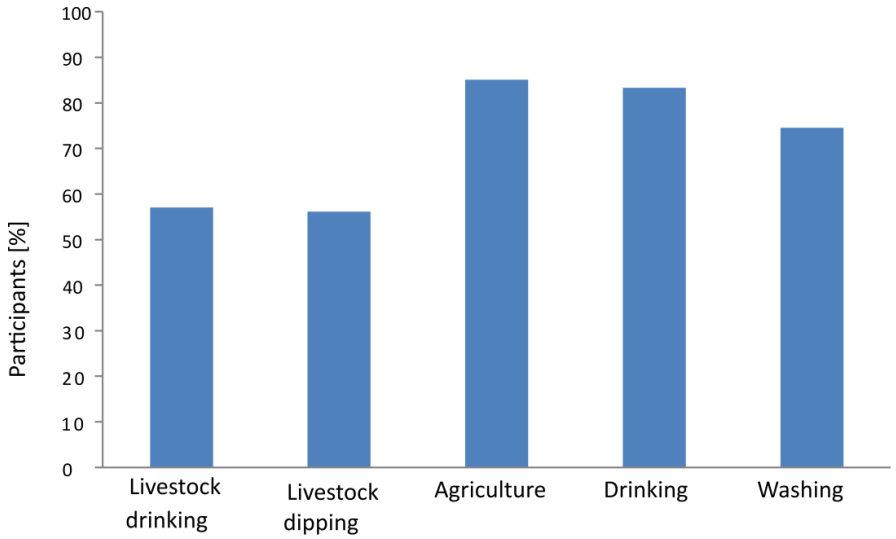

Fig. 6.1: Different uses of the Ewaso Narok wetland (114 participants in the survey 2016).

This comes in terms with KW results showing that 60 % of the 300 interviewed people utilized the wetland for drinking and bathing purposes.

People were then asked if they disposed of anything directly into the wetland. Hesitation to answering questions was noticed. People understand that some practices are problematic, yet they still do them. The categories included fertilizer remains, plastic containers of fertilizers, cans of food, etc., soap or cleaning material when directly washing on the wetland, cattle manure (if they leave their animals long on the wetland), and if they chemically spray their cattle directly in the wetland. More than 50 % of the participants disposed of plastic, soap and cleaning material, and fertilizers directly in the wetland (Fig. 6.2). 30 % of the sampled people chemically sprayed their cattle inside the wetland area.

To understand possible pollutants or point source contributors, if they exist, the people were asked how they dispose of the remains of their fertilizers or cans (Tab. 6.1). 26 % of those

people burn the remains, thus polluting the air but not the wetland, but at times the ashes fly into the wetland, and 33 % bury them in holes. There was no specification of whether these holes were in the flooded part of the wetland or not. 29 % of the participants have a hole for disposing of things in the wetland area.

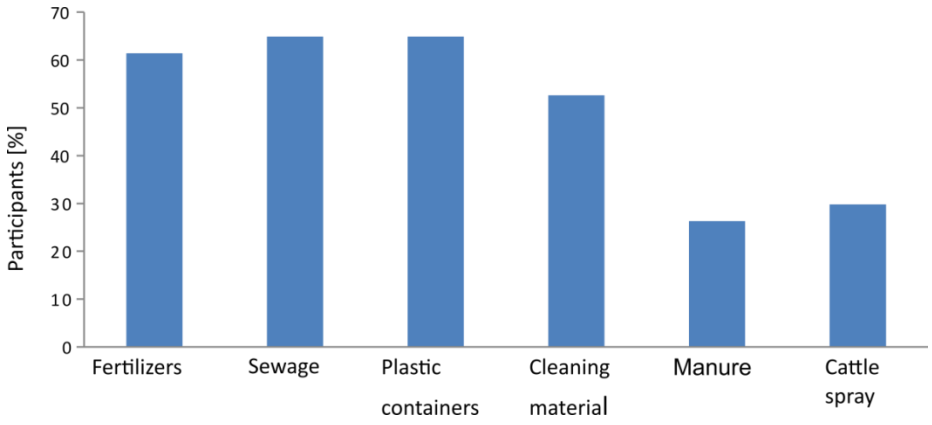

Fig. 6.2: Conscious disposal in the Ewaso Narok wetland. 2016 sampling campaign of 114 participants.

Tab. 6.1: Methods of disposal in the wetland.

Method of disposal in the wetland	Participants [%]
Burn	26
Bury in holes	33
Hole on site	29

Regarding agricultural practices, 54 % of the participants plant and farm inside the wetland as it is fertile, 28 % outside the wetland, and 18 % in both (Fig. 6.3). From the secondary data of KW, out of 339 participants, the reason for growing the crop is the high productivity, followed by the land not being suitable for other crops.

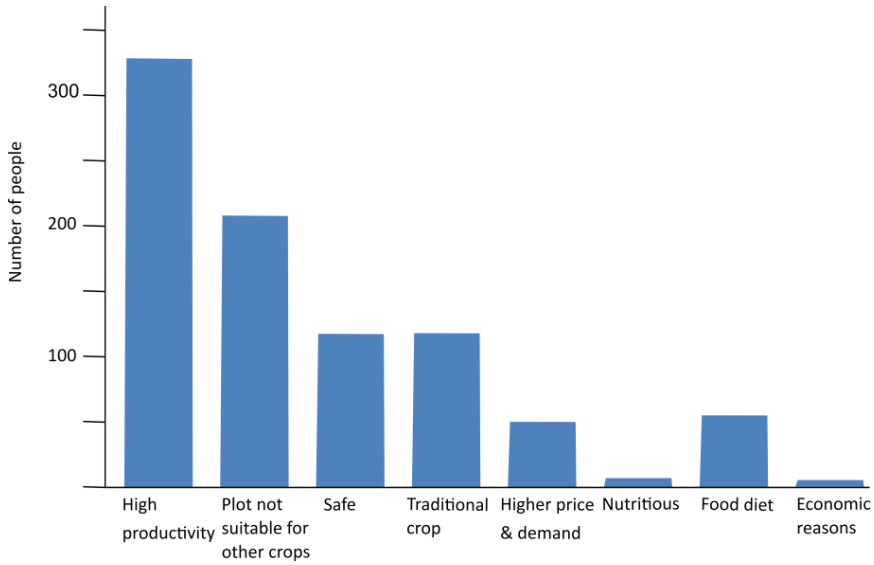

Fig. 6.3: Reasons for Ewaso Narok residents to grow crops. Source: secondary data of 339 participants (Kyalo Willy, 2015).

Though it is uncommon to use fertilizers in wetlands as they are fertile, people in Ewaso Narok still reported using them (Ngolo et al., 2018). Of the participants, 65 % used chemical fertilizers, and 35 % used manure. A remark is that people could be using both. Other reported fertilizers,

according to the participants, included diammonium phosphate (DAP), nitrogen phosphorus, and potassium (NPK), urea, and foliar feeds.

With respect to their drinking water, 87 % of the 114 participants relied on wells for drinking. Other alternatives involved pipes and water from the wetland. According to the participants, the associated problems with the wells in the area of Ewaso Narok included them being very salty, far forcing mainly women to walk miles to fetch water, owned by the rich and business people, dried up, and rarely maintained or fixed.

Taking the seasonality of water flow in the floodplain into account, the participants were asked about their experience with floods in the last years. 79 % of the participants believe that the wetland water becomes dirtier when floods are present. The participants back the argument by observed phenomena such as a change of color, the material carried, vegetation, dead animals, plastic, sewage, domestic things, clothes, fertilizers, unclear water, and water-born disease manifestation. Despite the observations mentioned above, people still drink the water due to a lack of alternatives. The attribution of 'bad' to floods was related to destruction by erosion.

Participants associating floods to 'good' explained it by less need to irrigate as large amounts of water are available. This, accordingly, provided the people with security and protection for the time being and the dry season. Furthermore, dirt and waste are pushed away and removed by the floods.

Throughout floods, participants leave their homes for a while, avoid the electric-fenced area of the wetland, and do not take their cattle to the wetland. Furthermore, pit latrines flood, fertilization use, and costs increase, and planting is stopped.

To conclude, people rely on the wetland for most of their daily livelihoods, including drinking. However, there is a lack of responsibility and awareness of the wetland's pollution and well-being, seen in the direct conscious disposal of fertilizers, manure, and plastic containers in the Ewaso Narok wetland. This accordingly points to the importance of water quality sampling and assessment.

The survey provided potential input points of water and pollution into the wetland for sampling and then modeling of the Ewaso Narok wetland. Obvious sources into the wetland are tributaries and the main river, while identifying and quantifying hidden contributions from groundwater, springs, or human-induced pollutants will be the purpose of the Mixing Cell Model (MCM) purpose, seen in the following chapters.

6.2. Characterization of the aquifer

This chapter describes the different characteristics of the aquifer. Analysis and interpretation of the aquifer conditions and classification of the geological units are based on the available geological information, including existing geological maps, lithological drilling logs, results of resistivity profiling methods, and own field data. The first chapter looks at the system from a larger perspective, whereas the second addresses the mineralogy and weathering of the topsoil layers.

6.2.1. Aquifer structure and properties

The basement is made of gneisses, schists, and quartzites that are overlaid by Tertiary volcanic rocks (MEMR, 1987; Republic of Kenya, 1987). The area of investigation is dominated by the Miocene Rumuruti phonolites and trachytes, which are fractured and weathered (Hackman, 1988; Republic of Kenya, 1987). The crystalline rocks' exposure is vivid in outcrops on top of hills, steep slopes, in river beds, and on the side roads (Fig. 6.4). More intense weathering is noticed along with fractures in saprock, as described in the wells drilling logs in the area.

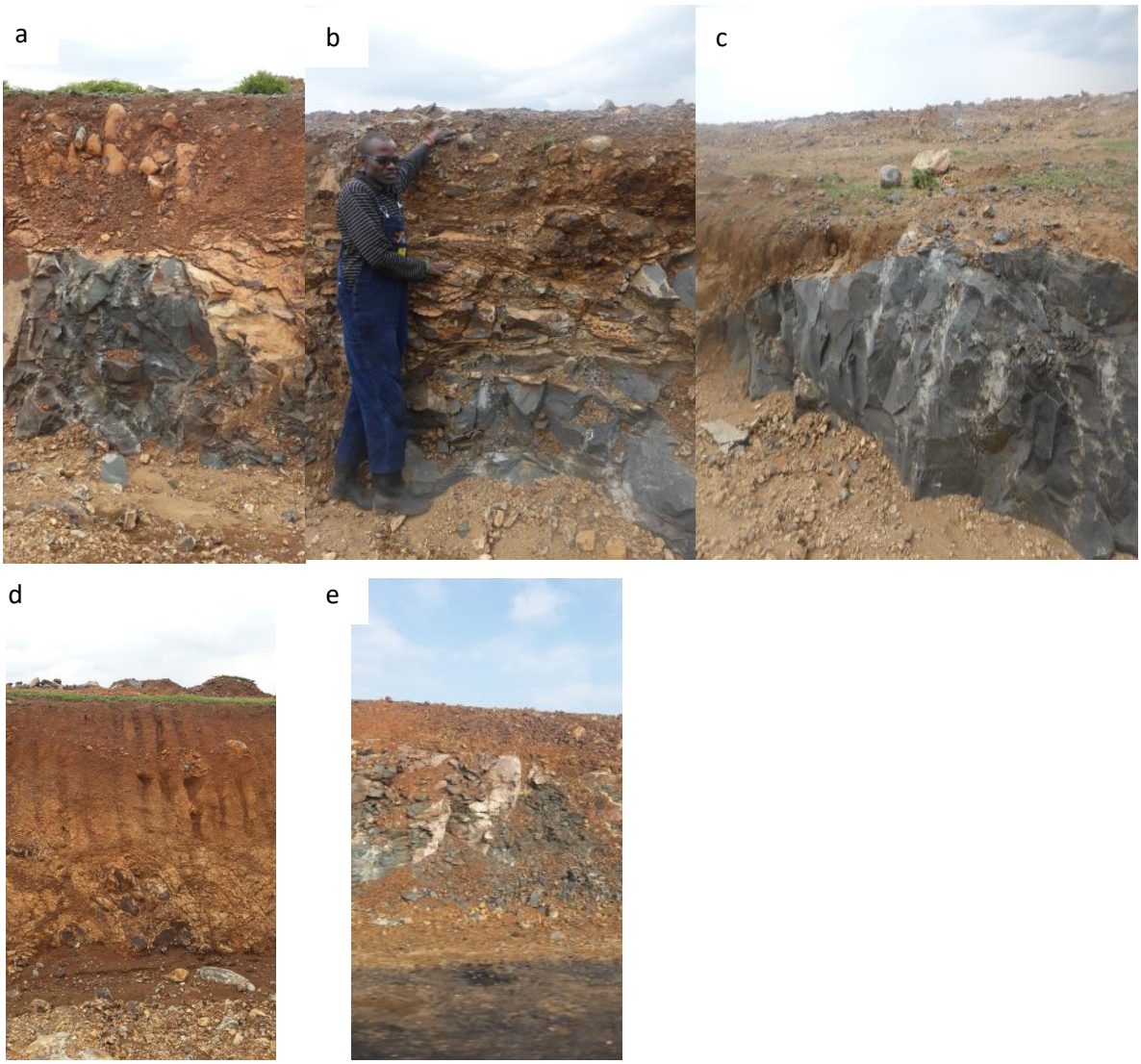

Fig. 6.4: Full exposure of the crystalline rocks (a, b, c) and regolith (d, e) on the roadsides of Ewaso Narok.

The rocks show varying degrees of weathering, from fresh phonolites to highly weathered ones. The depth of the weathering zones varies from around 0 to 150 m.b.s.l. (Fig. 6.5). Different weathered layers are noticed in between the phonolites, which include clay, tuff, or sand. The clay and sand are products of the Ewaso Narok wetland which was dammed by lava flows at various times. This might explain the fresh layers and the weathered ones that were on top then got covered, and then again, the top layers became weathered. The huge parts of the weathered profile can as well be affected by tectonic movements. The different water levels rising up and down from the stream or swamp affect the weathered and fresh phonolites. The

boreholes of the Shiva well, the Catholic Mission well, and Sosian well show more intensive weathering (Fig. 6.5). This might be related to their position as both wells lie within the wetland area that is flooded throughout the years. In addition, these wells all lie on the west side of the wetland, hinting at weathering being more intense on the west side. The Catholic Mission well is situated inside the delineated wetland flooded area. It consists mainly of weathered phonolites and taps the aquifer at around 85 m.b.s.l. compared to the rest of the wells tapping the aquifer at a level between 100 to 180 m. This is because the water level is higher, closer to the wetland. Furthermore, these wells lie in the lowest topographic areas explaining the weathering. Though Ol Maisor's topography is low, it is situated further away from the wetland water making it less vulnerable to water variations. Ol Maisor well lies 30 km northeast of the beginning of Ewaso Narok wetland. It is 178 m deep and consists mainly of phonolites. The aquifer is encountered at 157 m.b.s.l. There are some layers of tuffs and clay, but not much weathering is seen (Fig. 6.5). In addition, fractures are encountered. Shiva well lies around 8 km from Rumuruti town and is 158 m depth with the aquifer encountered at 140 m.b.s.l. It is made of weathered and fractured phonolites overlaid by weathered tuffs, clay, and volcanic rocks. Kifuku well lies in the upstream southeast of Ewaso Narok wetland. It is 152 m deep, and the main aquifer is encountered at 114 m.b.s.l. Kifuku area is underlain by superficial deposits overlying tuff calcrete deposits which further overly the Rumurti phonolites (Aqua Well, 2013). The drilling logs show mainly fresh phonolites and layers of agglomerates. Sosian well is 150 m depth and is situated north of Ewaso Narok wetland. The aquifer is encountered at 132 m.b.s.l. in the fresh phonolites. The geological formation (Fig. 6.5) shows that the main layers are weathered phonolites, with some layers of fresh phonolites. The top layers of all wells show illuviated clay, sand, and volcanic soils, typical residual soil formed from leaching and bioturbation. The perched aquifers are present around colluvial material, secondary clay, and laterites.

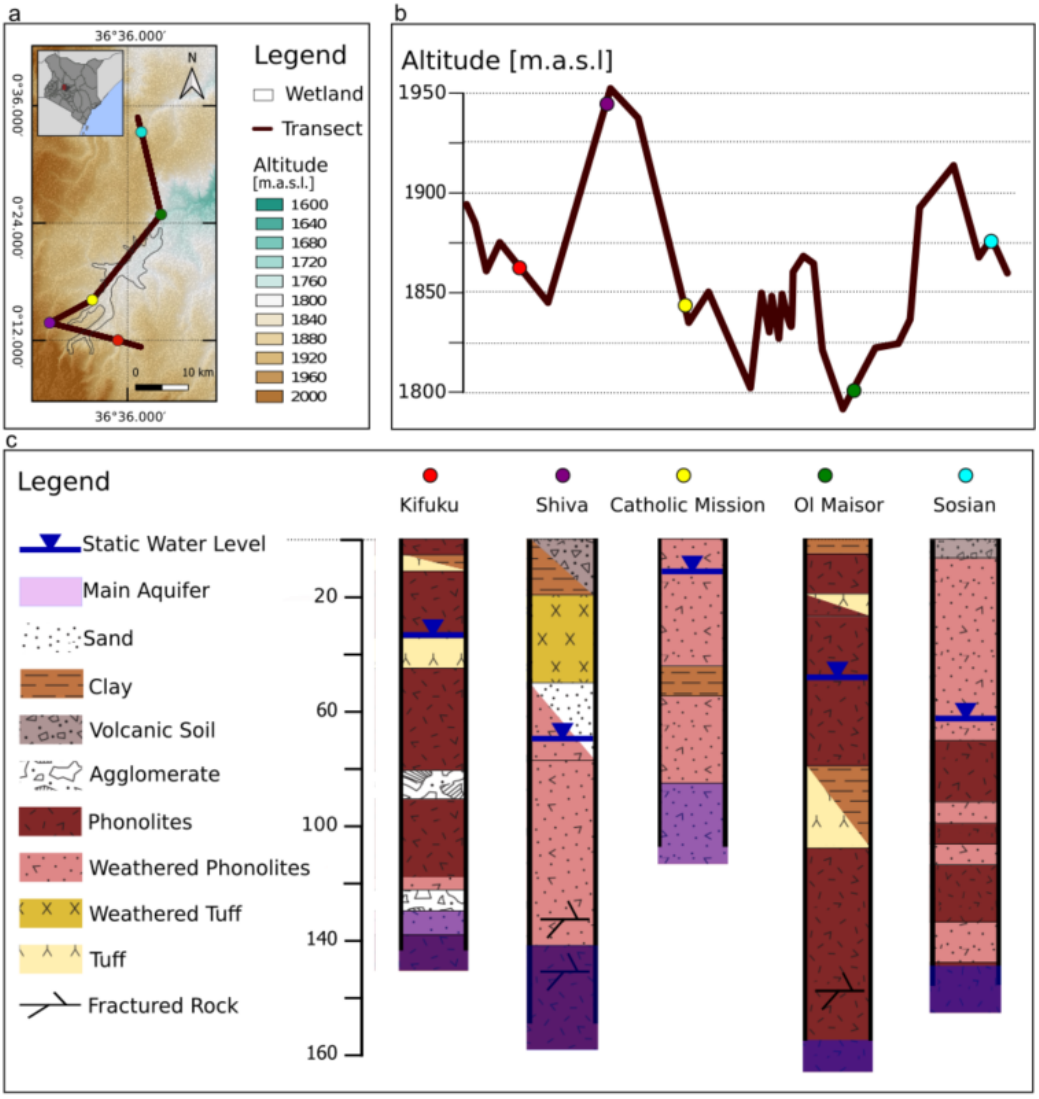

Fig. 6.5: The lithology and geology of selected wells in Ewaso Narok subbasin: a. The transect of the wells, b. The altitude of the wells, c. The lithology of the wells. Source: Drilling logs and earthexplorer.usgs.gov.

Porosities and permeabilities

The fresh rock of the crystalline basement in the Ewaso Narok wetland is made of granite and gneiss. Crystalline rocks are usually characterized by negligible porosity and permeability in terms of groundwater exploitability (Tab. 6.2). Granite, as part of the plutonic rocks, belongs to an aquifuge (Todd, 1959), a formation that has no interconnected openings. It, accordingly, does not enable absorption or water transmission. Its porosity ranges between 10^{-4} – 1 % (The Open University, 2006). Gneiss, as part of the metamorphic rocks, has completely obliterated the original porosity and permeability of the original rock (Lachassagne et al., 2021). The total porosity and drainage porosity of rocks decrease with age.

However, with fracturing and weathering, the igneous rocks and the weathered crystalline rock become more permeable and connected (Fass, 2004). Alteration processes can increase the rocks' fracture permeability and total porosity (Tab. 6.2). It further induces substantial changes in the mineralogical composition and properties of the aquifer system and has important implications for hydraulic properties (Briški et al., 2020; Walter et al., 2018). Weathered granite

and its regolith, the upper part of the basement in Ewaso Narok, possess higher permeability due to the leaching of clay minerals, iron, and calcium (Alexander, 1983; Chen et al., 2019; Rossi & Graham, 2010). Gneisses weathered profiles are characterized by strong clay and iron oxide and hydroxide enrichment, with higher porosities, median pore throat size, and a decrease of bulk density (Walter et al., 2018). In highly fractured regions, granite tends to be more pervious than gneiss (Stober & Bucher, 2007).

Tab. 6.2: Representative values of porosity and specific yield of selected geological formations (after Hamill & Bell, 2014; Morris & Johnson, 1967).

Geological formation	Porostiy [%]	Specific yield [%]
Dense crystalline rock	0 - 5	0 - 3
Fractured crystalline rock	5 - 10	2 - 5
Weathered crystalline rock	20 – 40	10 - 20

Different factors govern the water movement in weathered rocks. In granite, for example, it is the thickness and disposition of weathered materials and the nature of the unconsolidated-solid interface, along with joints, fissures, and vein systems (Alexander, 1983).

Weathering on higher grounds in Ewaso Narok's Basement System seems to be different from in the floodplain (Wachira, 2014; WRMA, 2013c). On high grounds, the depth of weathering is shallow, and the degree of decomposition of rocks is sufficiently limited that succeeding formations of different kinds have widely differing permeability. Gneisses in Ewaso Narok floodplain weather more easily than the more massive granites and migmatites in higher grounds (Ministry of Agriculture, 1983). The gneisses in the interfluves and in the high ground are less permeable, and their connecting fracture zones provide aquifers. In the floodplain of Ewaso Narok, the deep and advanced sub-surface decay of the saprolite has produced a thick zone of permeable material. This was observed in the exposed roadsides on the field (Fig. 6.4) and came in terms with the literature description (ESGHS, 2012).

In some parts of the Ewaso Narok wetland, the saprock is purely made of the weathered gneisses above the fresh crystalline basement. On other parts of the Ewaso Narok wetland, igneous and metamorphic rocks (mainly phonolites) are situated above the fresh crystalline basement. These igneous and metamorphic rocks have low primary porosity if they are unweathered and unfractured. Their permeability is very small to negligible (Davis & Turk, 1964), ranging from 0.01 to 20 m/day (Tab.6.3). Their porosity, accordingly, comes in the form of secondary porosity in fractures (Paron et al., 2013). They accordingly can hold water only in networks of fractures and faults (Paron et al., 2013) or interflow layers (Kulkarni et al., 2000). Water will then move through vertical fissures and horizontal interflow layers.

Phonolites, with their dense, thick flow and massively unjointed nature, are the most spread rock in the Ewaso Narok wetland. They have a total porosity of 2 – 4 % (Tab.6.3), with permeabilities ranging between 0.1 – 20 m/day. Faults in the weathered phonolites and fresh rock in Ewaso Narok can act as aquifer and channel flow conducting the water along the fault's axis. This is the case in the Ewaso Narok river and the streams around it where faults act as trough-like depression of the water table along the length allowing the water to only feed the aquifer through these zones (Aqua Well, 2013; Aquatreat, 2013). As the water moves through these faults, it reaches the flat-lying aquifers and moves mainly northwards (Aqua Well, 2013;

Aquatreat, 2013). At other times, faults impede flow due to hydraulic discontinuities. When faults are filled with clay and laterites, they act as barriers to the lateral flow (Wachira, 2014).

Tab.6.3: Material with its porosity, permeability, and transmissivity (The Open University, 2006).

Material	Total porosity [%]	Drainable porosity [%]	Comments	Permeability [m/day]	Tranmissivity [m^2/day]
Alluvium			Poorly sorted deprived from volcanics	1 - 10	2 - 200
Volcanic soils	40 – 60	<1 – 5	Variable		
Conglomerates	2 – 25	1 – 4	Mostly basaltic	0.01 - 0.5	3 - 50
'Core' basalts	2 – 5	< 0.1 – 4	Thermally altered and dykeintruded	0.001 - 0.05	0.1 - 100
Basalt sheets (traps) moderately old	4 – 10	<1 – 2	Several flows, no pyroclasts,		
Basaltic formations and pyroclasts	5 – 40	2 – 8	Increases with content of scoria, several flows with pyroclastics	0.01 - 20	2 - 100
Basaltic interflows of a lava flow	20 – 50	5 – 15	Breccia at the top and bottom		
Basalt flows	0.8 – 20	0.1 – 8	Dense to highly vacuolar	10^{-5} - 10	2 - 100
Pumices	50 – 85	< 0.1 – 1	Non- connected pores, unfractured		
Phonolitic ignimbrites	20 – 60	0.5 – 8	Dense to poorly welded tuff	10^{-6} - 0.01	0.1 - 10
Phonolites	2 – 4	1 – 6	Dense flows	0.1 - 20	20 - 1500

Other rocks in the study area are laterites, clay, and tuffs. Tuffs in Ewaso Narok floodplain owe their impermeability to the preponderance of ignimbrites and decomposed clayey pumice tuffs (Aquatreat, 2013). Ewaso Narok floodplain is a riverine wetland with permanent inundation and periodic soil saturation (Finlayson et al., 2001). The delineated part of the wetland is made from alluvial sediments. Laterites and clay clog the fractures in the weathered phonolite rocks, leading to low permeability in the area (ESGHS, 2012). When degraded and exposed to air, they form a hard crust hindering the water infiltration, thus causing more runoff. The Kinangop tuffs in the Ewaso Narok area are impermeable. They owe their impermeability to the preponderance of ignimbrites and decomposed clayey pumice tuffs.

Aquifers

As described, two principal confined aquifers, the regional and the local, are reported in the area of Ewaso Narok wetland in addition to the perched aquifer (Section 2.3.7). However, according to a map from WRA (2020), there seem to be several aquifer systems in the area. All groundwater samples belong to the Mount Kenya, and Aberdare volcanic aquifer, except for GW1, belonging to the Olobolossant plain aquifer system (Fig. 6.6). There is no available information about these other aquifers, the difference in their transmissivity, or in their characteristics.

The aquifers in the Laikipia plateau are no exception to aquifers in crystalline rocks and, accordingly, are heterogeneous and have irregular configurations with variable hydraulic characteristics over short distances (Bannerman & Ayibotele, 1984). The aquifers in the Ewaso Narok wetland do not occur as a continuous system, but the nature of the basement profile dictates their occurrence. Drilling wells combined with maps show that two aquifers, the regional and the local, exist (Aqua Well, 2013, Groundwater Survey, 1988, MEMR, 1987, Republic of Kenya, 1987).

The Ngelesh phonolites, or regional confined aquifer, was described by Sikes (1934) as the main aquifer in the Laikipia plateau. It is normally encountered within the weathered altered phonolites and the welded tuffs (Aqua Well, 2013), more precisely between Middle and Lower Rumuruti Phonolites. The aquifer further occurs in old land surface deposits, composed of sediment clasts and gravel in the clayey matrix (Groundwater Survey, 1988), and is developed between the saprolite and saprock of the various lava flows. The water is struck within the fractured zones of the phonolites. Accordingly, it gives rise to the local springs (Republic of Kenya, 1987).

The regional aquifer discharges to major joint swarms trending ENE (Aqua Well, 2013; MEMR, 1988) and to Ewaso Narok wetland. The aquifer's confinement (Kibson Consult, 2014; Republic of Kenya, 1987) is indicated by the difference between varying water levels (Fig. 6.5). The confinement is due to silicate weathering into clay material, which forms an impermeable layer above the aquifer (Hackman, 1988).

Weathering profile aquifers generally show confined to semi-confined conditions (Wright, 1992). They act as a storage layer for the infiltrating water, which eventually percolates into the underlying fractured rock aquifer, or as a reservoir for underground storage. Data of five wells from WRAP (Republic of Kenya, 1987) and further drilling wells gathered from owners show a big variation of transmissivities. The transmissivity closer to Ewaso Narok wetland (wells EGW53 and EGW32) varies between 14.8 to 30.7 m^2/day.

The second aquifer is the weathered crystalline basement rock (uppermost aquifer), referred to as the local aquifer. It occurs at times above the regional confined aquifer in the Ewaso Narok area. Just as the name suggested, this aquifer occurs in the weathered and fractured exposed gneisses basement (ESGHS, 2012; Kibson Consult, n.d.). Most of the groundwater is found in the thin layers of dark biotite schists. The only example of a well drilled in this aquifer is Kifuku well (Fig. 6.5). The transmissivity is 5.2 m^2/day (Republic of Kenya, 1987).

Both of the aquifers mentioned above are the exploitable groundwater resource in the Ewaso Narok area. Most of the yield to successful boreholes is the regolith with the deep-weathered bedrock (saprock) (Chilton & Foster, 1995; Chilton & Smith-Carington, 1984). The difference between the two aquifers' transmissivity values indicates that the regional aquifer could feed the local aquifer.

The perched aquifers in the area, seen in drilling wells, mainly occur in the decomposed weathered phonolites flow due to chemical weathering or by stream moving (Aqua Well, 2013; Geolink Associates, 2010; Groundwater Survey, 1988). They occur, in addition, in tuffs and in their contact with phonolites (Aqua Well, 2013). For example, the porous tuffs and Lapilli tuffs are well-developed aquifers and behave similarly to gravels and sand aquifers widespread in the area (Aqua Well, 2013). Further perched aquifers are formed in the lateritic zones, in the murram mantling high ground and lower depressions (ESGHS, 2012), and in the sediments of the alluvial system (Notter, 2003) along the main drainage channel (Paron et al., 2013).

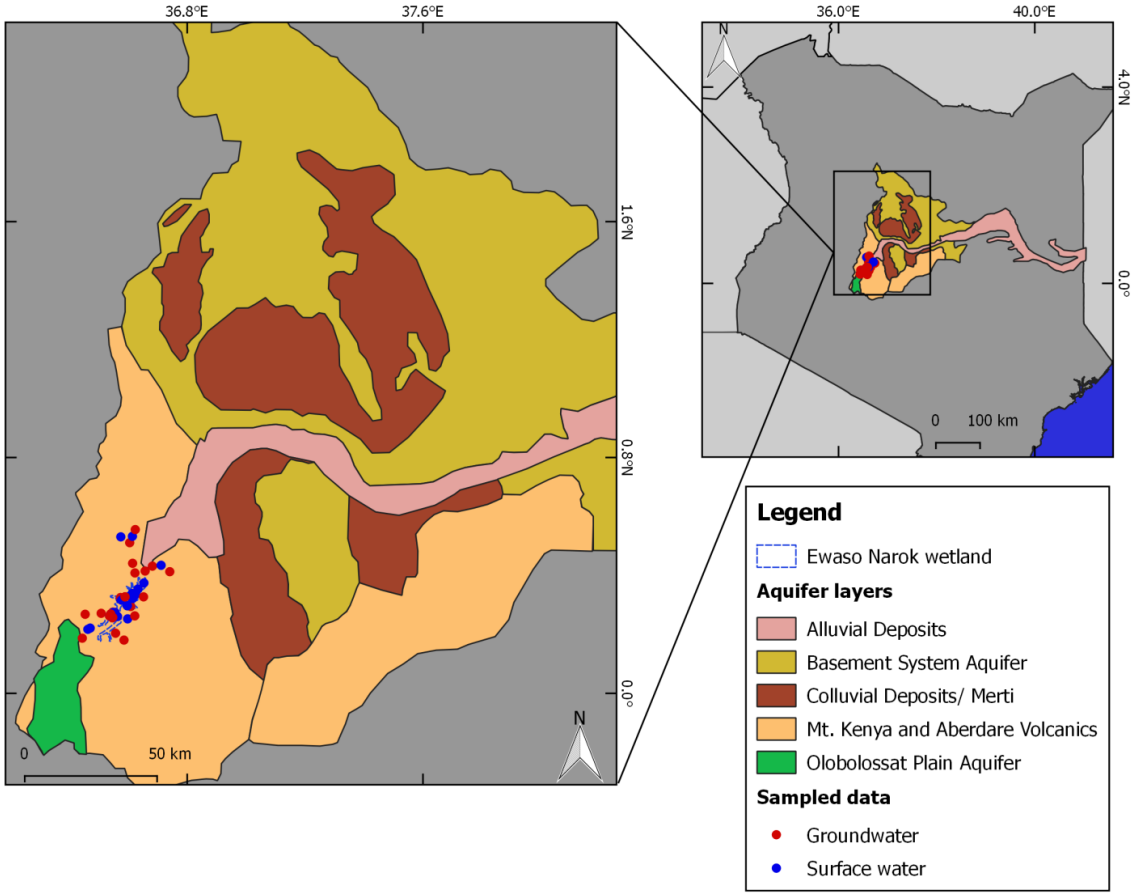

Fig. 6.6: Aquifers around the Ewaso Narok wetland. Georeferenced and modified after WRA (2020).

Recharge

There are two recharge mechanisms, direct and indirect, according to Allison et al. (1994), Allison (1988), and Foster (1988). Direct recharge is added to the aquifer through the unsaturated zone by direct percolation of rainfall, which can happen in the wetland. But, the percolating water may be used to fill soil moisture deficits and maybe be evapotranspirated before reaching the groundwater reservoir. Indirect recharge includes surface water, flood water entering the wetland through its beds, and water stored in fractured zones, which flows laterally.

Soils in Ewaso Narok wetland are made of Phaeozems and Solonchaks, thus allowing small amounts of water, if at all, to pass through (Aqua Well, 2013). The wetland lies in compact middle Rumuruti phonolites (Ewaso Narok Phonolites), making direct percolation of rainwater or recharge not possible unless it is through fissures, as weathered and fissured metamorphic rocks may contain isolated groundwater reserves. Schotterer and Müller (1985) emphasized that only a limited groundwater recharge occurs (Republic of Kenya, 1987) in volcanic slope regions in recharge areas. Ewaso Narok wetland lies on lower slopes where the groundwater usually emerges (Republic of Kenya, 1987).

Ewaso Narok river's side beds contain in addition clay, sand, and gravel (iron-stained quartz sand), which enable more water to flow through them. On the lower, steeper courses of the river courses, volcanic gravel is noticed. This means that runoff along the river courses is possible.

A further indication of the groundwater recharge status is that most of the tributaries rising on the Upper and Middle Volcanic Slopes are perennial, while tributaries rising on the volcanic of Laikipia Plateau are ephemeral (Samoka, 2010). This comes in terms with the calculated transmissivity values reported by Republic of Kenya (1987) discussed above.

6.2.2. Weathering and mineralogy

To understand the weathering processes in the Ewaso Narok wetland, 22 sampled soil and rocks (Tab. 5.2) were analyzed for their mineralogical content, major and trace elements, and content of carbon, nitrogen, and sulfur using XRD, XRF, and CNS (App. 7, App. 8, and App.9).

Samples taken from the same location are interpreted together, and a comparison of all the different locations is summarized in the end. Different layers of the river course soils (Fig. 6.7) and the exposed saprolite (Fig. 6.8) were observed on the field.

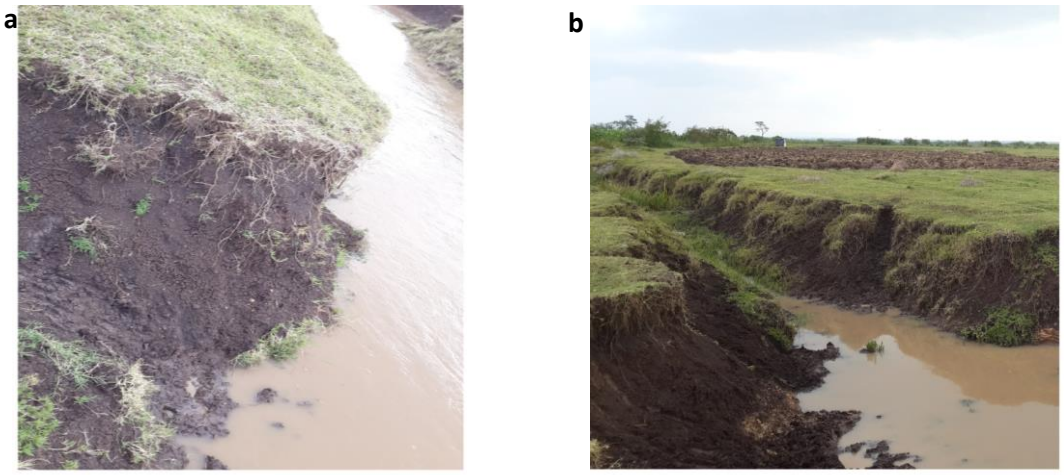

Fig. 6.7: Cross-section exposure of river course soils in the middle of Ewaso Narok: a. zoomed in profile, b. zoomed out profile.

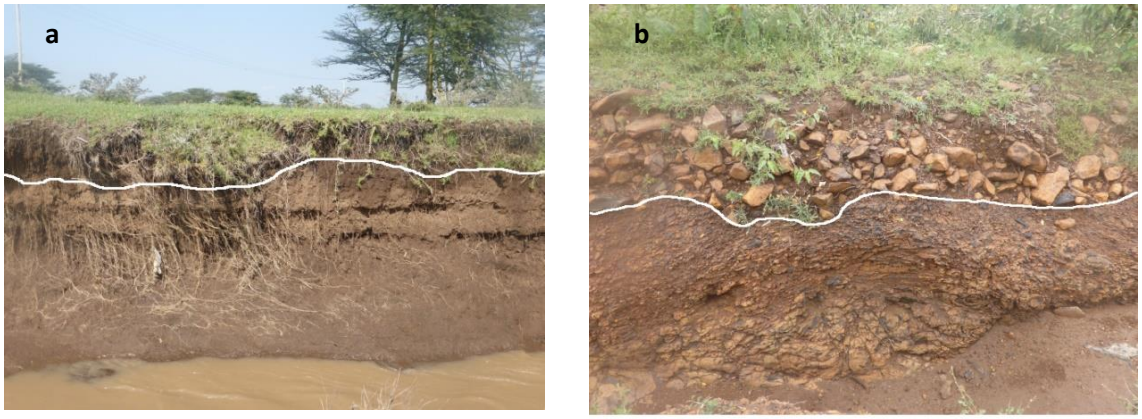

Fig. 6.8: Different layers (separated by a white line) and their weathering observed on the river courses in Ewaso Narok: a. the riverside, b. flooded wetland.

Continuously cultivated agricultural land

The continuously cultivated agricultural area, situated in the wet floodplain, is characterized by black and dark brown silt and clay mixed with murram. The two regolith samples are taken from

the same location but at different depths (R1: 70- 80 cm b.g.l, R2: 100- 110 cm b.g.l) (Fig. 5.1). The content of organic material is higher on the top layers, as vegetables are planted there. In both samples, illite/muscovite forms the main component, followed by K-feldspar, then calcite, then plagioclase, goethite, and a small percentage of quartz (Fig. 6.9). The elemental composition is similar in both samples, with an average of 45 % of SiO_2, 19.5 % of Al_2O_3 with 8 % of Fe_2O_3, and 7.5 % of CaO. The CIA index displayed an average of 64 %.

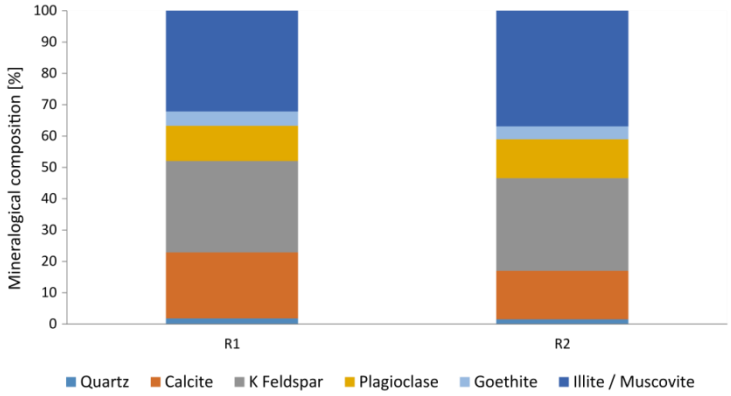

Fig. 6.9: Mineralogical composition of the samples R1 and R2 taken in the continuously cultivated agricultural land.

Fish ponds (grazing)

The fish ponds area is situated in the wet floodplain next to the furrow, where grazing takes place. It is characterized by brown, blackish, and murram soil. The four samples from this area are taken from the same grazing location (Fig. 5.1) but different depths (R3: 30- 65 cm b.g.l; R4: 100- 116 cm b.g.l; R5: 140 cm b.g.l; R6: 170- 178 cm b.g.l). The main component is K-feldspar followed by illite/muscovite. Other minerals composing these samples include goethite, quartz, kaolinite, and plagioclase (Fig. 6.10). Quartz is only present in the top layer and calcite in the deeper ones. Kaolinite is only present in the middle depth samples (R4 and R5).

Regarding the elemental composition, SiO_2 drops from 52 to 43 % with depth. The sample's elemental composition further constitutes of Al_2O_3 (average of 21 % for R3, R4, R5, and R6), then by Fe_2O_3 (average of 11.1 %). K_2O makes up an average of 3.1 %, and the rest of the oxides make up less than 1.5 %, except for CaO in deeper levels constituting 3 %, then 8 %. The CIA index drops from 84 to 60 % with depth. This again hints at higher weathering rates in the upper parts. The content of organic material increases with depth from 9 to 13.6 %.

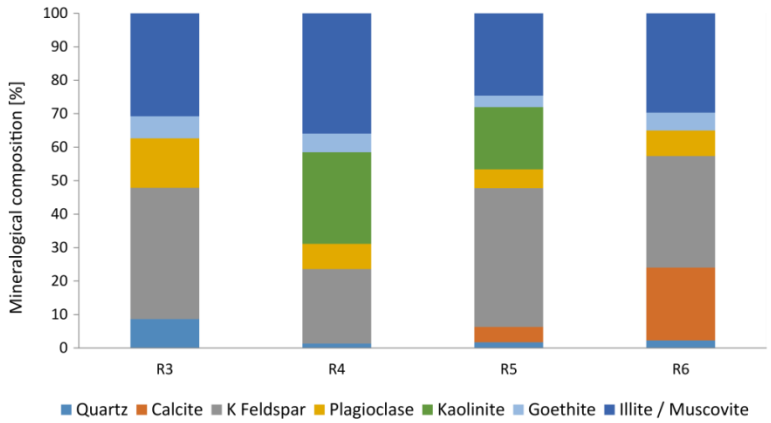

Fig. 6.10: Mineralogical composition of the samples R3, R4, R5, and R6 taken in the fish ponds (grazing).

River regolith (grazing)

This grazing area is in the flooded part of the wetland, surrounded by exposed phonolites, and is characterized by hard dark brown clay. The two samples are taken from different locations (Fig. 5.1) from the river regolith and at different depths (R7: 120 cm b.g.l.; R8: 76 cm b.g.l.). In both samples, illite/ muscovite form the main component, followed by K-feldspar, then plagioclase, quartz, and goethite (Fig. 6.11). The content of organic material is 7-8 %.

The CIA of R7 and R8 is 75 % and 79 %, respectively. Regarding the elemental composition, SiO_2 makes up 56.5 % in R6 and 55.6 % in R7. Al_2O_3 shows an average of 18.5 %, followed by Fe_2O_3, making up 9.5 %, K_2O around 3 %, and Na_2O with around 2 %, followed by TiO_2 of 1 %. The rest of the oxides contribute to less than 1 %.

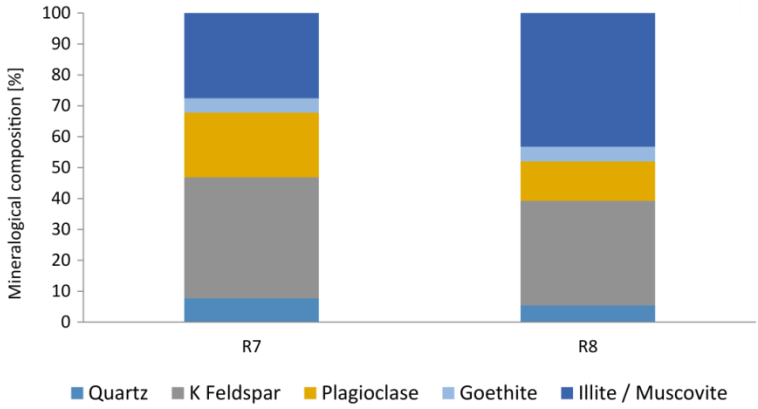

Fig. 6.11: Mineralogical composition of the samples R7 and R8 taken in the river regolith (grazing).

River regolith (seasonally cultivated)

River regolith samples R9, R10, and R11 (Fig. 5.1), are situated in the wet floodplain, in a seasonally cultivated area, characterized by dark brownish colours, that broke easily, was very soft, and well sorted. The samples are taken from the same location from different depths (R9: 31 cm, 60 cm and 90 cm b.g.l.). The content of organic material increases with depth. Illite/ muscovite forms the main component, followed by K-feldspar (6.12). Minor percentages of goethite, quartz, and plagioclase are present. R9 is the only sample from all the samples with a quartz percentage of more than 10 %. Plagioclase is only detected in the upper layers, whereas

calcite is in the deeper ones. Higher weathering rates in the upper layers are seen as K-feldspar increases with depth and goethite decreases with depth.

The CIA index decreases from 78 to 62 % with depth, again hinting at weathering being more dominant at the top layers. The element composition, both of R9 and R10, show similar results, of SiO_2 making up almost 53 %, Al_2O_3 making up 19 %, Fe_2O_3 making up 10.5 %, K_2O making up 2.9 %, and MgO, CaO, and Na_2O making up between 1 to 3 %.

Sample R11, however, shows slightly lower values of SiO_2 with 47 %, Fe_2O_3 making up 9 %, and CaO making up to 6.7 %. All the rest of the oxides make up less than 3 %.

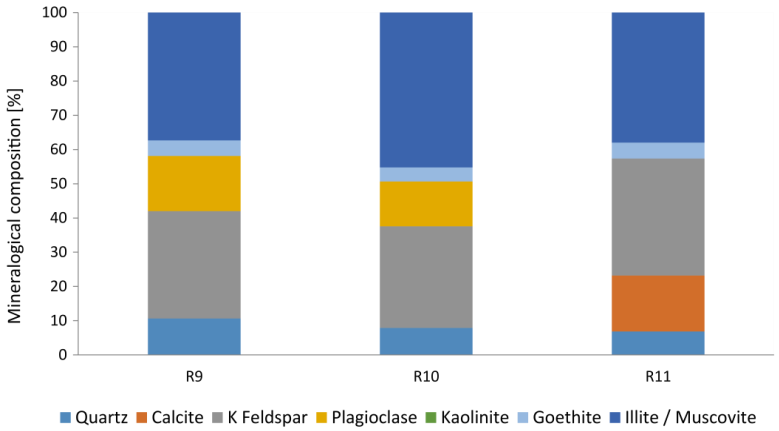

Fig. 6.12: Mineralogical composition of the samples R9, R10, and R11 taken in the river regolith (seasonally cultivated).

River courses (grazing)

R13 and R14 are sampled outside the wet flooded, yet on the stream in a grazing area (Fig. 5.1). The two samples are taken from the same location from different depths (R13: 100 cm b.g.l, R14: 160 cm b.g.l). Illite/ muscovite form the main component (6.13). In the upper part, plagioclase prevails, while in the deeper layers, K-feldspar prevails. Calcite is detected in the deeper sample. K-feldspar increases with depth, confirming more weathering in the upper layers. Sample R12 is sampled from an adjacent location at a depth of 130 cm b.g.l. It has a similar composition to both R13 and R14, with a small percentage of kaolinite. The content of organic material is 7.8 % in R12 and 8.6 %, and 9.5 % for R13 and R14.

The CIA drops from 81 to 76 % with depth. The elemental composition of the three samples shows similar compositions. SiO_2 is the highest of all samples, with an average of 52.2 %. Al_2O_3 shows an average of 21 %, followed by Fe_2O_3 of around 10 %, K_2O around 3 %, and all the other oxides less than 2 % except for R14 with CaO of 2.6 %.

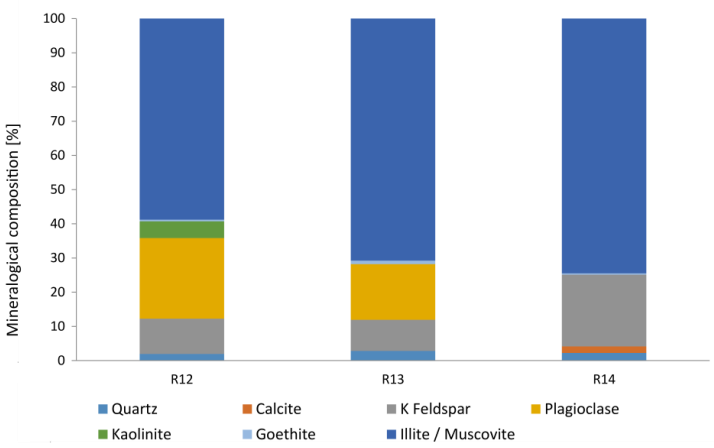

Fig. 6.13: Mineralogical composition of the samples R12, R13, and R14 taken in the river courses (grazing).

Papyrus area (slash and burn)

The papyrus area within the wet floodplain is characterized by dark-colored soils. The two sediment samples from this area are taken in indifferent depths (S1: 89 cm b.g.l.; S2: 128 cm b.g.l.). The content of organic material increases with depth from 9 to 14.5 %. In the upper part (S1), illite/ muscovite form the main component, while K-feldspar prevails in the deeper one (Fig. 6.14). Kaolinite is only detected in the upper layer and calcite in the deeper one. Additional proof for higher weathering rates in the upper part gives the increase in the percentage of goethite, quartz, and plagioclase with depth. But, the presence of goethite and plagioclase in both samples hints that weathering occurs at both depths.

The CIA drops from 83.8 to 60.4 % with depth. Regarding the elemental composition, SiO_2 also drops from 54 to 43 %, indicating silicate weathering on the top layers. Al_2O_3 drops from 22.5 to 19 %. CaO increases from 0.6 to 9 %. The occurrence of the other elements shows no variation with depth.

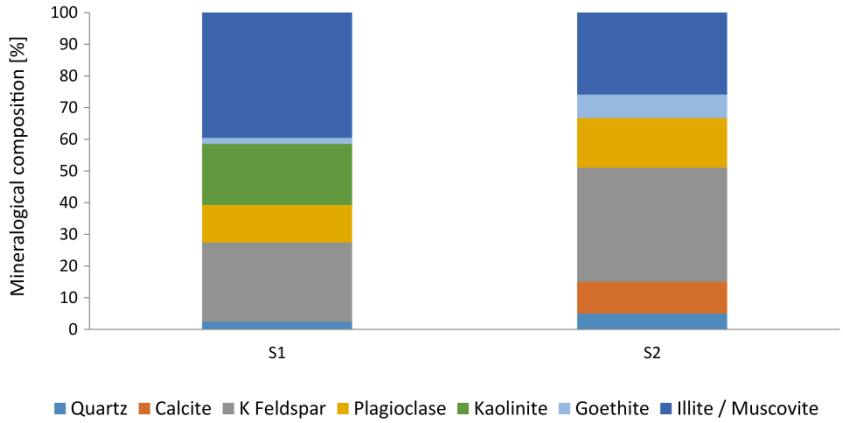

Fig. 6.14: Mineralogical composition of the sediment samples in the papyrus area (slash and burn) taken from a profile at different depths (S1: 89 cm b.g.l.; S2: 128 cm b.g.l.).

Papyrus flooded area (continuously cultivated)

The flooded Papyrus area is characterized by dark black, fertile, and sandy alluvial soil. The three sediments are taken from different locations and depths (S3: 40 cm b.g.l.; S4: 120cm b.g.l.; S5: 50cm b.g.l.). The mineral composition of the three samples is very similar, with illite/muscovite being the main component. A smaller percentage of kaolinite and k-feldspar further prevail

(Fig. 6.15). Intense weathering is indicated as no plagioclase, and little K-feldspar exists. The content of organic material varies between 14.6, 15.2, and 18.7 % for S4, S3, and S5, consecutively. Their elemental composition is similar, with around 49 % SiO_2 , followed by Al_2O_3 (19 %) and Fe_2O_3 (10.5 %). With the exception of K_2O (1.1 %) and TiO_2 (1.2 %), the other oxides make less than 1 %. Compared to all the samples taken K_2O is the lowest and P_2O_5 the highest value in those three samples. The three samples are organic-rich, with high levels of total nitrogen and total carbon. An average CIA index of 89 % for the three samples proves intense weathering in the flooded area.

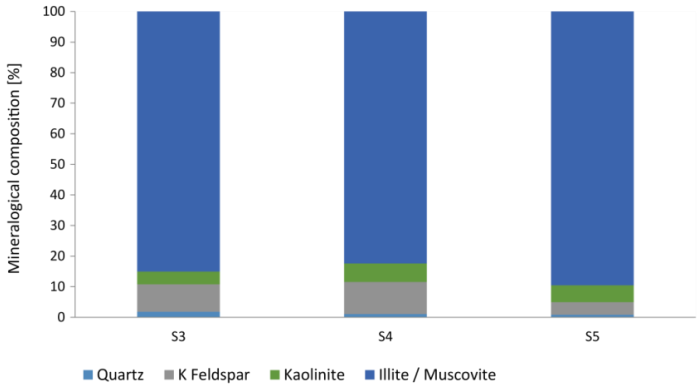

Fig. 6.15: Mineralogical composition of the samples S3, S4, and S5 taken from the papyrus flooded area (continuously cultivated).

Rocks

The rocks (samples R15, R16 and R17) were collected from different locations from the exposed fractured rock in the Ewaso Narok floodplain: laterite / murram (Fig. 6.16) and two basalts (Fig. 6.17 and 6.18).

Fig. 6.16: Laterites from the R15 sampled in the field: a. Outside view, b. Inner view.

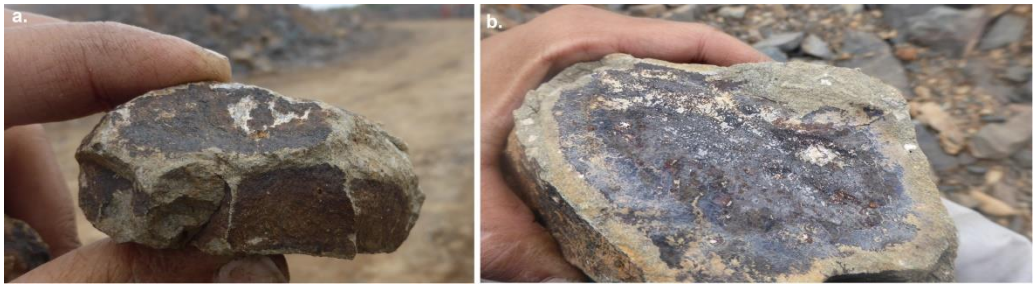

Fig. 6.17: Field samples of basalt (R16): a. The whole rocks, b. Parts of the rock.

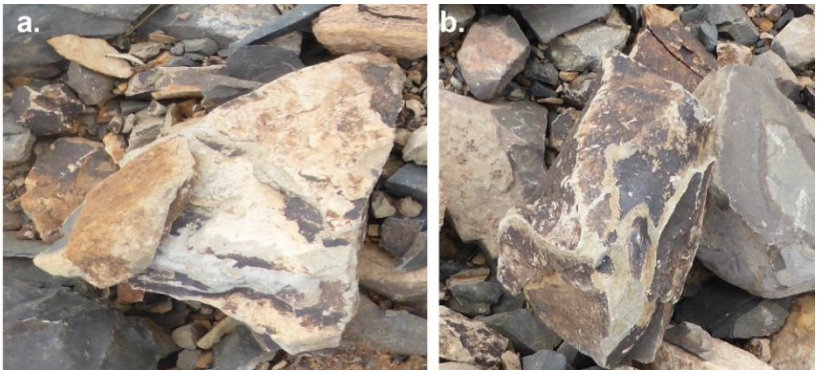

Fig. 6.18: Field samples of basalt (R17): a. The whole rock, b. Parts of the rock.

Half of the mineral composition of the **laterite** (R15) is K-feldspar, followed by kaolinite (25 %) and goethite (9 %), both of which are a result of weathering. Illite/muscovite constitutes around 8 % and plagioclase less than 6 % and 1 % quartz (Fig. 6.19). The laterite (R15), locally called murram (Fig. 6.16), is formed by leaching after intensive and long-lasting weathering in dry and wet conditions. They are rich in iron, and aluminum giving them the red color (Aqua Well, 2013; WRMA, 2013b). The elemental composition shows SiO_2 (41 %), Al_2O_3 (9 %), and Fe_2O_3 (22 %) as main components. Other oxides higher than 1 % included MnO (3 %), Na_2O (1.1 %), and K_2O (4 %). The CIA is 77 %. The lateritic weathering leaches silica and magnesia and leaves a residue mainly of iron hydroxides. Lateritic deposits form an impermeable lateritic soil which usually is less than 7m thick (Bell, 2013). The LOI result of R15 were 8.38%.

The two basaltic rocks differ in their mineralogical composition. R16 is mainly composed of K-feldspar (56 %) with contributions of Illite/muscovite (21 %), kaolinite (18 %), and a small percentage of plagioclase and goethite (Fig. 6.19). The elemental composition shows SiO_2 prevailing (53 %), with Al_2O_3 (24 %) and Fe_2O_3 (6.5 %). Na_2O makes 2.7 %, K_2O of 6 %, and all other oxides less than 1 %. The CIA is 73 %. R17 has a higher content of K-feldspar (76 %), followed by kaolinite (18 %), illite/ muscovite (10 %), and goethite (5 %) (Fig. 6.19). Its elemental composition was similar to sample R15 (App. 7) . The CIA is 75 %. The percentage of K_2O in samples R15, R16, and R17 are higher than in other samples (App. 8). The LOI results of samples R16 and R17 are 6.14 % and 7.81 %, respectively.

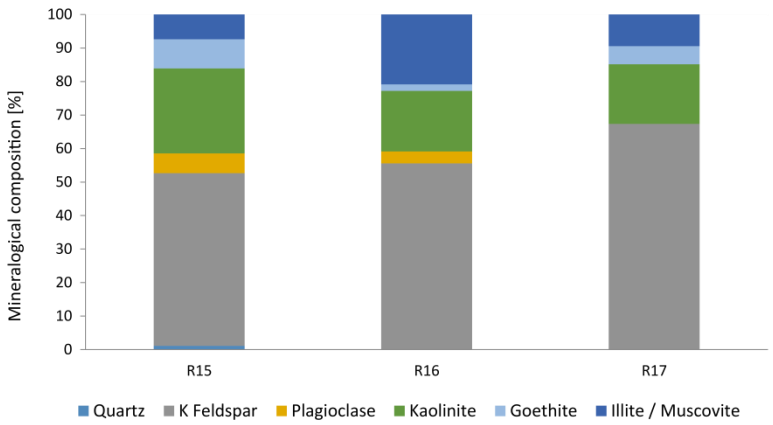

Fig. 6.19: Mineralogical composition results of Laterite R15, Phonolite R16, and R17.

Comparison of samples

In most of the samples illite/muscovite prevail (Fig. 6.20). Illite results from the weathering of silicates, mainly feldspar, and muscovite. K-feldspar is the second dominant mineral and makes most of the solid rocks. If the samples were totally weathered, all feldspar would have been decomposed into clay minerals. The K-feldspar increases with depth, confirming more weathering on top. The weathering profile is further composed of kaolinite, goethite, and small proportions of quartz and calcite. Goethite is formed from the weathering of magnetite and demonstrates extreme leaching. The sequence of weathering products, going from montmorillonite over kaolinite to gibbsite, reflects the increasing leaching intensity. It removes silica and cations from the rock (Appelo & Postma, 2005). Kaolinite, the weathered form of plagioclase feldspar, is present in the three rock alluvial sediments samples and two of the regolith samples. Al_2O_3 can be correlated with feldspars and clay minerals (e.g., kaolinite). However, the percentage amount of Al_2O_3 does not change even though those of kaolinite and feldspar do.

In the form of goethite, iron-hydroxide is present from the weathering of iron-rich minerals and indicates prolonged ferralitic weathering (Appelo & Postma, 2005). Its presence is visible in most of the samples except for the sediments (Fig. 6.20).

Calcite exists in some samples and is usually deposited by either groundwater solutions or hydrothermal solutions and most commonly has a biogenic origin (Nichols, 2009). The calcite source is the calcrete deposits and calcareous sediments in the area originating from the Miocene sedimentary rocks and the Samburu episode (Aquatreat, 2013; ESGHS, 2012; Hackman, 1988; Kibson Consult, n.d.; Republic of Kenya, 1987). Calcite is found at a depth of around 90 to 140 cm from the ground surface. Ca^{2+} variation is noticed as water goes up and down in the sampling when flooding occurs.

The muscovite's weathering sequence is muscovite → muscovite/ montmorillonite → montmorillonite → kaolinite (Gour et al., 2014; Stoch & Sikora, 1976). This weathering from muscovite to kaolinite is seen in Equation 6.1.

$$2KAl_2(Si_3AlO_{10})(OH)_2 + 2H^+ + 3H_2O \text{—->} 1.5Al_4(Si_4O_{10})(OH)_8 + 2K^+ \quad \text{(Eq. 6.1)}$$

All samples had muscovite, and some had kaolinite in addition. Thus they were either not weathered or totally weathered, or the kaolinite is from another source. Another explanation is that the main weathering product was illite and not muscovite. But, it is impossible to differentiate both in the XRD. However, the literature shows that illite is widespread in the area and that muscovite is less common yet was produced during the Samburu episode.

Illite occurs as an altered form of muscovite and feldspar in weathering. Illite is similar to muscovite but has lower K_2O content and higher H_2O content than muscovite (Fanning et al., 1989; Srodon & Eberl, 1984). Illite is a product of mica's weathering or collapse of the high-charge smectite layer around K-ions (Thompson & Ukrainczyk, 2002).

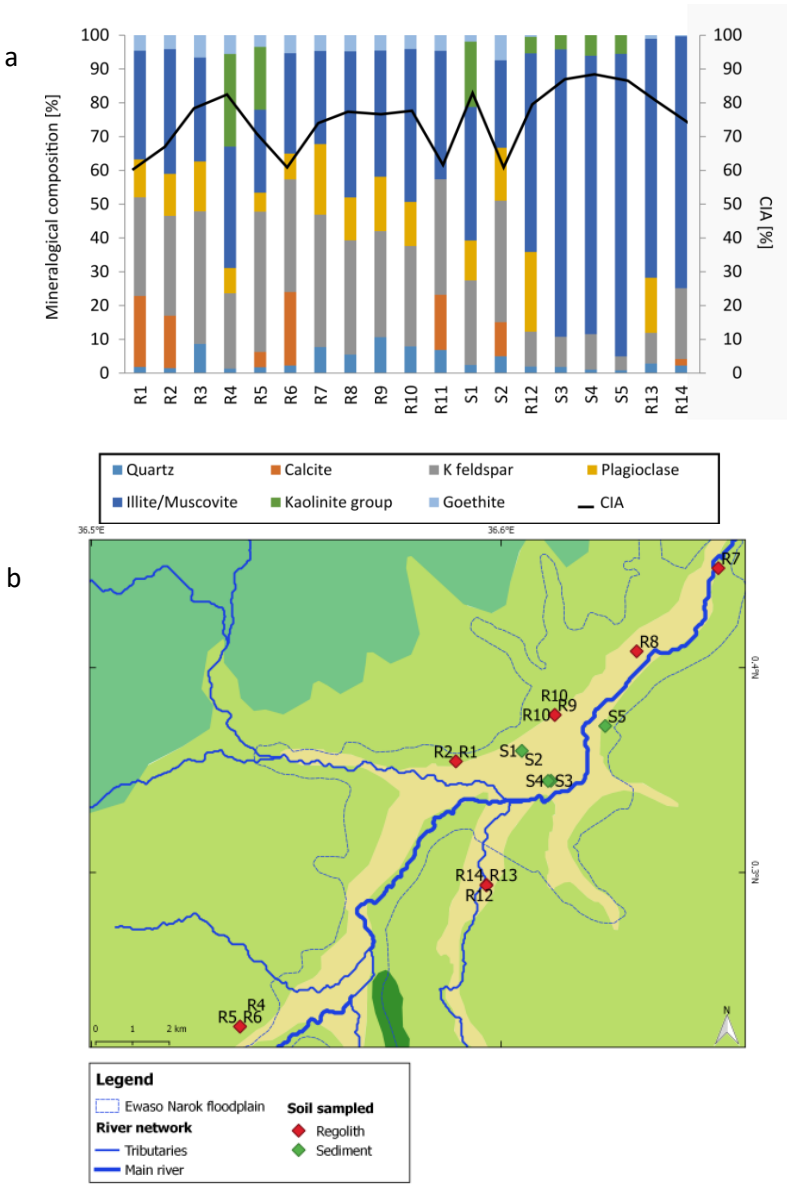

Fig. 6.20: Samples taken from the alluvial year-round flooded wetland sediments (S) and the saprolite's regolith (R): a. The mineralogical composition and CIA values, b. Location of the samples, drawn on the geological map (cp. Fig. 2.9, p.19).

To sum up, silicate weathering is dominant in the Ewaso Narok wetland, with the top areas being more weathered, as seen in LOI results and feldspar content in the soil. The CIA ranged between 65 and 91 % depending on the kind of soil, the depth, the area's use, and its weathering. The highest CIA is seen in the sediment samples (organic layer) in the floodplain, followed by the solid rocks (bedrock) and top layers, indicating high weathering in the upper layers. High values of LOI are in the sediments confirming organic content. The weathering profile mainly compromises of K-feldspar and illite/muscovite with mixed proportions of plagioclase, kaolinite, calcite at times, and small amounts of quartz and goethite. Laterites soil is encountered, displaying an average of 41 % of SiO_2, with Al_2O_3 as 19 % and Fe_2O_3 as 22 % with the remaining percentages for MnO, MgO, CaO, K_2O, Na_2O, P_2O5, TiO_2, and SO_3.

The top layers are dominated by kaolinite and with Fe^{2+} in the form of goethite. Although parents' rocks are variable, progressive leaching of the more mobile elements Na^+, K^+, Mg^{2+}, is

evident in the saprolite. As iron and aluminum are the least mobile elements, they are found in the upper parts of the weathering profiles as hydroxides or as residual minerals. As these layers are destroyed by erosion, they move by mechanical processes, more precisely colluvial on slopes and river water suspension.

Al_2O_3 varies between 17 and 24 % and tends to be concentrated in the residual weathering products because of its low solubility (Ceryan, 2012). FeO remains relatively constant even though it might change from ferric to ferrous (Ceryan, 2012). There was a big range in the samples as the saprolite samples showed Fe_2O_3 of 23 %, whereas others did not exceed 7 %.

The amount of MgO is below 1.5 % in all the samples. MgO is leached and removed in the early stages of the chemical weathering, but a certain amount is retained in the clay's mineral structure, where it is adsorbed (Ceryan, 2012).

As expected, all sediment, regolith, and rock samples can be traced back to the Miocene Cenozoic volcanic rocks of the Laikipia plateau described in Chapter 2.3.2 and 2.3.4 (Tab. 2.3 and Tab. 2.4). The sediments (S1 to S 5) indicate basalt, basanite, and basaltic andesite as the rock source (Fig. 6.21). The hard rock indicates basaltic trachyandesite and tephrite andesite as the rock sources (Fig. 6.21). The regolith indicates basalt, basaltic andesite, trachybasalt, and tephrite basanite as the rock source. The layers above the crystalline basement in the Ewaso Narok area range from alkali-basalts to trachytes and phonolites (Republic of Kenya, 1987). As the weathering of basalt leads to the formation of kaolinite and iron oxide goethite (Asio & Jahn, 2007), the results come in terms with the mineralogical results presented above.

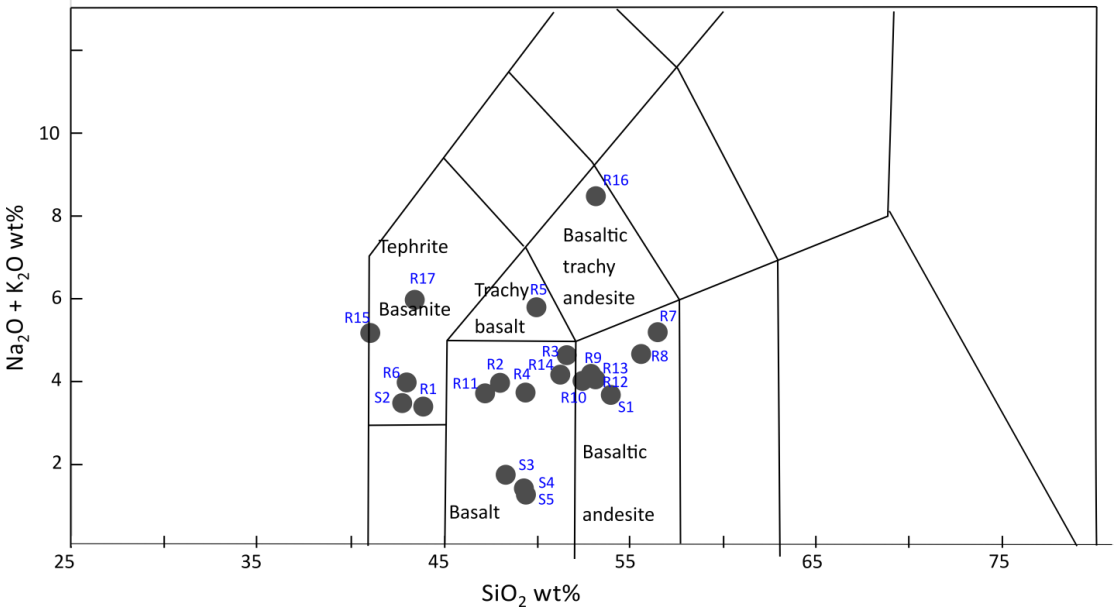

Fig. 6.21: Total alkali-silica (TAS) diagram of the samples (after Maitre et al., 2002).

A detailed description of the results shows that R1, S2, R6, R15, and R17 are weathering products of tephrite basanite. Samples R2, R3, R4, R11, R14, S3, S4, and S5 are a weathering product basalt. R5 is weathered from trachybasalt, and more precisely, potassium-trachybasalt according to the relative amounts of Na_2O and K_2O as Na_2O minus two is less than K_2O. R7, R8, R9, R10, R12, R13, and S1 are weathering products of basaltic andesite. R16 is a weathering product of basaltic trachyandesite, and more precisely, shoshonite as $Na_2O - 2 \leq K_2O$.

6.2.3. Water dynamics

6.2.3.1. Piezometer installations and water flow

Ten piezometers (twenty pairs) were placed at different depths and locations to evaluate the magnitude of vertical flow (Fig. 6.22). GW31, installed next to another piezometer, shows **stagnant water** as no head gradient exists between both piezometers. GW14, installed next to another piezometer, shows that the water flows **vertically downward** to recharge the groundwater. The shallow piezometer intercepts a higher hydraulic head than the deeper one. The eight other piezometer pairs installed for water flow measurements show that on the wet floodplain, no change is noticed after floods, and the water gradient is zero. Regarding the area outside the wetland after floods, a recharge is noticed in two piezometers, indicating direct local recharge and infiltration. In the rest of the piezometers in the floodplain and river courses, discharge is noticed at all times, indicating that groundwater feeds the surface water, as seen further with the springs.

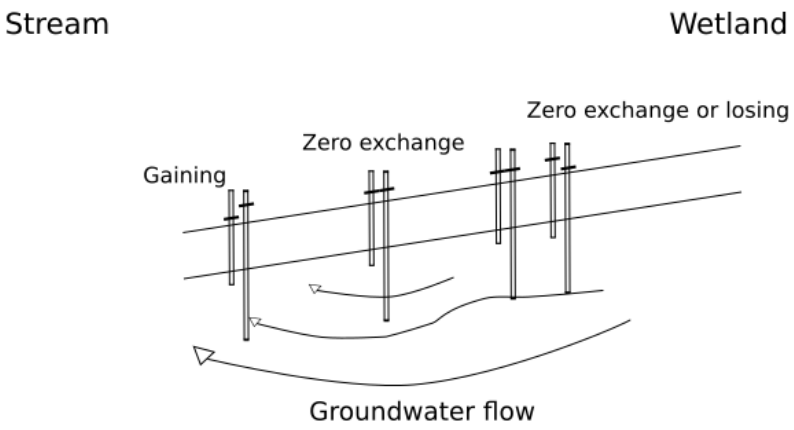

Fig. 6.22: Cross-section showing the piezometer results. The vertical lines indicate the position of open-ended piezometers, and the horizontal bars show the water level in them.

6.2.3.2. Creation of piezometric maps

Using the measured water levels collected by Muriuki Karugi (2016) and calibrated water table in addition to the piezometers installed and data acquired from WRMA, the groundwater flow direction was calculated. Data sets were integrated from different sources. They were compared with the data available from the literature, and it was found that they interplace each other feasibility. A map is generated (Fig. 6.23).

The water tables rise and fall with time. However, the general groundwater flow is northeastward in the Middle and Lower Phonolite series of the Plateau series, both inside the wetland and surrounding area. An exception occurs in a small part of the lower basin in the wetland (Fig. 6.24), especially during the summer. In this part, groundwater flows from both the north and south part, as seen from the installed piezometers results. It is important to remember that along with the Ewaso Narok River, there is high fracturing intensity, and accordingly, the hydraulic gradient is expected to be high.

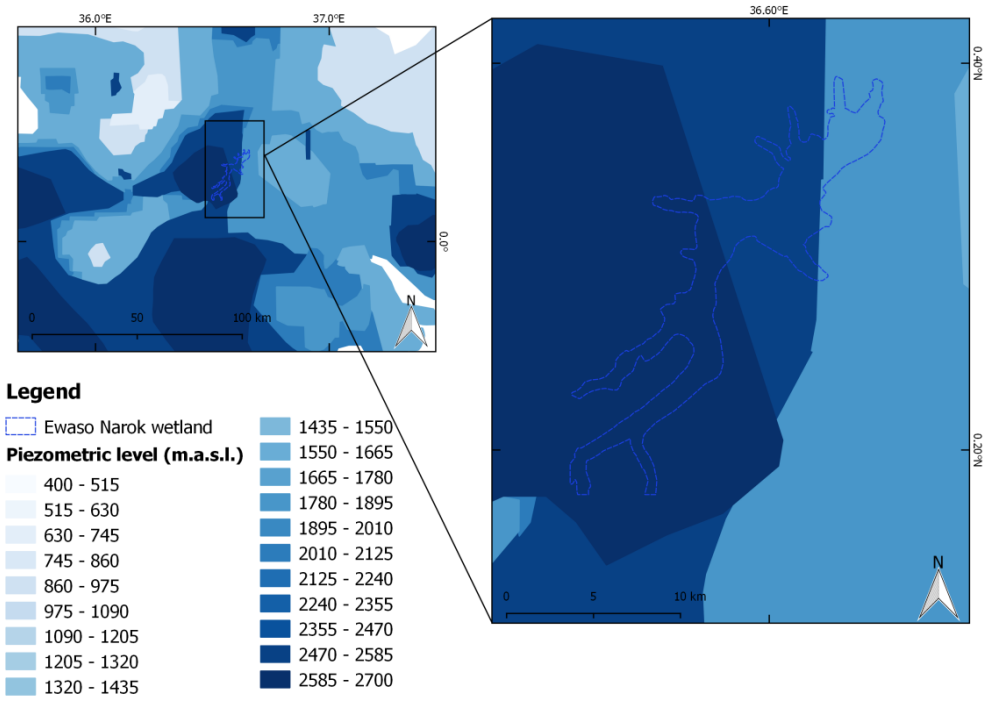

Fig. 6.23: Groundwater flow and piezometric levels. Sources: WRMA/ drilling logs/ Paron et al. (2013).

Wells from secondary sources were additionally used to add to the available data. In addition, their positions, depths, and SWL were recorded, which accounts for the water level in this case (the elevation or level of the water table in a well when the pump is not operating). It is important to keep in mind that the static groundwater levels at different points were not measured simultaneously, thus might lead to uncertainties. Further uncertainties in hydraulic heads may arise from the DEM elevation data.

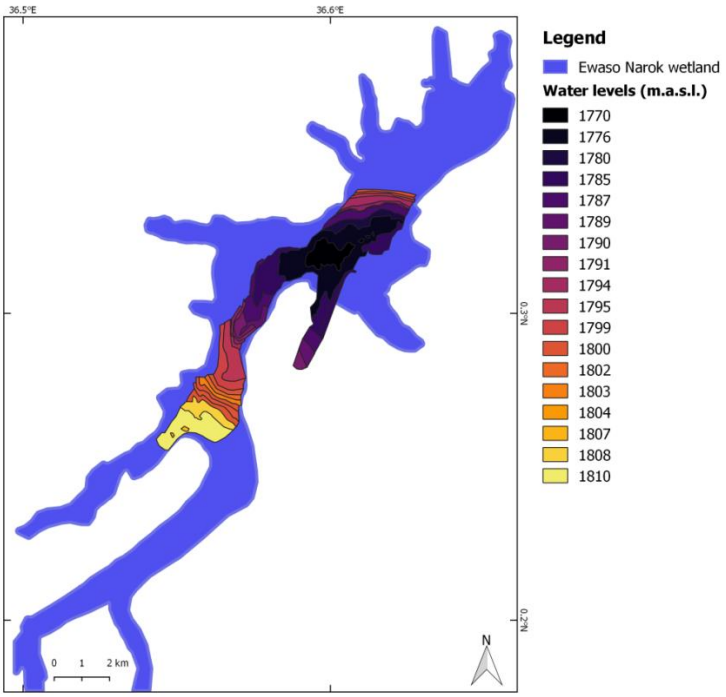

Fig. 6.24: Water levels inside the wetland. Sources: Field measurement and Muriuki (2016).

6.3. Water composition

The following section discusses groundwater and surface water composition. It starts with in-situ water parameters (App. 1), followed by hydrochemical water analysis (App. 2). The water quality results are discussed afterward, followed by the stable water isotopes (App. 3) and the hydro-geochemical processes occurring in this system.

Surface water points are divided into the tributary streams leading to the wetland, the main river inside the wetland, the wetland when flooded, the wetland dry, the effluent, and the dams.

Groundwater is divided into shallow groundwater, deep groundwater, and the spring. The shallow groundwater is sampled at wells and piezometers up to 3 m depth. The deep groundwater is sampled at pumping wells between 10 and 200 m depth.

6.3.1. In-situ parameters

The specific electric conductivities (EC) representing surface water's mineralization ranged between 94 and 1,697 µS/cm (Fig. 6.25 and Fig. 6.26). The median was 189 µS/cm, and most of the samples were between a narrow range of 133 and 224 µS/cm. The outliers were the effluent [1697 µS/cm], SF51 [395µS/cm], SF26 [570 µS/cm]. The EC values of groundwater ranged between 272 and 4,470 µS/cm with a median of 1,342 µS/cm, and most of the samples ranged between 934 and 1,594 µS/cm. The pH values of surface water showed both basic and acidic water, whereas the groundwater had a bigger range of basic and acidic samples. The outlier to the surface water is the effluent [pH = 9.2] (Fig. 6.25). Oxygen content (O_2) varied both in surface water and groundwater. However, most of the samples had a concentration between 85 and 103 mg/l for surface water and 44 and 90 mg/l for groundwater. Outliers are GW11 [161.7 mg/l] and GW41 [174.4], SF33 [20.1], and SF34 [52.6] (Fig. 6.25). The redox potential was higher for surface water than for groundwater samples. The outlier is the effluent [81.7 mV], SF39 [754.7 mV], and GW5 [-152.8 mV] (Fig. 6.25).

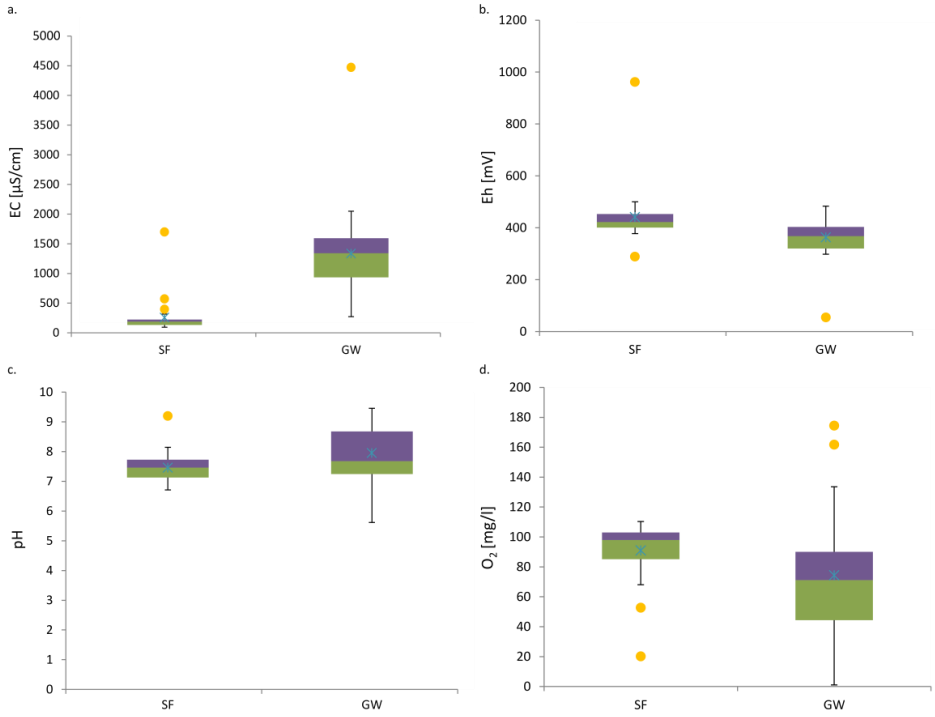

Fig. 6.25: Boxplot of in-situ measured parameters for surface water and groundwater: a. Electric conductivities, b. Redox potential, c. pH values, d. Oxygen content.

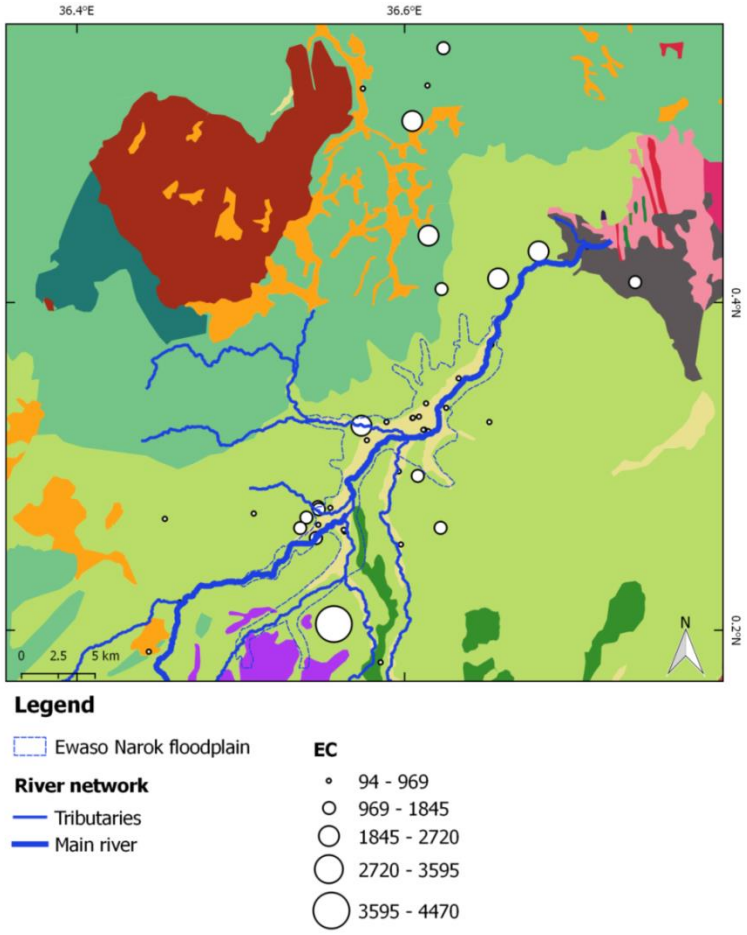

Fig. 6.26: Specific electric conductivity (EC) of the sampled water points, drawn on the geological map (cp. Fig. 2.9, p.19).

6.3.2. Hydrochemical water analysis

The results of the water sampling are seen in App. 2. For graphical representation, ***Udluft*** and ***Piper*** diagrams were chosen to display the composition of anions and cations (Güler et al., 2002). Certain selected determinant values are presented in the following (Tab. 6.4). Calcium, magnesium, chloride, silica, and sulfate were higher values were higher for groundwater than surface water. Samples whose ion charge balance errors were higher than |10 %| were discarded from any further analyses.

Tab. 6.4: Selected parameters' range values in surface and groundwater.

Determinant	Source and value	
	Surface Water	Groundwater
pH	6.7 - 9.2	5.6 - 9.5
Calcium [mg/l]	0.9 - 24	1.8 - 121
Magnesium [mg/l]	1.2 - 4.3	0.3 - 42.9
Chloride [mg/l]	4.9 - 123.2	7.4 - 253
Silica (SiO_2) [mg/l]	12.3 - 34.5	5.2 - 66.4
Sulfate (SO_4) [mg/l]	2.4 - 39.1	4.1 - 128.8

The water type in both surface water and groundwater is mainly classified as Na^+-K^+-HCO_3^--type, as sodium plus potassium and bicarbonate, is the predominant cation and anion, respectively (Fig. 6.27). This is typical water influenced by ion exchange. The shallow dug wells, and the water of the dam had water of sodium chloride type, whereas the installed piezometers, some deep wells, and the spring had sodium chloride water type.

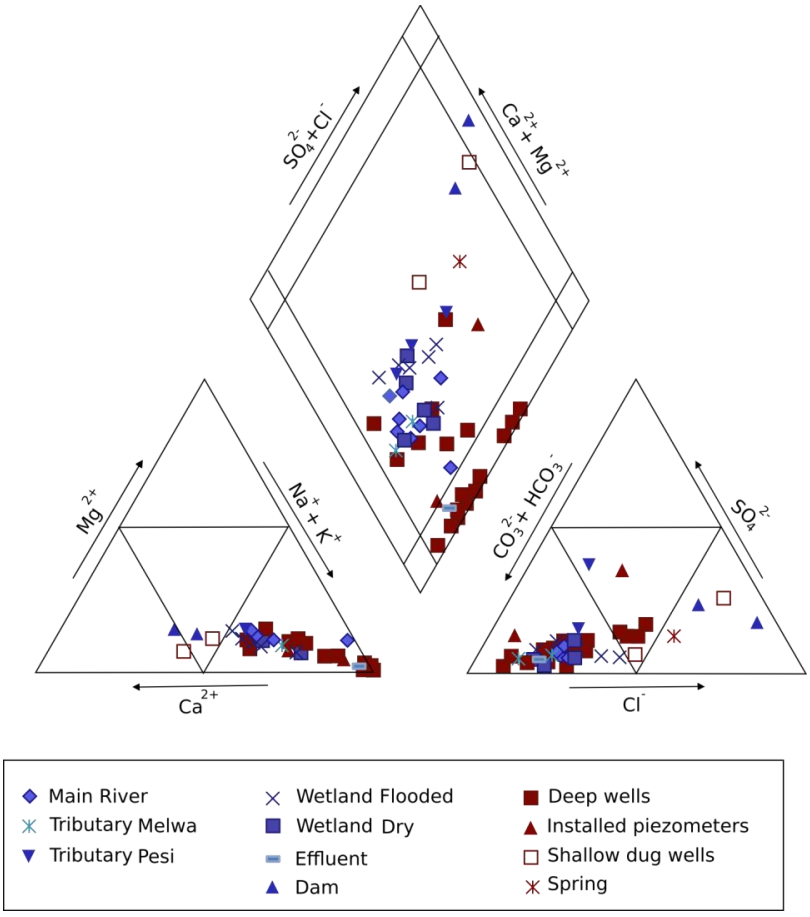

Fig. 6.27: Piper diagram for the surface water and the groundwater sample points.

The above for-mentioned results were compared with the Piper classification diagram for anion and cation facies after (Back, 1966; Morgan & Winner, 1962) in terms of major-ion percentages.

Sodium bicarbonate is a result of the weathering of silicate minerals in igneous rocks. As the aquifer and rocks contain silicate minerals, this might be another indication for its weathering leading to higher silica values between 12.3 and 34.5 mg/l in surface water and between 5.2 and 66.4 mg/l in groundwater. Silica released by weathering is transported underground and along river water. Part of it remains in the weathering zone, as it precipitates in the joints and fractures of the rocks as silica. Bicarbonate tends to predominate in water in areas where vegetation is grown profusely (Hem, 1985), which might be the reason for the surface water as the wetland is heavily dense with vegetation.

The groundwater results (Fig. 6.28) follow similar hydrochemical trends, showing similar lines with slight yet moderate differences, given the subgroup's spatial variabilities. Silica differs between all the subgroups, nitrate is higher in deep wells, and sulfate is lower in shallow wells. A noticeable difference exists between the deep and shallow wells. The piezometer results lie between the deep and shallow wells emphasizing the fact that it taps the groundwater. The spring shows similar results to the groundwater in general, emphasizing that some groundwater feeds the surface water. No clear distinction between the water in both the confined aquifers in terms of quality is observed.

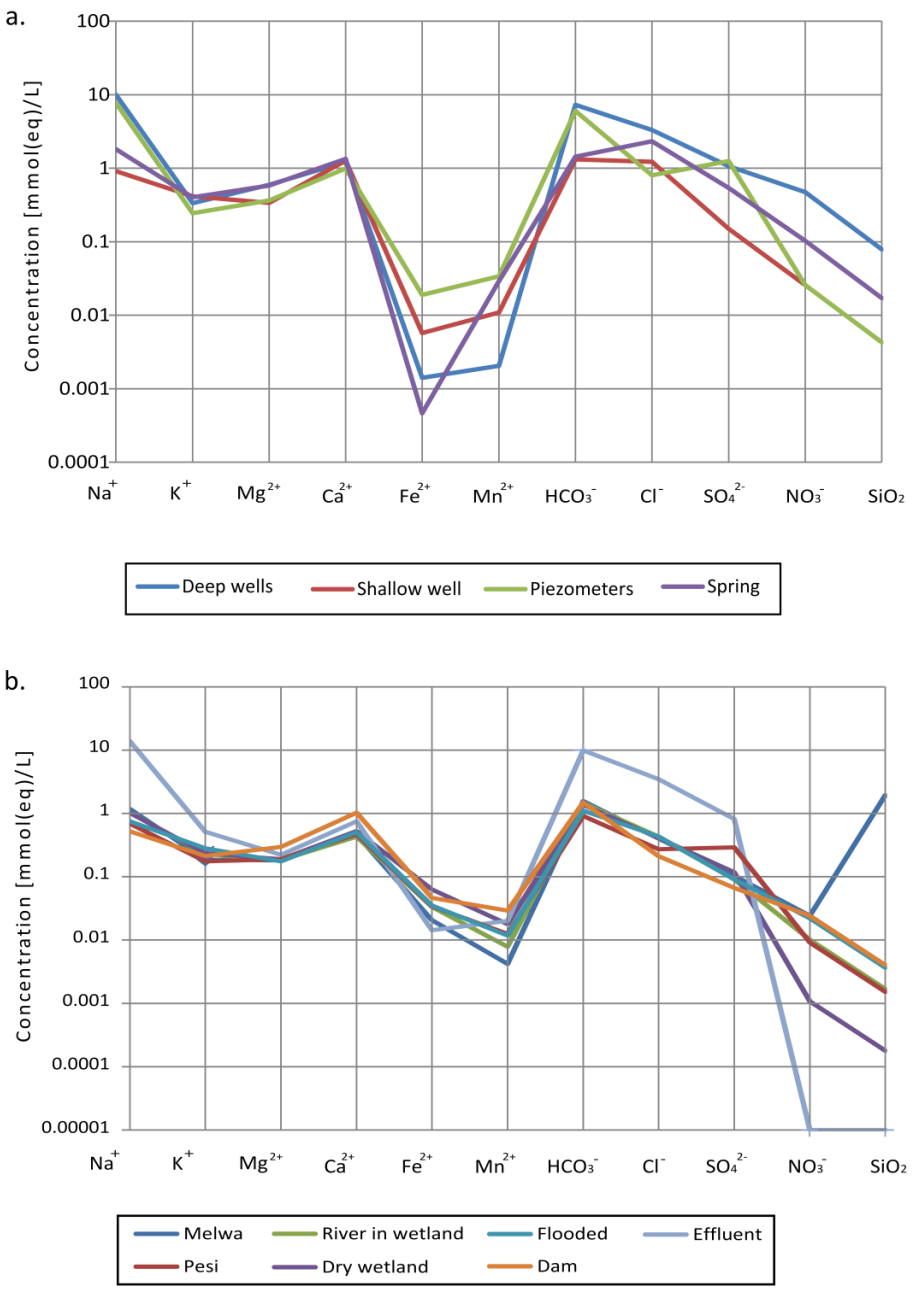

Fig. 6.28: Schoeller diagrams based on the average values of a. Groundwater and b. Surface water.

The surface water samples (Fig. 6.28) have similar hydrochemistry and follow the same trends except for the effluent. Silica, however, differs and is highest in the tributary Melwa, upstream of the wetland, and very low in the dry wetland. The effect of silicate weathering on water chemistry is primarily the addition of cations and silica. Accordingly, HCO_3^- and SiO_2 were used as indicators of silicate weathering (Appelo & Postma, 2005). The tributary Pesi, again upstream of the wetland, has a higher sulfate content compared to the rest of the surface water samples. The surface water samples taken in the dry period in the wetland have lower nitrate. The composition of the river in the wetland is comparable to the composition of his tributary streams, Pesi and Melwa.

TDS of the sampled points

Total dissolved solids (TDS) comprise dissolved inorganic salts and organic matter in water. TDS originates mainly from natural sources, sewage, agricultural and industrial runoff, and wastewater. The TDS is high in the groundwater samples, except for samples GW24 and GW41. In addition, GW1, GW32, GW31, and GW11 are in the middle range. In regards to surface water, all are in the same range except for the effluent SF21 (Fig. 6.29). The EC results (Fig. 6.26) are similar to TDS results. The groundwater points with low EC are GW11, GW24, GW41, GW31, GW1, and GW32. GW32 and GW31 are shallow wells, and GW11 is the spring. Samples GW24 and GW41 seem to be recharged from a different aquifer, or there might be faults allowing rain to reach them in the area. GW1 seems to be recharged from a shallower aquifer (will be elaborated upon in section 6.3.4).

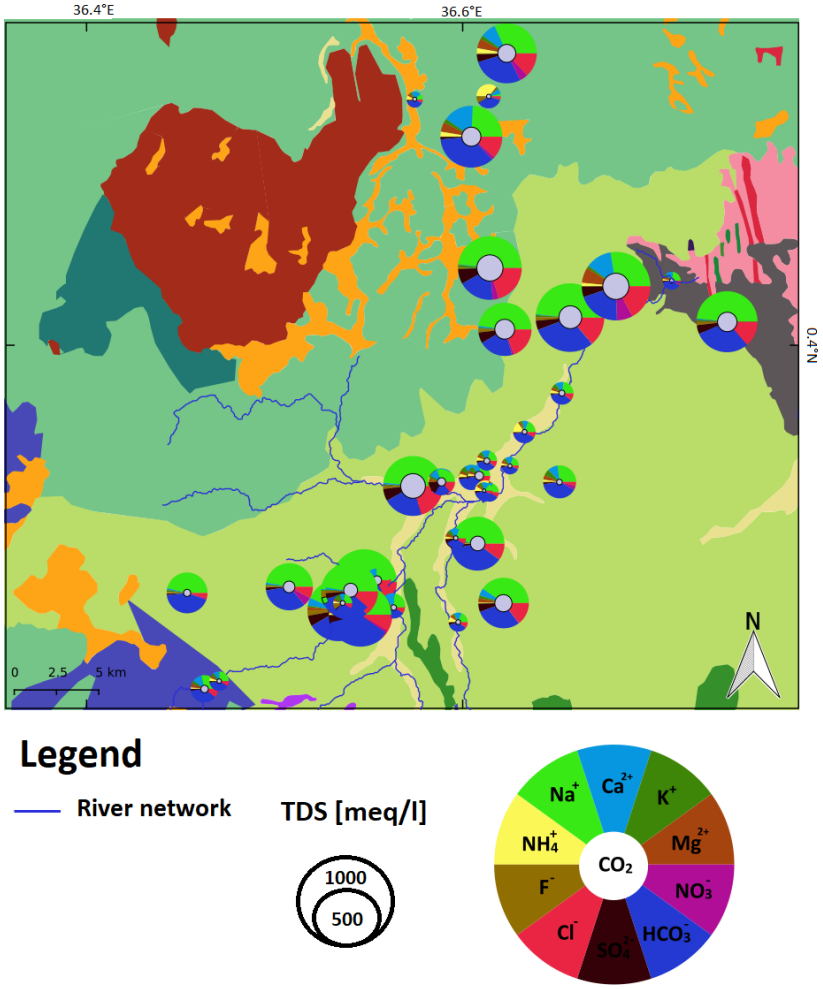

Fig. 6.29: Udluft diagram of the sampled water points, drawn on the geological map (cp. Fig. 2.9, p.19).

6.3.3. Water quality

Surface water from the stream and the wetland are used not only for drinking but for irrigation. Irrigation is widespread in the flooded parts of the wetland and the outside parts, where water is pumped directly from the wetland. The groundwater is mainly used for drinking and the ranching industry. The water quality of the sampled groundwater and surface water is discussed in this section. The detailed description starts with nitrogen compounds, fluoride, and

phosphate. The rest of the elements/constituents are compared to the health guidelines of WHO (2011) and KEBS (2015), and irrigation guidelines FAO (1985).

6.3.3.1. Nitrogen compounds

Wetlands usually help in the removal of nitrate (Gersberg et al., 1983; Van Oostrom & Russell, 1994; Zhu & Sikora, 1995) through two available mechanisms; the plant uptake and denitrification (Ingersoll & Baker, 1998; Lin et al., 2002; Van Oostrom & Russell, 1994; Xue et al., 1999; Zhu & Sikora, 1995). However, if the carbon source is not sufficient (Wu et al., 2014), at times, the enhancement of denitrification is required by planting the wetland (Lin et al., 2002). This is especially the case if the source is nitrate-rich agricultural runoff and polluted groundwater. Many studies focus on denitrification, but not many address the effect of the denitrification process on groundwater systems' hydrochemistry and on measuring denitrification in aquifer sediments (Smith et al., 1991).

Ewaso Narok wetland is known for the use of ammonia and nitrogen compounds as fertilizers (Kyalo Willy, 2016; own survey, 2016; UNESCO-WWAP, 2006). Nitrite and nitrogen compounds are indicators of pollution, usually from the disposal of sewage or organic waste. Nitrate is a result of domestic, agricultural, and industrial practices. In Ewaso Narok wetland, nitrate is attributed to excessive agriculture, the application of inorganic nitrogenous fertilizers and manure, animal or human sewage (oxidation of nitrogenous waste products in human and animal excreta) (WHO, 2016). High nitrate in shallow groundwater can be a result of leaching from livestock by rainfall. The impact of leached fertilizer nitrogen on groundwater is slow to develop because the transport of solutes through the unsaturated zone between the land surface and groundwater table is slow (Hem, 1985).

Fertilizers containing inorganic nitrogen and waste containing organic nitrogen are decomposed to ammonia, which is oxidized to nitrite and nitrate in the soil. Nitrate is used by plants and its surplus moves to groundwater. Once the nitrate reaches the aquifer, it will contaminate it for decades, even if nitrate loading on the surface is reduced (WHO, 2016).

The WHO (2011) sets a limit of 50 mg/l for nitrate in drinking water, whereas that of Kenya (KEBS, 2015) stands by 45 mg/l (Tab.4.2, Tab. 4.3). The surface water samples in general (Fig. 6.30) show less than 5 mg/l of nitrate, indicating that most of the NO_3^- has been denitrified into NO_2^- in the wetland. In specific, the sampled points during the dry period show a very low amount of nitrate. The tributary Melwa has relatively higher nitrate levels (0.9 mg/l and 2.1 mg/l), whereas only at one point in Pesi is the nitrate level higher (1.7 mg/l). The river water has a medium range as its water combines the water of both Melwa and Pesi tributaries (not detectable to 2.2 mg/l). The flooded wetland samples have higher nitrate values. This can be explained by the runoff of agricultural fields. However, this does not come to terms with Hemond and Benoit (1988), where flash floods show that the NO_3^- concentrations are usually lower, suggesting denitrification and nutrient removal or simple dilution.

Groundwater (Fig. 6.31) shows higher detectable nitrate values compared to the surface water samples. Four of the deep groundwater samples from boreholes (GW49, GW52, GW46, and GW23) showed high concentrations of NO_3^- [67 mg/l, 73 mg/l, 193 mg/l, and 65 mg/l], which exceeded values of the 50mg/l recommended guideline of the WHO (2011) and KEBS (2015).

This might suggest that the rest were denitrified to NO_2^- as seen in the nitrite values below. This indicates that existing NO_3^- was removed by denitrification in water with lower redox potentials (Mitsch & Gosselink, 2000). This process occurs at redox conditions below 250 mV (Mitsch & Gosselink, 2000). Most redox potentials were below 250 mV, allowing denitrification (Mitsch & Gosselink, 2000). The water in boreholes with the high NO_3^- values comes most from anthropogenic sources, and more precisely, from point pollution of sewage or agriculture as faults are common. Accordingly, these waters are leached from agricultural fields and then infiltrated into the groundwater without having been denitrified in an area where there were fractures.

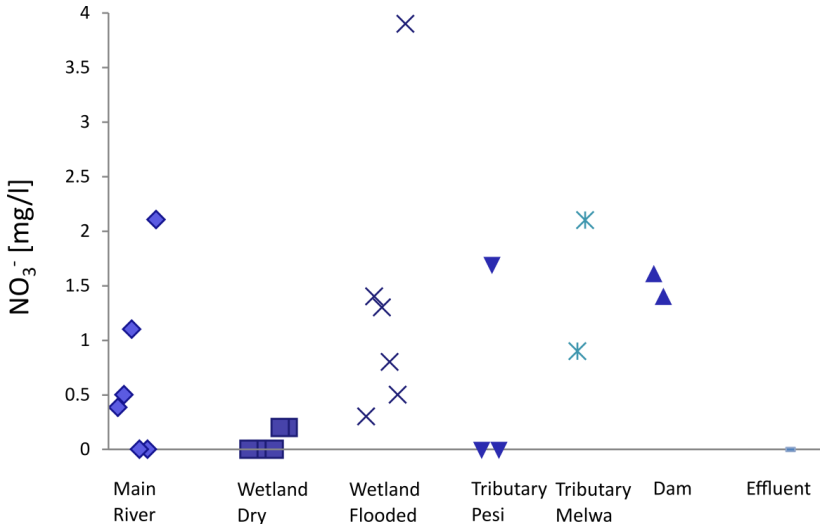

Fig. 6.30: Nitrate content of the surface water samples.

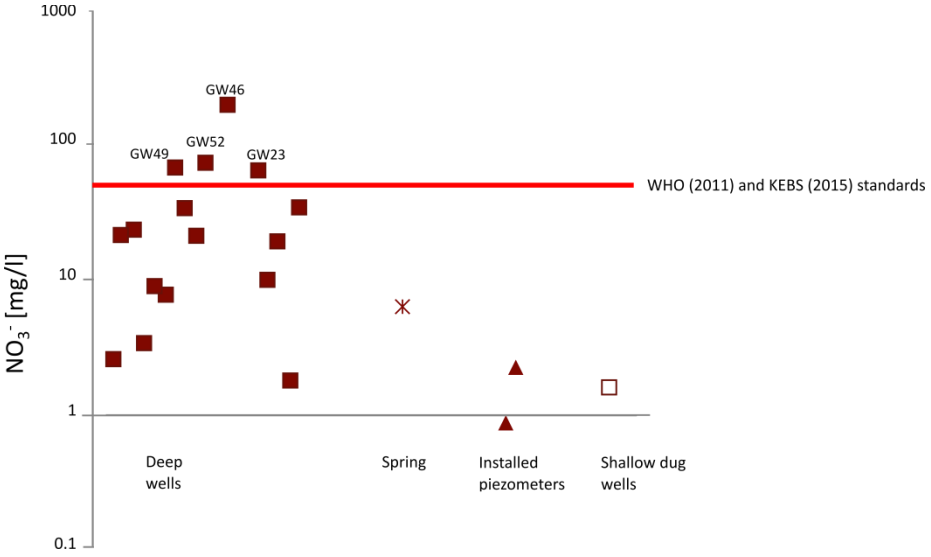

Fig. 6.31: Nitrate content of the groundwater samples compared to the recommended WHO (2011) and Kenyan standards (KEBS 2015) of 50mg/l. The y-axis is presented on a logarithmic scale for a better presentation of the results.

In regards to spatial distribution, the sampled points with the high nitrogen compounds, higher than the WHO (2011) guidance limit for ammonium and nitrate and higher than KEBS (2015) for nitrite, are mainly in the delineated flooded area of the wetland (Fig. 6.32). Few samples have high amounts of two nitrogen compounds.

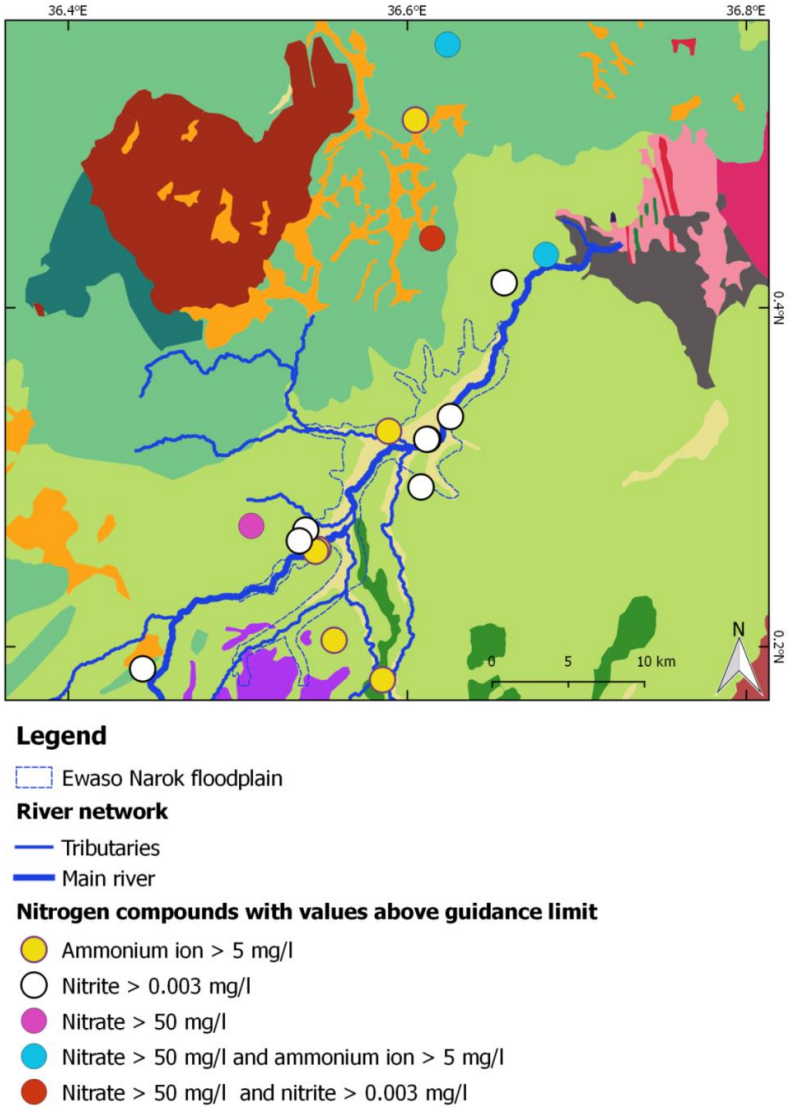

Fig. 6.32: Spatial distribution of the sampled water points with elevated levels of nitrogen compounds, drawn on the geological map (cp. Fig. 2.9, p.19).

The acceptability threshold values for nitrite differ between 0.003 mg/l (KEBS,2015) and 3 mg/l (WHO, 2011). While none of the water samples exceed the WHO (2011) threshold, three samples from surface water and six groundwater samples exceed the KEBS (2015) value. All three surface water samples are located downstream of the flooded area (Fig. 6.32). They are close to each other, ranging from Pesi inlet to the wetland (Fig. 2.2) and further on, thus showing a distinct spatial distribution. The surface water is used for irrigation, and it is important to take precautions as the limit of nitrite is exceeded. The groundwater points with high nitrites, on the other hand, are in the upstream and the outlet, always close to the water source (stream or flooded area).

In regards to ammonium, there is no place stating the drinking limit of it; however, for irrigation standards, it should be < 5 mg/l. The ammonium ion is a waste product of animals' metabolism and is relatively nontoxic to humans (Ismadji et al., 2015). However, it is toxic to most crop species if its recommended limit is exceeded. Bacteria and fungi convert organic nitrogen to ammonium through the ammonification or mineralization process.

Most of the surface water points lie around the 5 mg/l limits of ammonium, with a few samples exceeding the limit (Fig. 6.33). The samples exceeding the limit are sampled in the dry period and in the river itself and Pesi in addition to the dam. Another conclusion drawn from the ammonium ion exceeding the recommended standards is that ammonia fertilizer or wastewater is introduced in the supply system as the amount of ammonium is more than 1 mg/l (Ayers et al., 1985).

Regarding ammonium ions in groundwater (Fig. 6.34), the spring water, the shallow wells, and several deep wells water exceed the irrigation limit advised. Two of these deep groundwater wells have high nitrate levels in addition to the ammonium ion. The high level of ammonium in groundwater indicates point pollution.

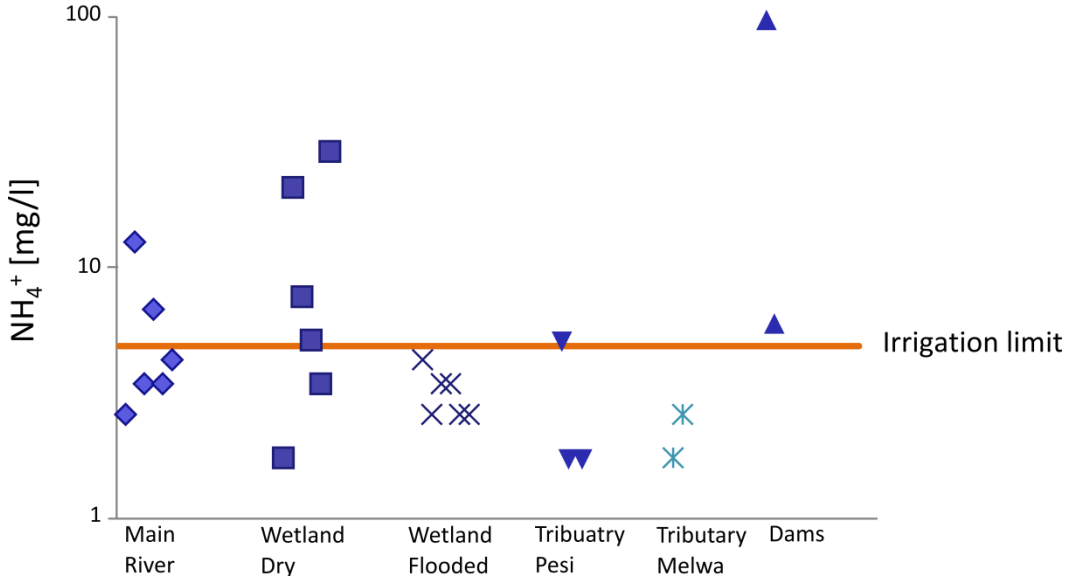

Fig. 6.33: Ammonium ion content of the surface water samples compared to the FAO recommended irrigation limit. The y-axis is presented on a logarithmic scale for a better presentation of the results.

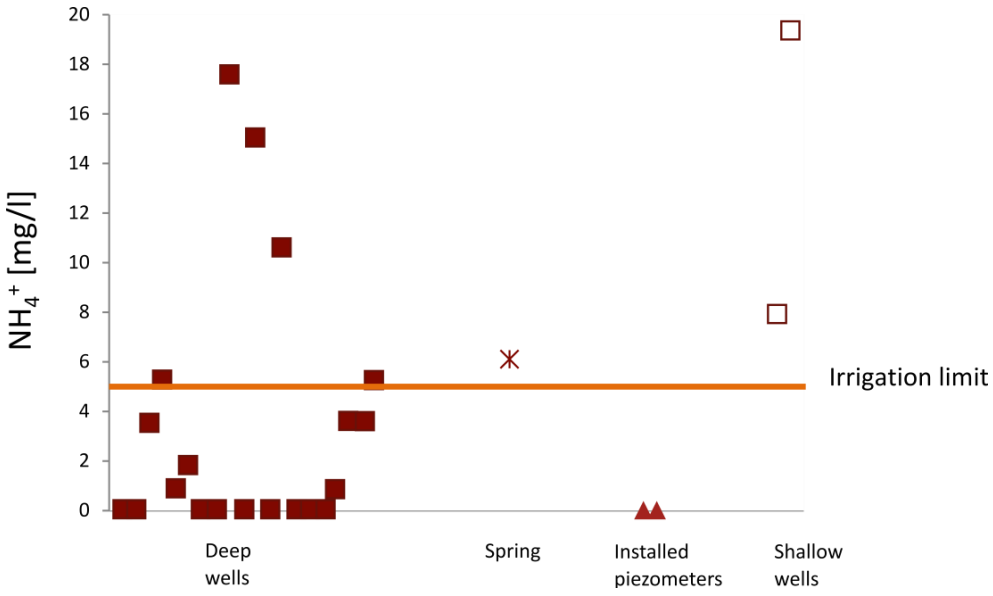

Fig. 6.34: Ammonium ion content for the groundwater samples compared to the FAO recommended irrigation limit.

6.3.3.2. Fluoride

With regard to groundwater, several patterns in fluoride behavior have been observed in Kenya. Higher fluoride concentrations are obtained in discharge areas rather than in recharge areas, with a trend of fluoride enrichment along the direction of flow (Gaciri & Davies, 1993). Groundwater and lake water, in comparison to other water sources, show considerably higher fluoride contents (Gaciri & Davies, 1993).

When looking at the depth of boreholes, the higher concentration was observed, the deeper the borehole was (Mjengera et al., 1997; Nair & Manji, 1984). However, research by Mageto (2011) and Marieta (2007) shows that depth did not play a role, but it was the geological formation and the mineral content that led to the differences.

The fluoride sources have been linked mainly to the volcanic activity, the composition of alkaline volcanic rocks, their chemical weathering, and breakdown. Volcanic rocks, especially amorphous rocks, are easily weathered, and accordingly, when washed away, they carry fluoride components into the surface and groundwater (Mageto, 2011).

Due to volcanoes, it is not rare for fluor ions, F^-, to attain concentrations well above the upper limit permitted for drinking water, especially in soft acidic water (Hem, 1985). As rainfall infiltrates through rocks, it gets enriched in fluorides and percolates into the groundwater (Mageto, 2011; Marieta, 2007). Volcanic ash is rich in fluorides, and water seeping through it is enriched. High temperatures, and geothermal activities, increase the solubility and mobility of fluoride ions in groundwater (Mageto, 2011).

Other fluoride resources are due to the residence time of dissolved fluorides in the waters that involve species of Ca^{2+} and F^-. In addition, fluorides are injected into the hydrological system by industrial operations or through atmospheric precipitation and dissolution of salt crusts (Gaciri & Davies, 1993).

The alkaline volcanic rocks of this work's studied area consist of trachytes, phonolites, and basalts. When these rocks are weathered, they dissociate into minerals such as micas (phlogopite, adularia), carbonate salts, and hydroxide (wollastonite, brucite, dolomite, trona, tremolite), that act as good sinks for fluoride ions (Marieta, 2007). The weathering of fluoride-bearing minerals like muscovite, which is common in the research area, besides industrial and agricultural sources, is another source of fluoride in groundwater (Appelo & Postma, 2005). Most fluoride-rich groundwater is usually characterized by sodium-bicarbonate water type (Brindha & Schneider, 2019).

Regarding fluoride, both the KEBS (2015) and the WHO (2011) agree on 1.5 mg/l as the drinking limit. Most of the surface water points (Fig. 6.35) are below the WHO (2011) standards with three exceptions; one part of the wetland when flooded, the effluent, and the dam.

Most groundwater samples (Fig. 6.36) have high fluoride levels above the WHO (2011) and KEBS (2015). The two exceptions are the installed piezometer and the spring water. The geology of the area explains the high levels of fluoride in the groundwater. The values suggest a general increase of fluoride with depth. This could also be attributed to the different geological formations.

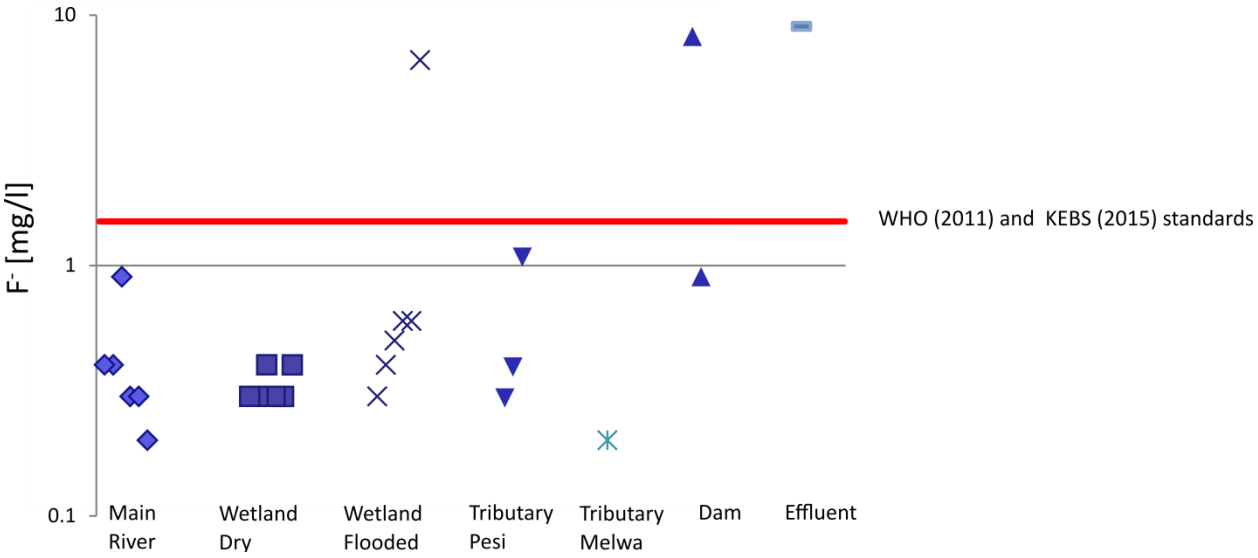

Fig. 6.35: Fluoride content of the surface water samples compared to the recommended WHO (2011) and Kenyan standards (KEBS 2015) of 50mg/l. The y-axis is presented on a logarithmic scale for a better presentation of the results.

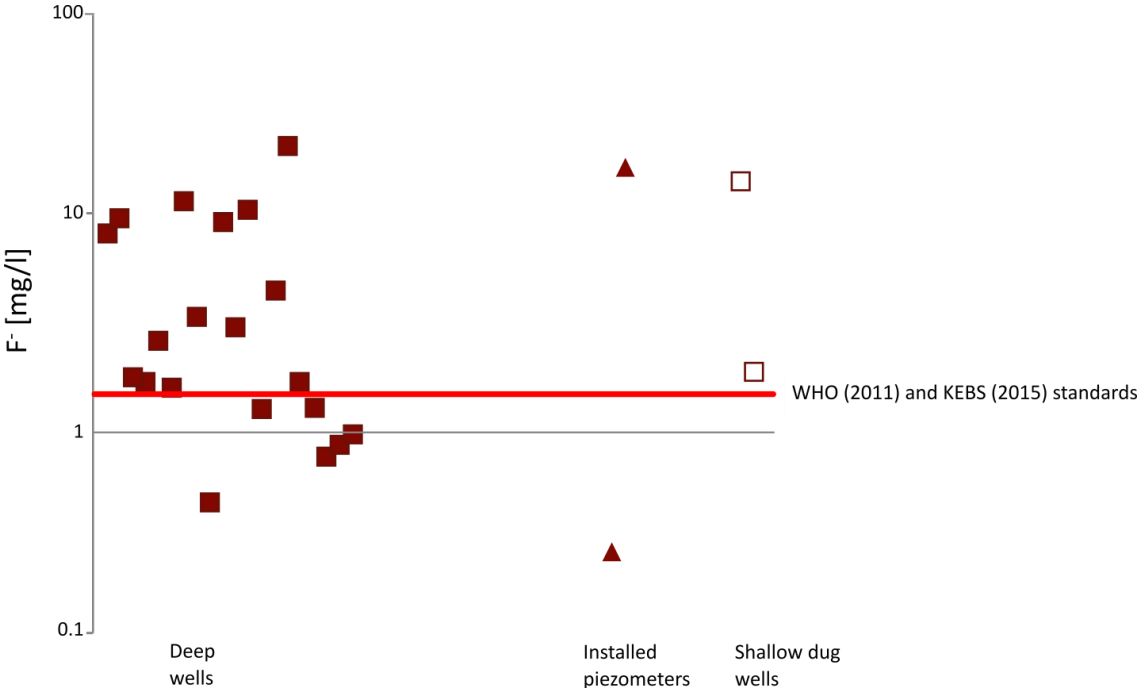

Fig. 6.36: Fluoride content of the groundwater samples compared to the recommended WHO (2011) and Kenyan standards (KEBS 2015) of 50mg/l. The y-axis is presented on a logarithmic scale for a better presentation of the results.

The spatial distribution of fluoride concentration shows that in the upstream flooded part of the wetland, the amount of fluoride is higher than in the area around it (Fig. 6.37). In the wetland's downstream part, no wells lie in the flooded delineated part. A trend is noticed in regard to groundwater samples showing that the further the distance from the wetland, the lower the value of fluoride is.

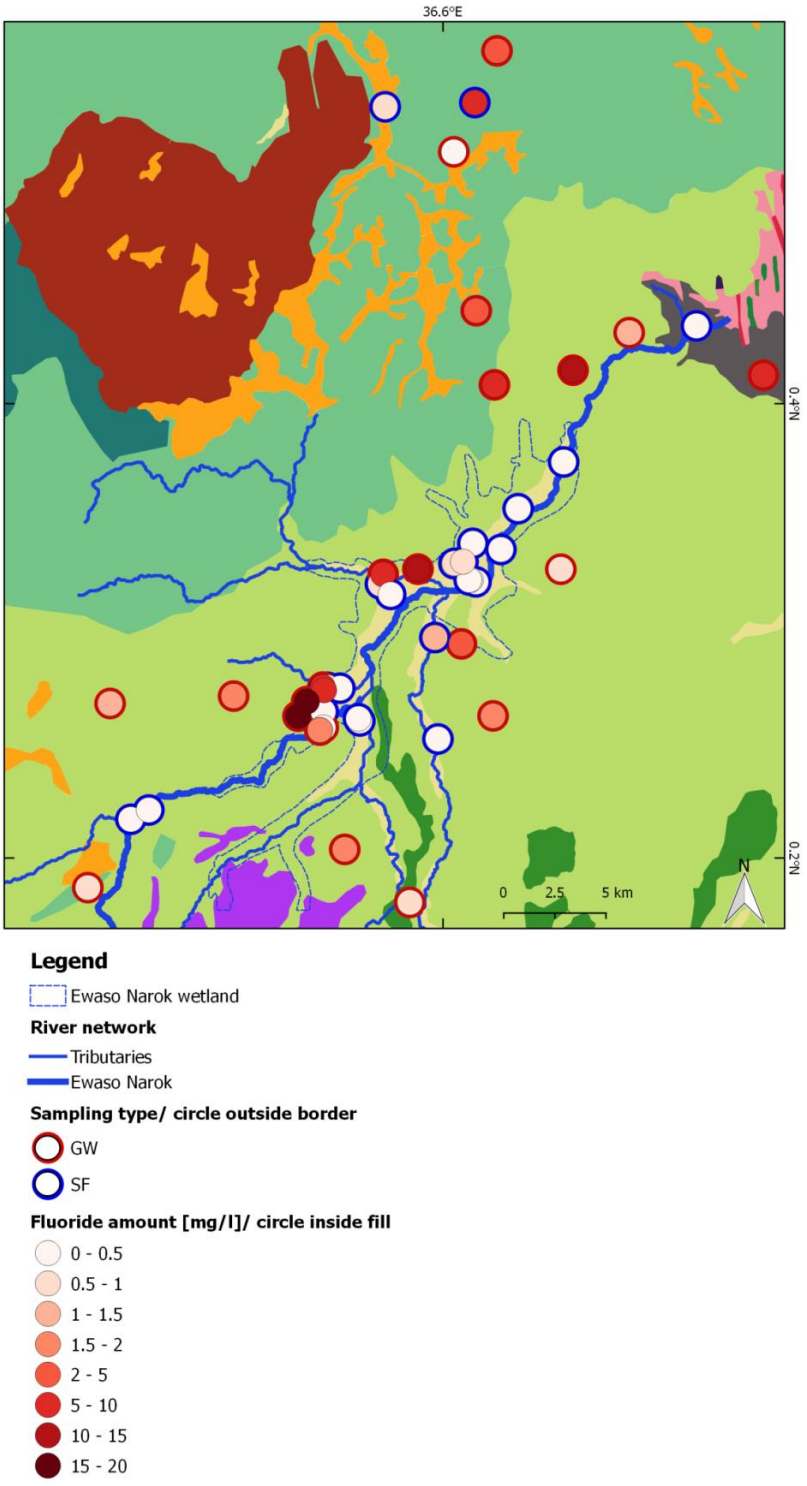

Fig. 6.37: Fluoride spatial distribution in the Ewaso Narok area, drawn on the geological map (cp. Fig. 2.9, p.19).

6.3.3.3. Phosphate

Phosphate sources are wastewater treatment plants and industrial discharges. Non-point sources are the natural decomposition of rocks and minerals, agricultural runoff, animal input, and wildlife. A large percentage of the phosphate in water is precipitated from the water as iron phosphate or stored in partially decomposed organic material.

While the WHO (2011) did not set a standard limit, the KEBS (2015) limit is 2.2 mg/l. Three surface water points were on the edge of the Kenyan standards. Two of these points were sampled from the Pesi River's inlet into the wetland (SF25, SF26) and the middle part of the wetland (SF35).

6.3.3.4. Water compared to health guidelines

The groundwater, as stated earlier, is the major drinking source for the local population. Surface water is used both for domestic and irrigation purposes. Accordingly, the dissolved water species were evaluated compared to the WHO (2011) and KEBS (2015) (Tab. 4.2, Tab. 4.3, and Tab. 4.4).

As fertilizers were applied in the area, the water samples were tested for the content of nitrogen, phosphorous (cp. sub-chapter 6.3.3.1. and 6.3.3.3), and potassium. Fertilizers further contain Cl^-, Ca^{2+}, and SO_4^{2-}. Accordingly, NO_3^-, Cl^-, Ca^{2+}, and SO_4^{2-} were set as indicators of anthropogenic influences (Van der Weijden and Pacheco, 2003). As described in chapter 6.3.3.1, the **nitrate** values were exceeded in 16 % of the groundwater samples (Fig. 6.38). High nitrogen uptake causes problems with vitamin A shortages and is linked to colorectal cancer, thyroid disease, and neural tube defects (Ward et al., 2018). According to the KEBS (2015), **nitrite** values are 0.003 mg/l compared to the WHO (2011) of 3 mg/l and were exceeded in 11 % of the surface water samples and in 24 % of the groundwater samples. This indicates fertilizer use and pollution. Regarding sulfate, chlorine, and calcium, the water samples were generally of acceptable quality. Only 8 % of the groundwater samples exceed the Ca^{2+} threshold value. The **chlorine** taste threshold is 250 mg/l and was exceeded by 12 % of the groundwater samples.

Regarding the geogenic influences and contamination, **fluoride** and **manganese** were used as indicators. **Fluoride** guideline levels were exceeded in 11 % of the surface water samples and 70 % of the groundwater samples (Fig. 6.38) (cp. sub-chapter 6.3.3.2.). This is striking as groundwater is the major drinking source, and regulations should be enforced. Health problems associated with excess fluoride include problems with bones, teeth, and neurological development (Brazier, 2018). **Manganese** could be derived from the weathering of manganese-containing silicate minerals or redox processes within the wetland. The WHO (2011) drinking standards set the limit at 0.4 mg/l for **manganese**, and according to the KEBS (2015), it is 0.1 mg/l. 11 % of groundwater samples and 36 % of surface water points exceeded the WHO (2011) limit, and 40 % of the groundwater samples and 93 % of the surface water according to the KEBS (2015) guideline (Fig. 6.38).

The **aluminum** guideline value of 0.9 mg/l, according to WHO (2011), was exceeded in 77 % of the surface water samples and 12 % of groundwater samples. In comparison, the KEBS (2015) sets the limit by 0.2 mg/l, meaning that all surface water points exceeded it, and 16 % of the groundwater points. As high concentrations of fluoride exist in the wetland area, the aluminum's solubility increases (Hem, 1985).

Further noticeable pollution that exceeded the recommended WHO (2011) threshold values were given for iron, arsenic, and copper. The drinking water guideline value for **iron** is 0.3 mg/l (WHO 2011). All sampled surface water points had higher levels than the guideline and 8 % of the groundwater samples.

Two groundwater points, GW44, situated downstream of the wetland, and GW17, situated upstream of the wetland, had higher contents of **arsenic** than the drinking guideline value (0.01 mg/l). Arsenic in drinking water is considered one of the most significant environmental causes of cancer in the world (Chung et al., 2014). Its source is either leaching from geological formations or anthropogenic sources (Chung et al., 2014; Shankar et al., 2014). In this area, the geological formations do not seem to contain arsenic; accordingly, it may derive from pesticides, fertilizers, or other major contamination sources. Extreme precautions should be taken, and an immediate solution is needed to prevent harm to the people drinking the water. Arsenic leads to carcinogenicity in humans, and intake over a long period causes arsenic poisoning.

One groundwater sample (GW9) exceeded the recommended guideline of **copper**. Most of the surface water points were within the recommended pH range. However, several groundwater points failed to satisfy this recommended range. To conclude, given these high levels of iron, manganese, and aluminum, it is highly likely that there will be laundry staining, coating, and deposits in pipes making the water not acceptable in terms of public acceptability.

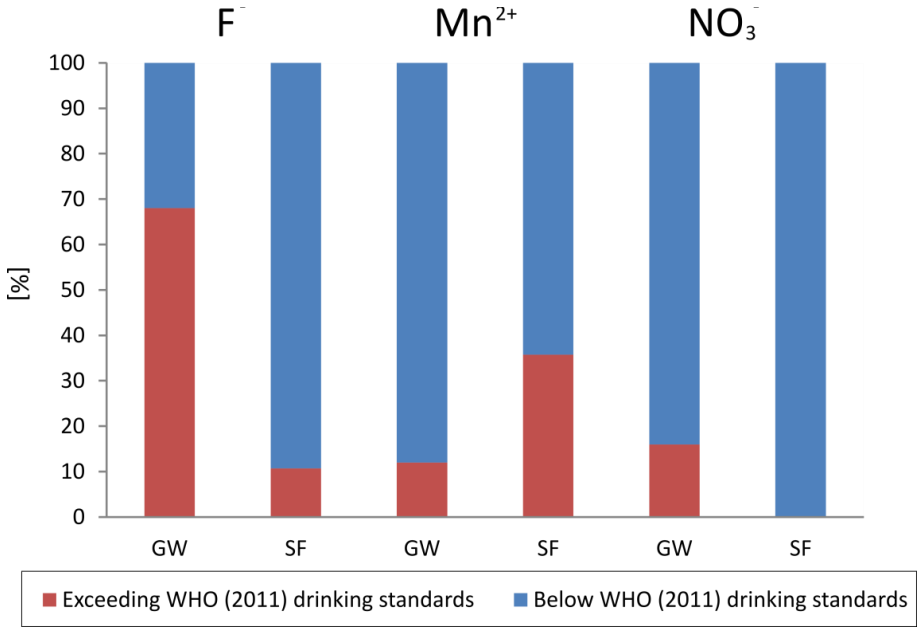

Fig. 6.38: Stacked bar charts of the percentage of fluoride, manganese, and nitrate in surface water and groundwater samples exceeding the WHO guidelines (2011).

In order to understand the water quality in terms of public health, the degree of health-related water quality (DHWQ) is calculated (Fig. 6.39 and App. 6). It is calculated as the sum of the WHO (2011) exceeded guidelines values (Burghof, 2017). The DHWQ of the samples which were exceeded included and decided upon for this calculation the following constituents: iron, fluoride, nitrate, manganese, arsenic, and aluminum. Zero indicated no guideline exceeded, and three indicated three guidelines exceeded (App. 6).

Only four sample points that lie outside the delineated flooded wetland show zero guidelines being exceeded, thirteen points show a value of one guideline exceeded and are located in the wetland outlet, and the delineated flooded area mainly. Eight points show a value of two, meaning two guidelines exceeded inside the wetland flooded area with seven other points outside that area. Nine points show a very high value, six of which are in the flooded area, meaning three guidelines exceeded, and one point shows a value of four guidelines exceeded.

Water quality may indicate a water source, although biogeochemical processes may modify the chemical signature (Gilvear & Bradley, 2000).

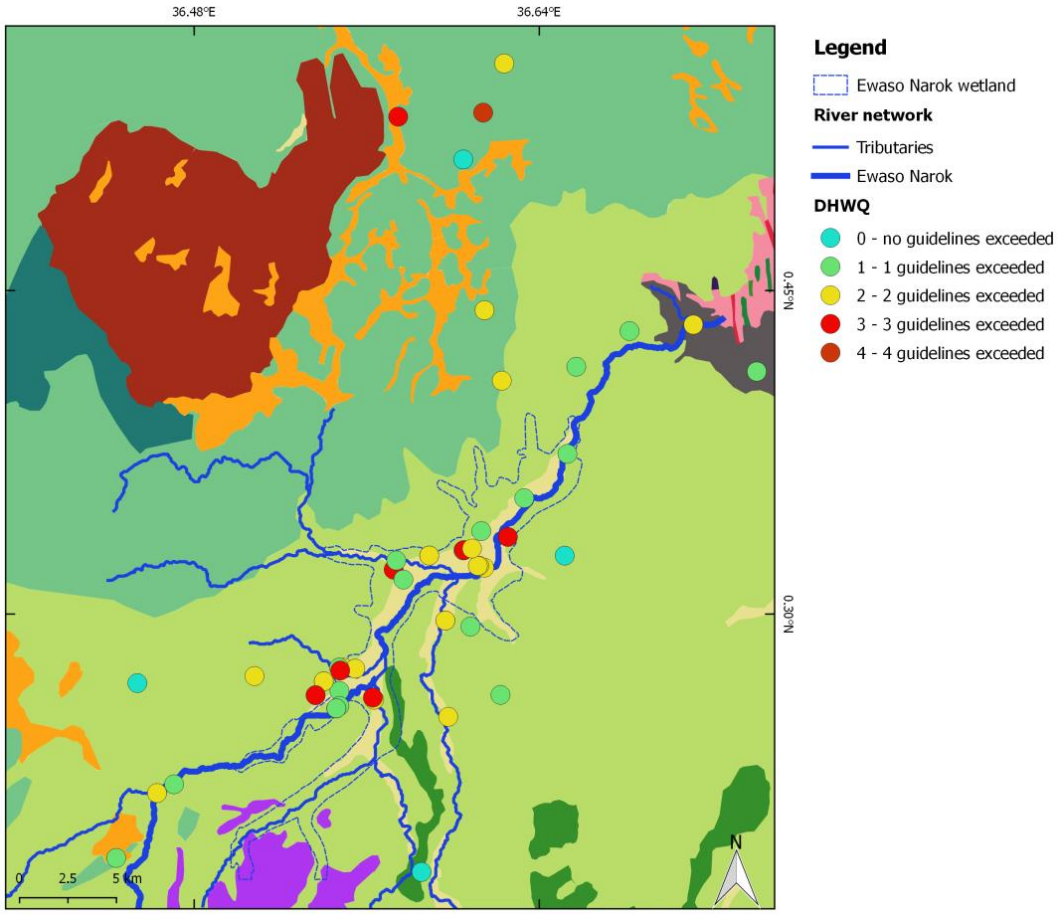

Fig. 6.39: The calculated DHWQ value for the sampled water points compared to the recommended WHO (2011) guidelines, drawn on the geological map (cp. Fig. 2.9, p.19).

6.3.3.5. Water quality compared to irrigation guidelines

As reported by the survey, fertilizers are frequently used in the wetland and usually supply the plants with nitrogen, phosphorous, and potassium with secondary nutrients and sulfate. These nutrients include iron, chlorine, copper, manganese, zinc, molybdenum, and boron. Salts are present in irrigation water but in small amounts and originate from the dissolution or weathering of rocks and soils (Joshi et al., 2009). Groundwater salinity in volcanic rocks results from atmospheric inputs, climatic conditions, and rock weathering (Kovalevsky et al., 2004). Water quality-related problems in irrigated agriculture include salinity, water infiltration rate, and specific ion toxicity. The salinity in soil or water reduces the soil-water availability, slowing crop growth and restricting root development, which leads to yield reduction. Infiltration and the rate at which irrigated water enters the soil are reduced when there are high sodium and low calcium in the soil or water. Certain ions, for example, sodium, chloride, and boron, if in high concentrations, accumulate in the leaves, and extend elsewhere in the plant, causing damage and yield reduction. Excessive nutrients can reduce yield and quality (Ayers & Westcot, 1985).

Following the irrigation limit of the FAO (1985) (see Chapter 4.4.3 Tab. 4.3), the guideline threshold for irrigation for **chloride** was exceeded in 36 % of the groundwater samples. In

regards to **calcium**, 12 % of groundwater samples exceed the irrigation limit. The potassium limit was exceeded by 24 % of the groundwater samples, and 8 % of the surface water samples and 24 % of the groundwater samples had higher **sulfate** values than the irrigation standards.

The **manganese** level was exceeded in 65 % of the surface water points and 12 % of the groundwater points. 16 % of groundwater samples were above the recommended irrigation limit of nitrate. Almost all the surface water and groundwater values of ammonium ions exceeded the irrigation limit. The **fluoride** irrigation limit was exceeded in 15 % of the surface water samples and in 80 % of the sampled groundwater samples. Finally, the HCO_3^-'s limit was exceeded in almost all the groundwater samples and in 24 % of the surface water samples. Accordingly, for irrigation purposes, surface water is more suitable than groundwater. However, certain constituents, such as manganese, fluoride, and ammonium, and their values in surface water are alarming and damaging for the crops. As the surface water is under threat, precautions must be taken in using the groundwater as an alternative for irrigation.

In terms of salinity (Fig. 6.40), most of the groundwater samples (20 out of 25) showed a moderate degree of restriction on use (DRU), while most of the surface water showed no restriction on use. In terms of infiltration (Fig. 6.40) evaluation problems due to low salinity and high SAR, most of the groundwater samples (22 out of 25) showed a moderate to severe degree of restriction on use. In contrast, all the surface water samples showed a moderate to severe degree of restriction on use. The groundwater samples that showed no restriction on use in terms of infiltration showed moderate restriction on use in terms of salinity. All the ones that showed a severe degree of restriction on use in terms of infiltration showed a moderate degree of restriction on use in salinity. The spatial distribution regarding DRU in terms of salinity (Fig. 6.41) shows almost all the samples in the delineated flooded part of the wetland having a moderate degree, whereas surrounding the wetland upstream and downstream show no DRU in terms of salinity.

Spatially, in the flooded part of the wetland, the sampled points, whether surface water or groundwater, showed severe to moderate degree of restriction in terms of infiltration (Fig. 6.41), in addition to the Western part next to the wetland.

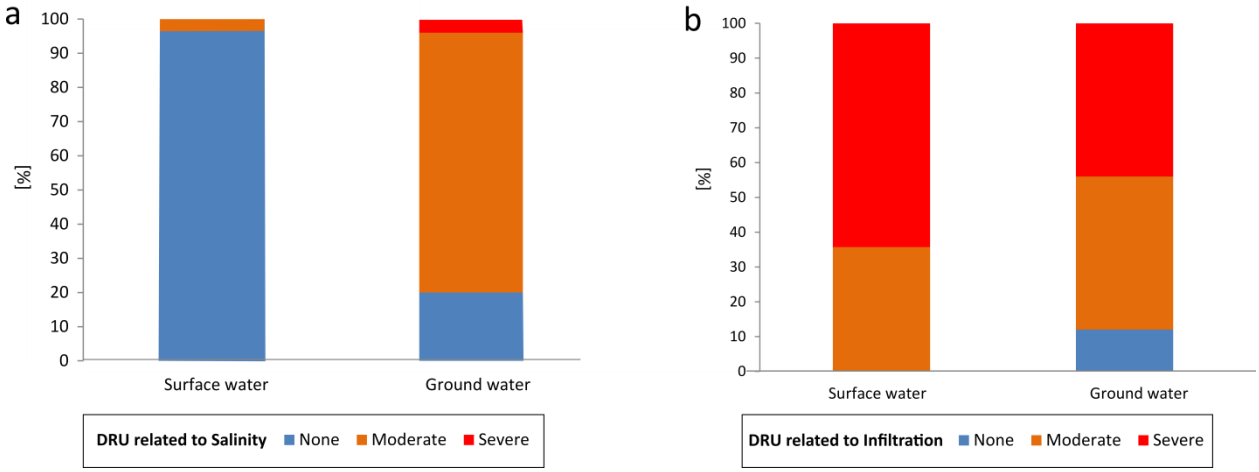

Fig. 6.40: Stacked bar charts of all samples showing percentages of a. DRU related to salinity (FAO, 1985) and b. DRU related to infiltration (FAO, 1985).

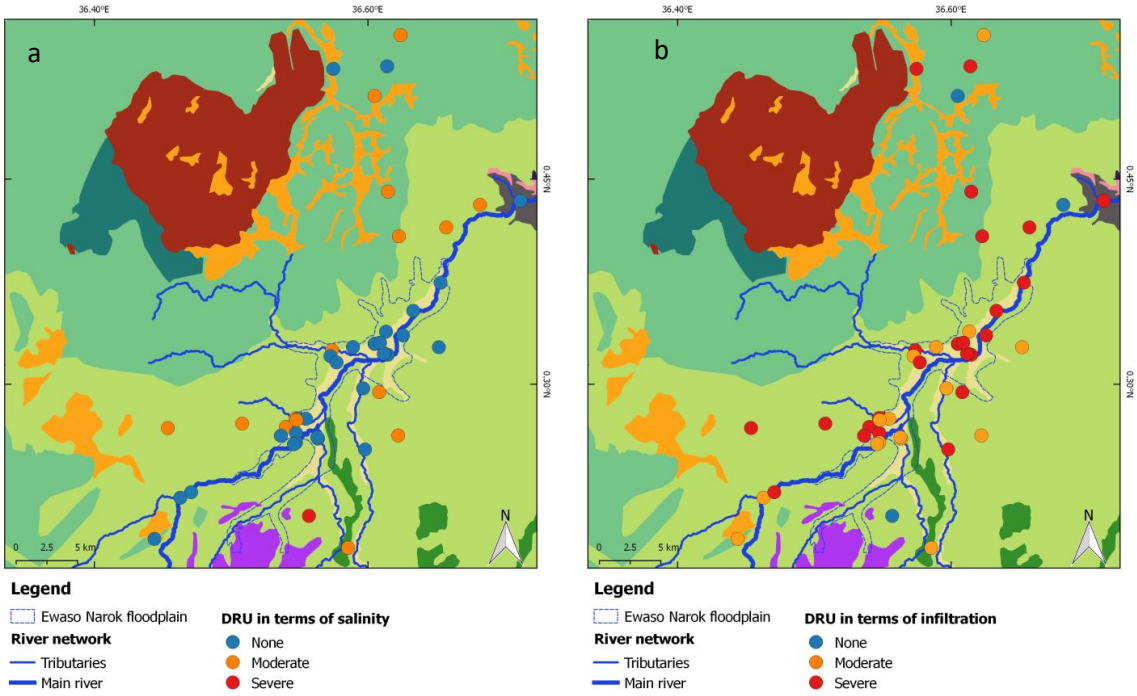

Fig. 6.41: Spatial distribution of DRU, drawn on the geological map (cp. Fig. 2.9, p.19): a. Related to salinity (FAO, 1985), b. Related to infiltration (FAO, 1985).

6.3.4. Stable water isotopes

The isotopic compositions of $\delta^{18}O$ and $\delta^{2}H$ in the surface water and groundwater were analyzed for the sampling campaign in July/ August 2016. The results are presented in the delta (δ) notation relative to V-SMOW (App. 3) in ‰.

The results are analyzed and presented as two groups; surface water (Fig. 6.42) and groundwater
(Fig. 6.43), wherein both linear correlation of $\delta^{2}H$ versus $\delta^{18}O$ is drawn. The approach was to interpret the spatial distribution of selected environmental isotopes. The Global Meteoric Water Line (GWML) is defined after Craig (1961) as $\delta^{2}H = 8\ \delta^{18}O + 10$. The Local Meteoric Water Line (LMWL) used is from Kericho's station **$\delta^{2}H = (7.96 \pm 0.35)\ \delta^{18}O + (11.35 \pm 0.96)$** (Rietti-Shati et al., 2000) as precipitation data did not exist.

The $\delta^{18}O$ values of surface water ranged between -3.28 to 1.24 ‰, while its $\delta^{2}H$ values ranged between -7.6 to 14.7 ‰ (Fig. 6.42). The non-weighted regression generated from all the sampled surface points yields a line of $\delta^{2}H = 4.9\ \delta^{18}O + 8.4$. Most of the surface samples plotted around the LMWL and the GMWL and showed no significant effect from evaporation, with the exceptions of samples SF12, SF29, SF51, SF20, and SF21. The main feeding source of the dam samples (SF51 and SF53) is rainwater, as indicated by the owners, showing as expected high values of $\delta^{2}H$ and $\delta^{18}O$.

Other exceptions deviating from the general behavior of the surface water were samples plotting above the global and local meteoric water lines (SF34, SF35, SF40) (Fig. 6.42). These samples could be contaminated by organic matter as they were taken in the middle of the wetland area in agricultural fields where flooding happened and the water was turbid.

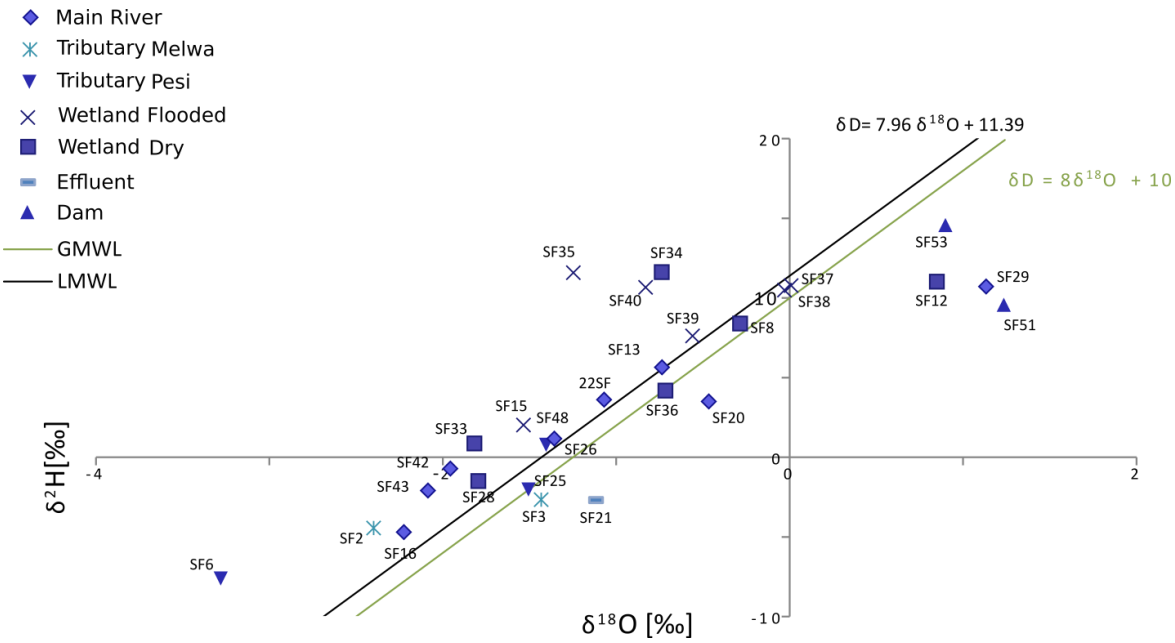

Fig. 6.42: $\delta^{18}O$ versus $\delta^{2}H$ for surface water samples (main river samples from Ewaso Narok, and its tributaries Pesi and Melwa), flooded, and dry wetland samples, dams, and effluent drawn with the global meteoric water line (GWML) and the local meteoric water line (LMWL).

The beginning upstream part of the Melwa and Pesi stream samples are depleted in both $\delta^{2}H$ and $\delta^{18}O$ values, indicating a direct release from a groundwater source without much attenuation and evaporation. Pesi upstream (SF6) has the most depleted isotopic signature [$\delta^{2}H$ = -3.28 ‰, $\delta^{18}O$ = -7.6 ‰]. The stream develops progressively with more enriched $\delta^{18}O$- and $\delta^{2}H$- signatures in the downstream direction that lies below the LMWL yet above the GMWL, thus showing almost no evaporation signs. Melwa stream is sampled at two points; the upstream one is more depleted. Both points show no effect of evaporation.

The samples along the flow path of the Ewaso Narok river situated in the wetland show different isotopic results depending on the tributary feeding the river (Pesi, S. Aiyam, and Mathenga) (for geographic location check Fig. 2.2). Water sampled from the tributaries S. Aiyam (SF29) and Mathenga (SF20) show evaporation effects, whereas water coming from Pesi direction does not show. Due to the very slow flow velocity in the furrow next to the main river (SF16) evaporation effects can be expected, but the isotopes' results do not prove this expectation. The downstream part of the Ewaso Narok river (SF43 and SF42) shows low values of $\delta^{18}O$ and $\delta^{2}H$, yet a bit higher values than upstream (SF16, SF22, SF29). This can be attributed to their different source and location as they originate from a different stream. The most downstream sampled point on the Ewaso Narok river (SF48) lies on the LMWL, indicating almost no to minimal evaporation and mixing of water. This indicates a major source that does not go through evaporation that feeds the wetland.

To sum up, the water upstream and along the flow of the Ewaso Narok river is more depleted in heavy isotopes than the downstream. This could be a result of the mixture of local water and regional water. The low values of $\delta^{2}H$ and $\delta^{18}O$ suggest a possible connection to the groundwater and that the surface water is fed by it.

The sampled points during the dry period show that one sample is influenced by evaporation (SF12) with enriched $\delta^{2}H$ and $\delta^{18}O$ values, two sampled points lie on the GMWL, and the rest

show depleted signatures of δ^2H and $\delta^{18}O$ and no evaporation signs. One would assume that there would be more evaporation as no rain has fallen during the last weeks before the sampling, and some of the water remains unmoved. However, more depleted water was noticed, again hinting at groundwater contribution. The upstream area showed negative values, which again indicates groundwater flow contribution and discharge from higher mountains. The different mixing of groundwater and surface water occurs as different non-evaporated sources feeding the wetland with depleted water and probably originate from either local effluents or springs or the tributaries. The mixing of different water is shown in SF36 as both waters from SF28 and SF12 contribute to the water's signature.

Water samples taken during the same period but once the flash floods started show negative values of $\delta^{18}O$ yet positive ones of δ^2H, which can happen as both are highly dynamic, especially during and after precipitation events (Rothfuss et al., 2015). All the samples plotted above the GMWL and LMWL and did not show evaporation effects. This can be attributed to the high intensity of the rainfall events, thus causing more depletion in δ^2H and $\delta^{18}O$ signatures (Rietti-Shati et al., 2000).

Few surface water samples taken during the floods show more depleted values in comparison to samples during the dry period. However, many samples taken during the flooding are close in signature to the samples taken during the dry time. This hints at a connection to a perched aquifer and its fast exchange with the river water, hence evaporation effects are not vivid. In addition, this points to the fact that the wetland groundwater water feeds the wetland and contributes to the mass balance as the dry period has depleted results and no clear evaporation effect.

The surface water can be clustered into different groups. The main streams that contributed to the wetland show low values of $\delta^{18}O$- δ^2H. As the streams join together to form the Ewaso Narok river, the δ^2H and $\delta^{18}O$ signature gets enriched. The water in the wetland has different isotopic signatures, some enriched and others depleted. There is a clear indication of groundwater flow contribution to the wetland and mixing of water. Floods further play an important role in the making up of the signatures.

Groundwater values of $\delta^{18}O$ values ranged between -3.76 and 0.53 ‰, and δ^2H values between -18.7 and 6.9 ‰ (Fig. 6.43). The range of ^{18}O signatures of the groundwater clearly indicates that the water is not of fossil origin. Studies of fossil groundwaters in Africa show 2 ‰ more depletion in ^{18}O-values if fossil groundwater existed (Darling et al., 1987; Sklash and Mwangi, 1991; Sonntag et al., 1979).

Shallow hand-dug wells (GW5, GW32) are left open without any seal or cover. GW5 contains enriched values of the isotopes and lies below the GMWL, showing a clear evaporation effect. GW32 shows lower values of isotopes $\delta^{18}O$ and δ^2H lying above the LMWL and the GMWL and is three meters deep. As it shows no effect of evaporation even though it is not sealed from the top, it is reasonable to assume that it is tapping the water table and containing groundwater that has not passed through evaporation. The evaporation trend of GW5 shows similarity to Clark's (2015) study, where he explained the low slope by strong evaporation from the soil column, enhancing the kinetic fractionation effects.

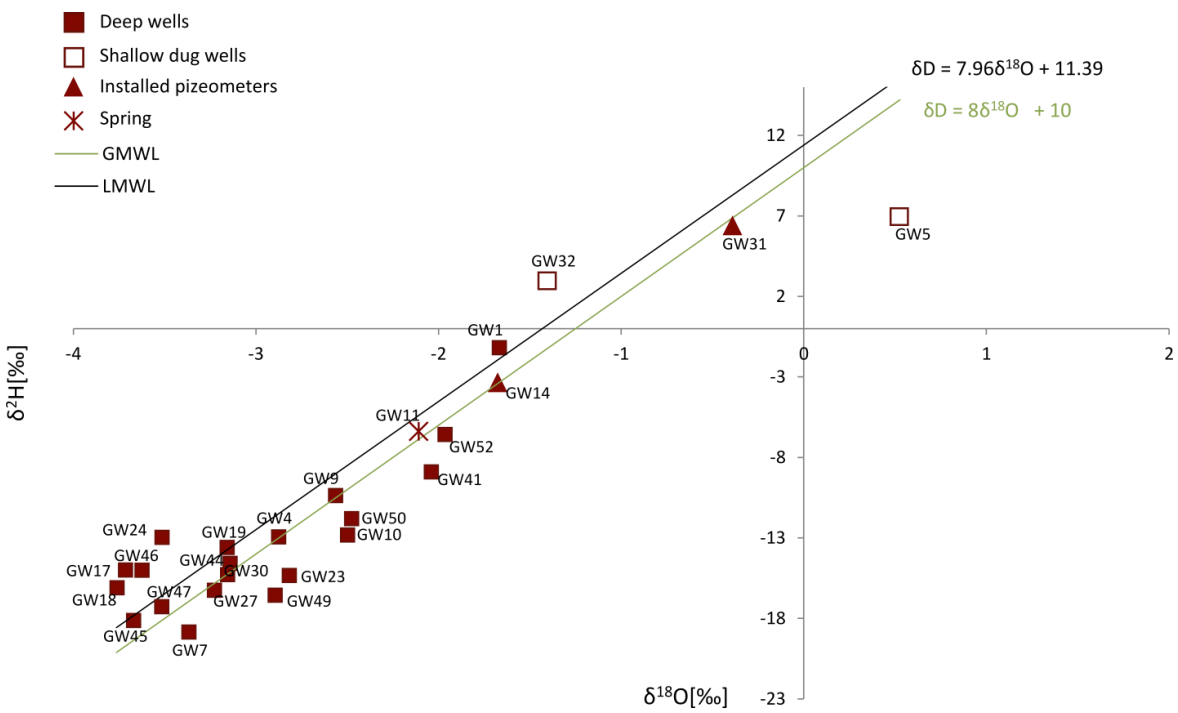

Fig. 6.43: $\delta^{18}O$ versus $\delta^{2}H$ for groundwater samples (deep wells, shallow wells, installed piezometers, and spring) drawn with the global meteoric water lines (GMWL) and the local meteoric water line (LMWL).

The two installed piezometers (GW31: 1.8 m deep; and GW14: 2.4 m deep) in the wetland plot almost on the GMWL yet below the LMWL, suggesting minimal to no evaporation effect. The deeper piezometer (GW14) shows depleted values of $\delta^{2}H$ and $\delta^{18}O$, almost resembling those of the deep wells, suggesting a beginning of groundwater recharge. Another explanation is that the surface water infiltrates to the groundwater during floods. As described above, surface water samples taken during floods carry water with the lowest signature of $\delta^{2}H$ and $\delta^{18}O$. This might happen especially on the wetland's fringe area or in the river courses where the soil is more than saturated. The floods lasted for hours, thus possibly replenishing the top layers close to the surface in the semi-arid environment.

The non-weighted regression from the deep wells (40 to 180 m) is $\delta^{2}H = 5{,}7\ \delta^{18}O + 3.7$. Seven of the twenty deep wells lie below the GMWL, showing some signs of evaporation. Groundwater may have an evaporated signal due to the evaporation of surface water prior to infiltration or evaporation of soil moisture from the unsaturated zone (Clark, 2015). Seven of the rest of the wells lie on or between the GMWL and LMWL, indicating minimum to no signs of evaporation. The rest of the wells lie above the LMWL, thus suggesting no evaporation at all. There are multiple explanations for the depleted signatures of the $\delta^{2}H$ and $\delta^{18}O$. The wells might indicate another source of recharge with not much water attenuation, suggesting that the main source of recharge is not the wetland surface water but water that has infiltrated into the system from a different source. This might be a source from higher altitude, cooler, and more humid climate. The water accordingly flows laterally and recharges these wells in the Ewaso Narok catchment, which is fairly deep. This comes in terms with previous studies, including Earth Scope (2012), Gichuki (2002), Republic of Kenya (1987), Samoka (2010), and Sklash and Mwangi (1991), suggesting that the main recharge occurs in Mount Kenya, Aberdare Ranges, and the Laikipia Mountains more specifically the Nyandarua mountain ranges. Rainfall runs in the Mau

escarpments infiltrating into the groundwater systems through the Basarlonian fractures and shear zones into the groundwater store and then flows to feed aquifers in the nearby areas of Ewaso Narok wetland (Earth Scope, 2012; Gichuki, 2002; Republic of Kenya, 1987; Samoka, 2010; Sklash and Mwangi, 1991).

Another explanation might be direct recharge from rainfall with evaporation effects (Republic of Kenya, 1987; Sklash and Mwangi, 1991). Ewaso Narok wetland has a lower elevation, warmer temperatures, and greater evaporation of falling precipitation before recharge, and a rise in elevation leads to a more negative signature of the stable isotopes. Furthermore, Craig (1961) suggested that the rain partially evaporates as it falls through the dry atmosphere in East African rain.

The deep wells GW52 and GW41, positioned outside the flooded area, have a higher signature than the rest of the wells, indicating a connection to another, maybe more local recharge area. GW1 showed the most enriched values of $\delta^{18}O$ and $\delta^{2}H$. It is located upstream at a depth of 10 m.b.s.l., next to a man-made open reservoir. Accordingly, water from the reservoir might be partially recharging the water in this well.

The spring sample (GW11) plots between the GMWL and the LMWL showing the most depleted signature of $\delta^{2}H$ and $\delta^{18}O$ in comparison to all of the surface water samples. The spring water has similar water to the deep wells GW52 and GW41, thus confirming that the spring is connected to local recharge (Fig. 6.43). GW4 shows similar results to the rest of the wells even though it is part of the local aquifer (as discussed in Sections 6.2.1 and 6.3.1). This might suggest a possible link between both the confined aquifers.

The spatial variation of the deep wells depicts zoning (Fig. 6.44). All wells with depleted water lie upstream of the wetland. The wells with groundwater signatures close to the LMWL and GMWL are inside the delineated part of the wetland. Wells with water with evaporation effects are, with one exception, always outside the delineated part of the wetland and seem to be a bit further away from the river distance-wise.

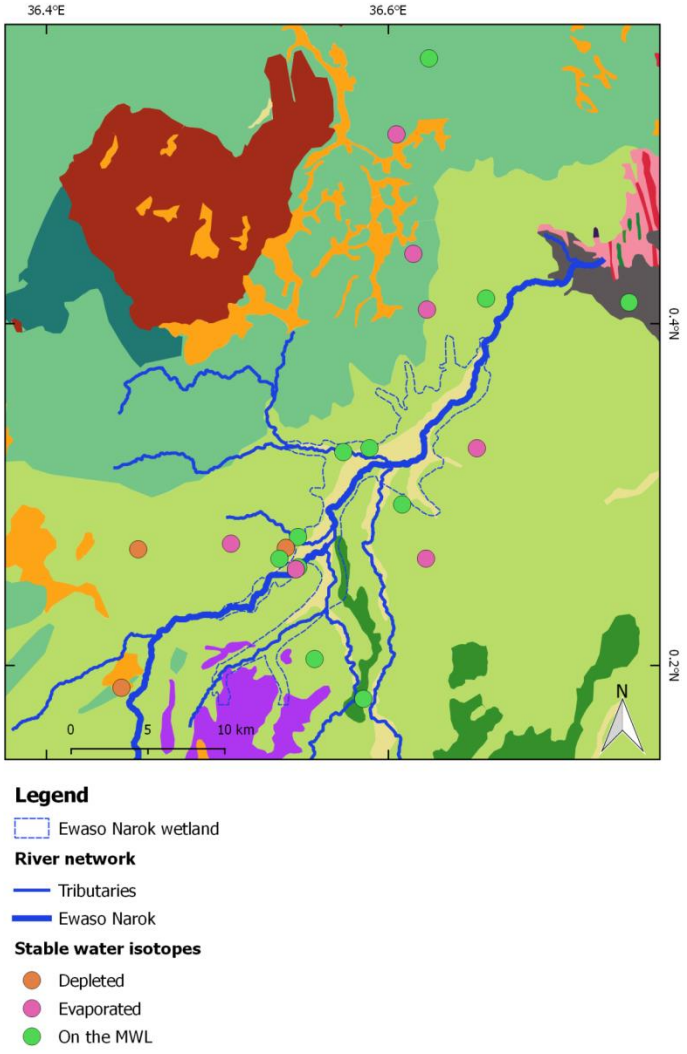

Fig. 6.44: Spatial distribution of $\delta^{18}O$ and $\delta^{2}H$ signatures of groundwater samples characterized by depleted, evaporated, or located on the MWL., drawn on the geological map (cp. Fig. 2.9, p.19).

Comparing surface water and groundwater:

The groundwater samples have lower signatures of $\delta^{2}H$ and $\delta^{18}O$ than the surface water, suggesting that the majority of the surface water does not make a significant and direct contribution to the groundwater. Due to temporal variations, some surface water might infiltrate into the groundwater, especially during flash floods. Additionally, the groundwater is recharged from higher altitudes, as explained beforehand (Fig. 6.45).

The depleted ephemeral streams feeding the Ewaso Narok wetland have a similar isotope signature to the spring and installed piezometers. This suggests a possible link between the sampled groundwater and surface water, possibly that the surface water source might be from increased heights.

The generated non-weighted regression from all the surface and groundwater samples is $\delta^{2}H = 6.8\ \delta^{18}O + 8.8$ (n= 53 and $r^{2}= 0.8577$). The gradient of this regression line is with 6.8 less than eight, indicating that mixing and minor evaporation effects enrich the isotopic composition mainly along the stream and the Ewaso Narok wetland.

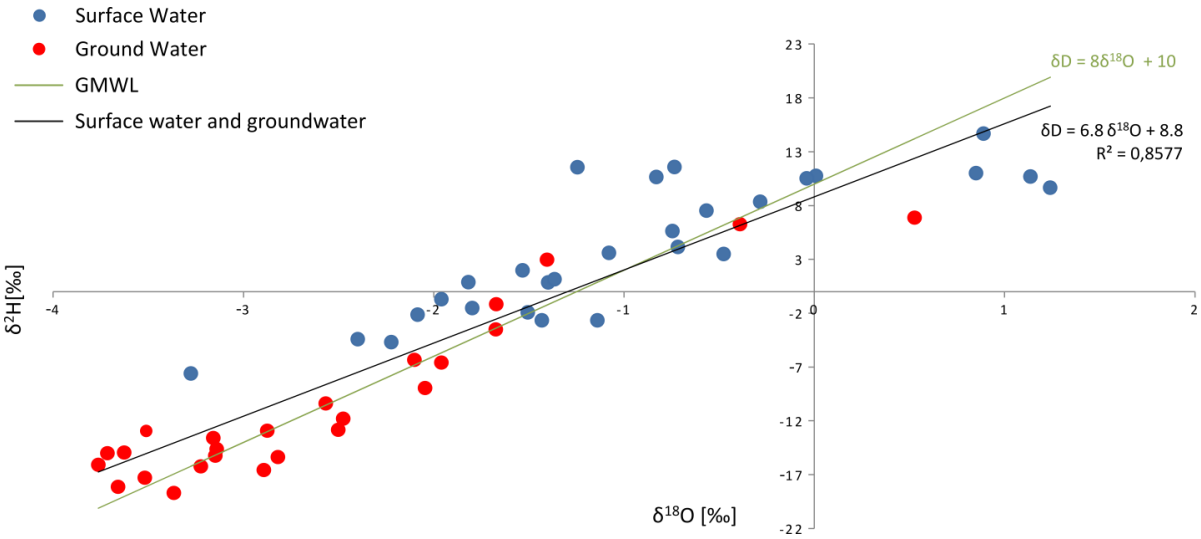

Fig. 6.45: $\delta^{18}O$ versus $\delta^{2}H$ for surface water and groundwater samples with the global meteoric water lines (GWML) and the generated non-weighted regression.

Conclusions

- There are two sources of recharge of groundwater; local and regional aquifers (cp. Samoka 2010).
- There is an indication that the regional confined aquifer system is recharged from high altitudes and that it reaches Ewaso Narok wetland by lateral flow of groundwater. Part of the infiltrated water rises in springs. The local aquifer occurs in the weathered basement rocks. Recharge is either by direct infiltration of rainwater along fissures and fractures in the weathered zones of the rocks or by indirect infiltration of the runoff along with the river courses.
- Surface water is a mixture of water from various sources such as tributaries, rainwater, and groundwater.
- The spring water's similarity to the shallow wells suggests that they have a similar mode of recharge, which could be from the groundwater.
- The similarity of results between the dry and wet sampling of surface water shows a clear connection to a perched aquifer, and exchange with the river happens quickly that the evaporation effects are not vivid.
- Two perched aquifers exist (one under the ephemeral stream and the other under the wetland).
- Flash floods contribute to the negative and low values of both the isotopes.
- Ephemeral streams bring in water with depleted isotopes signatures to the wetland.

Geographic grouping

The Ewaso Narok wetland is relatively small in size; however, an attempt at a geographic grouping is performed with four areas: upstream, middle, downstream, and outlet (Fig. 6.46).

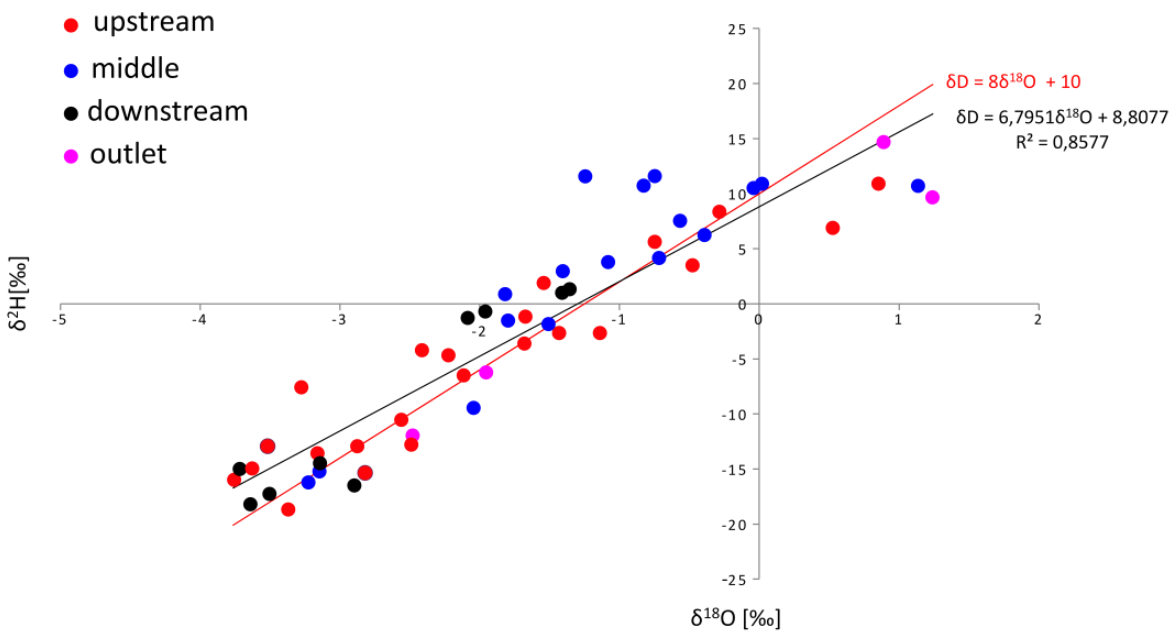

Fig. 6.46: Geographic grouping of $\delta^{18}O$ versus $\delta^{2}H$ for surface water and groundwater samples.

The upstream group (Fig. 6.46 red) has different $\delta^{18}O$ and $\delta^{2}H$ signatures even though the main clustering seems to be in the lower and middle of the graph, as they represent different streams. Those streams contain more depleted isotopes due to groundwater influences. As this type of water mixes with the stagnant wetland water, it gets enriched.

The middle part of the wetland (Fig. 6.46 blue) seems to be clustered close to each other with depleted signatures of $\delta^{18}O$ and $\delta^{2}H$. Few other blue points lie between -2 and 0 ‰ for $\delta^{18}O$.

The geographic grouping of samples suggests a similar mode and a recharge source in the exact regions for the downstream samples (Fig. 6.46 black), which are clustered in the lower left part of the graph. They represent wells in the downstream part of the wetland with similar depleted signatures of $\delta^{18}O$ and $\delta^{2}H$. The other cluster of downstream samples (Fig. 6.46 black) is around the x-axis, representing the surface water points.

The surface water downstream is more depleted than the middle part of the wetland, even though the precipitation, as described in literature and reports, is the same all over. This hints at the groundwater contributing to the wetland in the outlet (Fig. 6.46 purple).

Nitrate

Three of the four wells with elevated nitrate levels (cp. section 6.3.3) show evaporation impact (Fig. 6.47). In terms of location, three wells lie in the lower basin and one in the outflow of the wetland. All four are in the vicinity of a huge ranching industry for cows.

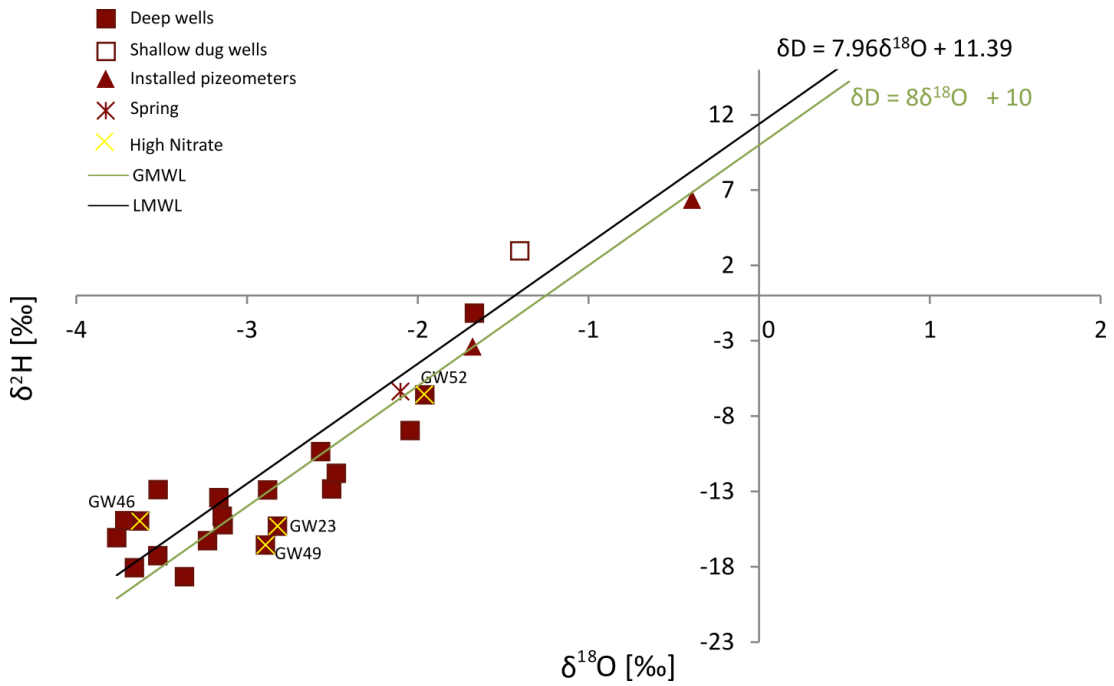

Fig. 6.47: Elevated nitrate shown in the results of the isotopes.

Deuterium and Chloride

Two different exponential lines (labeled as **a** and **b**) can be derived from the relationship between deuterium and chloride(Fig. 6.48). The R square of 0.729 (calculated using **STATA SE16)** shows a significant negative correlation (strong effect size after Moore (2008)) between δD and chlorine (Tab. 6.5). The 95 % confidence interval for the regression shows that when the two graphs collide, the correlation is not significant, as seen in the high chlorine.

The upper points (points that fit the **b line trend**) are mainly groundwater points, except for surface points inside the flooded part of the wetland (Fig. 6. 49). The upper points seem to be closely clustered in the upstream part of the wetland, with a few surface water points at the outlet and middle part of the wetland. The lower points forming the **a line trend** in the graph are groundwater points and surface water points at the outlet of the wetland and downstream, and surface water points inside the wetland (Fig. 6.49).

Tab. 6.5: Correlation between deuterium and chloride.

Source	Sum of Squares	Degree of freedom	Mean Squares
Model	4046.2	4	1011.5
Residual	1501.0	48	31.3
Total	5547.2	52	106.7

Number of observations	52
R^2	0.73
Adj. R^2	0.71
Root Mean Squared Error	5.6
Res. Dev.	322.4

Deuterium	Coef.	Std. Error	t	P >|t|	[95 %] of obs	
b1	-6.5	0.7	-8.9	0	-8	-5.1
b0	-8.8	1.6	-5.3	0	-12.1	-5.5
c1	15.9	2.5	6.3	0	10.9	21
c0	32.5	6.3	5.2	0	19.8	45.1

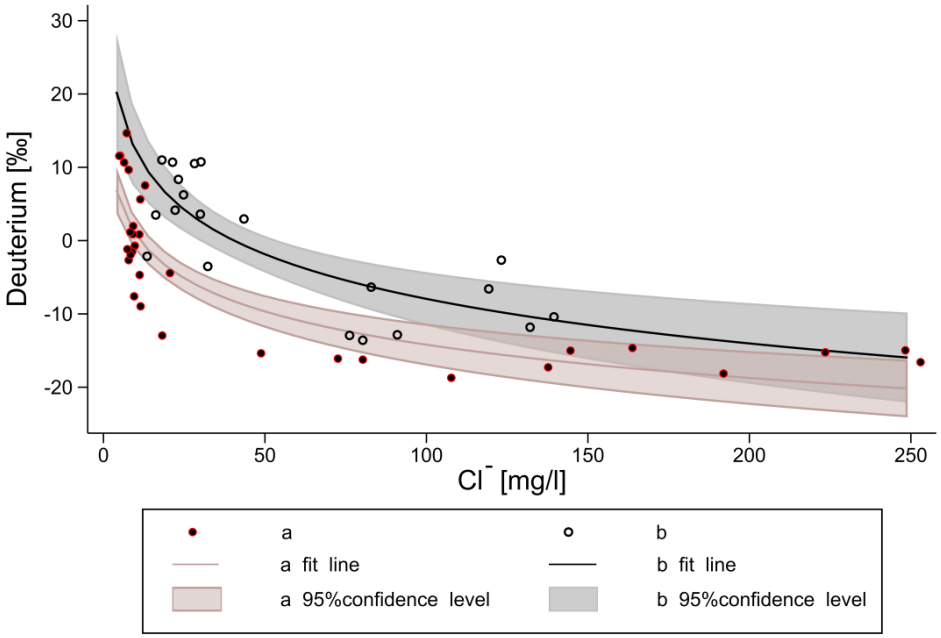

Fig. 6.48: **δ^2H [‰] versus chloride [mg/l] for the water sampled points with two trend lines labeled as a and b and their confidence level.**

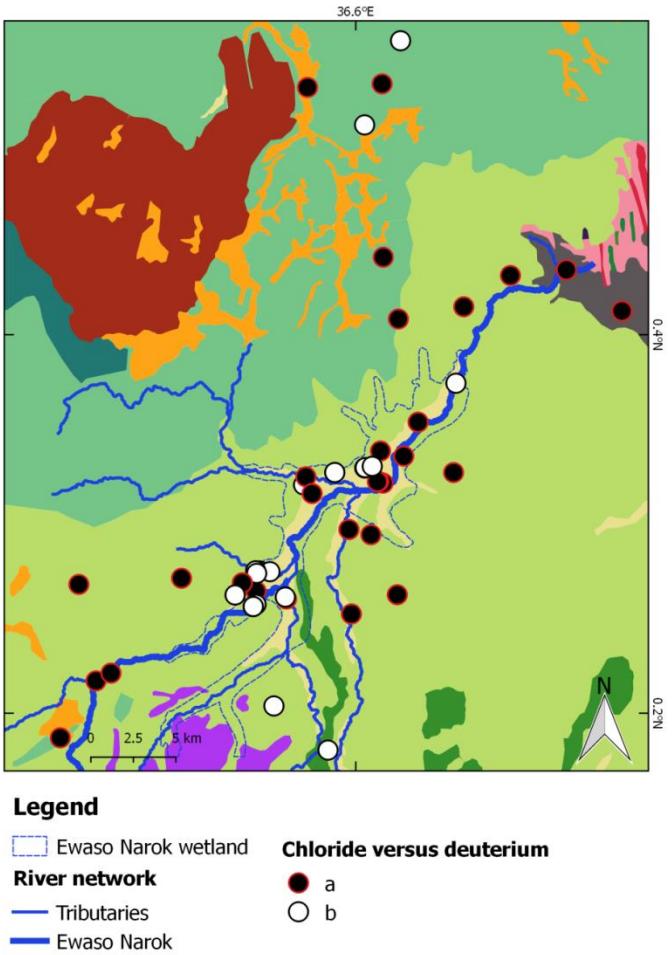

Fig. 6.49: **δ^2H [‰] versus chloride [mg/l] for the sampled points, drawn on the geological map (cp. Fig. 2.9, p.19), with a and b labels (cp. Fig. 6.48).**

The chloride was plotted with depth to check for any trends (Fig. 6.50a). Two regression lines are drawn when trying to exclude the first point from the regression and while including it as it is an influencing point. The chloride concentrations seem to increase with depth. Different geological layers can bear different chlorine levels. As the Ewaso Narok river, with its low chloride water, is a gaining river, it is recharged from groundwater with higher chloride values; the top layers show lower chlorine levels.

The EC again behaves similarly to chloride and shows a significant link to depth (Fig. 6.50b), with no difference when including and disregarding the first point in the regression. This then relates to higher deuterium levels and less evaporation influence.

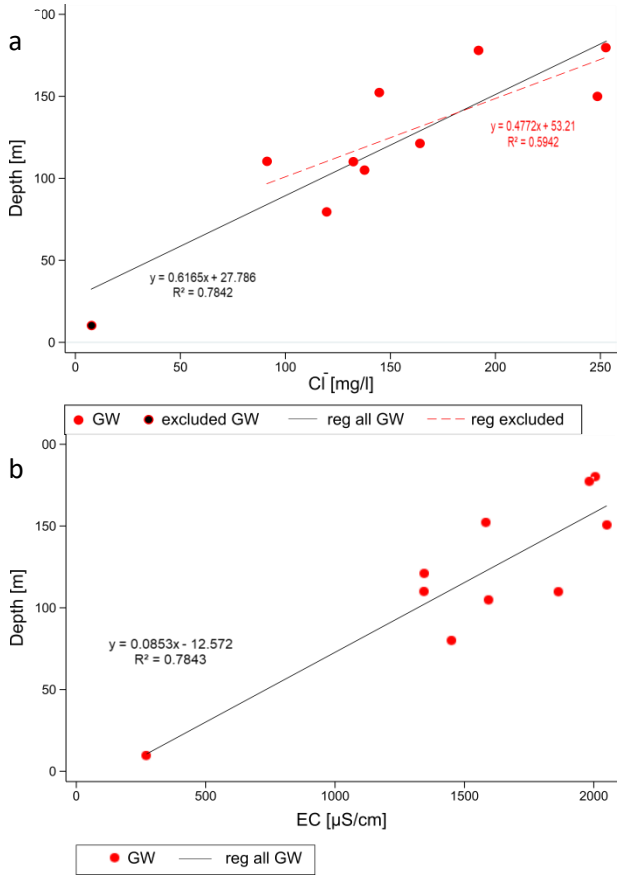

Fig. 6.50: Graphs for groundwater points of a. Depth versus chloride. The regression is drawn twice, once for all the groundwater points and once while excluding one groundwater sample, b. Depth versus electric conductivity.

Since all the surface water points have chloride levels less than 35 mg/l, only the groundwater samples with depleted values of deuterium were drawn with chloride to see if there is a geographical link (Fig. 6.51). The values with the highest chlorine values (>150 mg/l) and depleted deuterium are mainly centered around the wetland outlet.

Lamontagne et al. (2005) showed that groundwater with high Cl^- values and depleted ^2H can be recharged locally within a floodplain or originates from regional groundwater recharge. On the other hand, large floods and bank recharge tend to have depleted signatures of both the stable isotopes and lower chloride concentrations (Lamontagne et al., 2005; Simpson & Herczeg, 1991), which is not the case with the samples with high Cl^- concentrations in Ewaso Narok wetland or river. Transpiration of groundwater deprived of floodplain recharge keeps the

isotopic signature unchanged, but the Cl^- concentration increases (Brunel et al., 1995; Lamontagne et al., 2005), and this can explain some samples. The samples with the middle values of chloride (50 – 150 mg/l) and depleted deuterium are closest to the wetland (Fig. 6.51) and were not sampled throughout flash floods. In addition, they show depleted values of both isotopes, suggesting large floods might be somewhere closer to where the recharge is; higher mountains or regional groundwater recharge.

There is a clustering of the chloride levels and deuterium depending on the geology; Upper, Middle, and Lower phonolites. Another noticeable trend is that the piezometer further away from the river is more depleted in O^{18} and H^2 than those closer to it, indicating possible recharge in the floodplain area. The trend is somewhat similar in groundwater wells too.

Due to the lack of samples from local rainwater and the large range of Cl^- concentration, the evidence is not entirely conclusive. However, the trends show influence from regional groundwater recharge, transpiration, and groundwater discharge derived from floodplain water and local recharge.

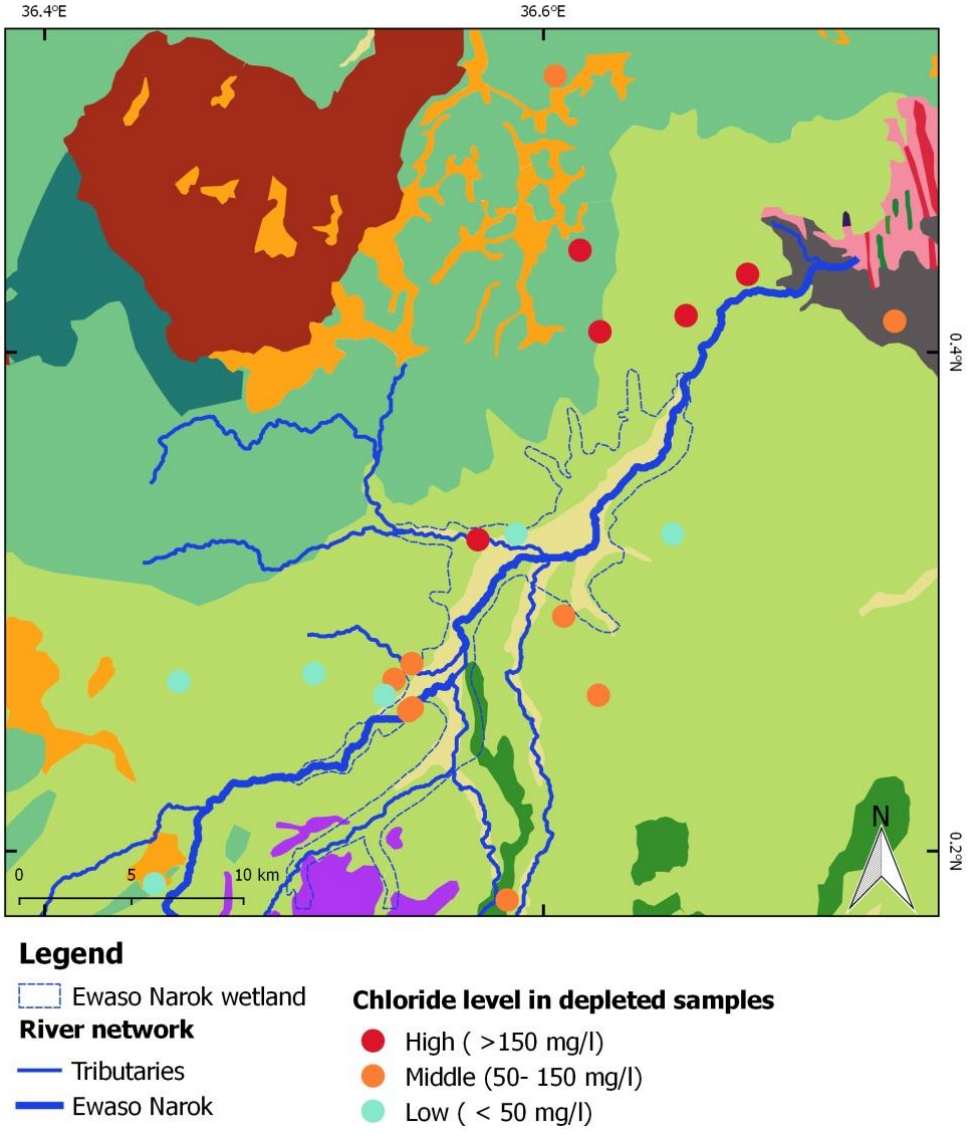

Fig. 6.51: Spatial distribution of chloride levels in depleted groundwater samples, drawn on the geological map (cp. Fig. 2.9, p.19).

To understand the indirect effect of depth on Cl^-, structural equation modeling (mediated regression) is performed using STATA SE16 (Fig. 6.52), and the results are presented (Tab. 6.6).

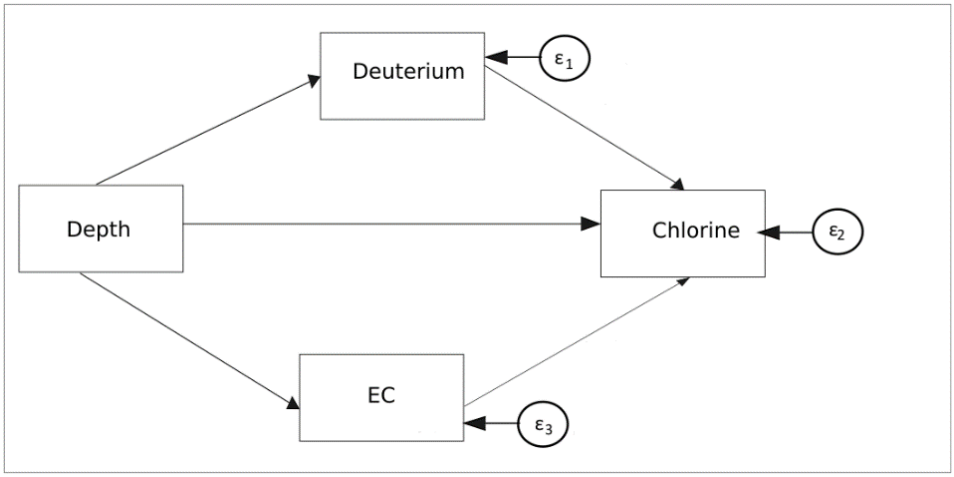

Fig. 6.52: Path diagram of the indirect effect of depth on chlorine. Rectangles represent variables, circles latent variables (composite score of other variables), and straight lines the regression or directional path between variables.

Tab. 6.6: Direct, indirect, and total effects of depth on chlorine.

Direct effect						
	Coef.	Std. Error	z	P >|z|	[95 % Conf. Interval]	
Structural						
Deuterium						
Depth	-0.146	0.02	-7.48	0.00	-0.184	-0.108
Chlorine						
Deuterium	2.039	2.093	0.97	0.330	-2.064	6.143
EC	0.073	0.027	2.74	0.006	0.021	0.125
Depth	**0.576**	0.299	1.93	0.054	-0.01	1.161
EC						
Depth	9.201	2.711	3.39	0.001	3.888	14.515
Indirect effect						
	Coef.	Std. Error	z	P >|z|	[95 % Conf. Interval]	
Structural						
Deuterium						
Depth	0	(No path)				
Chlorine						
Deuterium	0	(No path)				
EC	0	(No path)				
Depth	**0.375**	0.346	1.08	0.279	-0.304	1.054
EC						
Depth	0	(No path)				
Total effect						
	Coef.	Std. Error	z	P >|z|	[95 % Conf. Interval]	
Structural						
Deuterium						
Depth	-1.460	0.02	-7.48	0.000	-0.184	-0.108
Chlorine						
Deuterium	2.039	2.094	0.97	0.330	-2.064	6.143
EC	0.073	0.027	2.74	0.006	0.021	0.125
Depth	0.951	0.290	3.27	0.001	0.382	1.520
EC						
Depth	9.201	2.711	3.39	0.001	3.89	14.515

Depth has a direct causal effect on deuterium and on EC. Both deuterium and EC have a direct causal effect on chlorine. The indirect effect of depth on Cl^- which runs over deuterium and EC is

0.375 (64.7 %) (Tab. 6.6) of the direct effect of the depth. However, this is insignificant and might not be clear because it is a small sample (n < 10). To better estimate, bootstrapping is used to get overestimating, getting influential points only, while giving the confidence interval. The results show that with 80 % confidence, the indirect effect is at least 7 % but not more than 1.2 fold the direct effect (Tab. 6.7).

Tab. 6.7: Bootstrapping result of depth on Cl^- running over deuterium and EC with 80 % confidence interval.

Relation	Observed Coef.	Bootstrap Std. Err.	z	P >|z|	Normal- based [80 % Conf. Interval]	
indirect	0.375	0.451	0.83	0.406	-0.203	0.953
direct	0.576	0.386	1.49	0.135	0.082	1.070
total	0.951	0.375	2.54	0.011	0.471	1.431
q_ind_total	0.394	0.672	0.59	0.557	-0.467	1.255
q_ind_direct	0.651	0.453	1.44	0.150	0.0713	1.232
q_total_direct	1.651	0.453	3.65	0.000	1.071	2.232
diff_direct_indirect	0.201	0.751	0.27	0.789	-0.762	1.163
perc_of_indirect_from_total	0.395	0.672	0.59	0.557	-0.467	1.255
perc_of_indirect_direct	0.651	0.453	1.44	0.150	**0.071**	**1.232**

6.3.5. Hydro-geochemical processes

6.3.5.1. Principal component analysis (PCA)

Multivariate statistical analysis was performed for the hydrochemical data of the samples. The PCA was run on the **following** twelve variables EC, pH, Na^+, K^+, Mg^{2+}, Ca^{2+}, Cl^-, SO_4^{2-}, HCO_3^-, Fe^{2+}, Mn^{2+}, SiO_2, F^-, and NO_3^-. In addition, variables with more than 15 % of values below the LOD (Montcoudiol et al., 2015) were removed. PCA was used to identify the major processes controlling and affecting the hydrochemistry of the water sampled (Belkhiri et al., 2010; Moya et al., 2015). The results show that the variables are significantly correlated. It is decided to pick three components based on the eigenvalues and the scree plot (Tab. 6.8).

Tab. 6.8: Rotated component matrix of the three components.

Rotated Component Matrix[a]			
	Component		
	1	2	3
Na^+ [mg/l]	0.931		
EC [µS/cm]	0.906		
Cl^- [mg/l]	0.888		
SO_4^{2-} [mg/l]	0.887		
HCO_3^- [mg/l]	0.770		
F^- [mg/l]	0.696		
pH	0.656		
Mg^{2+} [mg/l]		0.929	
Ca^{2+} [mg/l]		0.901	
NO_3^- [mg/l]		0.723	
K^+ [mg/l]		0.697	
Si [mg/l]		0.686	
Mn^{2+} [mg/l]			-0.823
Fe^{2+} [mg/l]			-0.630
Extraction Method: Principal Component Analysis. Rotation Method: Varimax with Kaiser Normalization.			
a. Rotation converged in 5 iterations.			

The three components explain 77 % of the variance. Na^+, EC, Cl^-, SO_4^{2-}, HCO_3^-, F^-, and pH show positive loadings to **component 1**. All of these variables, with the exception of Cl^- and SO_4^{2-} are mainly related to silicate weathering, where cations and HCO_3^- are released to water, resulting in an increased EC. Cl^- and SO_4^{2-} indicate an anthropogenic influence or wastewater contamination from manure. Mg^{2+}, Ca^{2+}, NO_3^-, K^+, and Si show positive loading to **component 2,** which corresponds to the weathering of feldspar and cation exchange with the clay minerals and precipitation of secondary clay minerals. A limited supply of oxygen in pore space due to soil flooding leads to oxygen depletion. The Eh is reduced, followed by denitrification, and reduction of iron, manganese, and sulfate (Pezeshki & DeLaune, 2012).Fe^{2+} and Mn^{2+} show positive loadings to **component 3** and are linked to redox processes. Component 1 accounts for 46.3 % of the variance, component 2 for 22.8 %, and component 3 for 7.9 % (Tab. 6.9).

Silicate weathering expressed by PCA1 is the major process controlling the hydrochemistry of groundwater and surface water. The hydrochemistry is further affected by anthropogenic influences, mainly manure. To a lesser extent, the hydrochemistry is related to cation exchange with clay minerals. Furthermore, the hydrochemistry is slightly influenced by biogeochemistry and the reduction of manganese and iron. Influences from other processes are small and might only occur in a few samples, as they were not detected by PCA. Drawing the two main influencing PCA's 1 and 2 in a PCA plot shows two distinct groups, surface water and groundwater (Fig. 6.53). An overlap and scattering of some points away from the groups are noticed. However, an increase in mineralization from surface water to groundwater is evident.

Tab. 6.9: Total variance explained from the PCA result.

	Total Variance Explained								
	Initial Eigenvalues			Extraction Sums of Squared Loadings			Rotation Sums of Squared Loadings		
Component	Total	Variance %	Cumulative %	Total	Variance %	Cumulative %	Total	Variance %	Cumulative %
1	6,487	46.338	46.338	6.487	**46.338**	46.338	5.210	37.218	37.218
2	3,199	22.849	69.186	3.199	**22.849**	69.186	3.813	27.236	64.454
3	1,106	7.903	77.089	1.106	**7.903**	77.089	1.769	12.635	77.089
4	0.809	5.779	82.868						
5	0.618	4.414	87.283						
6	0.485	3.467	90.750						
7	0.461	3.294	94.044						
8	0.329	2.347	96.391						
9	0.245	1.747	98.138						
10	0.126	0.900	99.038						
11	0.072	0.516	99.555						
12	0.042	0.301	99.856						
13	0.014	0.102	99.958						
14	0.006	0.042	100.000						

Performing the HCA using Ward's linkages method, two clusters of surface water and groundwater are observed, similar to the trend observed in the PCA plot. The plausibility of clustering confirms the links between the cluster groups based on the location and type of sampled water, piezometer versus deep wells versus shallow wells. This supplies two main groups showing SF and GW that will be worked with in the following chapters. Sub-clustering using all the different hydrochemical parameters and isotopes is discussed in detail in section 6.4.

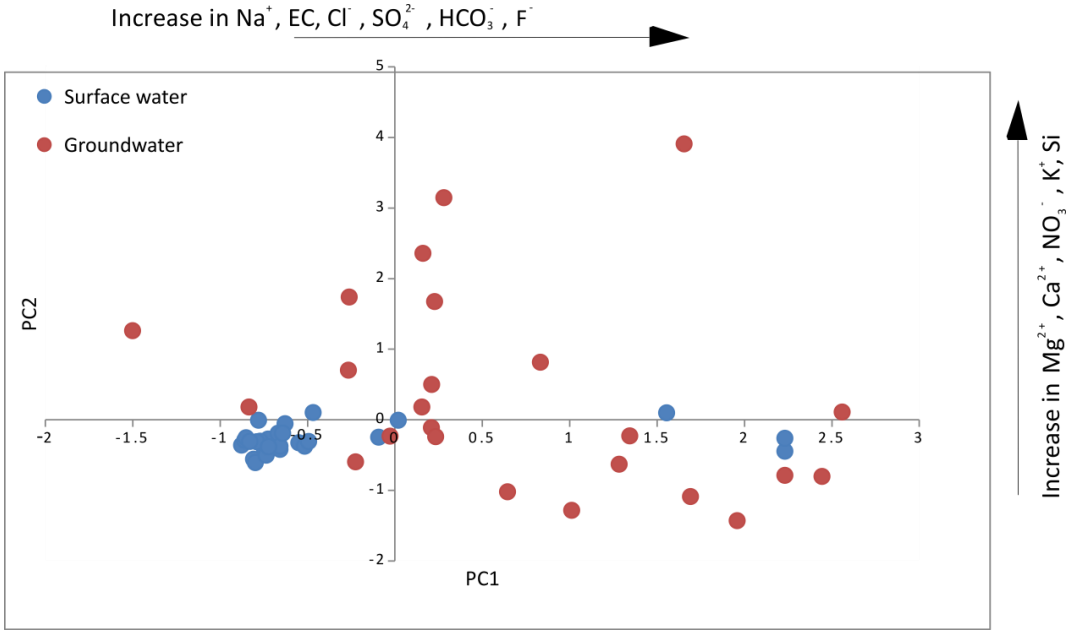

Fig. 6.53: Scatterplot of the two main principal components (PC1 and PC2) showing surface water and groundwater samples' distribution.

6.3.5.2. Calculation and evaluation of stoichiometric relations of dissolved ions

The chemical composition of water is related to the rock, which is being weathered. To identify the main hydro-geochemical processes occurring in this system and strengthen the PCA finding from the previous chapter, the stoichiometric relations of the dissolved ions are calculated and evaluated (Hem, 1985; Liang et al., 2018; Sracek & Zeman, 2004).

Ca^{2+}, Na^{+} rich mineral dissolution, is the primary process responsible for their high amounts in water. As CaO and Na_2O are both soluble in water, they either stay in the water or combine with epidote, hornblende, and plagioclase during weathering (Ceryan, 2012). As described in subchapter 6.2, chemical weathering is high in the area. Accordingly, it is typical to find the water enriched in Na^{+} and Ca^{2+} (max concentrations of 412 mg/l and 121 mg/l respectively) relative to K^{+} (maximum concentration of 30.3 mg/l), as they are released to weathering solutions in preference to K^{+} (Nesbitt et al., 1980). According to the X-ray diffraction, **plagioclase feldspar** (anorthite and albite) were identified. Thus, their weathering is most likely leading to the observed enrichment of Ca^{2+} and Na^{+} (Hem, 1985). Potassium is abundant in lower amounts and is from **k-feldspar** and its weathering. K-feldspar is relatively resistant to chemical weathering (Goldich, 1938). As large cations are preferentially retained on clay minerals (Domenico & Schwartz, 1998; White & Brantley, 2018; Wiklander, 1964), K^{+} is retained in preference to Na^{+} in addition to many other sinks being available for K^{+}, but not for Na^{+} (Hounslow, 2018). Anorthite and albite are more susceptible to weathering, yielding metal cation and silica to the solution and forming clay minerals with aluminum (Domenico & Schwartz, 1998; White & Brantley, 2018). In addition, the hydrolysis of feldspar produces **kaolinite,** which was vivid in the XRD results.

Muscovite/Illte was as well identified in the field and in the XRD results. Muscovite's weathering results in kaolinite. Illite is an altered form of muscovite and feldspar weathering. It is produced as well from plagioclase. Calcite is noticed as well and is from plagioclase or from chemical precipitation once Ca^{2+} and HCO_3^{-} have been dissolved.

The system had high levels of silica concentrations, which is explained by the feldspar chemical weathering. SiO_2 concentrations show a decrease with the increase in weathering. As silica has an intermediate behavior, part of it remains fixed, forming new clay minerals, and the other part is removed in the water (Ceryan, 2012; Tardy, 1971) during weathering. Silica released by weathering is transported underground and along river water. Part of it might remain in the weathering zone as it precipitates in the rocks' joints and fractures as silica.

Feldspar dissolution's chemical reactions can yield theoretical dissolution lines based on how many moles of each anion and dissolved silica the feldspar releases. For the dissolution of anorthite the Ca^{2+}: SiO_2 ratio has a 1:1 slope. The theoretical dissolution line for albite is Na^+: SiO_2 of 1:2 slope (Appelo & Postma, 2005). The theoretical dissolution line of k-feldspar is K^+: SiO_2 slope of 1:2. Na^+ surface water points plots above and below the albite's theoretical dissolution line, proving its (Fig. 6.54a). Regarding Na^+ of groundwater, a few points plot around the 1:2 theoretical dissolution line, but most of the sampled points lie high above. The Na^+ source is silicate dissolution of Na-feldspar, like albite or any other member of the plagioclase solid solution series between albite and anorthite (Fisher & Mullican, 1997).

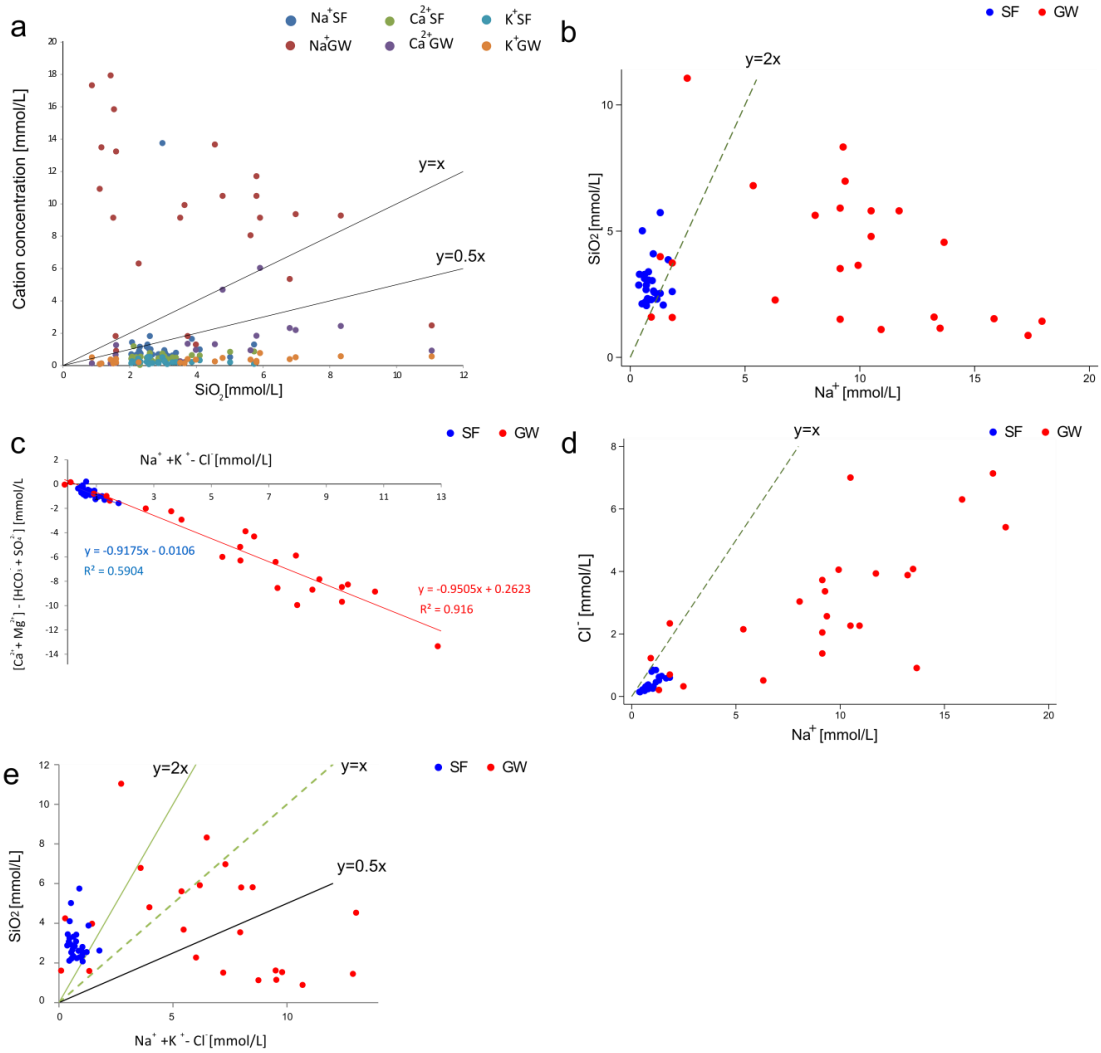

Fig. 6.54: Stoichiometric relations graphs showing silicate weathering and cation exchange for surface water and groundwater: a. Anorthite, albite, and k-feldspar weathering, b. Albite weathering, c. Sodium ion and chloride ion, d.($Na^+ + K^+ - Cl^-$) versus ($Ca^{2+} + Mg^{2+}$) - ($HCO_3^- + SO_4^{2-}$), e. ($Na^+ + K^+ - Cl^-$) versus silica.

K^+ of surface water points all plot below the 1:2 theoretical dissolution line of K-feldspar. The same applies to the groundwater samples. Ca^{2+} in surface water lies below the anorthite theoretical dissolution line. Some of the groundwater points lie on the anorthite line, but many lie below it. This indicates that the main source of Ca^{2+} is anorthite dissolution. Other sources of Ca^{2+} in water in this area are from carbonates (Kovalevsky et al., 2004), clay, calcite of hornblendes, also called amphiboles, and pyroxenes (Appelo & Postma, 2005). Ca^{2+} preference of the soil is attributed to the organic phase of the soil. Stronger binding of Ca^{2+} to organic soil is noted in the literature (Naylor & Overstreet, 1969; Van Bladel & Gheyi, 1980).

The distribution of data points indicates cation exchange between **Ca^{2+} and K^+** with respect to the occurrence of clay minerals. Kaolinite, mainly as potassium in illite, is incorporated and cannot be removed by further ion-exchange reactions (Domenico & Schwartz, 1998). Exchange of cations on the clay happens as the floor of the wetland is of clay. Na^+ and Ca^{2+} are removed by surface runoff through the weathering zone to groundwater or streams. The relative exchange property of the cations in the clay mineral (e.g., montmorillonites) has been stated by Ronov (1945) as $Na^+ < H^+ < K^+ < Mg^{2+} < Ca^{2+}$.

The graph of Na^+ versus SiO_2 with the line of slope 1:2, shows that feldspar weathering is the dominant source of Na^+ (Appelo & Postma, 2005) in surface water points (Fig. 6.54b). The effluent sample is an outlier and accordingly is disregarded from all the following hydro-geochemical calculations. The groundwater points show lower SiO_2 to Na^+ ratios and are induced by an increase of Na^+ during cation exchange or precipitation of clay minerals other than kaolinite, retaining the SiO_2 in the solid solution (Appelo & Postma, 2005) after Burghof (2017).

Another possible source of Na^+ in the surface water is NaCl, as Na^+: Cl^- ratio in the surface water is around one (Fig. 6.54c). The relationship between Na^+ and Cl^- has been used to identify the mechanism for acquiring salinity in semiarid to arid regions and quantify the atmospheric contributions (Sarin et al., 1989; Singh et al., 2005) after Tiwari and Singh (2014).

All the samples plotting above 1 indicate Na^+ released from silicate weathering reactions (Meybeck, 1987). Most of the sampled groundwater show Na^+: Cl^- above one, indicating albite as the source of Na^+. The surface water samples show similar results, indicating albite weathering. However, they lie closer to the 1:1 line that indicates NaCl as a possible source for Na^+ (Hounslow, 2018). The high values show that there is no contribution from atmospheric precipitation and that the high levels of major ions are derived from weathering of silicate rock minerals or anthropogenic sources (Tiwari & Singh, 2014). The lower molar ratio (Na^+: Cl^- less than 1) suggests ion exchange of Na^+ for Ca^{2+} and Mg^{2+} in clay.

In order to check if ion exchange occurs, (Na^++ K^+- Cl^-) is plotted against (Ca^{2+}+ Mg^{2+}) - (HCO_3^-+ SO_4^{2-}) (Fig. 6.54d). The slope value of -1 indicates the ion exchange between Na^+, Ca^{2+}, and Mg^{2+} (McLean et al., 2000). Both surface water, as well as groundwater indicate ion exchange with slopes close to the theoretical value of -1 (-0.9175 and -0.9505, respectively).

The SiO_2 versus non-halite sodium (Na^+ + K^+ - Cl^-) value is calculated (Fig. 6.54e). Fifteen groundwater samples are impacted by cation exchange, five samples contain a considerable amount of ferromagnesian minerals, and five are clearly influenced by albite dissolution. In regards to surface water samples, twenty-five samples have a considerable amount of ferromagnesian minerals, two are from albite source, one is influenced by cation exchange.

The spatial distribution based on weathering impact shows that Na^+ derives from albite dissolution occurring outside the flooded area of the wetland (Fig. 6.55). Most of the ferromagnesium minerals and their weathering, indicating that sodium is from plagioclase occurred in the wetland flooded area with a few exceptions. The rest of the samples in the flooded area show that sodium excess results from the cation exchange.

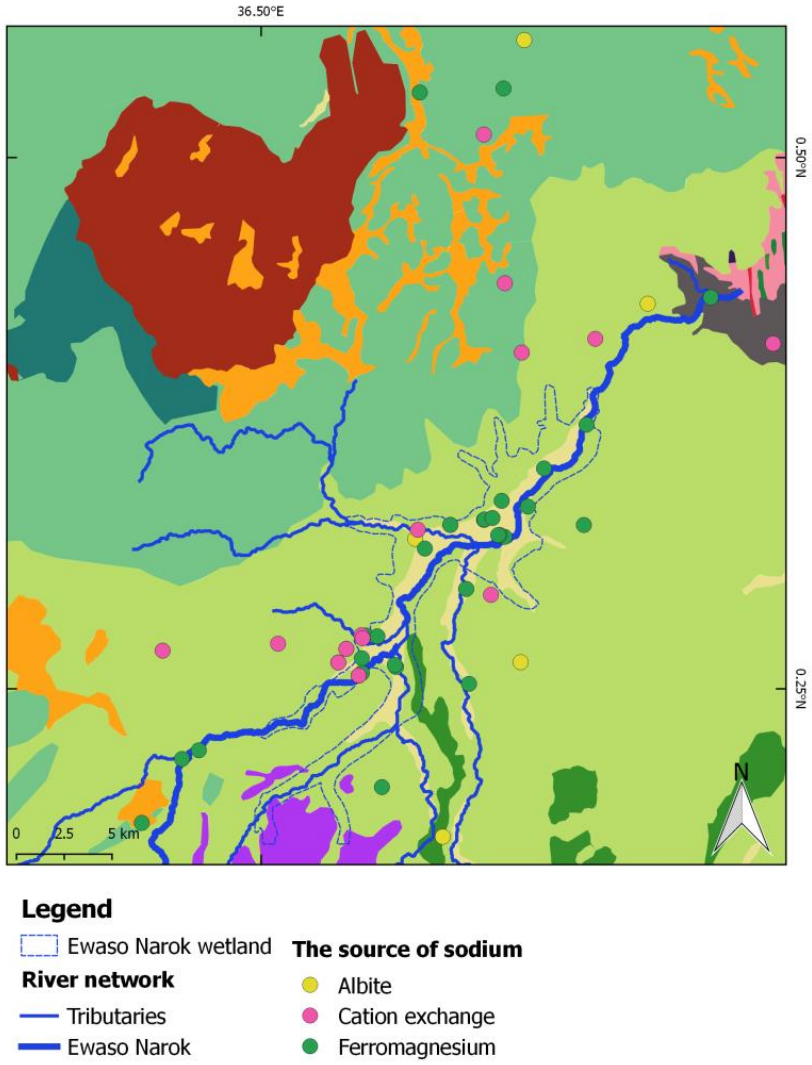

Fig. 6.55: Spatial distribution of the weathering impact as depicted in the water composition of the various sampling points, drawn on the geological map (c.p Fig. 2.9, p.19).

Schoeller (1977) proposed chloro-alkaline indices (CAI) to give insight to the base-exchange reaction between groundwater and its host environment:

$$\text{CAI I} = \frac{Cl^- + (Na^+ + K^+)}{Cl^-} \qquad \text{(Eq. 6.2)}$$

$$\text{CAI II} = \frac{Cl^- + (Na^+ + K^+)}{SO_4^{2-} + HCO_3^- + CO_3^{2-} + NO_3^-} \qquad \text{(Eq. 6.3)}$$

All groundwater samples, with the exception of the spring, have negative values for both CAIs, indicating chloro-alkaline disequilibrium. This means that the reaction is a cation-anion exchange reaction, where Ca^{2+} or Mg^{2+} in groundwater is exchanged with Na^+ or K^+ in the host rocks. This confirms the SiO_2 versus ($Na^+ + K^+ - Cl^-$) analysis.

Further proof of feldspar weathering is the positioning of the surface water samples below or almost on the 1:1 line of ($Na^+ + K^+$) versus total cations (Fig. 6.56a). The samples which show lower ($Na^+ + K^+$) concentrations seem to result from Ca^{2+} versus Na^+ exchange reaction. Less than half of the groundwater points lie on the 1:1 line, but the rest are under it.

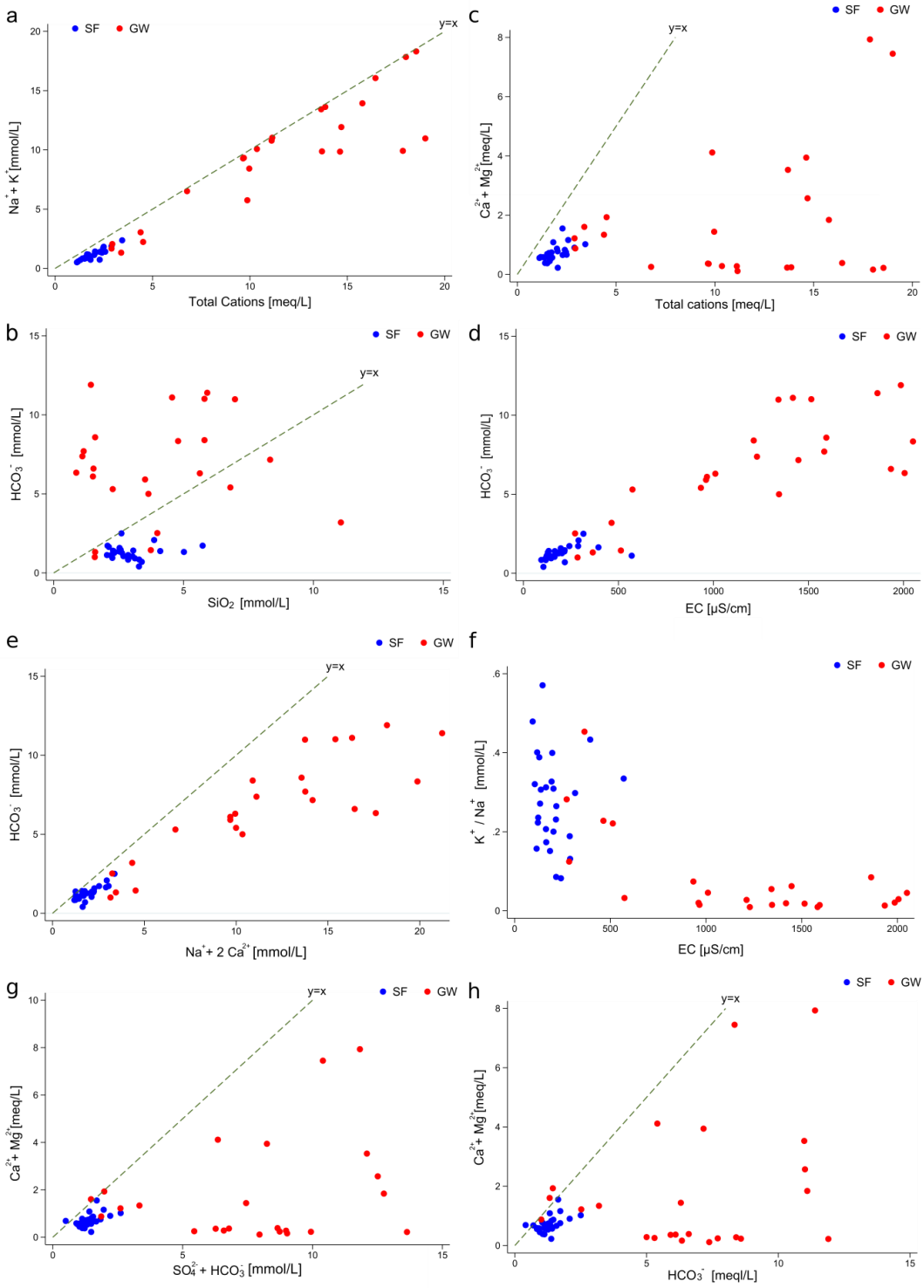

Fig. 6.56: Stoichiometric relation graphs for sampled surface water and groundwater points: a. $Na^+ + K^+$ versus total cations, b. $Ca^{2+} + Mg^{2+}$ versus total cation, c. Bicarbonate versus silica, d. HCO_3^- versus EC. e. ($Na^+ + 2Ca^{2+}$) versus HCO_3^-, f. K^+/Na^+ versus EC , g.($HCO_3^- + SO_4^{2-}$) versus ($Ca^{2+}+ Mg^{2+}$), h. HCO_3^- versus ($Ca^{2+}+ Mg^{2+}$).

The (Ca^{2+} + Mg^{2+}) versus total cations plot (Fig. 6.56b) shows that all samples lie below the 1:1 aquiline. (Ca^{2+} + Mg^{2+}) accordingly contribute highly to the total cations indicating silicate weathering. In general, if bicarbonate is less than or equal to silica (Fig. 6.56c), then albite is weathered. As silicate weathering is the main process happening, silica is released in the solution, as discussed before.

EC versus HCO_3^- (Fig. 6.56d) further confirms silicate weathering as one of the major mineralization sources. Most of the surface water samples show lower mineralization compared to groundwater samples, except for a few.

While surface water shows ratios of HCO_3^- / (Na^+ + 2 Ca^{2+}) around 1 (Fig. 6.56e), suggesting plagioclase weathering (Van der Weijden & Pacheco, 2003), groundwater samples lie below the 1:1 line suggesting another source of mineralization. Surface water had higher K^+/Na^+ ratios than groundwater points with the exception of four wells (Fig. 6.56f), indicating either contact with vegetation and soil (King et al., 2014) or high rates of k-feldspar weathering (Burghof, 2017).

Samples lying on the 1:1 line (Fig. 6.56g) suggest that these ions resulted from the weathering of carbonates or sulfate minerals (Cerling et al., 1989; Datta and Tyagi, 1996). The surface water was scattered below yet close to the 1:1 line. Few lie to the left side, indicating that an excess of (Ca^{2+} and Mg^{2+}) in surface water may be due to calcite's dissolution. Samples shifted to the right (excess of (SO_4^{2-} + HCO_3^-) over (Ca^{2+} and Mg^{2+})) indicate after Cerling et al. (1989) and Fisher & Mullican (1997) a contribution from a non-carbon source, and thus to a contribution from silicate weathering. This applies to both the surface water points and the groundwater points being affected by cation exchange with clay minerals, as the wetland floor is made of clay. If (Ca^{2+} and Mg^{2+}) originate solely from carbonate and silicate weathering, they will be balanced by alkalinity alone, which is not the case, especially in groundwater (Fig. 6.56g). This is additionally proved by the (Ca^{2+} + Mg^{2+}) to HCO_3^--ratio (Fig. 6.56h). Only a few samples from surface water and even fewer from groundwater plot close to the 1:1 ratio indicating weathering of carbonate rocks.

A value of bicarbonate/silica > 10 indicates carbonate weathering, and a value < 5 indicates silicate weathering (Hounslow, 2018). The results show that all of the samples have a bicarbonate/silica value of less than five, with three exceptions of groundwater (GW45: 8.3, GW49: 7.3, and GW17: 6.7).

According to Kovalevsky et al. (2004), the lithology of aquifers can be identified if the ratio of (Ca^{2+}+ Mg^{2+}) versus (Na^++ K^+) is less than 1, then there is silicate weathering, and above 1 show carbonaceous influences. With the exceptions of the shallow hand-dug wells and the dam, most of the surface water and groundwater points lie below 1 (Fig. 6.57a).

Sodium bicarbonate is a result of the weathering of silicate minerals in igneous rocks. Bicarbonate tends to predominate in water in areas where vegetation grows profusely (Hem, 1985).

To further understand the other possible sources of dissolution, Ca^{2+}/Mg^{2+} are plotted (Fig. 6.57b). If their molar ratio is greater than 2, it indicates the dissolution of silicate minerals (Katz et al., 1997), which is almost all the surface points sampled and some groundwater points. The rest of the groundwater points show Ca^{2+}/Mg^{2+} that is greater than 1 yet smaller than 2,

indicating a more dominant calcite contribution from the rocks (Mayo & Loucks, 1995). The ratio of Ca^{2+}/Mg^{2+} seems to decrease with the distance from weathering; the deeper the points sampled, the less the weathering and more fresh rock and the Ca^{2+}/Mg^{2+} decreases. The groundwater points are accordingly plotted as Ca^{2+}/HCO_3^- (Fig. 6.57c), with the suspected calcite (attained from Fig. 6.57c and are GW4, GW10, GW7, GW45, GW52, GW47, and GW17) dissolution marked. If the ratio is 1:2, then calcium and bicarbonate solely originated from calcite. If it is 1:4, it is from dolomite weathering (Subramani et al., 2010). The results show that three of the suspected samples originate from calcite weathering.

Further proof of calcite dissolution can be derived from Ca^{2+}/SO_4^{2-}- ratio (Fig. 6.57d). After Das & Kaur (2001) indicates a ratio of 1:2, the dissolution of gypsum or anhydrite, both of which do not exist in the study area. When the samples have excess calcium, there is an additional geochemical process, as is the case with surface water points. In the groundwater samples, excess sulfate over calcium indicates the removal of calcium from the system, likely by calcite precipitation.

An increase in salinity demonstrated by Cl^- with a relative increase in Ca^{2+} and Mg^{2+}, indicating that the carbonate weathering in the aquifer was done by chloride-bearing water (Fig. 6.57e). Chloride is usually linked to evaporation or anthropogenic influence, including potassium fertilizers (Kresic, 2006) or micas dissolution.

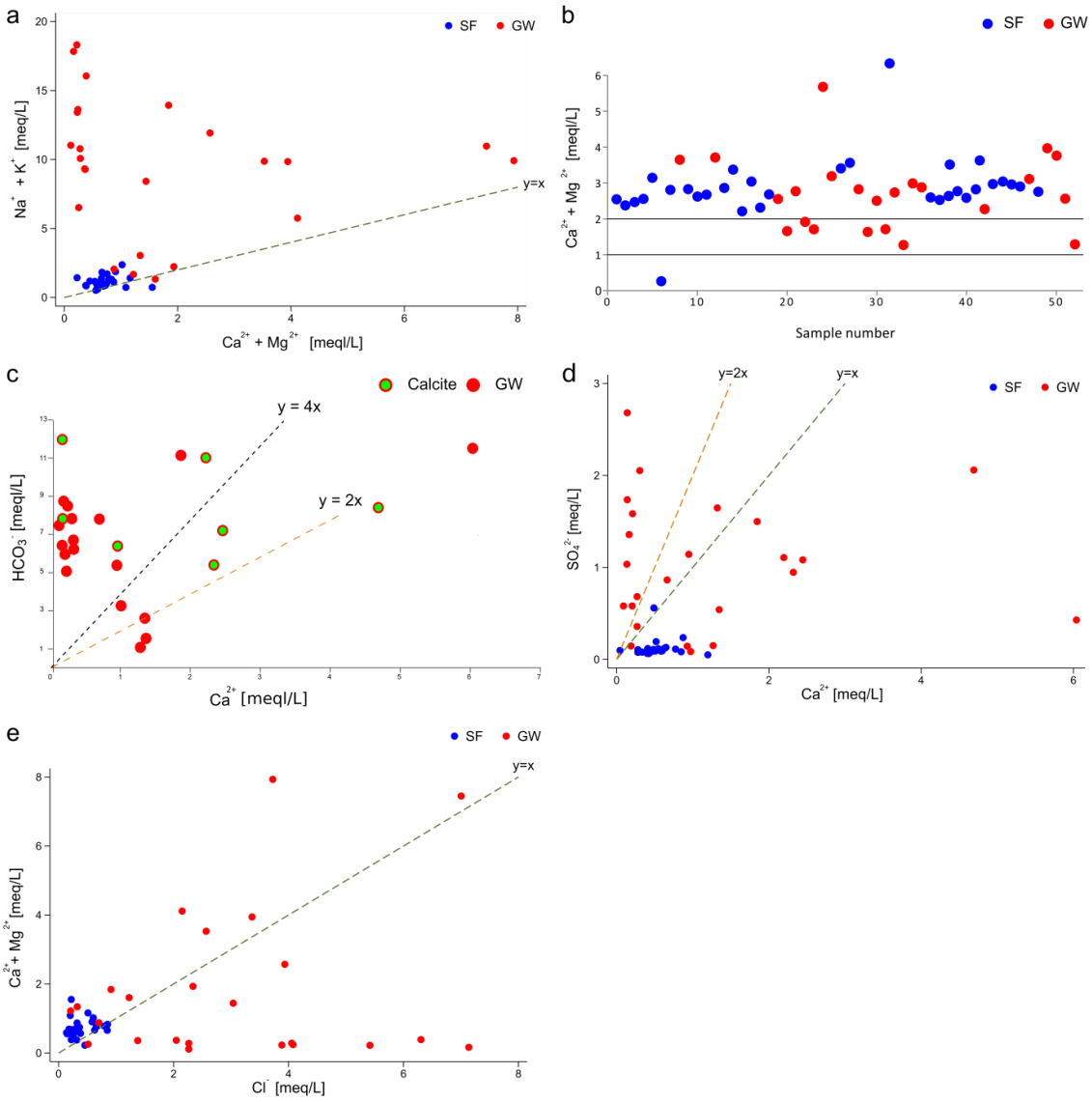

Fig. 6.57: Stoichiometric relation graphs for surface water and groundwater points showing different influences: a. $Na^+ + K^+$ versus $Ca^{2+} + Mg^{2+}$, b. Ca^{2+}/Mg^{2+}, c. Ca^{2+} versus HCO_3^- with suspected calcite samples marked, d. Ca^{2+} versus SO_4^{2-}, e. $Ca^{2+} + Mg^{2+}$ versus Cl^-.

Redox sensitive species

Soil flooding means a limited supply of oxygen in pore space. This leads to oxygen depletion and reduced soil oxidation-reduction potential (Eh), followed by denitrification, reduction of iron, manganese, and sulfate (Pezeshki & DeLaune, 2012). These trends are observed in iron and manganese plots (Fig. 6.58a and Fig. 6.58b). Two outlier points were disregarded from the presentation in the following redox-sensitive species graphs.

Fe^{2+} concentrations are observed mainly in the surface water samples, emerging from the dissolution of abundant ferrous oxides and silicates (Frankenberger, 1994) and the reduction of iron hydroxides. The redox potential of the samples with high Fe^{2+} was above the given threshold of 100 mV (Mitsch & Gosselink, 2000). However, the determination of redox potentials in the field is difficult, and values should always be regarded with caution (Appelo and Postma 2005).

Detectable concentrations of Mn^{2+} are observed above and below the threshold of 225 mV (Mitsch & Gosselink, 2000). Mn^{2+} concentrations are higher in the surface water samples and in four groundwater samples (Fig. 6.58b) and are linked to the reduction of manganese hydroxide.

The NO_3^- concentrations (Fig. 6.58c) were mainly detected in groundwater samples with reducing conditions (below 250 mV). This means that these samples were not yet denitrified, even though the redox potential is below 250 mV. Two groundwater samples with detectable NO_3^- concentrations were an exception showing oxidizing conditions (redox potential above 250 mV). This might indicate that existing NO_3^- was removed by denitrification in water with lower redox potentials (Mitsch and Gosselink 2007).

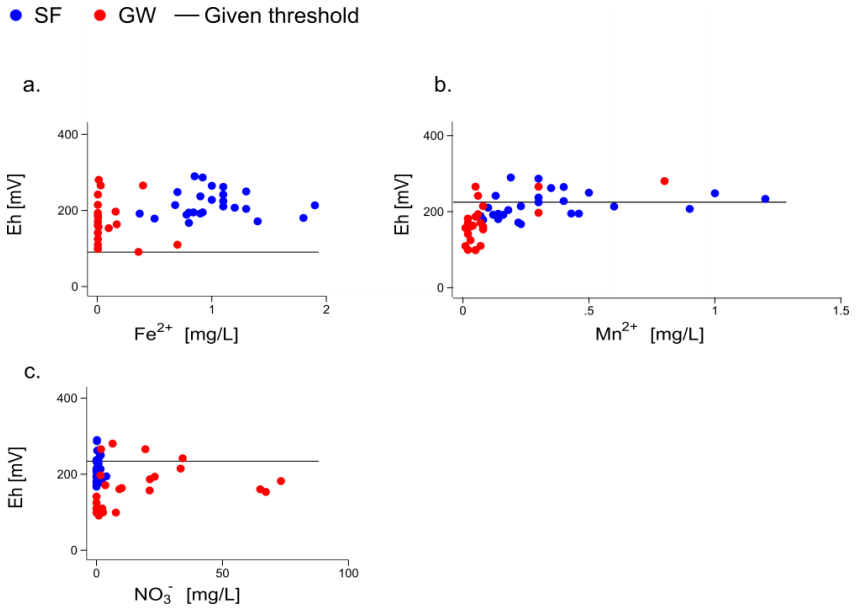

Fig. 6.58: Plots of redox-sensitive species: a. Fe^{2+} versus Eh, b. Mn^{2+} versus Eh, c. NO_3^- versus Eh.

Land use effect and evaporation

Sulfate and chloride (Fig. 6.59a) show a correlation in the groundwater samples, indicating surface contamination from manure or wastewater. TDS is high because of land-use effects. Accordingly, it cannot be reliable for Gibbs's calculation.

The molar ratio of Na^+/Cl^- is used to identify evaporation processes in groundwater (Subramani et al., 2010) to rule out the evaporation impacting the groundwater samples. The groundwater points show more of an inclined trend with Na^+/Cl^- ratio decreasing with increasing salinity (EC) (Fig. 6.59b), which again hints at the removal of sodium by ion exchange. This indicates that evaporation is not the major geochemical process controlling groundwater chemistry, which comes in terms with the results of the isotopes (Section 6.3.4). Chloride in groundwater originates from natural or anthropogenic sources that include fertilizers, animal wastes, and leakages from landfills (Appelo & Postma, 2005).

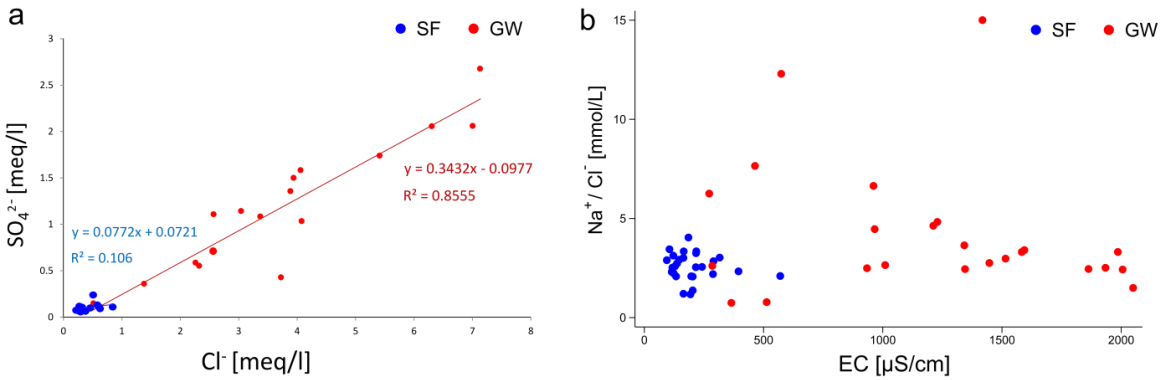

Fig. 6.59: Plots of sampled surface water and groundwater showing: a. Cl^- versus SO_4^{2-}, b. Na^+/Cl^- versus EC.

6.4. Statistical analysis and classification

A hierarchical cluster analysis was carried out using ***Ward's method***, applying a ***squared Euclidean distance*** as the distance or measure of similarity (Fig. 6.60). This analysis took the distance of two clusters as the average of the distances between all pairs of cases with one member of the pair from each of the clusters. This makes it possible to determine the optimum number of sub-aquifer units or clusters that are needed to work with. In the next stage, hierarchical cluster analysis for sub-grouping was rerun by zooming into each cluster to refine the connectivity amongst the sub-aquifer units in view of geographical and geological aspects.

The **SPSS®** computer code used for the cluster analysis performed in the hydrochemical water data analysis used the following; T_W, pH, Redox, DO, TDS, EC, all major ions (Ca^{2+}, Cl^-, NO_3^-, HCO_3^-, K^+, Mg^{2+}, Na^+, PO_4^{3-}, SO_4^{2-}), minor elements (NO_2^-, Fe^{2+}, Mn^{2+}, Al^{3+}, SiO_2, CO_2, Sr^{+2}, NH_4^+, BO_3^-, Br^-, F^-), and trace cations (As, Cd, Cr, Cu, Ni, Pb, Zn, Sr), as well as stable water isotopes ($\delta^{18}O$, δ^2H).

The cluster analysis was used first to define water bodies (sections that display similar hydrochemistry and isotopes) and then to find the hydrochemical "relationship" between different surface water and groundwater points. Later, it helped divide the aquifer into cells or compartments (a subdivision of the aquifer into sub-aquifer units) with similar hydrochemical characteristics.

The dendrogram results are presented as relative distances on a scale of 0 - 25 (Fig. 6.60). These detailed dendrograms' results will help decide which sampled points can be combined together as a cell in the MCMsf model with average unique hydrochemical values. The dendrogram shows the clusters of water sources and the possible spatial correlation between them. Cluster 1 is mainly made of surface water points, whereas cluster 2 is mainly made of groundwater points. Clusters 1 and 2 are not related at all. In order to elaborate further, the cluster analysis was run again on cluster 1 (twice) and cluster 2 (Fig. 6.61). Cluster 1 is divided into six sub-cluster (1.1, 1.2, 1.3, 1.4, 1.5, and 1.6). Sub-clusters 1.1 and 1.2 are related but not related to sub-cluster 1.3. All three show a weak link to 1.4. Cluster 1.5 and cluster 1.6 are related but are not at all related to 1.1, 1.2, 1.3, and 1.4. Cluster 2 is divided into three sub-clusters (2.1, 2.2, and 2.3). Sub-clusters 2.2 and 2.3 are related to each other. However, they are not related to 2.1. The different clusters were given different colors and displayed on the map. Sub-cluster 1.1 is made of surface water points, including the furrow in the wetland downstream, a flooded

sample in the wetland, two river points upstream of the wetland (next to the fish ponds), and the inlet from Pesi and Mathera (Fig. 6.61).

Sub-cluster 1.2 comprises surface water from the end part of the wetland. These points lie on the right side of the river and channel, even though some are flooded, and others were sampled when dry. This sub-cluster includes the last sampled point in the river that brings all the water together.

Sub-cluster 1.3 is (Fig. 6.61) built by flooded samples and dry samples, the river itself in the upstream part of the wetland. Sub-cluster 1.4 is represented by one flooded sample in the wetland. Sub-cluster 1.5 comprises surface water samples entering the wetland from the left (Melwa's direction), a well in the same area upstream, a piezometer in the middle part of the wetland, the river close to it, and a dam in the end part of the wetland. Sub-cluster 1.6 is made of two groundwater wells, one left to the wetland and another right of the wetland, the spring upstream to the wetland, and the canal leading to the wetland from Pesi.

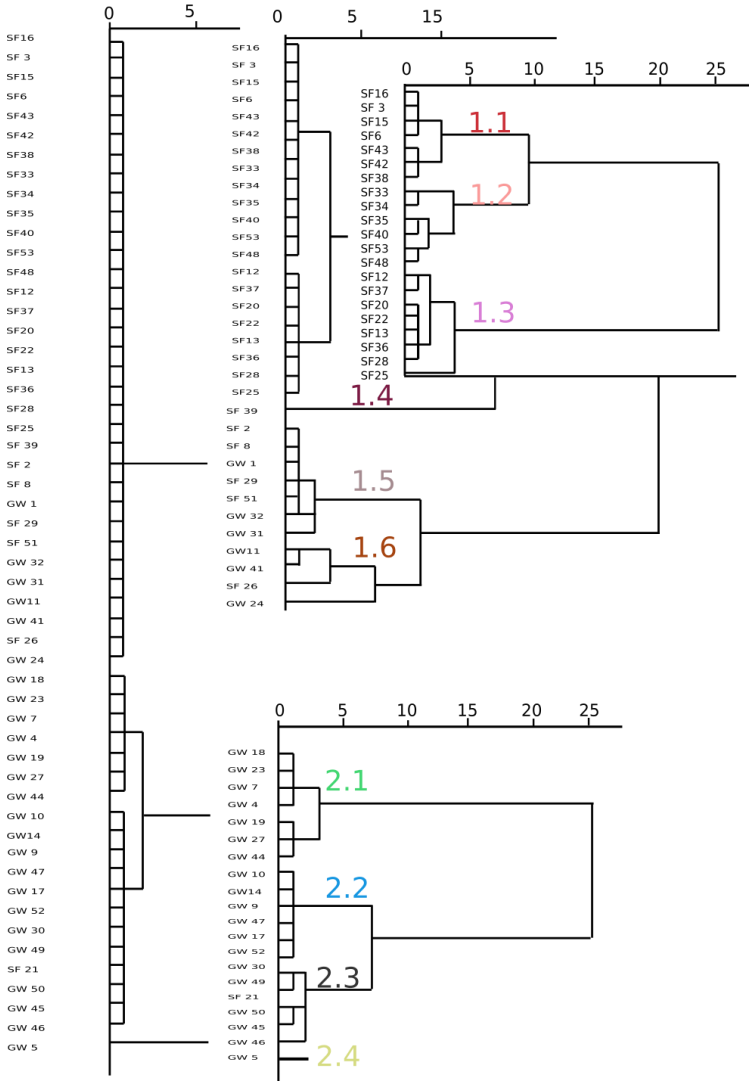

Fig. 6.60: Dendrogram obtained from the SPSS® cluster analysis using Ward Linkage on the sampled hydrochemical data. Each cluster is marked with a different color. For its location, cp. Fig. 6.61.

In regards to groundwater cluster 2, sub-cluster 2.1 consists of borehole samples mainly in the upstream part with one exception (GW44) (Fig. 6.61). Sub-cluster 2.2 is made of the piezometer

in the upstream part and three wells next to it, and two boreholes in the end part of the wetland. Sub-cluster 2.3 is composed of wells at the end of the wetland, with the exception of one in the middle part (lying very close to the wetland's river) and the effluent. Sub-cluster 2.4 is made of the shallow well in Pesi.

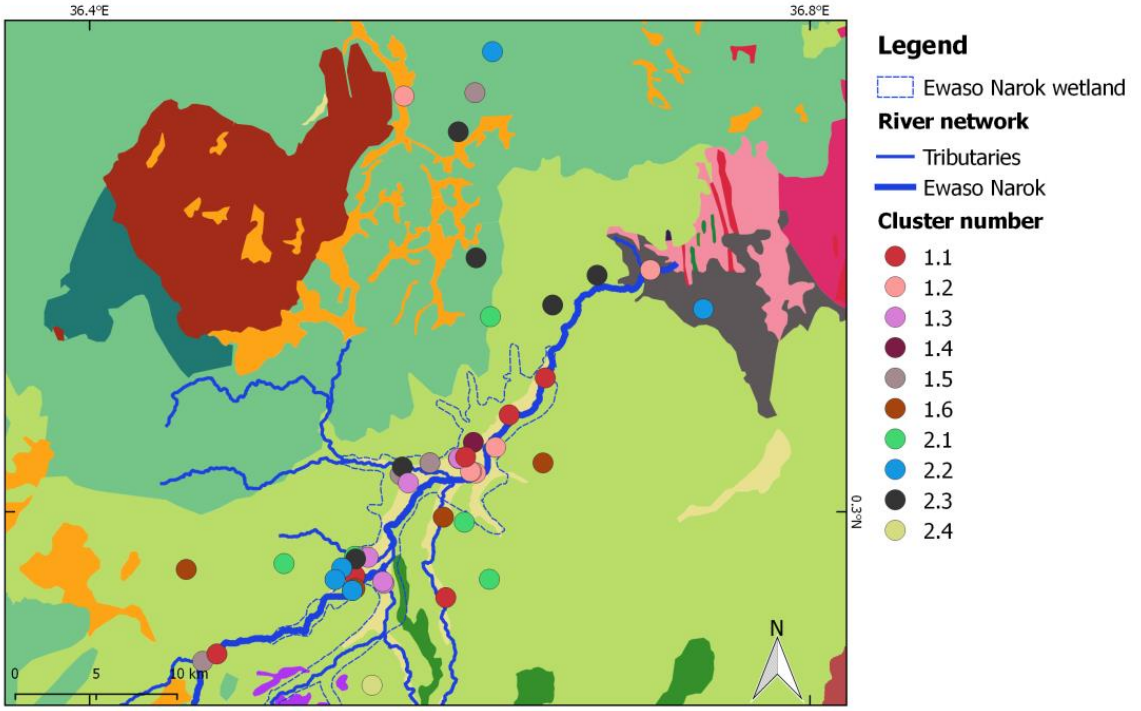

Fig. 6.61: Clusters of the sampled water (Fig. 6.60) in the Ewaso Narok wetland, drawn on the geological map (cp. Fig. 2.9, p.19).

6.5. Model setup

6.5.1.1. Data acquisition and processing

The first task was to create a shared hydrological and hydrochemical database based on all the hydrological information gathered in the wetland and catchment.

The primary data used was based on the sampling campaign of July-August 2016, as it provided comprehensive and up-to-date surface and groundwater quality data. The sampling took place throughout dry and rainy times, including flash floods. Some more gathered data included was provided by the Water Resource Management Authority (WRMA, 2016), and others were published by the Ministry of Water Development and data drilling by well-owners. In case current data was not available, the average of previous years, if it existed, was taken. For those data, the significant error and standard deviation were calculated, and only after being minimum were considered (App. 12 and App. 13).

A hydrochemical database (App. 14) with a unified format has been established for Ewaso Narok hydrological basin to characterize, classify, and discretize the groundwater and surface water basin into sub-water units. Similarly, it was also aimed at characterizing the optional sources of recharge and/ or pollution recharging and contaminating the aquifer.

6.5.1.2. Single-cell model

Single-cell MCM modeling was used to depict the potential contributors and the hydraulic connectivity for every proposed compartment in the modeled system. It also aimed at confirming possible water flow movement from groundwater into the wetland. In addition, it provided the ability to assess both the active sources of recharge and the active sources of pollution, if existing. However, following the limited number of constraints (mass-balance equations), with respect to the number of unknowns for each cell (in the single-cell mode), the optimization provides only a feasible assessment of the active sources rather than quantitative fluxes.

As for the optimization, when applying the MCMsf to a single-cell model configuration, it was asserted that there are more tracers than the unknown sources of recharge to obtain meaningful results (Adar et al., 1988). Accordingly, a feasible solution is a solution given all the above-mentioned satisfies and yields in a feasible assessment of the active sources. Initially, all the hydrochemical elements were assigned the same weight in constructing the set of constraints to make it 100 % conservative. Further refinement was performed using those dissolved minerals, which were in almost hydrochemical equilibrium with the rock minerals, as neither dissolution nor precipitation could occur. More than 50 iterations using different parameters were performed for every cell, but only the results with relatively small water balance differences were included used.

As accurate quantitative fluxes are not available for any of the identified flows, and since no water pumping is reported in the modeled area, the model was performed in “percentage mode” where the “Outflow” is assigned to 100 % while all the fluxes will be assessed relative to the 100 % downstream outflow flux. Although the rate of evaporation and evapotranspiration might be significant, it is not included in the water and mass balance expressions due to the lack of evaporation data.

6.5.1.3. Multi-cell model

Based on the single-cell model, the multi-cell modeling (MCM) was applied for a comprehensive quantitative assessment of the surface-groundwater flow pattern over the wetland. MCM provides the ability to assess both the water fluxes from active sources of recharge and the active sources of pollution if existing. It should depict local shallow groundwater’s relative contribution to the global water budget of the wetland.

As for the optimization, when applying the MCMsf to a multi-cell model configuration, it was asserted that the last cell is the output cell from the modeled flow system. The abstraction rate for all the cells is set to zero, neglecting any water diversions (if it exists) and evaporation. Not having any measured discharge data, we operate on relative mode using percentage, where the last cell is assigned with an outflow rate of 100 %. This set-up ensured that the fluxes are calculated as relative percentages of the total inflow into each cell and as percentages of the total outflow or recharge into the entire modeled flow system, which in this case is the entire wetland domain. Initially, all the hydrochemical elements were assigned the same weight to provide all constituents with the same weighting capacity in the optimization scheme. However, later in the result, the actual dissolved minerals that were in almost hydrochemical equilibrium with small balance differences can be identified. These minerals were, therefore, almost

conservative elements as they could not dissolve further, and no precipitation could occur. Common tracers are a necessity for comparison in the single-cell and multiple-cell versions.

6.5.2. Assigning potential contributors

The potential natural sources of groundwater and surface water recharge into the wetland and into the modeled aquifer are discussed below. However, as this is cell-specific, a detailed description is shown in each cell separately. It is verified that all chosen potential sources have a hydrological potential to flow into a specific cell-based on topography, piezometric potential, and geological feasibility. In addition, a point that is part of a cell cannot be a potential source into another cell.

Potential natural groundwater recharge sources into the wetland are represented as wells, springs, and piezometers located in the study area. Different wells surround the wetland, and as fractures and fissures exist, groundwater may contribute to the surface flow providing the local piezometric head reaches the surface and beyond. The source of groundwater replenishment of these wells is in the upper hills and mountains.

Potential natural sources of surface water recharge into the wetland include streams and water from the surrounding channels and the wetland itself. Besides the Ewaso Narok river as the wetland's main source, the tributaries Pesi, Melwa, and Aiyam as well as the channel parallel to Ewaso Narok, although known as the furrow, and the effluent from the stone cutting (SF21) contribute to the wetland.

6.5.3. Conceptual framework

A schematic diagram of the Ewaso Narok modeled system (Fig. 6.62) is presented below after readjustments based on the single-cell model mode's successful runs.

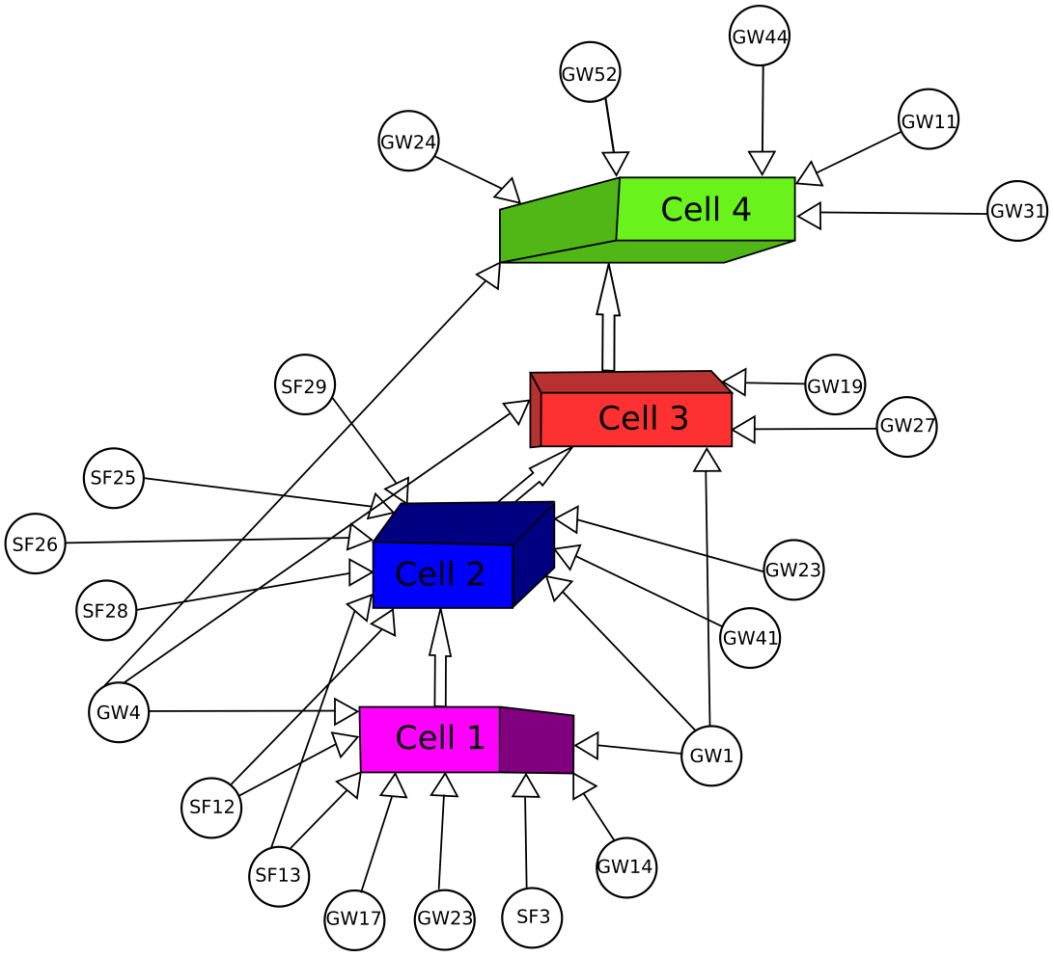

Fig. 6.62: A schematic flow pattern of MCM based on the single-cell modelings' successful runs.

Cell 1 has input from the following sources GW1, GW14, SF3, GW23, GW17, SF13, GW12, and GW4. Source refers to the flow component that contributes water and mass of dissolved constituents, single boreholes, and surface water points in this case. The output flux of this cell is into the downstream cell (cell 2) to maintain water balance in this modeled aquifer. Cell 2 accordingly has input from the previous cell (cell 1), in addition to GW1, GW41, GW23, SF12, SF13, SF28, SF26, SF25, SF29. The output flux of this cell is into the downward cell 3, with inflow from GW1, GW4, GW19, and GW27. The output flow of this cell is into the downstream cell 4. Further sources to cell 4 are GW11, GW31, GW44, GW52, GW24, and GW4. A selection of tracers (hydrochemical and isotopic constituents) are made for each cell.

6.5.4. Cell selection

Based on the cluster analysis (the hydrochemical and isotopic similarities) of the available water sampled points (discussed in Section 6.4) and the geographic location (proximity to each other), the aquifer in Ewaso Narok wetland was discretized into four compartments (Fig. 6.63); **upstream, middle, downstream and outlet** for modeling.

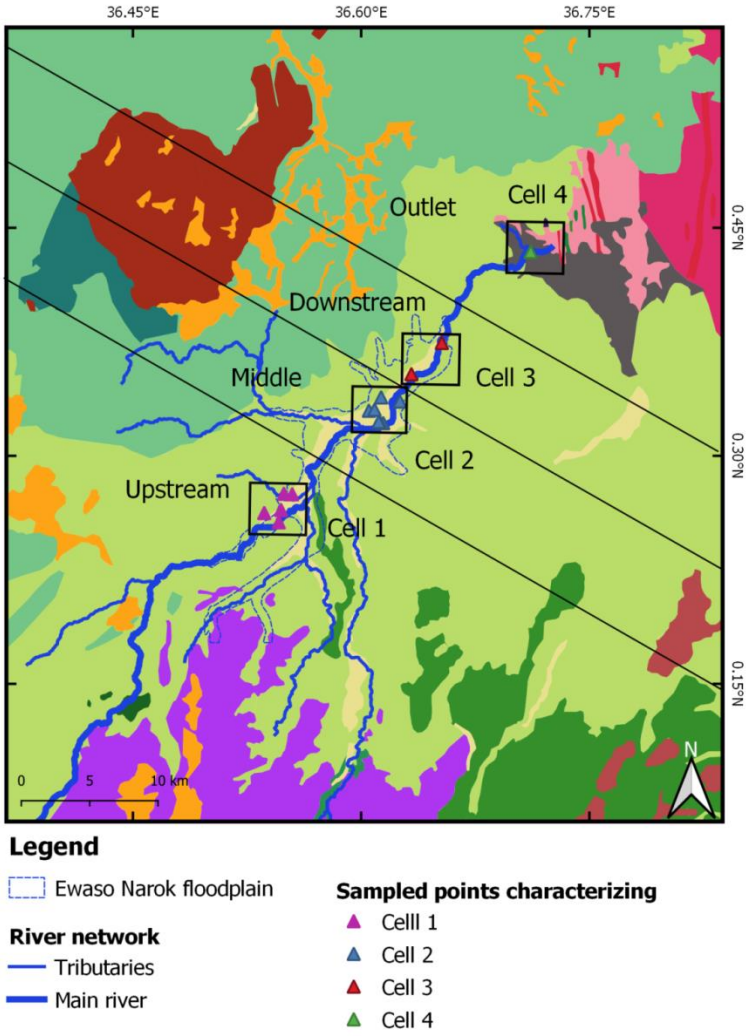

Fig. 6.63: The division of the wetland into four homogenous compartments and the sampling points' location drawn on the geological map (cp. Fig. 2.9, p.19).

The cells were initially presented on the dendrogram to see if they belong to the same subcells and then accordingly decide how to characterize and select them (Fig. 6.64).

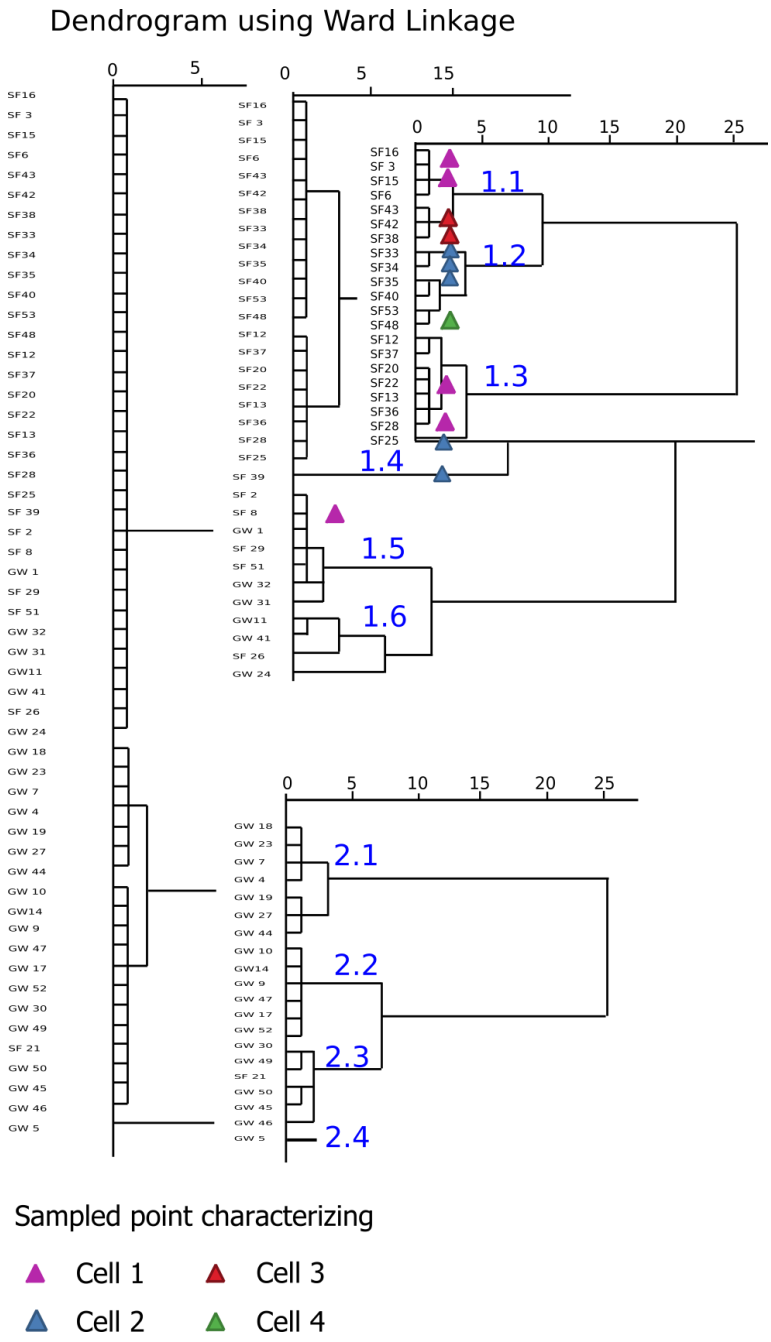

Fig. 6.64: Presenting the potential points making up the selected cells on the dendrogram with a different symbol for each cell's characterization.

The obvious sources into the wetlands are the side-streams tributaries and the main river, while identifying and quantifying the hidden contributions from groundwater, springs, and or human-induced pollutants was the goal and the purpose of the MCM. The criteria for selecting points to belong to a cell included: the points being surface water points, the points having similar hydrochemical traits, and isotopes traits meaning they belong to the same cluster or a very close cluster, the points being geographically close to each other. A challenge was encountered in regards to the surface water, as some samples were taken during flash floods. Due to the resulting dilution compared to those sampled before the floods, less hydrochemical similarities between the results from the dry and flood times exist.

The first cell was selected in the upstream part of the wetland, where most of the tributaries join to make up the main inflow. The second cell was more of stagnant water in the river, and channel around it, in the middle part of the wetland. The selected points belong to a similar kind of water. Cell 3 consisted of two samplings of the river. The area around these points lacked further access. The two points selected had similar hydrochemical characteristics (cluster 1.1 in Fig. 6.64). The last cell is the only reachable area of the river, where all the points join, and the river becomes several meters wide.

Cell 1: Upstream wetland section

Based on geology, geographic distances, and similarity in hydrochemical values, the average hydrochemical and isotopic composition of all of those points was assigned to characterize cell 1 (Tab. 6.10, Fig. 6.65). Different versions and names were prepared at selecting the first cell (cell 1, cell 1_1, cell 1_2). The common characteristic is that the points are all surface water in the wetland's upstream. It included five sampling points (2016 sampling campaign: SF8, SF20, SF22 SF15, and SF16) along the river. All points display different yet similar hydrochemical compositions. In the cluster analysis, SF15 and SF16 belonged to sub-cluster 1.1, SF20, SF22 belonged to 1.3, whereas SF8 belonged to 1.5 (Fig. 6.64). SF20 and SF22 are from the river in the wetland, where local farmers pump water from the canals for irrigation. SF16 is at the beginning of the furrow. SF15 is in the wetland next to the furrow. SF8 is at the beginning of the wetland, where papyrus fills the area. SF15 and SF20 were sampled after the flash floods occurred. In addition, the external data points ESF1, ESF2, and ESF3 were included in the characterization of cell 1.

Tab. 6.10: Different versions for characterizing cell 1.

Cell name and version	Cell 1	Cell 1_1	Cell 1_2
The average composition of points	SF8		
	SF15	SF15	
	SF16	SF16	SF16
	SF20	SF20	SF20
	SF22	SF22	SF22
	ESF1	ESF1	
	ESF2		
	ESF3	ESF3	

Possible groundwater inflow into Cell 1 might be characterized by water from wells (GW1, GW4, GW9, GW7, GW10, GW17, GW18, GW19, GW23, GW24), one piezometer (GW14), and the spring (GW11). Potential natural surface water sources include water coming from the small surrounding streams (SF2, SF3 lying exactly on the river, and SF15). Additional contributions might be generated through surface streams characterized by river water SF12 and river water SF13, which join the wetland from the east. The last possible source of water is a polluted effluent, Point SF21, from the stone-cutting factory.

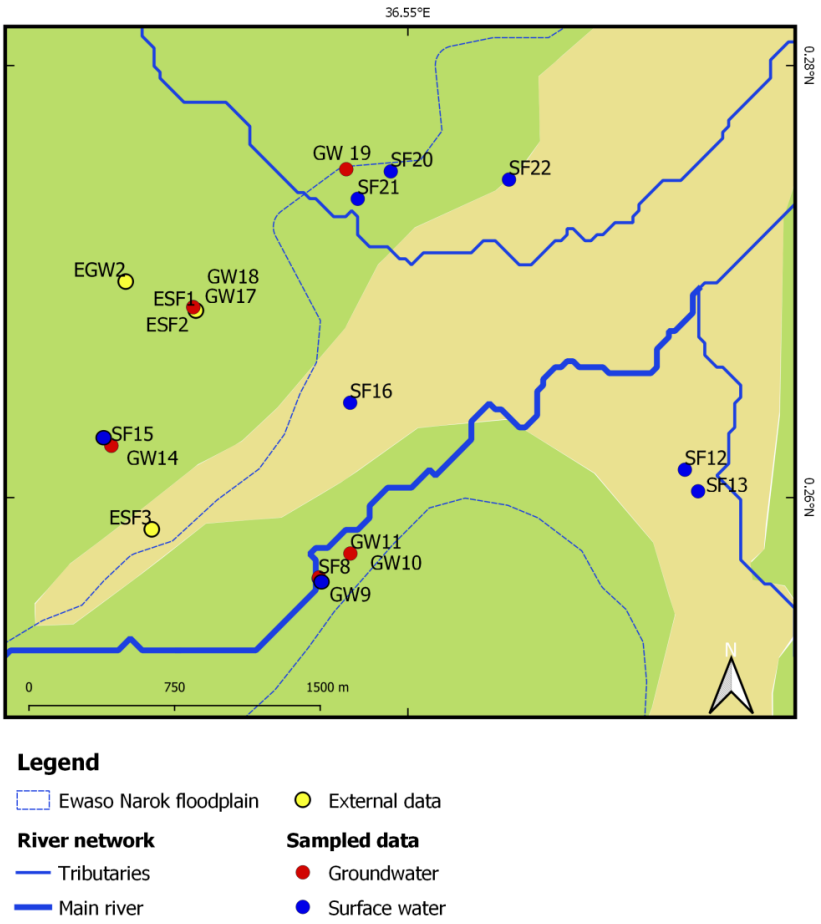

Fig. 6.65: Upstream area of the wetland showing the different points used to select cell 1, drawn on the geological map (cp. Fig. 2.9, p.19).

Cell 2: Middle part of the wetland

The second cell selected represents the middle part of the wetland. Just like the selection of cell 1, different versions of cell 2 were tested (cell 2, cell 2_1, Cell 2_NF, cell 2_2) (Tab. 6.15 6.11, Fig. 6.66). The average of the ions and isotopes from all these below-mentioned points was used to characterize Cell 2. The different points in cell 2 belong to sub-clusters 1.1, 1.2, 1.3, and 1.4 and are chemically and in regards to the location close to each other. It is important to note that the same sources may contribute to more than one cell. A source that supplied cell 1 can be included as sources feeding cell 2 provided they can flow in one streamline into cell 1 and in addition in another streamline into cell 2; meaning it also flows directly into cell 2 but not through cell 1 (SF12, SF13). SF12 is taken from the water in the wetland. SF13 is taken from the river inside the wetland.

Tab. 6.11: Different versions for characterizing cell 2.

Cell name and version	Cell 2	Cell 2_1	Cell 2_NF	Cell 2_2
The average composition of points	SF33	SF33	SF33	SF33
	SF34	SF34	SF34	SF34
	SF35			SF35
	SF36	SF36	SF36	
	SF37	SF37		
	SF38	SF38		
	SF39	SF39		
	SF40			SF40

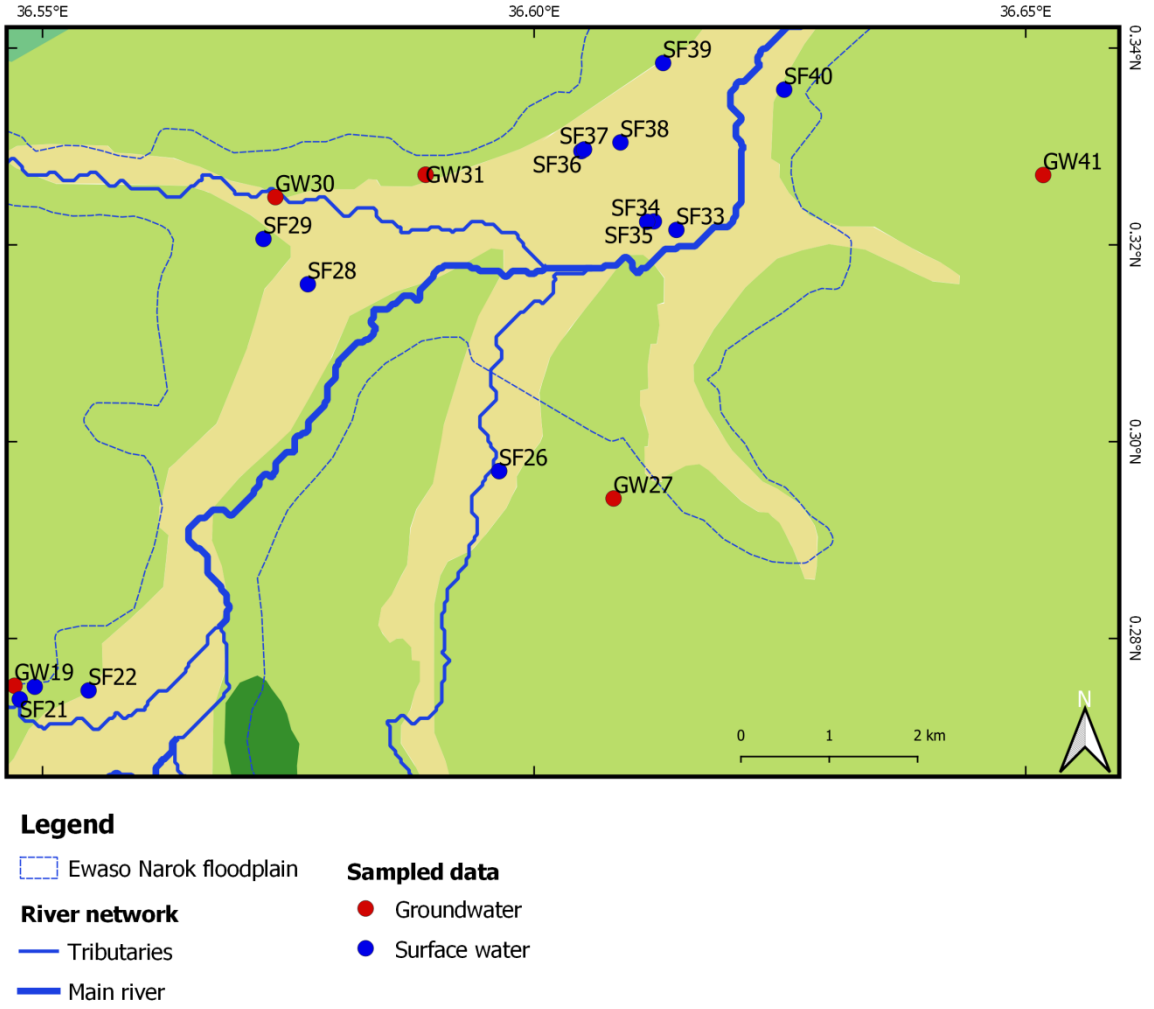

Fig. 6.66: Middle area of the wetland showing the different points used to select cell 2, drawn on the geological map (cp. Fig. 2.9, p.19).

Possible inflow into cell 2 is from Cell 1 (with its variation meaning cell 1, cell 1_1, cell 1_2), water coming from point SF6 (one of the tributaries), point SF12 and point SF13, and water from Melwa direction from SF25, SF26, and from the West streams from SF29, and SF28. Another possible inflow derives from the spring (GW11), and two piezometers (GW14, GW31). Taking groundwater flow direction into consideration, possible inflows might be contributed from wells (GW 1, GW 4, GW 7, GW 9, GW 10, GW 17, GW 18, GW 19, GW 23, GW 24, GW 27, GW 30, GW 41).

Cell 3: Downstream of the wetland

The third cell selected was in the downstream part of the wetland and includes only two river water samples (SF42 and SF43) (Tab. 6.12, Fig. 6.67). Both sampling points lie close to each other and belong to the same cluster in the multivariable cluster analysis. The flow, as noticed by qualitative observation, is with moderate velocity (and quantitatively, as shown by Bours (2016) 10 m^3/s in comparison to cell 2 that is slower). This might be a qualitative indication for additional enhanced groundwater contribution downstream of the lagoons. It included SF42 and SF43, which lie exactly on the river.

Tab. 6.12: Characterization of cell 3.

Cell name	Cell 3
The average composition of points	SF42 SF43

Possible inflow into cell 3 derives from upstream contribution from Cell 2 with its variations, SF6, and points that are not included in the characterization of cell 2 (e.g., SF38 and SF39, when cell 2_2 is used as a possible inflow). Additional sources are the spring GW11, the piezometers GW14 and GW31, and several wells (GW 1, GW 4, GW 7, GW 9, GW 10, GW 17, GW 18, GW 19, GW 23, GW 24, GW 27, GW 30, GW 41, GW 44, GW 47) (Fig. 5.2).

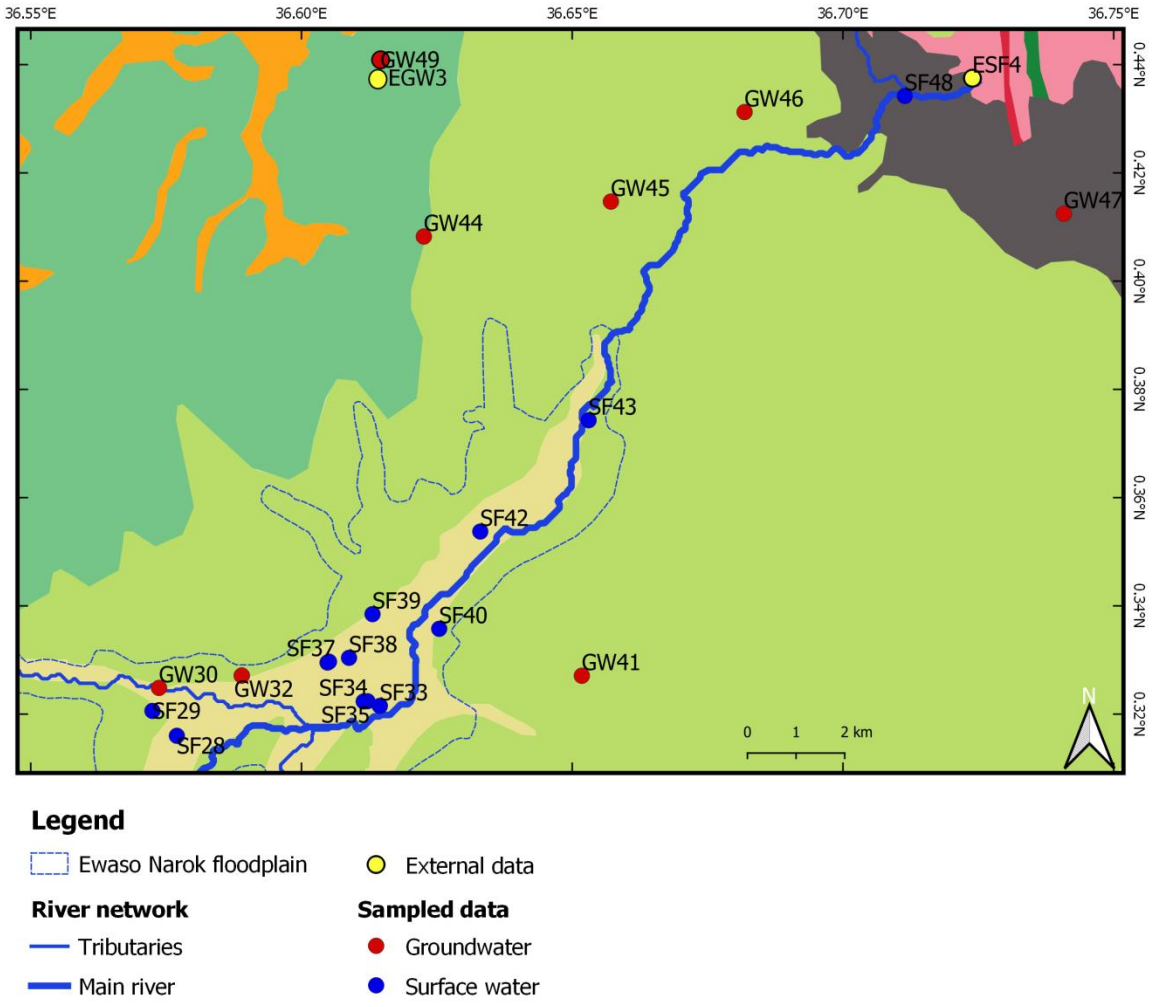

Fig. 6.67: Downstream area of the wetland showing the different points used to select cell 3, drawn on the geological map (cp. Fig. 2.9, p.19).

Cell 4: Outlet of the wetland

The fourth cell selected was at the end part of the wetland (SF48), where all the water sources converge together. Two different versions at the selection and characterization of cell 4 were made (Tab. 6.13, Fig. 6.68).

Tab. 6.13: Different versions for characterizing cell 4.

Cell name and version	Cell 4	Cell 4_NF
The average composition of points	SF48	SF48 ESF4

In cell 4, only SF48 is taken into account as a cell. As SF48 was sampled during flood times, a second cell (Cell 4_NF) combines SF48 with ESF4, a data set from the Water Resource Department in the area (App. 13).

Possible inflow into cell 4 comes from surface water from Cell 3 and groundwater from GW1, GW 4, GW 7, GW 9, GW 10, GW 17, GW 18, GW 19, GW 23, GW 24, GW 27, GW 30, GW 41, GW 44, GW 47, GW 45, GW 46, GW 49, GW 50, and GW 52.

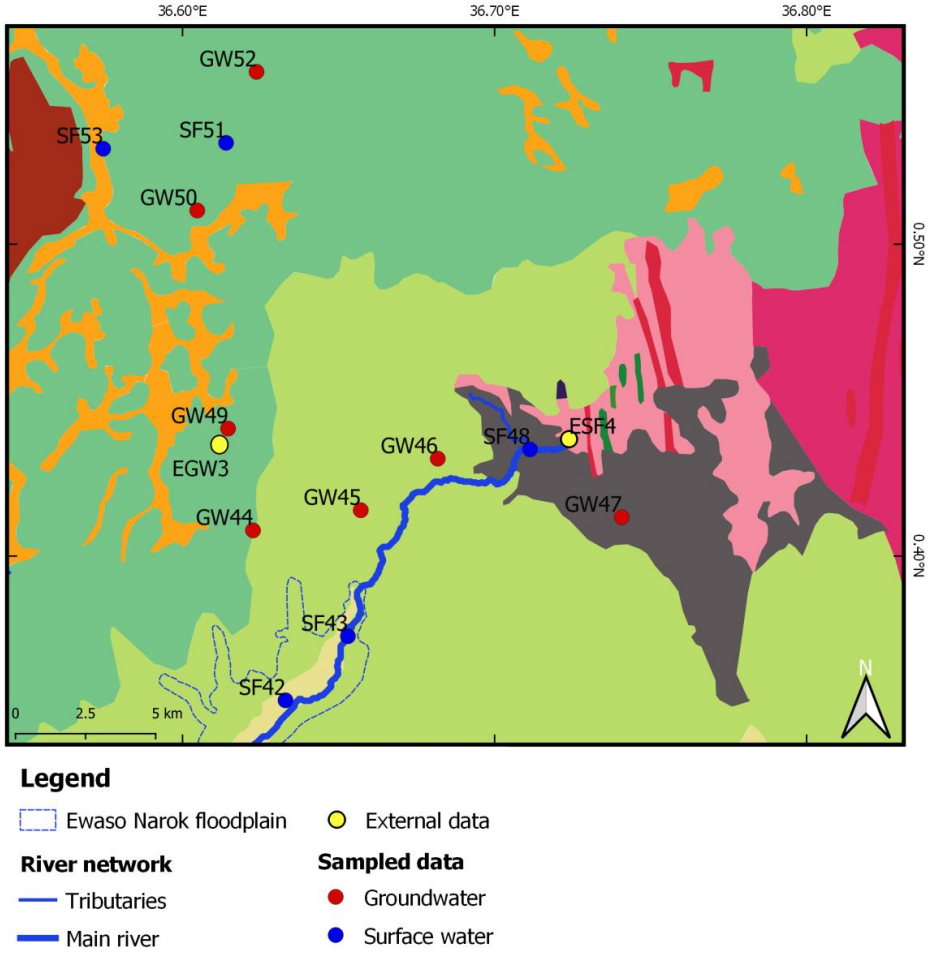

Fig. 6.68: Outlet area of the wetland showing the different points used to select cell 4, drawn on the geological map (cp. Fig. 2.9, p.19).

6.6. Hydrochemical and isotopes modeling

This part discusses the single-cell MCM modeling and the Multi-cell MCM modeling results.

6.6.1. MCM single-cell version

The hydrochemistry and isotopes of the groundwater, stream water, channel, and flooded wetland were used to identify possible hydraulic connectivity within the local aquifer and between the wetland's water and the groundwater underneath. While the multivariable cluster analysis helped establish similarities between the various water sources, the Mixing Cells Modeling approach was implemented to quantify the mixing rates between the active water sources that contribute to specific surface water points, which combines 'water cells' in Ewaso Narok wetland. The results of the single-cell version of MCM are presented below for each cell. The map showing the 'cells' locations' and the contributors is presented in Figure 6.69 and in the single-cell conceptual model (Fig. 6.62). The construction of the compartmental flow pattern in Ewaso Narok allows a better vision of the results and linkages between the different cells and hydrological compartments.

When running the MCMsf to a single-cell model configuration, it was asserted that there are more tracers than the unknown sources of pollution to obtain meaningful results; feasible assessment of active sources given the limited number of constraints. Accordingly, a feasible solution is a solution given all the above-mentioned satisfies and yields in a feasible assessment of the active sources.

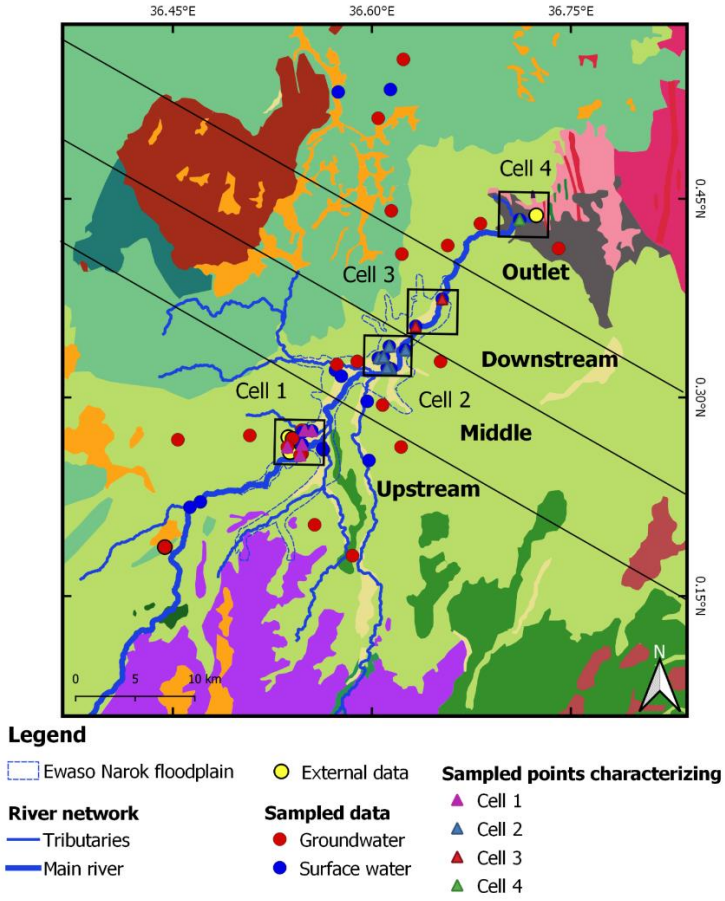

Fig. 6.69: Location of potential contributing points (own and external data) with a different symbol characterizing each cell, drawn on the geological map (cp. Fig. 2.9, p.19).

6.6.1.1. Cell 1: Upstream wetland section

Four different scenarios using 19 tracers were applied to define the various sources for the upstream wetland section (cell 1) using the single-cell model (Tab. 6.14).

Tab. 6.14: Results of supported potential sources to cell 1 using single-cell modeling.

Scenario 1

Cell 1	
Contributor	**portion of total inflow [%]**
SF3	25,30
GW4	1,50
SF12	1,10
SF13	65,70
GW23	4,80
GW17	1,70
Percentage difference	16,29
# of Tracers	19
EC, Mn^{2+}, Mg^{2+}, Na^{+}, K^{+}, Ca^{+2}, PO_4^{3-}, HCO_3^{-}, Cl^{-}, NO_3^{-}, SO_4^{2-}, F^{-}, Al^{3+}, Cu^{2+}, Zn^{2+}, SiO_2, $\delta^{18}O$, $\delta^{2}H$, TDS	

Scenario 2

Cell1_1	
Contributor	**portion of total inflow [%]**
SF3	28,70
GW4	2,20
SF12	2,20
SF13	62,90
GW23	1,20
GW17	2,70
Percentage difference	25,87
# of Tracers	19
EC, Mn^{2+}, Mg^{2+}, Na^{+}, K^{+}, Ca^{+2}, PO_4^{3-}, HCO_3^{-}, Cl^{-}, NO_3^{-}, SO_4^{2-}, F^{-}, Al^{3+}, Cu^{2+}, Zn^{2+}, SiO_2, $\delta^{18}O$, $\delta^{2}H$, TDS	

Scenario 3

Cell1_2	
Contributor	**portion of total inflow [%]**
SF3	34,10
GW4	0
SF12	0
SF13	65,10
GW23	0,20
GW17	0,70
Percentage difference	18,95
# of Tracers	19
EC, Mn^{2+}, Mg^{2+}, Na^{+}, K^{+}, Ca^{+2}, PO_4^{3-}, HCO_3^{-}, Cl^{-}, NO_3^{-}, SO_4^{2-}, F^{-}, Al^{3+}, Cu^{2+}, Zn^{2+}, SiO_2, $\delta^{18}O$, $\delta^{2}H$, TDS	

Scenrio 4

Cell 1	
Contributor	**portion of total inflow [%]**
SF12	24.90
SF3	70.40
GW17	2.20
GW4	2.40
Absolute water difference	0.62
# of Tracers	18
EC, Mn^{2+}, Mg^{2+}, Na^{+}, PO_4^{3-}, HCO_3^{-}, NO_3^{-}, Fe^{2+}, Al^{3+}, Br^{-}, SiO_2, $\delta^{18}O$, As^{5+}, SO_4^{2-}, NH_4^{+}, Zn^{2+}, Cr^{2+},pH,	

Source SF13 is by far the most dominant contributor to Cell 1 in the first three scenarios. In scenario 1, SF13 contributes to 65.7 % of the total inflow, followed by SF3 (25.3 %). SF12 with 1.1 %, and the groundwater contribution is 4.8 % from GW23, 1.7 % from GW17, and 1.5 % from GW4.

Cell 1_1's contribution in scenario 2 is from source SF13 with 62.9 %, followed by 28.7 % from SF3, 2.7 % from GW17, and around 7 % from groundwater (GW4, GW17, GW 23) and SF12. The main contributors, SF13 and SF3, are both rivers feeding the wetland. Cell 1_2 in scenario 3 is also mainly fed by SF13, making up 65.1 % of the total flow, followed by SF3 with 34.1 %. In this scenario, GW4 and SF12 do not show any contribution to the system, and both GW23 and GW17 contribute less than 1 %.

Scenario four seems to be the best-case scenario as it has a very small water error balance (0.62). The result shows that the majority of the water in this upstream section of the wetland originates from the two tributaries, Melwa (SF3), contributing to 70 % of the flow, and Pesi (SF12), contributing to 25 % of the flow. Real flow in reality and on the field is seen as the tributaries flow and come together, forming the wetland. Groundwater contributes to 5 % of

the flow from sub-aquifer units characterized by the wells in the same area from well GW17 and upstream close to Pesi (GW4).

6.6.1.2. Cell 2: Middle part of the wetland

Five different scenarios using 19 tracers were applied to define the various sources for the middle part of the wetland section (cell 2) using the single-cell model (Tab. 6.15).

Tab. 6.15: Results of supported potential sources to cell 2 using single-cell modeling.

Scenario 1

Cell 2	
Contributor	**portion of total inflow [%]**
Cell1	11.60
SF28	22.20
SF13	48.20
SF12	16.10
GW41	1.80
GW23	0.10
Absolute water difference	13.91
# of Tracers	20
Na^{+}, pH, $\delta^{18}O$, TDS, As^{5+}, Cr^{2+}, Al^{3+}, SO_4^{2-}, NO_3^{-}, HCO_3^{-}, NH_4^{+}, PO_4^{3-}, Mg^{2+}, Fe^{2+}, Mn^{2+}, F^{-}, SiO_2, Ca^{2+}, Cu^{2+}	

Scenario 2

Cell2_1	
Contributor	**portion of total inflow [%]**
SF11	0
SF12	25.20
SF13	0
GW23	0
SF28	59.90
SF29	11.80
GW41	1.10
Cell1_1	1.90
Percentage difference	24.37
# of Tracers	19
EC, Mn^{2+}, Mg^{2+}, Na^{+}, K^{+}, Ca^{+2}, PO_4^{3-}, HCO_3^{-}, Cl^{-}, NO_3^{-}, SO_4^{2-}, F^{-}, Al^{3+}, Cu^{2+}, Zn^{2+}, SiO_2, $\delta^{18}O$, $\delta^{2}H$, TDS	

Scenario 3

Cell2_NF	
Contributor	**portion of total inflow [%]**
SF11	0
SF12	18.30
SF13	23.40
GW23	0
SF28	48.40
SF29	8.00
GW41	0
Cell1	1.90
Percentage difference	16.52
# of Tracers	19
EC, Mn^{2+}, Mg^{2+}, Na^{+}, K^{+}, Ca^{+2}, PO_4^{3-}, HCO_3^{-}, Cl^{-}, NO_3^{-}, SO_4^{2-}, F^{-}, Al^{3+}, Cu^{2+}, Zn^{2+}, SiO_2, $\delta^{18}O$, $\delta^{2}H$, TDS	

Scenrio 4

Cell2_NF	
Contributor	**portion of total inflow [%]**
SF11	0
SF12	18.90
SF13	25.50
GW23	0
SF28	47.10
SF29	5.60
GW41	0
Cell1_1	3.00
Percentage difference	15.18
# of Tracers	19
EC, Mn^{2+}, Mg^{2+}, Na^{+}, K^{+}, Ca^{+2}, PO_4^{3-}, HCO_3^{-}, Cl^{-}, NO_3^{-}, SO_4^{2-}, F^{-}, Al^{3+}, Cu^{2+}, Zn^{2+}, SiO_2, $\delta^{18}O$, $\delta^{2}H$, TDS	

Scenario 5

Cell2_2	
Contributor	**portion of total inflow [%]**
SF12	21
SF6	20.80
SF28	37.30
SF29	0
Cell1_1	20.90
Percentage difference	26.34
# of Tracers	19
EC, Mn^{2+}, Mg^{2+}, Na^{+}, K^{+}, Ca^{+2}, PO_4^{3-}, HCO_3^{-}, Cl^{-}, NO_3^{-}, SO_4^{2-}, F^{-}, Al^{3+}, Cu^{2+}, Zn^{2+}, SiO_2, $\delta^{18}O$, $\delta^{2}H$, TDS	

In scenario 1, groundwater constitutes a small part of the flow (2 %) in the middle part of the wetland. Yet this is a noticeable amount given the fact that there are floods throughout this time. The groundwater sources are east and west of the wetland. However, as more samples

are included in the cell averaging, the flow source is the previous cell and the two new incoming water streams (Pesi) and SF12.

The main contribution in scenario 2 is from SF28, making almost 60 % of the inflow, followed by SF12, which contributed to 25 %, and SF29 contributing to 12 %, and GW41 contributing to 1.1 %. Cell 1 contributed to 1.9 % of the flow in cell 2.

While the first two scenarios included flooded samples, scenarios 3 and 4 show the results without floods to ensure that only base flow is taken into account. Cell 1 and Cell 1_1 are contributors simultaneously. The results are very close in scenarios 3 and 4. Cell 2 gets its contribution mainly from SF28 (48.4 % and 47.1 %), followed by SF12 (around 19 %), and SF13 (around 24 %), and SF29 (around 7 %). Groundwater does not appear in the contribution list, and cell 1 contributes in a minor amount.

In scenario 5 (cell 2_2), a higher absolute error compared to the other scenarios is noticed. This is because no groundwater was included as a potential contributor. This is a clear hint that groundwater could contribute to the cell's recharge. The rest of this scenario's contribution is from SF28, making up 37.3 % of the flow, followed by almost equal shares of around 20 % from the previous cell (cell1_1), SF12, and SF6.

To conclude, under all scenarios, the middle part of the wetland represented by cell 2 shows a very small contribution from the upper cell (Cell 1), reflecting very low fluxes along the mainstream within the lagoon. The recharge is mainly from surface water. However, there is a clear indication that there is a small contribution from groundwater. There was no significant difference in the simulation results between including or removing the flooded samples from the cell characterization.

6.6.1.3. Cell 3: Downstream of the wetland

Three scenarios using 19 tracers were applied to define the various sources for the downstream part of the wetland section (cell 3) using the single-cell model (Tab. 6.16).

In scenario 1, Cell 3's contribution is mainly from the previous cell, cell 2, making up to 60 % of the inflow, followed by a high groundwater contribution (GW27) with 40 %. As the percentage difference is relatively large, another main active water source with a unique hydrochemical composition might exist.

In scenario 2, SF38 is included as a potential contributor as it is not part of the characterization of the previous cell (cell2_2). The percentage difference decreases accordingly by 15 %. The contribution from groundwater increases as GW1 (40 %) further adds to the flow in addition to GW27 (6.1 %). Cell2_2 contributes to only 15 % of the flow, whereas SF38 contributes to the remaining.

In scenario 3, SF6 is included as a potential source not only to cell 2 only but also to cell 3. At first glance, this does not seem feasible, but it is as the wetland is channelized in reality. The results show one of the possible missing sources in the previous scenarios. The contribution from SF6 is 56.7 %, followed by SF36 contributing to 10.6 %, and the groundwater contributing to 5 % from GW27. The percentage difference immediately drops in this scenario compared with the two previous ones.

Tab. 6.16: Results of supported potential sources to cell 3 using single-cell modeling.

Scenario 1

Cell 3	
Contributor	**Portion of total inflow [%]**
GW27	40
Cell2_1	60
Percentage difference	74,91
# of Tracers	19
EC, Mn^{2+}, Mg^{2+}, Na^{+}, K^{+}, Ca^{+2}, PO_4^{3-}, HCO_3^{-}, Cl^{-}, NO_3^{-}, SO_4^{2-}, F^{-}, Al^{3+}, Cu^{2+}, Zn^{2+}, SiO_2, $\delta^{18}O$, $\delta^{2}H$, TDS	

Scenario 2

Cell 3	
Contributor	**Portion of total inflow [%]**
GW27	6,10
GW38	38,7
GW1	40
Cell2_2	15,10
Percentage difference	49,44
# of Tracers	19
EC, Mn^{2+}, Mg^{2+}, Na^{+}, K^{+}, Ca^{+2}, PO_4^{3-}, HCO_3^{-}, Cl^{-}, NO_3^{-}, SO_4^{2-}, F^{-}, Al^{3+}, Cu^{2+}, Zn^{2+}, SiO_2, $\delta^{18}O$, $\delta^{2}H$, TDS	

Scenario 3

Cell 3	
Contributor	**Portion of total inflow [%]**
GW27	5
Cell2_2	1
SF6	56,7
SF36	10,6
SF38	26,6
Percentage difference	29,79
# of Tracers	19
EC, Mn^{2+}, Mg^{2+}, Na^{+}, K^{+}, Ca^{+2}, PO_4^{3-}, HCO_3^{-}, Cl^{-}, NO_3^{-}, SO_4^{2-}, F^{-}, Al^{3+}, Cu^{2+}, Zn^{2+}, SiO_2, $\delta^{18}O$, $\delta^{2}H$, TDS	

6.6.1.4. Cell 4: Outlet of wetland

Two scenarios using 19 tracers were applied to define the various sources for the outlet of the wetland (cell 4) using the single-cell model (Tab. 6.17).

Tab. 6.17: Results of supported potential sources to cell 4 using single-cell modeling.

Scenario 1

Cell4	
Contributor	Portion of total inflow [%]
GW10	0
GW4	0
GW52	1.00
Cell3	99.00
Percentage difference	42.07
# of Tracers	19
EC, Mn^{2+}, Mg^{2+}, Na^{+}, K^{+}, Ca^{+2}, PO_4^{3-}, HCO_3^{-}, Cl^{-}, NO_3^{-}, SO_4^{2-}, F^{-}, Al^{3+}, Cu^{2+}, Zn^{2+}, SiO_2, $\delta^{18}O$, $\delta^{2}H$, TDS	

Scenario 2

Cell4_NF	
Contributor	Portion of total inflow [%]
GW10	0
GW4	0
GW52	1.00
Cell3	99.00
Percentage difference	40.40
# of Tracers	19
EC, Mn^{2+}, Mg^{2+}, Na^{+}, K^{+}, Ca^{+2}, PO_4^{3-}, HCO_3^{-}, Cl^{-}, NO_3^{-}, SO_4^{2-}, F^{-}, Al^{3+}, Cu^{2+}, Zn^{2+}, SiO_2, $\delta^{18}O$, $\delta^{2}H$, TDS	

In both scenarios, the main contribution to cell 4 is from the previous cell (Cell 3), making up 99 % of the inflow. There is a minor contribution of 1 % from a well (GW52). The lack of identified active contribution from groundwater may be attributed to scarce groundwater samples along this part of the wetland. The percentage difference again is high in both scenarios and means that there is a main active source that feeds cell 4, which is not accounted for in the optimum mass balance.

6.6.1.5. Summary of single-cell modeling

In the single-cell modeling optimization scheme, the number of constraints, which is equivalent to the number of hydrochemical parameters plus one, is only slightly bigger than the unknowns.

Therefore, the assessed global optimum for the objective function is rather more of a 'domain' than a 'sharp optimal point'. Therefore, the results indicate a range of relative flux values rather than unique values.

The above-presented results can be combined to form a summary of the single-cell model using the same trace elements. Different scenarios for each cell yielded potential outcomes (Tab. 6.18).

Tab. 6.18: Summary of the single-cell model results using the same tracers.

Single-cell model			
Cell name	**Contributor**	**portion of Cell inflow [%]**	**Difference in cell [%]**
Cell1_1			25.87
	GW1		
	SF3	28.7	
	GW4	2.2	
	SF12	2.2	
	SF13	62.9	
	GW14		
	GW23	1.2	
	GW17	2.7	
Cell2_1			24.37
	SF11		
	SF12	25.2	
	SF13		
	GW23		
	SF28	59.9	
	SF29	11.8	
	GW41	1.1	
Cell3			77.54
	GW27	40	
	SF38		
	SF40		
Cell 4	**GW10**		42.07
	GW4		
	GW52	1	
from single-cell2_1	**Cell1_1**	1.90	
from single-cell3	**Cell2_1**	60.00	
from single-cell4	**cell3**	99.00	

6.6.2. MCM multi-cell version

In this section, two terms are used. The **best-case scenario** is the one with the lowest water balance difference. The **most feasible scenario** is the scenario where the tracers used resulted in a feasible solution in all the following single-cell modeling and multi-cell modeling. This means that the most feasible solution in the multi-cell version was used even if it was not the best-case scenario.

6.6.2.1. Potential sources that are active contributors in single-cell

All sources found to be active contributors in the aforementioned single-cell version process are assigned inflows as potential contributors in the multi-cell version simulations (Tab. 6.19, Tab. 6.20, Tab. 6.21, Tab. 6.22).

Tab. 6.19: Potential contributors to cell 1.

Name	Elaboration
GW4	Well
GW17	Well
GW23	Well
SF3	Surface water
SF12	Surface water
SF13	Surface water

Tab. 6.20: Potential contributors to cell 2.

Name	Elaboration
GW41	Well
SF12	Surface water
SF28	Surface water
SF29	Surface water
Cell 1	

Tab. 6.21: Potential contributors to cell 3.

Name	Elaboration
GW27	Well
Cell 2	

Tab. 6.22: Potential contributors to cell 4.

Name	Elaboration
GW52	Well
Cell 3	

Different scenarios were accordingly run as the real hydrochemical link and paths are not known. These scenarios were run with different cell versions and with different potential sources and similar tracers. It was asserted that geologically and hydrologically, that was feasible. The model was first run, where three cells are introduced into the MCMsf system. Three different scenarios are presented, where the first two scenarios are similar though the first does not take flooding into account, and the second with the flooding samples considered. The third scenario includes a source that is harder to detect because of channelization. It is important to note that the decision to include that exact cell (cell 1 versus cell1_1, for example) was based on choosing a cell that yielded an output. Once the cells were all included in one trial, some trials did not give a result meaning the equations leading to the optimization solution could not be solved. The results are summarized in Tab. 6.23 and Table 6.24. All scenarios build on hydrogeology being one criterion and the sources that were active in the single-cell model as a second criterion.

6.6.2.2. Results of multi-cell modeling using three cells

The results in both the first and second scenarios are very similar (Tab. 6.23 and Tab. 6.24). In both scenarios, Cell 1 contributes to less than 3 % of the system's total inflow. The following sources: SF3, SF12, GW23, SF13, GW17, and GW4 in both scenarios were found to be active contributors. In scenario one, SF13 contributes to 1 % of the total inflow of the system. This translates to SF13, making up 67.2 % of cell 1 inflow. The rest in cell 1_1 inflow is divided as 11.9 % from SF12, 10.8 % from SF3, 7.9 % from GW4, 1.7 % from GW23, and 0.4 % from GW17.

In scenario 1, Cell 2_NF shows that the percentage of total inflow is from SF28, making up 32.8 % of the whole system's inflow, 16.6 % from SF29, and SF12 and SF13, each contributing to 25

%. Even though GW41 was a contributor in the single-cell model, it contributed to zero percent in this case.

Scenario 2 shows similar behavior in cell 1_1, where SF13 makes up 2.8 % of the total inflow in the system translating to 67.2 % of the inflow in cell 1_1. SF3 contributes to 10.8 %, SF12 to 11.9 %, SF3 to 7.9 %, GW23 to 1.7 % followed by 0.4 % from GW17. Cell 2_1 shows that the percent of total inflow to the system is from SF12 with 31.6 %, followed by 10.9 % from SF29, and 6.5 % from SF28.

Cell 3 shows that the contribution is solely from GW27, making up 30.9 % of the total inflow in scenario 1 and 46.8 % in scenario 2. The difference in the inflow amount is due to the cell's make-up and, thus, the floods. More inflow is observed going through cell 3 at the time of floods.

The in-between real flow from cell 1 to cell 2 is 0.73 and 1.55 % of volume/time in scenario 1 and scenario 2, respectively, and that from cell 2 to cell 3 is 29.12 and 17.8 % of volume/time.

The rate of inflow is calculated as the flux divided by the pumping rate of the last cell. The rate of pumping, in this case, is non-existent and accordingly is assigned a small positive value of 0.1, and it is not relevant to this case.

In scenario 3, the active sources in cell 1 contribute to a very small percentage of the total inflow (SF13 to 0.1 %). This translates to SF13 contributing to 56.3 % of cell 1's inflow, followed by SF12 (17.6 %) and SF3 (16.5 %), and the groundwater sources GW4 contributing to 7.1 % and GW23 with 2 % and GW17 to 5 %. Cell's 2 main contributors are SF12, making up 79.1 %, and SF28 with 20.9 %. This translates to 0.5 % of the total inflow of the system.

As SF6 is included as a potential active source in cell 3, the inflow percentage in the whole system is contributed by cell 3. SF6 contributes to 57.3 % of the cell inflow, followed by SF38 (30.4 %) and two groundwater wells (GW1: 6.2 %, GW27: 5.5 %). This is the same percentage contributed to the whole system. The percentage difference decreases dramatically from the two previous scenarios to 17 % in this scenario. The in-between real flow is 0.11 from cell 1_1 to cell 2_2 and 0.51 from cell 2_2 to cell 3.

Tab. 6.23: Results of multi-cell modeling using 3 cells.

MCM 3 cells					
Scenario 1			**portion of total inflow [%]**	**portion of cell inflow [%]**	**Flux [% of v/t]**
Cell1_1	GW1	x			
	SF3		0.2	10.8	0.06
	GW4		0.1	7.9	0.04
	SF12		0.2	11.9	0.06
	SF13		1.0	67.2	0.37
	GW14	x			
	GW23		0.0	1.7	0.01
	GW17		0.0	0.4	0.0
Cell2_NF	SF11	X			
	SF12		17.1	25.3	6.40
	SF13		17.1	25.3	6.39
	GW23	X			
	SF28		22.2	32.8	8.30
	SF29		11.2	16.6	4.19
	GW41	X			
Cell3	GW27		30.90	100.0	11.55
	SF38	x			
	SF40	x			
from cell		to cell	**Flux [% of v/t]**		
Cell1_1		Cell2_NF	0.73		
Cell2_NF		Cell3	29.12		
outflow from cell3		0.1		**Percentage difference**	42.66
Scenario 2			**portion of total inflow [%]**	**portion of cell inflow [%]**	**Flux [% of v/t]**
Cell1_1	GW1	x			
	SF3		0.5	10.8	0.13
	GW4		0.3	7.9	0.09
	SF12		0.5	11.9	0.14
	SF13		2.8	67.2	0.78
	GW14	x			
	GW23		0.1	1.7	0.02
	GW17		0.0	0.4	0.01
Cell2_1	SF11	x			
	SF12		31.6	64.5	8.70
	SF13	x			
	GW23	x			
	SF28		6.5	13.2	1.78
	SF29		10.9	22.3	3.00
	GW41		0.0	0.0	0.00
Cell3	GW27		46.8	100.0	12.90
	SF38	x			
	SF40	x			
from cell		to cell	**Flux [% of v/t]**		
Cell1_1		Cell2_1	1.55		
Cell2_1		Cell3	17.8		
Outflow from cell 3		0.1		Percentage difference	52.48

Tab. 6.24: Results of multi-cell modeling using 3 cells (continued).

Scenario 3			portion of total inflow [%]	portion of cell inflow [%]	Flux [% of v/t]
Cell1_1	GW1	x			
	SF3		0	16.5	0.00
	GW4		0	7.1	0.00
	SF12		0	17.6	0.00
	SF13		0.1	56.3	0.04
	GW14	x			
	GW23		0	2.0	0.00
	GW17		0	5.0	0.00
Cell2_2	SF28		0.1	20.9	0.08
	GW1		0.0	0.0	0.00
	SF12		0.4	79.1	0.29
Cell3	SF38		30.4	30.6	21.98
	GW27		5.5	5.5	3.96
	SF6		57.3	57.6	41.39
	GW1		6.2	6.3	4.51
from cell		to cell	**Flux [% of v/t]**		
Cell1_1		Cell2_2	0.11		
Cell2_2		Cell3	0.51		
Outflow from cell 3		0.1		Percentage difference	17.79

6.6.2.3. Results of multi-cell modeling using four cells

Different scenarios are executed with the four cells, and only four with relatively adequate water balance are chosen to demonstrate the results (Tab. 6.25 and Tab. 6.26), where cell 1_1, cell 2_1, cell 2_2, cell 3, cell 4, and cell 4_NF are chosen:

Tab. 6.25: Results of multi-cell modeling using 4 cells.

MCM 4 cells					
Scenario 1			**portion of total inflow [%]**	**portion of cell inflow [%]**	**Flux [% of v/t]**
Cell1_1	**GW1**	**x**			
	SF3		0.4	17.8	0.06
	GW4		0.1	3.4	0.01
	SF12		0.1	5.7	0.02
	SF13		1.5	69.6	0.22
	GW14	**x**			
	GW23		0.1	2.9	0.01
	GW17		0.0	0.6	0.00
Cell2_1					
	SF11	**x**			
	SF12		21.6	50.7	3.26
	SF13	**x**			
	GW23	**x**			
	SF28		0.0	0.0	0.00
	SF29		21.0	49.3	3.16
	GW41		0.0	0.0	0.00
Cell 3	**GW27**		47.8	100.0	7.21
	SF38	**x**			
	SF40	**x**			
Cell 4	**GW10**	**x**			
	GW4	**x**			
	GW52		7.60	100.0	1.14
From cell		**To cell**		**Real number [v/t]**	
Cell1_1		**Cell2_1**		0.37	
Cell2_1		**Cell3**		8.94	
Cell3		**Cell 4**		53.79	
Outflow from cell 4		0.1			
Percentage difference		64.93			
Scenario 2			**portion of total inflow [%]**	**portion of cell inflow [%]**	**Flux [% of v/t]**
Cell1_1	**GW1**	**x**			
	SF3		0.0	0.0	0.00
	GW4		0.2	11.9	0.05
	SF12		0.8	40.9	0.18
	SF13		0.8	42.2	0.19
	GW14	**x**			
	GW23		0.1	1.9	0.01
	GW17		0.0	3.1	0.01
Cell2_NF	**SF11**	**x**			
	SF12		9.2	15.3	2.11
	SF13		21.8	36.1	4.98
	GW23	**x**			
	SF28		14.5	24.0	3.31
	SF29		14.8	24.6	3.30
	GW41	**x**			
Cell3	**GW27**		32.9	100.0	7.52
	SF38	**x**			
	SF40	**x**			
Cell4_NF	**GW10**	**x**			
	GW4	**x**			
	GW52		4.70	100.0	1.08
From cell		**To cell**		**Real number [v/t]**	
Cell1_1		**Cell2_NF**		0.93	
Cell2_NF		**Cell3**		16.53	
Cell3		**Cell 4_NF**		59.7	
Outflow from cell 4		0.1			
Percentage difference		57.19			

Tab. 6.26: Results of multi-cell modeling using 4 cells (continued).

Scenario 3			portion of total inflow [%]	portion of cell inflow [%]	Flux [% of v/t]
Cell1_1	GW1	x			
	SF3		0.7	15.9	0.16
	GW4		0.2	3.8	0.04
	SF12	x			
	SF13		3.3	77.7	0.78
	GW14	x			
	GW23		0.1	2.6	0.03
	GW17	x			
Cell 2_2	SF11	x			
	SF12		10.4	100.0	2.48
	SF13	x			
	GW23	x			
	SF28		0.0	0.0	0.00
	SF6		0.0	0.0	0.00
Cell 3	GW1		58.6	72.3	13.91
	GW27		22.4	27.7	5.32
	GW38		0.0	0.0	0.00
Cell 4	GW10	x			
	GW4	x			
	GW52		4.3	100.0	1.02
From cell		To cell		Real number [v/t]	
Cell1_1		Cell2_2		1.13	
Cell2_2		Cell3		4.56	
Cell3		Cell 4		59.97	
Outflow from cell 4		0.1			
Percentage difference		56.28			
Scenario 4			**portion of total inflow [%]**	**portion of cell inflow [%]**	**Flux [% of v/t]**
Cell 1_1	GW1	x			
	SF3		0.0	0.0	0.00
	GW4		0.0	0.0	0.00
	SF12	x			
	SF13		0.0	0.0	0.00
	GW14	x			
	GW23		0.0	0.0	0.00
	GW17	x			
Cell 2_2	SF11	x			
	SF12		0.0	0.0	0.00
	SF13	x			
	GW23	x			
	SF28		0.0	0.0	0.00
	SF6		0.0	0.0	0.00
Cell 3	GW1		7.6	7.8	3.07
	GW27		6.8	7.0	2.72
	SF38		28.9	29.6	11.59
	SF6		54.2	55.6	21.75
Cell 4	GW10	x			
	GW4	x			
	GW52		2.5	100.0	1.02
From cell		To cell		Real number [v/t]	
Cell1_1		Cell2_2		0	
Cell2_2		Cell3		0.38	
Cell3		Cell 4		59.47	
Outflow from cell 4		0.1			
Percentage difference		39.89			

Scenario 1:

The dominant contributor to cell 1 (represented as cell1_1) is SF13 with a 69.6 % inflow, followed by SF3 (17.8 %), SF12 (5.7 %), and groundwater from the wells GW4 with (3.4 %), and

GW23 with 2.9 %, and GW17 with 0.6 %. All this inflow sums up to around 2 % of the total inflow of the system (Tab. 6.25).

Cell 2_1 gets its contribution from SF29 and SF11, each making up 50.7 % of the cell inflow, which is 21.6 % of the system's total inflow. Cell 3 gets its contribution from GW27, which translates to 47.8 % of the system's total inflow. Cell 4's contribution is from GW52, making 7.6 % of the total inflow.

The in-between real flow is 0.37 % of volume/time from cell 1_1 to cell 2_1, 8.94 % of volume/time from cell 2_1 to cell 3, and 53.79 % of volume/time from cell 3 to cell 4.

Scenario 2:

The dominant contributor to cell 1 (represented as cell1_1) is SF13 with a 42.2 % inflow, followed by SF12 with a 40.9 % contribution, then GW4 with a contribution of 11.9 %, GW17 with 3.1 %, and GW23 with 1.9 %. As the change is mainly in the make-up of cell 2 and cell 4, the contribution and the percentage of total inflow in cell 1 do not change much (summing up to around 2 %).

The whole system's main contribution is from GW27 into cell 3 (32.9 %), followed by 21.8 % contribution from SF13 into cell 2 and 14.8 %, 14.5 % respectively from SF29, SF28, then by SF12 making up 9.2 %. The contribution from GW52 is almost 5 %, with less than 1 % from each of GW4, SF3, SF13, and GW23. The in-between real flow is 0.93 % of volume/time from cell 1 to cell 2, 16.5 % of volume/time from cell 2 to cell 3 is 59.7 % of volume/time from cell 3 to cell 4.

Scenario 3:

The dominant contributor to cell 1 (represented as cell1_1) is SF13 with a 77.7 % inflow, followed by SF3 with a contribution of 15.9 %, then GW4 with a 3.8 % contribution, and GW23 with 2.6 % (Tab. 6.25). This translates to 3.3 % of the total inflow to the system. Cell 2_2 gets its contribution from SF12, making up 10.4 % of the system's total inflow. Cell 3 gets its recharge mainly from GW1, making up 72.3 % of the cell inflow, which translates to 58.6 % of the system's total inflow. A further contribution is from GW27 of 27.7 % of the cell inflow making up 22.4 % of the total system inflow. Cell's 4 contribution is from GW52, making 4.3 % of the total inflow. The groundwater contribution to the whole system is more than 80 %.

The in-between real flow is 1.13 % of volume/time from cell 1_1 to cell 2_2, 4.56 % of volume/time from cell 2_1 to cell 3, and 59.97 % of volume/time from cell 3 to cell 4.

Scenario 4:

The difference between this scenario and scenario 3 is the addition of SF6 as a potential contributor in cell 3 (Tab. 6.26). All of the potential contributors do not contribute to any significant inflow into cell 1 and cell 2. The main contribution is SF6, making up 54.2 % of the total inflow meaning 55.6 % of cell 1's inflow. SF38 contributes to 28.9 % of the total inflow, which translates into 29.6 % of cell's 1 inflow. Both GW27 and GW1 accordingly make the rest of the contribution of around 7 % to the cell and to the whole system. GW52 is the only contributor to cell 4 water, making up 2.5 % of the system's total inflow.

The in-between real flow is 0 % of volume/time from cell 1_1 to cell 2_2, 0.38 % of volume/time from cell 2_1 to cell 3, and 59.47 % of volume/time from cell 3 to cell 4.

Comparing scenarios 1 and 2:

The results show that the main contribution in both scenarios is provided by seeping groundwater, as represented by GW27 (Tab. 6.25). However, the percentage of total inflow from GW27 to cell 3 drops from 47.8 % to 32.8 % from the scenario that includes samples obtained during the flood event versus those collected before the flood (do not include flood). Cell 2 gets lower inflow through it in the flood season. In addition, the total in-between cell inflow is higher in the scenario without floods.

The reasoning behind it is that during the flood, surface water dilutes the water storage in the lagoon relative to the amount that seeps out from the shallow groundwater. In addition, during floods, the water head in the lagoon is temporarily elevated, which decreases the hydraulic head difference between the lake and the groundwater piezometer head. The latter causes a decrease in the upward groundwater flux. Adding to that, a major source that contributes to the water, which is missing, is portrayed in the absolute difference in both scenarios. GW52 is the main contributor to cell 4 in both scenarios.

Comparing scenarios 3 and 4:

Scenario 3 and scenario 4 (Tab. 6.25) use different make-up of cell 2 (cell 2_2). This accordingly enables SF6 to be a possible contributor to cell 2. Scenario 4 includes SF6 as a potential contributor to cells 3 in addition. This changes the whole system's balance. The results show that in scenario 4, the main and almost all the contribution to the system is **cell 3** through SF6, SF38, and GW1 and GW27. The water flow through the first two cells is almost negligible and stagnant. The main recharge in between the cells happens between cell 3 and cell 4. In scenario 3, the main contribution to the system was similar from cell 3. However, both cell 1 and cell 2 contributed to the system too. The difference as well lies in the percentage contribution of groundwater to the whole system; in scenario 3, groundwater is the only contributor to cell 3 (in addition to cell 2_2), which is not the case in scenario 4 (groundwater in addition to surface water and cell 2_2's contribution).

The in-between real flow is lower in scenario 4 between cell 1_1 to cell 2_2 and cell 2_2 to cell 3. However, it is similar to cell 3 to cell 4. Furthermore, recall that the error was around 17 % only when running the multi-cell version on 3 cells in scenario 3 (Tab. 5.24). However, scenario 4 in this multi-cell (run of 4 cells) increases the error by at least 30 % more, meaning that there is a main source that contributes to the water during the flood times, vividly seen in the end part of the wetland, which is missing. GW52 is the main contributor to cell 4 in both scenarios.

6.6.2.4. Discussion of MCM results

Preferred scenarios on behalf of other scenarios

The three first scenarios present similar results (Tab. 6.25 and Tab. 6.26). Scenario 4 though representing the smaller error, shows that the first two cells' contribution is negligible (almost 0 %). This is explained by the fact that the area where cell 1 and cell 2 are located is known for having shallow water through them due to the high abstractions and irrigation rate. Due to the lack of data about the exact amounts, it was not included in the modeling.

The four different scenarios represent all the various possibilities of water flow in the Ewaso Narok wetland, depending on the time of year, the blocking of channels, the abstraction amounts, the ephemeral streams' drying, and the rain amount.

The best scenario compared to other scenarios would be scenario 3 from the three cells MCM run (Tab. 6.24) if the percentage error is the only criterion.

Explaining the error and its importance:

Running the multi-cell based on the scenarios, and running many iterations, makes it clear that there is a substantial error, a high negative one. Many attempts were performed to decrease the water balance error, and some yielded better results. The high negative error means that one or several additional hidden sources contributing to the mass balance are missing or are not identified. These might be pristine water of the wetland, water from the channel with human-made additions, floodwater, and groundwater within the floodplain.

The wetland is full of agriculture, grazing, and floodwater, bringing water from all over. Floods play a significant role in the characterization of the wetland. Recall that the samples in cell 2 onwards were mainly sampled during flash floods. An ending member contributing to the storage is missing, and its water mixes with the stagnant water in the floodplain. There are not enough sources to back up the water flow from cell 2 to cell 3 and not from cell 3 to cell 4. Cell three is made up of two points on the river. It was attempted to change the make-up of cell 2 to include floods and not include them. However, this did not change the fact that only two points were sampled downstream from there. The same applies to cell 4.

It is accordingly important to remember that the percentage error is one of many other parameters in this quantification and water flow determination, and its interpretation is of value. Determining the missing sources in the MCMsf that resulted in the absolute difference's high values is vital in lowering the absolute error in future studies. This can be achieved by sampling the wetland more often, during and without flash flood periods. In addition, drilling wells inside the delineated flooded wetland could better characterize the aquifer and might account for the missing sources. Locating more wells and boreholes in the area is of vital importance.

Challenges

Several challenges were encountered while using the MCM. These included performing many iterations as the potential sources could include any measurement with a hydrological potential to flow into a specific cell based on topography, piezometric potential, and geological feasibility. In addition, if a scenario does not yield a successful output, it is not possible to know which of the sources caused the failure because it uses different sets of equations that do not cross each other; thus, they do not lead to an optimum. Accordingly, the only way is trial and error.

Furthermore, the results presented in this work show a relative value of 100 %, as the pumpage and evapotranspiration values were not known. Measuring the real amount of pumping and evapotranspiration and including them in the model can help assess the real values of water inflow and contribution from groundwater to the Ewaso Narok wetland. In addition, it is important to try to find the missing hidden water source. This can be achieved by drilling artesian wells in the floodplain and conducting more sampling campaigns during dry and flood periods.

6.6.2.5. Summary and main finding from MCM

This research analyzed the spatial distribution along the Ewaso Narok wetland and the aquifer to assess both systems' potential links. Statistical cluster analyses, followed by single-cell modeling and then multi-cell modeling, indicate hydraulic connectivity between the wetland's surface water and the groundwater underneath. The water source in the wetland is the river and its tributary. However, there is enough evidence to show a clear link between the groundwater and the wetland. The groundwater feeds the wetland and contributes between 17 and 84 % to the wetland water (Tab. 6.25 and Tab. 6.26). Groundwater feeding the wetland is clear upstream of the wetland and even more vivid downstream of the wetland, as seen clearly in Cell 3, being the main contributor to the total amount of water in the system. This clearly shows that groundwater emerging in many perennial springs and seepages in the Ewaso Narok river often ends in the Ewaso Narok wetland and becomes baseflow.

This leads to the next finding that groundwater rises along preferential flow paths within the faults and fissure system to feed the wetland. This is not surprising given that the whole Ewaso Narok basin is a recharge/ discharge area with a deep groundwater table and locally shallow groundwater perched aquifer (Republic of Kenya, 1987). Another explanation is that the wetland's sides are permeable allowing groundwater discharge**.** The weathering profile, which is more advanced on the wetland side, acts as a porous aquifer contributing flow. Most groundwater flow in the upper-weathering profile is between the deep layers. When the recharge is intense, the water infiltrates and moves between fissures and fractures.

The middle part of the wetland is the only part where groundwater is not noticed as feeding the wetland. The main source feeding the wetland in this area is the contribution from the different streams. This might hint at the fact that there are not many fractures in this specific part of the wetland or that there is a clay layer that acts as a barrier preventing groundwater from feeding the wetland's surface water. Assuming faults, they might act as hydraulic barriers between the different aquifers preventing water replenishment and exchange. This suggests that the middle part of the wetland is relatively impermeable compared to the wetland's sides.

Floods play a major role in the functioning of the wetland. Even though most of the sampling occurred during flash floods, the groundwater percentage inflow was high. It is accordingly feasible to assume that it might be even more vivid in drier periods.

The gap between the inflow and outflow in the modeled cells clearly hints at a hidden undefined water source. This, coupled with the fact that there is a shallow water table, further suggests the existence of a semi-confined aquifer (artesian and pressurized) under the wetland, where the water leaks upwards from what was not sampled. The water from this semi-confined aquifer mixes with the floodplain water and changes its characteristics.

7. Summary, conclusions, and recommendations

Conflicts in the Ewaso Narok wetland area arise mainly due to the lack of water, making collecting field data and, more importantly, controlling and managing this scarce resource more difficult. This is further exacerbated and impeded by the lack of geological, hydrological, and water quality data in the Ewaso Narok wetland. As for any effective and integrated management of water resources, there is a need for proper aquifer characterization and an understanding of groundwater flow direction, recharge and discharge mechanisms, water flux and chemicals from and to groundwater, and the water chemistry processes. Aiming to address this data gap, this study successfully developed a hydrogeological and hydrochemical database. Furthermore, it quantitatively assessed the surface water - groundwater interactions, namely water recharge, discharge, and water flux. Given climate change and population growth, competition over water resources is expected to only intensify with time. The results of this work, mainly the hydrogeological characterization of the Ewaso Narok system and the modeling, allow regionally specific recommendations to be formulated, as the Ewaso Narok wetland is an example that applies to many other wetlands in Kenya.

In section 7.1, a general summary of the work with the challenges encountered is discussed. The characterization of the Ewaso Narok wetland, its setting, and its processes are discussed from a wider perspective in section 7.2. Despite the data scarcity and the challenges encountered, the results of this work allow for drawing valuable conclusions and recommendations, as seen in section 7.3 for improved wetland management, while taking into account the various interests of different groups.

7.1. Summary of the work

The Ewaso Narok wetland is a floodplain within a weathered basement aquifer and part of the largest drainage basin in Kenya (Ewaso Ngiro). The wetland was and still is intensively used for grazing and agricultural use to meet the growing increase in demand for food and water.

The hydrogeological characterization of the Ewaso Narok's aquifer system was challenging due to the limited data availability, incomplete datasets, and the lack of recent sampling. Therefore, an interdisciplinary approach was developed to understand the aquifer's structure, water dynamics, and water composition and to model this data-scarce wetland. The field data were collected using surveys, water, soil, and rock measurements. They were processed and analyzed while combined with data obtained from existing reports of various agencies, making the secondary data a backbone to fill gaps in this work. The survey results provided potential water points for modeling the Ewaso Narok wetland, as they determined locations of input of water as well as pollution into the wetland for sampling and then modeling the wetland.

The hydrogeological characterization of the Ewaso Narok aquifer, its setting, and processes were merged with field data from reports, drilling logs, and the survey results to develop a theoretical model. This was then used as the base for running the MCM mathematical modeling based on hydrochemistry and stable water isotopes to identify the water sources feeding the wetland. In addition, biogeochemical processes that may further modify the chemical signature were included in the analysis. Typical challenges of hydrological assessment and mathematical modeling were encountered (Arheimer et al., 2005; Kumar, 2014; Verhoeven et al., 2006).

Among these was developing water table contour maps, essential for any hydrological work, which involved combining different geo-referenced maps from reports while looking for water levels from literature and identifying well names and drilling well logs. Data validation was performed to correct errors, especially in the secondary recorded data. The data was assessed for its reliability. The task was more challenging as certain gaps in the database were identified, but there was no possibility of going back to the field due to security issues and conflicts between ranch farmers and pastoralists that led to ranch invasions, violence, and displacements in 2017.

Despite these challenges, this study shows that augmenting and combining the mixing-cell modeling approach with the survey, the aquifer's characterization, the water dynamics, and the water composition are of great value. This was the key element in determining the spatial hydraulic connectivity between the wetland's surface water and sub-aquifer units in this data-scarce area. Based on this study, it is concluded that the MCMsf is a good method to quantify the water inflow and that it provides meaningful results when limited information is available.

7.2. Discussion and characterization of the hydrogeological setting and processes

This section discusses the Ewaso Narok wetland as a discharge wetland in the bigger context of other wetlands in Africa. Furthermore, a characterization of the aquifer system with a focus on the surface water-groundwater interactions is summarized.

The geomorphology of the Ewaso Narok wetland, with its wide floodplain bounded by steep hill slopes, is typical of many African floodplains. However, the spatial response pattern is more site-specific, controlled by the sediments, the thick, fresh, and weathered phonolites, and fractures. The characteristics of the groundwater-surface water interactions along the Ewaso Narok river are not constant throughout the year as seasonal dynamics exist. However, a general trend is observed, which is crucial for the floodplain chemistry and water balance: The results prove the tight interaction between groundwater and floodplain water. It is evident that the Ewaso Narok wetland is a discharge wetland for at least a part of the year (Fig. 7.1), where groundwater plays a major role in the water balance of the wetland. This type of interaction, as seen by the composite of water balance factors, has been suggested before but never proven (Ministry of Agriculture, 1983). Gichuki (2002) further indicated that the Ewaso Narok subsystem, with its high rainfall and dense ground cover in the Nyandarua mountain ranges, provides most of the water during the dry seasons. Finally, according to Bours (2016), despite increased abstractions, a striking increase in discharge rates over the last four years (2010-2013) is observed at two gauge stations (5AC15 and 5AC10) in the middle and the outlet part of the Ewaso Narok. This is explained by the groundwater's contribution to this wetland resource's replenishment.

A further characteristic of discharge wetlands in arid and semi-arid regions is the presence of springs located at or just above the base of hills (Maltby & Barker, 2009), which is the case for the Ewaso Narok wetland. Furthermore, they do not provide proper floodwater storage but are responsible for increased vegetation and habitat diversity (Maltby & Barker, 2009).

In terms of surface water-groundwater interactions, this study's results confirm the spatial and temporal variability of groundwater inflow and outflow patterns of wetlands, as has been found

by other authors (Burghof, 2017; Hunt et al., 1996; Shedlock et al., 1993). The Ewaso Narok river, a small river flowing in an alluvial floodplain, resembles larger streams in regards to the interactions of groundwater and surface water being spatially diverse. Groundwater discharges to the gaining stream in the upstream and downstream parts of the basin. It further discharges in the tributaries, where the stream stage is greater than the adjacent and underlying groundwater head. Furthermore, by discharging into the stream, groundwater contributes to the flooding and thus indirectly contributes to the wetlands. Water discharge is then possible due to the fractured and weathered profiles underneath the Ewaso Narok river, as seen in this study.

In regards to surface water, a large flow is noticed, especially downstream of the wetland, which is characterized in the model as cell 3. In the upstream and middle parts of the wetland, lower inflow is observed, and the impact of abstractions and irrigation is visible. Cell 3 is the main contributor to the total amount of water in the system. Throughout the flood season, it gets lower groundwater contribution (from 47.8 % to 32.8 %) than during the drier periods. The reasoning is that surface water dilutes the wetland's water storage relative to the amount that seeps from the shallow groundwater. In addition, during floods, the water head in the wetland is temporarily elevated, which decreases the hydraulic head difference between the wetland and the groundwater piezometer head. The latter causes a decrease in the upward groundwater flux. Another explanation is that the dirt, waste, and heavy sediments that the floods carry, as reported by the inhabitants in the survey, end up blocking and lowering the inflow.

Two conclusions can be drawn from the fact that the middle part of the wetland, characterized as cell 2, does not show groundwater impact. The first is that the lower end of the wetland is made of an impermeable clay layer, and the weathering profile and rate along the river courses in this part are low, thus not allowing a large amount of water to be discharged. The second is that the faults could act as hydraulic barriers to the lateral flow as they are filled with clay.

Regarding recharge, infiltrated water reaches the local aquifer through preferential flow paths and fractures. This was seen in the piezometer results around the river at the beginning of the flooding, where the hydraulic gradient is directed away from the river. Lateral riverbank infiltration is thus induced to the floodplain groundwater. During the daytime, the hydraulic gradient inverts again, and only small amounts of water enter the aquifer. This water reaches the local aquifer, the perched aquifer, or is discharged back as springs. The sides of the river's profile show more weathering than the floodplain profile. This research could not clearly differentiate between the different sources of flooding, be it precipitation or over-bank flow, due to the lack of isotopes precipitation data. The isotope results for surface water in the dry period indicate that the wetland groundwater feeds the wetland and contributes to the mass balance. This is evident in the dry period samples that show results of depletion and no evaporation effect. In addition, the tributaries are more depleted in both the stable water isotopes $\delta^{18}O$ and $\delta^{2}H$. As the river moves downwards, the water is mixed, yet signs of depletion are still vivid, which suggests that the groundwater feeds the wetland in the downstream part. The isotope results indicate that groundwater from regional and local systems discharges to the river at various places across the floodplain.

Two systems characterize the wetland (Fig. 7.1): a regional confined aquifer system underlying the volcanic rocks and a local semi-confined aquifer system in the weathered profile of the

crystalline basement. Both the regional and the local groundwater systems are interconnected and thus interact and influence the wetland. There is no clear distinction between the water in each of the confined aquifers in terms of water quality and isotopes. However, a clear hydrochemical and isotopic difference exists between surface water and groundwater.

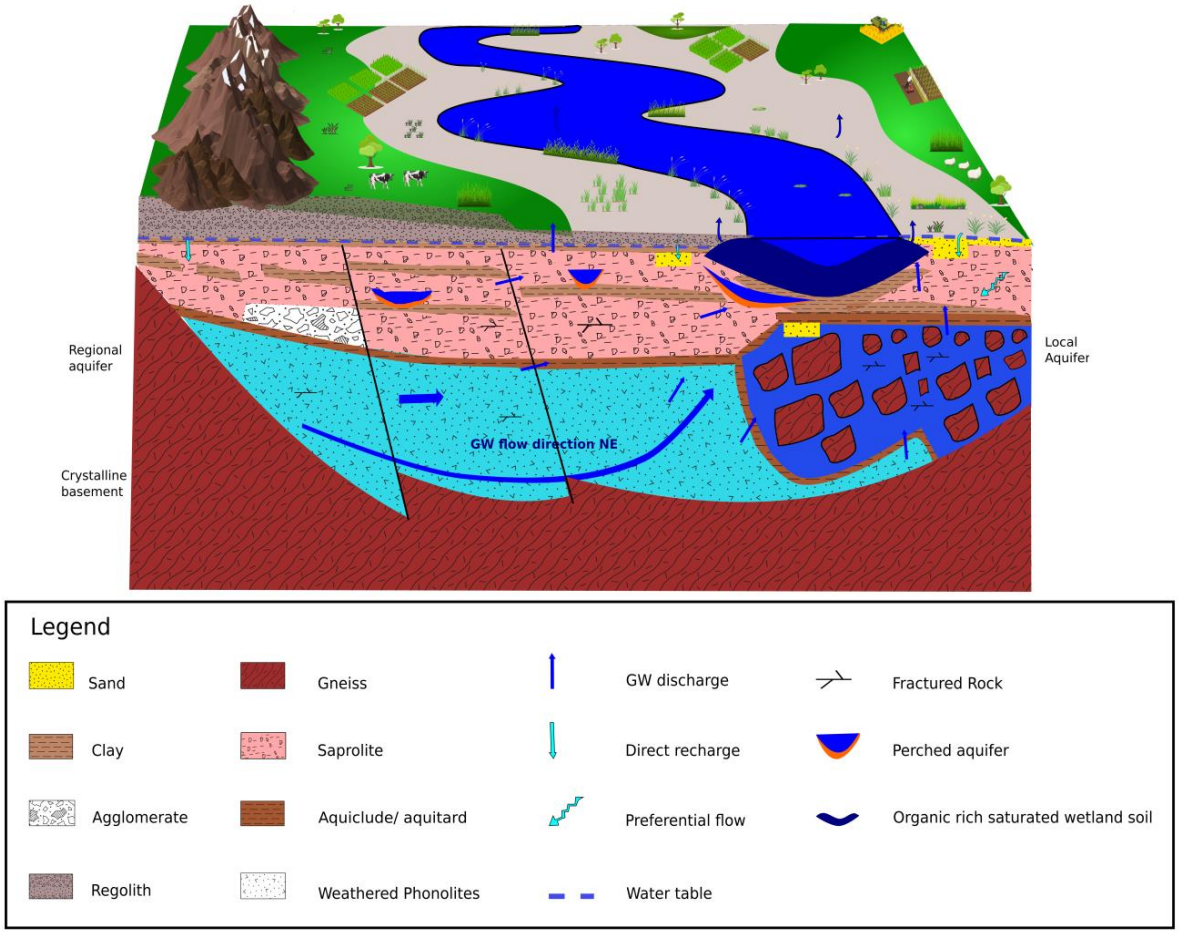

Fig. 7.1: Conceptualized diagram of the Ewaso Narok aquifer system.

The water from the springs circulates throughout the shallow system, whereas the plains' water passes underneath as part of the regional system. The groundwater of the regional aquifer is discharged upwards towards the local aquifer (Fig. 7.1). Furthermore, the regional aquifer directly discharges water to the unconfined aquifer and the wetland. The local aquifer is connected hydraulically to the weathering profile. The Ewaso Narok wetland is fed from both the aquifers (shallow groundwater contributes to 17 and 84 % of the wetland water) and is located on sediments, which are derived from alluvial transported weathered material of crystalline rocks. Within these weathered profiles, perched aquifers are present.

Chemical reactions on alluvial aquifers are usually more impacted by weathering rates and microorganisms' activities than by dissolution and precipitation of minerals, as the rate of water movement is fast. The hydrochemistry in Ewaso Narok is profoundly impacted by silicate weathering expressed in low ECs and high content of HCO_3^- and SiO_2 (Appelo & Postma, 2005). Secondary minerals are formed, such as clay (illite, kaolinite) and iron oxides (cp. sec. 6.2.2)(Appelo & Postma, 2005). The wetland is rich in organic compounds, as seen in the LOI results, even though more weathered clay minerals tend to hold fewer nutrients. Further

chemical reactions in the system are seen in the relatively high cation exchange capacity and the amount of dissolved ions.

The results show that indirect water recharge did not happen. The EC of groundwater of wells next to the wetland and close to the streams and Ewaso Narok river did not decrease. Furthermore, the evaporation effect was not observed in wells lying adjacent to the streams or in the river in the wetland's delineated flooded area. On the contrary, most wells showed a depleted signature of both stable water isotopes inside the delineated flooded area. In addition, during the flood event, the groundwater, which is charged in the high southern mountains, has a higher pressure gradient and thus is discharged into the floodplain. Most of the sampling occurred during flash floods, and despite that, the groundwater percentage inflow was high. It is accordingly feasible to assume that it might be even more vivid in drier periods.

7.3. Recommendations and management

People in the Ewaso Narok wetland rely on surface water for their livelihood, from drinking, irrigation, and washing cars to farming. On the other side, groundwater is mainly filled in tanks and buckets and taken home for drinking. As the main aim of this study was to quantitatively evaluate the surface water-groundwater interactions in the Ewaso Narok wetland in terms of water recharge/discharge and water flux, comparison and recommendations can be given below in terms of water quantity. Furthermore, this study assessed the Ewaso Narok wetland's water quality and compared it to the human drinking standards and irrigation guidelines. Accordingly, specific recommendations are given in terms of water quality.

This study's results show that the nature of the wetland resource, and more specifically, its groundwater and its quality, is not fully documented. For example, two gauging surface water stations are in the Lower Ewaso Narok (WRMA & LWF, 2013). However, the data collected from these gauging stations by WRMA focuses mainly on the flow quantity and lacks many important hydrochemical and biological parameters. There are currently no groundwater monitoring stations. This highlights the need for a proper establishment of monitoring stations both for surface water and groundwater and regular monitoring for establishing databases and building on the already established work of this study (appendices).

This study provides a database of the Ewaso Narok and solutions for dealing with data scarcity. It can further be used to:

- Provide input parameters in future crop growth simulation modeling and scenario building to assess other wetlands, catchments, and regional agricultural production potentials.
- Communicate essential information to decision-makers or locals using the wetland's resources for daily consumption and growing food.

Long-term measurements are important for hydrogeological works. This necessitates training a group of people to collect and monitor these stations. In addition, providing well owners and users with the measured results will improve the transparency and likelihood of future accessibility regarding research activities.

Furthermore, like many other studies, this research shows that management problems in the Ewaso Narok wetland include water quality degradation, catchment degradation, and water scarcity (Kibson Consult, 2014; WRMA & LWF, 2013).

Regarding water quality, the study results show that some dissolved water compounds, including nitrogen, manganese, and fluoride, exceeded the recommended WHO (2011) and KEBS (2015) health guidelines. Although the Ewaso Narok wetland probably provides water purification, applying less fertilizer is less costly and easier to realize than wetland restoration (Arheimer et al., 2005; Verhoeven et al., 2006).

Nitrate values in surface water during the flash floods were higher than during the dry period, probably due to washed-out agricultural fields. Groundwater shows partly high nitrate values exceeding the recommended WHO guidelines (2011). Nitrite values exceeding the recommended KEBS standards (2015) were noticed in both the surface water and groundwater points. These measurements are worrying, as high nitrogen uptake causes problems with vitamin A shortages and is linked to colorectal cancer, thyroid disease, and neural tube defects (Ward et al., 2018). As the nitrogen compounds guidelines are exceeded in some samples, assessing the nitrogen isotope to distinguish the artificial fertilizers from manure or nitrate formed from the nitrification of organic material is recommended. This will assist in determining the dominant nitrate source. In addition, a high potential of nitrate contamination is expected in the wetland as well GW52, located in the wetland's outlet, has more than 50 mg/l of nitrate, contributing to 5 to 7 % of the wetland's inflow. In the single-cell version, well GW23, located upstream of the wetland, appears to contribute to the middle part of the wetland (cell 2), and well GW52 appears to contribute to the wetland's outlet part (cell 4); thus, both groundwater wells are positive potential sources of recharge. This also applies to other elements and compounds found in higher amounts than the recommended WHO (2011) and KEBS guidelines (2015), especially fluoride and arsenic, as both were found mainly in groundwater samples, which are used for drinking. They, therefore, pose a direct threat to health. Arsenic in drinking water is considered one of the most significant environmental causes of cancer (Chung et al., 2014). It leads to human carcinogenicity, and intake over a long period causes arsenic poisoning. Its source is either leaching from geological formations or anthropogenic sources (Chung et al., 2014; Shankar et al., 2014). In this area, the geological formations do not seem to contain arsenic; accordingly, arsenic may derive from pesticides, fertilizers, or other major contamination sources. Regarding fluoride, health problems associated with its excess include problems with bones, teeth, and neurological development (Brazier, 2018). Extreme precautions should be taken, and an immediate solution is needed to prevent harm to the inhabitants drinking the water. Determining the source of pollutants and getting rid of them, being informed about their existence in the drinking water, and possibly finding other drinking sources or even limiting water usage of contaminated water are vital. This research indicates geogenic influences as the source of two contaminants, fluoride, and manganese.

As the results of this research show a strong link between groundwater and surface water, it is advised to address the water quality of both by building a technical basis for systematic monitoring of water quality. In addition, proper management of wastewater and agricultural runoff; subsequently, water treatment has to be promoted.

Regarding surface water and health, iron, aluminum, iron, and copper levels exceeded the recommended concentrations. Although these elements are less dangerous to humans, they still impact taste and cause laundry staining, coating, and pipes' deposits. The water is accordingly not satisfactory in terms of public acceptability. The locals should be informed of these impacts and advised on how to deal with them. Furthermore, to deal with the pollution and water quality issues, awareness campaigns are advised and should address the following:

1. The pollution effects and how to control them.

2. Proper sanitation practices and hygiene.

3. Good agricultural practices.

Investment in the construction of sewage, car wash, and toilets is important. Local inhabitants should be encouraged to use alternatives and not to chemically spray and water their livestock directly in the wetland. Finally, a set of rules and enforcement schemes should be established to avoid further pollution through individuals. If necessary, penalties on polluters should be enforced (WRMA & LWF, 2013).

The surface water sampled exceeded the recommended irrigation limits, mainly for manganese. As surface water is mainly used for irrigation, it is accordingly advised to cultivate crops that are not impacted by high manganese concentrations. Other constituents' content, such as fluoride, ammonium ion, potassium, and bicarbonate, were alarmingly high and pose a threat to crops. All the surface water samples implicated a moderate to severe degree of restriction on use. Regarding infiltration evaluation, problems arise due to low salinity and high SAR. This is a common problem in most wetlands of East Africa (Burghof, 2017). Similarly, most groundwater samples (22 out of 25) showed a moderate to severe degree, suggesting a restriction on use. As surface water is under threat from over-extraction and climate change, a precaution in using groundwater in irrigation as an alternative is necessary, as high values of certain constituents can damage the crops. The groundwater sampled exceeded recommended irrigation limits for chlorine, calcium, potassium, sulfate, manganese, nitrate, ammonium ion, fluoride, and bicarbonate. The results contradict the Republic of Kenya's (1987) findings that groundwater is safer than surface water in terms of quality. It is accordingly advised to find other sources for irrigation.

From the water quality results that exceeded the recommended irrigation limits, one can conclude that agriculture in the wetland seems less harmful than outside the wetland. This can be explained by de-nitrification in the wetland and the clay layer preventing the contaminants' infiltration. This comes in terms with Burghof's (2017) findings. Due to constraints, a biological analysis was not performed; accordingly, analyzing fecal bacteria and organic products is recommended.

With regard to water scarcity, the research shows that the water storage and water treatment infrastructure is of poor quality. The surveyed people report a reduction in the water quantity in the dry period, exacerbated by climatic factors and the watershed's degradation. This necessitates ending the illegal water abstraction and metering and monitoring the water abstraction points. This work demonstrates the direct link and the contribution of groundwater to the wetland. Accordingly, groundwater protection and prevention of over-abstraction are vital for the sustainable use of wetlands' resources.

Regarding catchment degradation, the research showed that many of the surveyed people do not know the water quality, the impact of certain practices, and their long-term effects. Furthermore, there is a lack of responsibility and awareness of the wetland's pollution and well-being seen in the direct disposal of fertilizers, manure, and plastic containers in the Ewaso Narok wetland. Educating people and investing in awareness campaigns on the sustainable use of water resources is important. Similarly, providing the locals with alternative water sources (e.g., roof water harvesting) and livelihood strategies is important. Another important measure is to provide people with equal and equitable resource access to the Ewaso Narok wetland and to ensure better compliance with the law to prevent conflicts. This can be achieved by involving stakeholders and enhancing capacity building. Additionally, coordination between CETRAD, WRMA, and other government offices is important. Finally, making Ewaso Narok maps, plans, and water quality data accessible to the public and the researchers is essential.

The Kenyan government has set policies since the 1990s for sustainable water management of the Ewaso Narok wetland. However, a lack of political will and adequate budgetary provision for implementing these policies and enforcing the legislation continues to allow water scarcity (Gichuki, 2002), despite WUA's establishment of plans for water management and conflict resolution (CETRAD, 2005) and the creation of the Lower Ewaso Narok Water Resource Association (WRMA & LWF, 2013).

It is recommended that the government better enforces the water laws and policies, adequately regulates pumping, and controls the illegal abstractions and pumping permits. This will not only positively impact the livelihood of inhabitants in the floodplain but also of the downstream water users as well. In addition, there is a need to create a platform for local and financial resource mobilization. Investment in new technologies and water development to use the water more efficiently, like drip irrigation and water storage, for instance, in small-scale dams, runoff, and roof catchment, is vital. Further financial investment should be made in infrastructure maintenance. Protecting and conserving the springs, the catchment, and the dams are necessary. Furthermore, developing a water allocation plan and promoting storage reservoirs would help address the water scarcity.

The Ewaso Narok wetland is the backbone of people's local livelihoods, and given the already growing tension around it, a holistic approach is recommended to managing it, as summarized below. This approach necessitates addressing both groundwater and surface water alike for the Ewaso Narok wetland's long-term sustainability in order to put an end to the human activities that pose a threat of extinction to it.

Recommendations to government and policymakers:

- Address the groundwater pollution as groundwater clearly contributes to the wetland.
- Protect the groundwater and surface water quality and quantity.
- Systematically monitor the quality to strengthen the technical basis for planning and managing surface water and groundwater resources.
- Inform locals about water quality and health impacts and provide advice on how to deal with the pollution.

- Educate local communities and invest in awareness campaigns about the sustainable use of water resources, pollution effects, proper sanitation practices and hygiene, and good agricultural practices.
- Provide the locals with alternative water sources and income strategies to ensure their livelihood.
- Encourage the locals to use alternative sources and not to chemically spray and water their livestock with water directly abstracted from the wetland.
- Enforce penalties on polluters if necessary.
- Ensure that people have equal and equitable resource access to the Ewaso Narok wetland and show better compliance with the law to prevent conflicts.
- Involve stakeholders and provide them with capacity building in management decisions and discussions.
- Enforce the water laws and policies, adequately regulate pumping, and control the illegal abstractions and pumping permits.
- Invest in new technologies and water development for more efficient water usage, like drip irrigation and water storage (e.g., in small-scale dams, runoff, and roof catchment).
- Invest in infrastructure maintenance and construction of sewage, car wash, and toilets.
- Invest in proper management of wastewater and agricultural runoff.
- Regularly sample, validate data, and share it via platforms.
- Establish monitoring stations both for surface water and groundwater.
- Train people to operate monitoring stations.
- Monitor and meter the water abstraction points.
- Provide the well owners with water quality data.
- Develop a water allocation plan and promote storage reservoirs.
- Coordinate work from CETRAD, WRMA, and other government offices.
- Make data, including maps, management plans, water quality, and quantity, accessible to the scientific community and the inhabitants.

Recommendations to local inhabitants and farmers:

- Apply less fertilizer, which is less costly and easier to realize than wetland restoration.
- Manage wastewater and agricultural runoff.
- Enroll in awareness campaigns.
- Cultivate crops that are not vulnerable to high manganese concentrations.
- Find another source for irrigation and fertilization if needed.

Recommendations to researchers for future work:

- Assess the nitrogen isotope to distinguish the artificial fertilizers from manure or nitrate formed from the nitrification of organic material.
- Analyze fecal bacteria and organic products.
- Use different modeling techniques and compare their result with this work.
- Conduct similar case studies of wetlands in different environments.
- Update and keep up-to-date hydrological data of the Ewaso Narok wetland.
- Understand the water situation in the downstream part of the wetland and the associated impacts from the upstream.

- Complete the missing datasets and update the data from boreholes.
- Sample the quality of the Ewaso Narok surface water and boreholes regularly and more frequently.

8. References

Adams, W. M. (1993). *Indigenous Use of Wetlands and Sustainable Development in West Africa.* Geogr. J. 159(2), 209–218. doi 10.2307/3451412

Adar, E. & Massoth, S. (2017). *MCMsf Manual*.

Adar, E. (1996). Quantitative evaluation of flow systems, groundwater recharge and transmissivities using environmental tracers. In *Manual on Mathematical Models in Isotope Hydrology: Vol. IAEA-TECDOC-910, Y. Yurtsever* (IAEA-TECDOC--910; pp. 113–154). International Atomic Energy Agency (IAEA). http://inis.iaea.org/Search/search.aspx?orig_q=RN:28020906

Adar, E. (1995). Assessment of groundwater fluxes and transmissivities by environmental tracers—Summary of theory, application and sensitivity analysis. In *Mathematical models and their applications to isotope studies in groundwater hydrology* (pp. 93–122). IAEA, , Vienna.

Adar, E. Rosenthal, E., Issar, A. S., & Batelaan, O. (1992). *Quantitative assessment of the flow pattern in the southern Arava Valley (Israel) by environmental tracers and a mixing cell model.* Elsevier Science Publishers B.V., J. Hydrol. 136, 333–352.

Adar, E., & Sorek, S. (1990). *Numerical method for aquifer parameter estimation utilizing environmental tracers in a transient flow system*.

Adar, E. & Sorek, S. (1989). *Multi-compartment modelling for aquifer parameter estimation using natural tracers in non-steady flow.* Adv. Water Resour. 12(2), 84–89. doi 10.1016/0309-1708(89)90006-7

Adar, E. & Neuman, S. P. (1988). *Estimation of spatial recharge distribution using environmental isotopes and hydrochemical data, II. Application to Aravaipa Valley in Southern Arizona, U.S.A.* J. Hydrol. 97(3), 279–302. doi 10.1016/0022-1694(88)90120-5

Adar, E. Neuman, S. P. & Woolhiser, D. A. (1988). *Estimation of spatial recharge distribution using environmental isotopes and hydrochemical data, I. Mathematical model and application to synthetic data.* J. Hydrol. 97(3), 251–277. doi 10.1016/0022-1694(88)90119-9

Adar, E. & Long, A. (1987). *Oxygen-18 and deuterium distribution in rainfall, runoff and groundwater in a small semi-arid basin: The Aravaipa Valley in the Sonora Desert, Arizona.* In proceedings of an International Symposium on the Use of Isotope Techniques in Water Resources Development (pp. 257-273). IAEA, Vienna.

Adar, E. & S. Neuman (1986). "*The use of environmental tracers (isotopes and hydrochemistry) for quantification of natural recharge and flow components in arid basins*". The 5th International Symposium on Underground Tracing, Athens, Greece, pp. 235-253.

Akeroyd, M. D., Tyerman, S. D., Walker, G. R., & Jolly, I. D. (1998). *Impact of flooding on the water use of semi-arid riparian eucalypts.* J. Hydrol. 206(1), 104–117. doi 10.1016/S0022-1694(98)00092-4

Alexander, J. (1983). *Hydrogeological investigations in a granite catchment, Dartoor, Devon* [PhD thesis]. University of Plymouth Polytechnic.

Allen, D. J., Darling, W. G., & Burgess, W. G. (1989). *Geothermics and hydrogeology of the southern part of the Kenya Rift Valley with emphasis on the Magadi-Nakuru area* [Report].

Allison, G. B., Gee, G. W., & Tyler, S. W. (1994). *Vadoze-Zone techniques for estimating groundwater recharge in arid and semiarid regions.* Soil Sci. Soc. Am. J. 58, 6–14. doi 10.2136/sssaj1994.03615995005800010002x

Allison, J. B. (1988). *A review of some of the physical chemical and isotopic techniques available for estimating groundwater recharge.* In I. Simmers (Ed.), Estimation of Natural Groundwater Recharge (pp. 49–72). Springer Netherlands.

Anhaeusser, C. R. (2014). *Archaean greenstone belts and associated granitic rocks – A review.* J. Afr. Earth Sci. 100, 684–732. doi 10.1016/j.jafrearsci.2014.07.019

Anthonj, C., Rechenburg, A., & Kistemann, T. (2016). *Water, sanitation and hygiene in wetlands. A case study from the Ewaso Narok Swamp, Kenya.* Int. J. Hyg. Environ. Health 219(7), 606–616. doi 10.1016/j.ijheh.2016.06.006

Appelo, C. A. J., & Postma, D. (2005). *Geochemistry, groundwater and pollution*, 2nd edn. CRC Press, Taylor & Francis Group.

Aqua Well (2013). *Kifuku Estate Limited* [Hydrogeological Survey Report AWS/2953/2013]. Compiled by: Njoroge S.N.

Aquatreat. (2013). *Kifuku Estate* [Water Quality Analysis: Physical & Chemical Tests].

Arheimer, B., Löwgren, M., Pers, B. C., & Rosberg, J. (2005). *Integrated catchment modeling for nutrient reduction: Scenarios showing impacts, potential, and cost of measures.* Ambio 34(7), 513–520.

Ashley, G. M., Mworia, J. M., Muasya, A. M., Owen, R. B., Driese, S. G., Hover, V. C., Renaut, R. W., Goman, M. F., Mathai, S., & Blatt, S. H. (2004). *Sedimentation and recent history of a freshwater wetland in a semi-arid environment: Loboi Swamp, Kenya, East Africa.* Sedimentology 51(6), 1301–1321. doi 10.1111/j.1365-3091.2004.00671.x

Asio, V., & Jahn, R. (2007). *Weathering of basaltic rock and clay mineral formation in Leyte, Philippines.* Philipp. Agric. Sci. 90(3), 192–204.

Ayers, R. S., & Westcot, D. W. (1985). *Water quality for agriculture* [FAO irrigation and drainage paper, 29 Rev. 1]. Food and Agriculture Organization of the United Nations.

Back, W. (1966). *Hydrochemical facies and groundwater flowpattern in northern part of Atlantic Coastal Plain* [US Geological Survey Professional Paper No. 498A]. US Government Printing Office. doi 10.3133/pp498A

Baker, B. H., & Wohlenberg, J. (1971). *Structure and Evolution of the Kenya Rift Valley.* Nature 229, 538–542. doi 10.1038/229538a0

Bannerman, R. R., & Ayibotele, N. B. (1984). *Some critical issues with monitoring crystalline rock aquifers for groundwater management in rural areas.* In proceedings, Harare Symposium July 1984. D. Walling, S. Foster, & P. Wurzel (Eds.), Challenges in African hydrology and water resources: IAHS Publ. no. 144.

Bas, M. J. L., Maitre, R. W. L., Streckeisen, A., & Zanettin, B. (1986). *A Chemical Classification of Volcanic Rocks Based on the Total Alkali-Silica Diagram.* J. Petrol. 27(3), 745–750. doi 10.1093/petrology/27.3.745

Bates, P. D., Stewart, M. D., Desitter, A. L., Anderson, M. G., Renaud, J.-P., & Smith, J. A. (2000). *Numerical simulation of floodplain hydrology.* Water Resour. Res. 36(9), 2517–2529.

Bear, J., & Verruijt, A. (1987). *Modeling Groundwater Flow and Pollution.* Springer Netherlands.

Belkhiri, L., Abderrahmane, B., & Mouni, L. (2010). *A multivariate Statistical Analysis of Groundwater Chemistry Data.* Int. J. Environ. Res. 5(2), 537–544.

Bell, F.G. (2013). *Engineering Properties of Soils and Rocks.* Butterworth-Heinemann

Berger, P. (1989). *Rainfall and agroclimatology of the Laikipia Plateau, Kenya.* Geographica Bernesia and Geographical Society of Berne.

Beuel, S., Alvarez, M., Amler, E., Behn, K., Kotze, D., Kreye, C., Leemhuis, C., Wagner, K., Willy, D. K., Ziegler, S., & Becker, M. (2016). *A rapid assessment of anthropogenic disturbances in East African wetlands.* Ecol. Indic. 67, 684–692. doi 10.1016/j.ecolind.2016.03.034

BGS (British Geological Survey) (2019). *Africa Groundwater Atlas.* Choubert

Blake, S., Henry, T., Murray, J., Flood, R., Muller, M. R., Jones, A. G., & Rath, V. (2016). *Compositional multivariate statistical analysis of thermal groundwater provenance: A hydrogeochemical case study from Ireland.* J. Appl. Geochem. 75, 171–188. doi 10.1016/j.apgeochem.2016.05.008

Borchers, U. (2013). *Die Trinkwasserverordnung 2012: Erläuterungen - Änderungen - Rechtstexte*. Beuth Verlag.

Borg, G., & Shackleton, R. M. (1997). *The Tanzania and NE-Zaire Cratons.* In M. de Wit & L. D. Ashwal (Eds.), Greenstone Belts (OUP) Greenstone Belts (pp. 608–619). Oxford University Press.

Bours, H. (2016). *Irrigation Water Requirements in the Ewaso Narok Swamp in Laikipia, Kenya Using the CropWat Model and their Influence on Downstream River Discharges* *Master's Thesis, unpublished]. University of Duisburg-Essen, Essen, Germany.

Boy, G. (2011). *Laikipia: A natural history guide.* Laikipia Wildlife Forum.

Brazier, Y. (2018). *Fluoride: Risks, uses, and side effects.* Retrieved from https://www.medicalnewstoday.com/articles/154164.php

Brindha, K., & Schneider, M. (2019). *Impact of Urbanization on Groundwater Quality.* In S. Venkatramanan, M. V. Prasanna, & S. Y. Chung (Eds.), GIS and Geostatistical Techniques for Groundwater Science (pp. 179–196). Elsevier. doi 10.1016/B978-0-12-815413-7.00013-4

Brinson, M. (1993). *Changes in the Functioning of Wetlands Along Environmental Gradients.* Wetlands 13, 65–74. doi 10.1007/BF03160866

Briški, M., Stroj, A., Kosovid, I., & Borovid, S. (2020). *Characterization of Aquifers in Metamorphic Rocks by Combined Use of Electrical Resistivity Tomography and Monitoring of Spring Hydrodynamics. Geosciences 10*(4), 137. doi 10.3390/geosciences10040137

Brunel, J.-P., Walker, G. R., & Kennett-Smith, A. K. (1995). *Field validation of isotopic procedures for determining sources of water used by plants in a semi-arid environment.* J. Hydrol. 167(1), 351–368. doi 10.1016/0022-1694(94)02575-V

Burdige, D. J. (1993). *The biogeochemistry of manganese and iron reduction in marine sediments.* Earth Sci. Rev. 35(3), 249–284. doi 10.1016/0012-8252(93)90040-E

Burghof, S. (2017). *Hydrogeology and water quality of wetlands in East Africa: Case studies of a floodplain and a valley bottom wetland* [Dissertation, published]. Rheinischen Friedrich-Wilhelms-Universität Bonn.

Burt, T. P., Pinay, G., Matheson, F. E., Haycock, N. E., Butturini, A., Clement, J. C., Danielescu, S., Dowrick, D. J., Hefting, M. M., Hillbricht-Ilkowska, A., & Maitre, V. (2002). *Water table fluctuations in the riparian zone: Comparative results from a pan-European experiment.* J. Hydrol. 265, 129–148. doi 10.1016/S0022-1694(02)00102-6

Butturini, A., Bernal, S., Sabater, S., & Sabater, F. (2002). *The influence of riparian-hyporheic zone on the hydrological responses in an intermittent stream.* Hydrol. Earth Syst. Sci. Discuss. 6(3), 515–526.

Bwangoy, J.B., Hansen, M. C., Roy, D. P., Grandi, G. D., & Justice, C. O. (2010). *Wetland mapping in the Congo Basin using optical and radar remotely sensed data and derived*

topographical indices. Remote Sens. Environ. 114(1), 73–86. doi 10.1016/j.rse.2009.08.004

Carlé, W. (1975). *Die Mineral- und Thermalwässer von Mitteleuropa: Geologie, Chemismus, Genese.* Wissenschaftliche Verlagsgesellschaft.

Carney, J. N. (1972). *The geology of the area to the east of Lake Baringo, Rift Valley Province, Kenya* [PhD thesis, unpublished]. University of London.

CDE, University of Bern, Switzerland. Retrieved from https://www.arcgis.com/apps/Cascade/index.html?appid=ea0d2abd26a64ad18dca60a9e514b457. Retrieved on 1 March 2021.

Cerling, T. E., Pederson, B. L., & Damm, K. L. V. (1989). *Sodium-calcium ion exchange in the weathering of shales: Implications for global weathering budgets.* J. Geol. 17(6), 552–554. doi 10.1130/0091-7613(1989)017<0552:SCIEIT>2.3.CO;2

Ceryan, S. (2012). *Weathering Indices for Assessment of Weathering Effect and Classification of Weathered Rocks: A Case Study from NE Turkey.* In I. A. Dar (Ed.), Earth sciences. IntechOpen. doi 10.5772/25740

CETRAD Center for Training and Integrated research in ASAL Development (2016). *CETRAD* data, cited with permission (Unpublished).

CETRAD Center for Training and Integrated research in ASAL Development (2005). *Upper Ewaso Ngiro River Basin Water Management Information Platform*. Survey on Development Priorities, Information Needs and Conflict Management Efforts. doi 10.7892/boris.71791

Charsley, T. J. (1984). *Notes on the geology of the Rumuruti area* (No. 106/1). Rep. Mines & Geol. Dept. Kenya, unpublished.

Chen, L., Hu, W., Zhu, L., Feng, Y., Min, Y., & Liu, L. (2019). *Study on Permeability Characteristics of Granites with Different Degrees of Weathering.* IOP Conf. Ser.: Earth Environ. Sci. 300, 022160. doi 10.1088/1755-1315/300/2/022160

Chilton, P. J., & Foster, S. (1995). *Hydrogeological Characterisation And Water-Supply Potential Of Basement Aquifers In Tropical Africa.* Hydrogeol. J. 3(1), 36–49. doi 10.1007/s100400050061

Chilton, P. J., & Foster, S. (1994). *Hydrogeological Characterisation And Water-Supply Potential Of Basement Aquifers In Tropical Africa.* Hydrogeol. J. 3, 36–49. doi 10.1007/s100400050061

Chilton, P. J., & Smith-Carington, A. K. (1984). *Characteristics of the weathered basement aquifer in Malawi in relation to rural water supplies.* In proceedings of the Harare Symposium,

Challenges in African Hydrology and Water Resources, July 1984 (p. 16). IAHS Pub no. 144.

Chittleborough, D. J. (1991). *Indices of weathering for soils and palaeosols formed on silicate rocks. Aust. J. Earth Sci.* 38(1), 115–120.

Choubert, G., & Faure-Muret, A. (1990). *Carte Geologique Internationale de l'Afrique.* Commission for the geological map of the world [Map]. CCGM & UNESCO.

Chung, J.Y., Yu, S.D., & Hong, Y.-S. (2014). *Environmental Source of Arsenic Exposure.* J. Prev. Med. Pub. Health 47(5), 253–257. doi 10.3961/jpmph.14.036

Clark, I. (2015). *Groundwater Geoctardistry and Isotopes.* CRC Press.

Clark, I., & Fritz, P. (1997). *Environmental Isotopes in Hydrogeology.* CRC Press.

Collins, B., McArthur, J. V., & Sharitz, R. R. (2004). *Plant effects on microbial assemblages and remediation of acidic coal pile runoff in mesocosm treatment wetlands.* Ecol. Eng. 23(2), 107–115. doi 10.1016/j.ecoleng.2004.07.005

Condie, K. C. (1998). *Episodic continental growth and supercontinents: A mantle avalanche connection?* Earth Planet. Sci. Lett. 163(1–4), 97–108. doi 10.1016/S0012-821X(98)00178-2

Cook, P.G. Herczeg Al. (eds) (2000). Environmental Tracers in Subsurface Hydrology. Springer US

Cook, H. E., Johnson, P. D., Matti, J. C., & Zemmels, I. (1975). *Methods of Sample Preparation and X-Ray Diffraction Data Analysis, X-Ray Mineralogy Laboratory, Deep Sea Drilling Project.* In Initial Reports of the Deep Sea Drilling Project, 28. US Government Printing Office. University of California, Riverside, 999–1007.

Craig, H. (1961). *Isotopic Variations in Meteoric Waters. Science* 133(3465), 1702–1703. doi 10.1126/science.133.3465.1702

Crawford, J., Hughes, C. E., & Lykoudis, S. (2014). *Alternative least squares methods for determining the meteoric water line, demonstrated using GNIP data.* J. Hydrol. 519, 2331–2340. doi 10.1016/j.jhydrol.2014.10.033

Dansgaard, W. (1964). *Stable isotopes in precipitation.* Tellus 16(4), 436–468. doi 10.3402/tellusa.v16i4.8993

Darling, W. G., Edmunds, W. M., Kinniburgh, D. G., & Kotoub, S. (1987). *Sources of Recharge to the Basal Nubian Sandstone Aquifer, Butana Region, Sudan.* IAEA: Vienna, 205–224.

Das, B. K., & Kaur, P. (2001). *Major ion chemistry of Renuka Lake and weathering processes, Sirmaur District, Himachal Pradesh, India.* Env. Geol. 40(7), 908–917. doi 10.1007/s002540100268

Datta, P. S., & Tyagi, S. K. (1996). *Major ion chemistry of groundwater in Delhi area: Chemical weathering processes and groundwater flow regime.* J. Geol. Soc. India 47, 179–188.

Davis, S. N., & Turk, L. J. (1964). *Optimum Depth of Wells in Crystalline Rocks.* Groundwater 2(2), 6–11. doi 10.1111/j.1745-6584.1964.tb01750.x

DeBusk, W. (1999). *Nitrogen Cycling in Wetlands* [Fact Sheet of the Soil and Water Science Department No. SL171]. World Health Organization (WHO).

Dijkshoorn, J. A. (Creator) (2007). *Soil and terrain database for Kenya (KENSOTER)*, version 2.0. ISRIC - World Soil Information.

Dirks, P., Blenkinsop, T. G., & Jelsma, H. A. (2009). *The Geological Evolution Of Africa.* In: Geology- Vol. IV. EOLSS Publications.

Dixon, A. B., & Wood, A. P. (2003). *Wetland cultivation and hydrological management in eastern Africa: Matching community and hydrological needs through sustainable wetland use.* Nat. Resour. Forum 27(2), 117–129. doi 10.1111/1477-8947.00047

Dixon, J. B., & Weed, S. B. (1989). *Minerals in Soil Environments*, 2nd edn. Vol. 1. SSSA Book Series. Soil Science Society of America, Inc.

Domenico, P. A., & Schwartz, F. W. (1998). *Physical and Chemical Hydrogeology*, 2nd edn. Wiley.

Drever, J. I., & Clow, D. W. (1995). *Weathering rates in catchments.* In A.F. White & S. L. Brantley (Eds.), Chemical Weathering Rates of Silicate Minerals, Vol. 31 (pp. 465–483). Min. Soc. of America. https://ci.nii.ac.jp/naid/10008768309/

Du Laing, G., Rinklebe, J., Vandecasteele, B., Meers, E., & Tack, F. M. G. (2009). *Trace metal behaviour in estuarine and riverine floodplain soils and sediments: A review.* Drever, Sci. Total Environ. 407(13), 3972–3985. doi 10.1016/j.scitotenv.2008.07.025

Earth Scope Geo-Hydro Services (ESGHS) (2012). *Shivas Farm Limited. Melwa Area, Laikipia West District*. Lr No. Marmanet/Melwa Block 1/ 2949 (Muhotetu) [Hydrogeological Assessment Report]. Consultant: Sebestian Namwamba.

Eggleton, R. A. (2001). *The regolith glossary: Surficial geology, soils, and landscapes.* Cooperative Research Centre for Landscape Evolution and Mineral Exploration.

Engle, M. A., Gallo, M., Schroeder, K. T., Geboy, N. J., & Zupancic, J. W. (2014). *Three-way compositional analysis of water quality monitoring data.* Environ. Ecol. Stat. 21(3), 565–581. doi 10.1007/s10651-013-0268-x

EPA (United States Environmental Protection Agency) (2008). *Methods for Evaluating Wetland Condition: Wetland Hydrology.* Office of Water, U.S. Environmental Protection Agency, Washington, DC.

Evanson, C., Njuguna, C., Kiteme, B., & Peter, E. (2014). *Sub Catchment Directory For Upper Ewaso Ngiro River Basin* (Revised). CETRAD.

Fanning, D. S., Keramidas, V. Z., & El-Desoky, M. A. (1989). *Micas.* In Minerals in Soil Environments, Vol. 1, 2nd edn. (pp. 551–634). Soil Science Society of America, Inc.

https://dl.sciencesocieties.org/publications/books/abstracts/sssabookseries/mineralsinsoile/551

FAO (Food and Agriculture Organization of the United Nations) (2019a). SOFI 2019—The State of Food Security and Nutrition in the World. Retrieved from http://www.fao.org/state-of-food-security-nutrition/en/. Retrieved on 8 December 2019.

FAO (Food and Agriculture Organization of the United Nations) (2019b). *Kenya at a glance*. FAO in Kenya. Retrieved from http://www.fao.org/kenya/fao-in-kenya/kenya-at-a-glance/en/

FAO (Food and Agriculture Organization of the United Nations) (2017). *Water for Sustainable Food and Agriculture.* A report produced for the G20 Presidency of Germany.

FAO (Food and Agriculture Organization of the United Nations) (2012). *FAO STAT.* Retrieved from http://www.fao.org/countryprofiles/index/en/

Farnham, I. M, Johannesson, K. H., Singh, A. K., Hodge, V. F., & Stetzenbach, K. J. (2003). *Factor analytical approaches for evaluating groundwater trace element chemistry data.* Anal. Chim. Acta. 490(1), 123–138. doi 10.1016/S0003-2670(03)00350-7

Farnham, I.M, Singh, A. K., Stetzenbach, K. J., & Johannesson, K. H. (2002). *Treatment of nondetects in multivariate analysis of groundwater geochemistry data.* Chemom. Intell. Lab. Syst. 60(1–2), 265–281. doi 10.1016/S0169-7439(01)00201-5

Fass, T. (2004). *Hydrogeologie im Aguima Einzugsgebiet in Benin/Westafrika* [PhD thesis]. University of Bonn.

Faulkner, S. P., & Richardson, C. J. (1989). *Physical and chemical characteristics of freshwater wetland soils.* In Hammer, D.A. (Ed.), Constructed wetlands for wastewater treatment, municipal, industrial, and agricultural. Lewis Publishers, Boca Raton.

Fedo, C. M., Nesbitt, H. W., & Young, G. M. (1995). *Unraveling the effects of potassium metasomatism in sedimentary rocks and paleosols, with implications for paleoweathering conditions and provenance.* J. Geol. 23(10), 921–924. doi 10.1130/0091-7613(1995)023<0921:UTEOPM>2.3.CO;2

Finlayson, C. M., Stevenson, N. J., Davidson (Eds.). (2001). *Wetland inventory, assessment and monitoring: practical techniques and identification of major issues.* In proceedings of Workshop 4, 2nd International Conference on Wetlands and Development, Dakar, Senegal, 8–14 November 1998. Darwin, Supervising Scientist Report 161. (pp. 11–22)

Fisher, J., & Acreman, M. C. (2004). *Wetland nutrient removal: A review of the evidence.* Hydrol. Earth Syst. Sci. 8(4), 673–685. doi 10.5194/hess-8-673-2004

Fisher, R. S., & Mullican, I., William F. (1997). *Hydrochemical Evolution of Sodium-Sulfate and Sodium-Chloride Groundwater Beneath the Northern Chihuahuan Desert, Trans-Pecos, Texas, USA.* Hydrogeol. J. 5(2), 4–16. doi 10.1007/s100400050102

Foster, S. S. D. (1988). *Quantification of groundwater recharge in arid regions: A practical view for resource development and management.* In I. Simmers (Ed.), Estimation of Natural Groundwater Recharge (pp. 323–338). D. Reidel Publishing Company.

Frankenberger. (1994). *Selenium in the Environment.* CRC Press.

Freeze, R. A., & Cherry, J. A. (1979). *Groundwater.* Englewood Cliffs, NJ, Prentice Hall.

Friedman, I., Redfield, A. C., Schoen, B., & Harris, J. (1964). *The variation of the deuterium content of natural waters in the hydrologic cycle.* Rev. Geophys. 2(1), 177–224. doi 10.1029/RG002i001p00177

Fritz, H., Abdelsalam, M., Ali, K. A., Bingen, B., Collins, A. S., Fowler, A. R., Ghebreab, W., Hauzenberger, C. A., Johnson, P. R., Kusky, T. M., Macey, P., Muhongo, S., Stern, R. J., & Viola, G. (2013). *Orogen styles in the East African Orogen: A review of the Neoproterozoic to Cambrian tectonic evolution.* J. Afr. Earth. Sci. 86, 65–106. doi 10.1016/j.jafrearsci.2013.06.004

Gaciri, S. J., & Davies, T. C. (1993). *The occurrence and geochemistry of fluoride in some natural waters of Kenya.* J. Hydrol. 143(3), 395–412. doi10.1016/0022-1694(93)90201-J

Gat, J. R. (1971). *Comments on the Stable Isotope Method in Regional Groundwater Investigations.* Water Resour. Res. 7(4), 980–993. doi 10.1029/WR007i004p00980

Geolink Associates. (2010). *AAA Growers Limited—Rumuruti* [Groundwater Resources Investigation Report].

Gersberg, R. M., Elkins, B. V., & Goldman, C. R. (1983). *Nitrogen removal in artificial wetlands.* Water Res. 17(9), 1009–1014. doi 10.1016/0043-1354(83)90041-6

Gibson, J. J., Birks, S. J., & Edwards, T. W. D. (2008). *Global prediction of δ_A and $\delta_2 H$- $\delta_{18} O$ evaporation slopes for lakes and soil water accounting for seasonality: Predicting evaporation line slopes.* Global Biogeochem. Cy. 22(2). doi 10.1029/2007GB002997

Gichuki, F. N. (2002). Water Scarcity and Conflicts: *A Case Study of the Upper Ewaso Ng'iro North Basin.* In H. G. Blank, C. M. Mutero, & H. Murray-Rust (Eds.), The changing face of irrigation in Kenya: Opportunities for anticipating changes in eastern and southern Africa, (pp. 113–134). International Water Management Institute.

Gichuki, N., Oyieke, H., & Ndiritu, G. (2001). *Assessment and monitoring of wetlands for conservation and development in dry lands: A case study of Kajiado District, Kenya* [Supervising Scientists Report 161]. Department of Environment and Heritage Darwin, Australia.

Gilvear, D. J., & Bradley, C. (2000). *Hydrological monitoring and surveillance for wetland conservation and management; a UK perspective.* Phys Chem Earth, Part B: Hydrology, Oceans and Atmosphere, 25(7–8), 571–588. doi.org 10.1016/S1464-1909(00)00068-X

Gilvear, D. J., Andrews, R., Tellam, J. H., Lloyd, J. W., & Lerner, D. N. (1993). *Quantification of the water balance and hydrogeological processes in the vicinity of a small groundwater-fed wetland, East Anglia,* UK. J. Hydrol. 144(1–4), 311–334. doi 10.1016/0022-1694(93)90178-C

Gleick, P. H. (1994). *Water, War & Peace in the Middle East.* Environ. Sci. Policy *for Sustainable Development*. 36(3), 6–42. doi 10.1080/00139157.1994.9929154

GlobE - Wetlands. (2014). *Wetlands in East Africa: Reconciling future food production with environmental protection- Annual progress report 2014*.

Godfray, H. C. J., Beddington, J. R., Crute, I. R., Haddad, L., Lawrence, D., Muir, J. F., Pretty, J., Robinson, S., Thomas, S. M., & Toulmin, C. (2010). *Food Security: The Challenge of Feeding 9 Billion People.* Science 327(5967), 812–818. doi 10.1126/science.1185383

GoK (Government of Kenya) (1994). *District Development plan, Laikipia District.* Government Press.

GoK (Government of Kenya) (1983). *Arid and Semi-arid Lands Branch Laikipia District – A Pre-investment Study of Human and Natural Resources,* Vol. 3. Ministry of Agriculture.

Golden, M. (1978). *The geology of the area east of Silale. Rift Valley Province, Kenya* [PhD thesis, unpublished]. University of London.

Goldich, S. S. (1983). *A study in rock-weathering.* J. Geol. 46, 17–58. doi 10.1086/624619

Gonfiantini, R. (1978). *Standards for stable isotope measurements in natural compounds.* Nature271(5645), 534. doi 10.1038/271534a0

Gounot, A.-M. (1994). *Microbial oxidation and reduction of manganese: Consequences in groundwater and applications.* FEMS Microbiol. Rev. 14(4), 339–349. doi 10.1111/j.1574-6976.1994.tb00108.x

Gour, D., Soumendu, C., & Nilanjana, D. C. (2014). *Weathering and Mineralogical Alteration of Granitic Rocks in Southern Purulia District, West Bengal, India.* Int. Res.J. Earth Sci. 2(4), 1–12.

Grannemann, N. G., & Sharp, J. M. (1979). *Alluvial hydrogeology of the lower Missouri River valley.* J. Hydrol., 40(1), 85–99. doi 10.1016/0022-1694(79)90089-1

Greenway, M. (2005). *The Role of Constructed Wetlands in Secondary Effluent Treatment and Water Reuse in Subtropical and Arid Australia*. Ecol. Eng. 25, 501–509. doi 10.1016/j.ecoleng.2005.07.008

Griffiths, P. S. (1977). *The geology of the area around Lake Hannington and the Perkerra River, Rift Valley Province, Kenya* [PhD thesis]. University of London.

Groundwater Survey (1988). *Ol Maisor Ranch* [Hydrogeological Investigation].

Guan, H., Hutson, J., Ding, Z., Love, A., Simmons, C., & Deng, Z. (Rose). (2013). *Principal component analysis of watershed hydrochemical response to forest clearance and its usefulness for chloride mass balance applications.* Water Resour. Res. 49. doi 10.1002/wrcr.20357

Gubanov, A. P., & Mooney, W. D. (2009). *New Global Geological Maps of Crustal Basement Age.* AGU Fall Meeting Abstracts, 53, T53B-1583.

Güler, C., Thyne, G. D., McCray, J. E., & Turner, K. A. (2002). *Evaluation of graphical and multivariate statistical methods for classification of water chemistry data.* Hydrogeol. J. 10(4), 455–474. doi 10.1007/s10040-002-0196-6

Guntenspergen, G. R., Peterson, S. A., Leibowitz, S. G., & Cowardin, L. M. (2002). *Indicators of Wetland Condition for the Prairie Pothole Region of the United States.* Environ Monit. Assess. 78(3), 229–252. doi 10.1023/A:1019982818231

Hackman, B. (1988). *Geology of the Baringo—Laikipia area* [Report No. 104]. Ministry of Environment and Mineral Resources.

Hackman, B. (1986). *The Sukuta Magie area* [Geological Map]. Kenya Mines & Geol. Dep. archives (unpublished).

Hahn-Weinheimer, P., Hirner, A., & Weber-Diefenbach, K. (1995). Röntgenfluoreszenzanalytische Methoden: *Grundlagen und praktische Anwendung in den Geo-, Material- und Umweltwissenschaften*, 2nd edn. Springer-Verlag. doi 10.1007/978-3-642-57848-9

Hamill, L., and Bell, F. U., (1986). *Groundwater Resources Development.* Britain Library Cataloguing in Publication Data London. pp. 151-158.

Hammer, D. A. (1989). *Constructed Wetlands for Wastewater Treatment: Municipal, Industrial and Agricultural.* CRC Press.

Harrington, G. A., Cook, P. G., & Herczeg, A. L. (2002). *Spatial and Temporal Variability of Groundwater Recharge in Central Australia: A Tracer Approach.* Groundwater 40(5), 518–527. doi 10.1111/j.1745-6584.2002.tb02536.x

Havens, K. E., Sharfstein, B., Rodusky, A. J., & East, T. L. (2004). *Phosphorus accumulation in the littoral zone of a subtropical lake.* Hydrobiologia 517(1), 15–24. doi 10.1023/B:HYDR.0000027334.05589.29

Hayashi, M., & Rosenberry, D. O. (2002). *Effects of Groundwater Exchange on the Hydrology and Ecology of Surface Water.* Groundwater 40(3), 309–316. doi 10.1111/j.1745-6584.2002.tb02659.x

Hazell, J. R. T., Cratchley, C. R., & Jones, C. R. C. (1992). *The hydrogeology of crystalline aquifers in northern Nigeria and geophysical techniques used in their exploration.* Geol. Soc. Spec. Publ. London 66(1), 155–182. doi 10.1144/GSL.SP.1992.066.01.08

Hebert, R., Barker, J. A., & Kitching, R. (1992). *New approaches to pumping test interpretation for dug wells constructed on hard rock aquifers.* Hydrogeology of Crystalline Basement Aquifers in Africa, Geol. Soc. Spec. Publ. London 1(66), 221–242.

Heinichen, G. (2015). *Water use related conflicts and resource management around a small wetland in central Kenya (Ewaso Narok, Laikipia)* [Masters Thesis, unpublished]. University of Cologne, Germany.

Heiri, O., Lotter, A. F., & Lemcke, G. (2001). *Loss on ignition as a method for estimating organic and carbonate content in sediments: Reproducibility and comparability of results.* J. Paleolimnol. 25(1), 101–110. doi 10.1023/A:1008119611481

Heiss, L. (2016). *The alluvium of the Namulonge wetland (Uganda), its contribution to subsurface water dynamics and composition* [Masters Thesis, unpublished]. Bonn University, Germany.

Heller, P. L., Beland, P. E., Humphrey, N. F., Konrad, S. K., Lynds, R. M., McMillan, M. E., Valentine, K. E., Widman, Y. A., & Furbish, D. J. (2001). *Paradox of downstream fining and weathering-rind formation in the lower Hoh River, Olympic Peninsula, Washington.* J. Geol. 29(11), 971–974. doi 10.1130/0091-7613(2001)029<0971:PODFAW>2.0.CO;2

Hem, J. D. (1985). *Study and Interpretation of the Chemical Characteristics of Natural Water,* 3rd edn. [US Geological Survey Water-Supply Paper 2254]. University of Virginia, Charlottesville. p. 263

Hemond, H. F., & Benoit, J. (1988). *Cumulative impacts on water quality functions of wetlands.* J. Environ. Manage. 12(5), 639–653. doi 10.1007/BF01867542

Hinkle, S. R., Duff, J. H., Triska, F. J., Laenen, A., Gates, E. B., Bencala, K. E., Wentz, D. A., & Silva, S. R. (2001). *Linking hyporheic flow and nitrogen cycling near the Willamette River: A large river in Oregon, USA.* J. Hydrol. 244(3–4), 157180. doi 10.1016/S0022-1694(01)00335-3

Hinsbergen, D. V., Buiter, S. H., Torsvik, T. H., Gaina, C., & Webb, S. J. (2011). *The formation and evolution of Africa from the Archaean to Present: Introduction.* Geol. Soc. Spec. Publ. 357(1), 1–8. doi 10.1144/SP357.1

Hogan, D. M., Jordan, T. E., & Walbridge, M. R. (2004). *Phosphorus retention and soil organic carbon in restored and natural freshwater wetlands.* Wetlands 24(3), 573–585. doi 10.1672/0277-5212(2004)024[0573:PRASOC]2.0.CO;2

Hollands, G. G. (1987). *Assessing the Relationship of Groundwater and Wetlands.* In J. A. Kusler and G. Brooks (Eds.) Wetland Hydrology. Proceeding of the National Wetland Symposium, (pp. 161–185). OMNIPRESS, The Proceedings Printer.

Hounslow, A. (2018). *Water Quality Data: Analysis and Interpretation.* CRC Press. doi 10.1201/9780203734117

Hughes, F. M. R. (1997). *Floodplain biogeomorphology.* Prog. Phys. Geogr.: Earth Environ. 21(4), 501–529. doi 10.1177/030913339702100402

Hunt, R. J., Krabbenhoft, D. P., & Anderson, M. P. (1996). *Groundwater Inflow Measurements in Wetland Systems.* Water Resour. Res. 32(3), 495–507. doi 10.1029/95WR03724

Hütter, L. A. (1994). *Wasser und Wasseruntersuchung: Methodik, Theorie und Praxis chemischer, chemisch-physikalischer, biologischer und bakteriologischer Untersuchungsverfahren*, 6. Aktual. Salle.

Ingersoll, T. L., & Baker, L. A. (1998). *Nitrate removal in wetland microcosms.* Water Res. 32(3), 677–684. doi 10.1016/S0043-1354(97)00254-6

Isaac, R. A., & Kerber, J. D. (2015). *Atomic Absorption and Flame Photometry: Techniques and Uses in Soil, Plant, and Water Analysis.* In L. M. Walsh (Ed.), Instrumental Methods for Analysis of Soils and Plant Tissue (pp. 17–37). SSSA. doi 10.2136/1971.instrumentalmethods.c2

Ismadji, S., Soetaredjo, F. E., & Ayucitra, A. (2015). *Clay Materials for Environmental Remediation.* Springer.

Johnsson, M. J., & Meade, R. H. (1990). *Chemical weathering of fluvial sediments during alluvial storage; the Macuapanim Island point bar, Solimoes River, Brazil.* J. Sediment. Res. 60(6), 827–842. doi 10.1306/212F9296-2B24-11D7-8648000102C1865D

Johnston, C. A. (1991). *Sediment and nutrient retention by freshwater wetlands: Effects on surface water quality.* Crit. Rev. Environ. Control 21(5–6), 491–565. doi 10.1080/10643389109388425

Jones, A., Breuning-Madsen, H., Brossard, M., Dampha, A., Deckers, J., Dewitte, O., Gallali, T., Hallett, S., Jones, R., Kilasara, M., Le Roux, P., Micheli, E., Montanarella, L., Spaargaren, O., Thiombiano, L., Van Ranst, E., Yemefack, M. , Zougmoré R., (eds.), *2013, Soil Atlas of Africa*. European Commission, Publications Office of the European Union, Luxembourg. 176 pp.

Joshi, D. M., Kumar, A., & Agrawal, N. (2009). *Assessment of the irrigation water quality of River Gana in Hairdwar District.* Rasayan J. Chem. 2, 285–292.

Judd, A. G. (1980). *The Use of Cluster Analysis in the Derivation of Geotechnical Classifications.* Environ. Eng. Geosci. 4, 193–211. doi 10.2113/gseegeosci.xvii.4.193

Jung, M., Burt, T. P., & Bates, P. D. (2004). *Toward a conceptual model of floodplain water table response: Floodplain Water Table Response.* Water Resour. Res. 40(12), W12409. doi 10.1029/2003WR002619

Junk, W. J., & Welcomme, R. L. (1990). *Floodplains.* In B. Patten & et. al. (Eds.), Wetlands and shallow continental water bodies, Vol. 1, (pp. 491–524) SPB Academic Publishing.

Kadlec, R. H., Wallace, S., & Wallace, S. (2008). *Treatment Wetlands.* CRC Press. doi 10.1201/9781420012514

Kaplan, D., Muñoz-Carpena, R., & Ritter, A. (2010). *Untangling complex shallow groundwater dynamics in the floodplain wetlands of a southeastern U.S. coastal river.* Water Resour. Res. 46(8). doi 10.1029/2009WR009038

Katz, B. G., Coplen, T. B., Bullen, T. D., & Davis, J. H. (1997). *Use of Chemical and Isotopic Tracers to Characterize the Interactions Between Groundwater and Surface Water in Mantled Karst.* Groundwater 35(6), 1014–1028. doi 10.1111/j.1745-6584.1997.tb00174.x

Kautz, C. Q., & Martin, C. E. (2007). *Chemical and physical weathering in New Zealand's Southern Alps monitored by bedload sediment major element composition.* Appl. Geochem. Metal interactions with natural organic matter and Watershed-scale geochemistry, 22(8), 1715–1735. doi 10.1016/j.apgeochem.2007.03.031

Kazimierz, R., Froehlich, K., & Mook, W. (2000). *Environmental Isotopes in the Hydrological, Principles and Applications*, Vol. 3. IAEE and UNESCO.

KEBS (Kenya Bureau of Standards) (2015). *Potable water—Specification. Kenya Standards* [EAS 12: 2014 ICS 13.060.20], 1st edn.

Key, R. M. (1992). *An introduction to the crystalline basement of Africa.* Hydrogeology of Crystalline Basement Aquifers in Africa from Wright, E.P. & Burgess W. G. Geol. Soc. Spec. Publ. 66, 29–57.

Key, R. M. (1987). *The geology of the Maralal Area* (No. 105; p. 93). Rep. Mines & Geol. Dep. Kenya.

Khan, S., Ahmad, I., Shah, M. T., Rehman, S., & Khaliq, A. (2009). *Use of constructed wetland for the removal of heavy metals from industrial wastewater.* J. Environ. Manage. 90(11), 3451–3457. doi 10.1016/j.jenvman.2009.05.026

Kibson Consult. (n.d.). AAA Growers Ltd.

Kibson Consult. (2014). *Ewaso Narok River for Shiva Farm Ltd. Farm A/Farm B* [Hydrogeological Assessment Report]. Ewaso Narok Water Management Unit. Compiled by: James K. Waititu, Nairobi, Kenya.

King, A. C., Raiber, M., & Cox, M. E. (2014). *Multivariate statistical analysis of hydrochemical data to assess alluvial aquifer–stream connectivity during drought and flood: Cressbrook Creek, southeast Queensland, Australia.* Hydrogeol. J. 22(2), 481–500. doi 10.1007/s10040-013-1057-1

King, B. C., Chapman, G. R., Robson, D. A., & McConnell, R. B. (1972). *Volcanism of the Kenya Rift Valley [and Discussion]*. Philos. Trans. Royal Soc. A PHILOS T R SOC A, 271(1213), 185–208.

KNBS (Kenya National Bureau of Statistics) (2019). *Population Projections.* Retrieved from https://www.knbs.or.ke/download/population-projections/

Koeniger, P., & Leibundgut, C. (2001). *Study of River Water Impacts on Groundwater during Flood Events in a Dry Flood Plain on the Upper Rhine Valley.* In Griebler C, Danielopol DL, Gibert J,Nachtnebel HP, Notenboom J (Eds.) Groundwater Ecology. Office for official publications of European Communities, Luxembourg. 369–374.

Kohler, T. (1987). *Land-use in Transition; Aspects and problems of small scale farming in a new environment; the example of Laikipia District, Kenya.* ASS.

Kovalevsky, V. S., Rushton, K. R., & Kruseman, G. P. (2004). *Groundwater studies: An international guide for hydrogeological investigations.* UNESCO.

Krause, S., Bronstert, A., & Zehe, E. (2007). *Groundwater–surface water interactions in a North German lowland floodplain – Implications for the river discharge dynamics and riparian water balance.* J. Hydrol. 347(3), 404–417. doi 10.1016/j.jhydrol.2007.09.028

Krauskopf, K. (1967). *Introduction to geochemistry*, 1st edn. McGraw-Hill.

Krauskopf, K. & Bird, D. (1995). *Introduction to geochemistry*, 3rd edn. McGraw-Hill.

Kresic, N. (2006). *Hydrogeology and Groundwater Modeling*, 2nd edn. CRC Press.

Kroner, A. (1977). *Precambrian mobile belts of southern and eastern Africa- ancient sutures or sites of ensialic mobility? A case for crustal evolution towards plate tectonics.* Tectonophysics 40(1–2), 101–135. doi 10.1016/0040-1951(77)90031-2

Kulkarni, H., Deolankar, S., Lalwani, A., Joseph, B., & Pawar, S. (2000). *Hydrogeological framework of the Deccan basalt groundwater systems, west-central India.* Hydrogeol. J. 8, 368–378. doi 10.1007/s100400000079

Kumar, C. P. (2014). *Groundwater data requirement and analysis.* GRIN Publishing.

Kyalo, Willy D. (2016): *Unpublished dataset*.

Lachassagne, P., Dewandel B., WYNS, R. (2021). *Groundwater in granitic and metamorphic rocks?*. Encyclopedia of the Environment. https://www.encyclopedie-environnement.org/en/water/groundwater-in-granitic-and-metamorphic-rocks/.

Lambs, L. (2004). *Interactions between groundwater and surface water at river banks and the confluence of rivers.* J. Hydrol. 288(3–4), 312–326. doi 10.1016/j.jhydrol.2003.10.013

Lamontagne, S., W. Leaney, F., & L. Herczeg, A. (2005). *Groundwater-surface water interactions in a large semi-arid floodplain: Implications for salinity management.* Hydrol. Processes 19(16), 3063–3080. doi 10.1002/hyp.5832

Langguth, H.R., & Voigt, R. (2004). *Hydrogeologische Methoden.* Sp

Larson, J. S. (2009). *Introduction – Methodologies for Wetland Assessment.* In The Wetlands Handbook (pp. 465–485). John Wiley & Sons, Ltd. doi 10.1002/9781444315813.ch21

Le Bas, M. J. (1971). *Per-alkaline Volcanism, Crustal Swelling, and Rifting.* Nature 230, 85–87. doi 10.1038/physci230085a0

Leemhuis, C., Amler, E., Diekkrüger, B., Gabiri, G., & Näschen, K. (2016). *East African wetland-catchment data base for sustainable wetland management.* Proc. Int. Assoc. Hydrol. Sci. 374, 123–128. doi 10.5194/piahs-374-123-2016

Liang, Z., Chen, J., Jiang, T., Li, K., Gao, L., Wang, Z., Li, S., & Xie, Z. (2018). *Identification of the dominant hydrogeochemical processes and characterization of potential contaminants in groundwater in Qingyuan, China, by multivariate statistical analysis*. RSC Advances 8(58), 33243–33255. doi 10.1039/C8RA06051G

Lin, Y.-F., Jing, S.-R., Wang, T.-W., & Lee, D.-Y. (2002). *Effects of macrophytes and external carbon sources on nitrate removal from groundwater in constructed wetlands.* Environ. Pollut. 119(3), 413–420. doi 10.1016/S0269-7491(01)00299-8

Lind, E. M., Morrison, M. E. S., & Hamilton, A. C. (1974). *East African vegetation.* Longman.

Lovley, D. R. (1991). *Dissimilatory Fe(III) and Mn(IV) reduction.* Microbiol. Mol. Biol. Rev. 55(2), 259–287.

LWF (Laikipia Wildlife Forum), KENWEB (Kenya Wetlands Biodiversity Research Team), NMK (National Museum of Kenya). (2013). *A Water Conservation Strategy for Laikipia County (2014-2018)*, 1st edn. Nanyuki, Kenya.

Macdonald, R. (2002). *Magmatism of the Kenya Rift Valley: A review.* Earth Environ. Sci. Trans. R. Soc. Edinburgh 93, 239–253. doi 10.1017/S0263593300000420

Machefert, S. E., & Dise, N. B. (2004). *Hydrological controls on denitrification in riparian ecosystems.* Hydrol. Earth Syst. Sci. 8(4), 686–694. doi 10.5194/hess-8-686-2004

Mageto, O. B. (2011). *Structural and geological control of fluoride levels in groundwater and deflouridation in Elemntaita, Nakuru County, Kenya* [BSc]. University of Nairobi.

Maitre, R. W. L., Streckeisen, A., Zanettin, B., Bas, M. J. L., Bonin, B., & Bateman, P. (2002). *Igneous Rocks: A Classification and Glossary of Terms: Recommendations of the International Union of Geological Sciences Subcommission on the Systematics of Igneous Rocks*, 2nd edn. Cambridge University Press.

Maltby, E., & Barker, T. (2009). *The wetlands handbook.* Wiley-Blackwell.

Marieta, M. W. (2007). *The distribution of fluoride ions in the groundwaters of the Baringo – Bogoria lake Basin* [Msc Thesis, unpublished]. Univeristy of Nairobi.

Margolis, L., & Chaouni, A. (2014). *Out of Water—Design Solutions for Arid Regions*. Birkhäuser.

Mathuva, J. M., MacOPiyo, L., Kironchi, J., & Thenya, T. (1997). *Pre-Drainage Environmental Impact Study (PDEIS) for Laikipia Wetlands, Laikipia District* [Technical Report]. University of Nairobi.

Maynard, J. B. (1992). *Chemistry of Modern Soils as a Guide to Interpreting Precambrian Paleosols.* J. Geol. 100(3), 279–289. doi 10.1086/629632

Mayo, A. L., & Loucks, M. D. (1995). *Solute and isotopic geochemistry and groundwater flow in the central Wasatch Range, Utah.* J. Hydrol. 172(1–4), 31–59. doi 10.1016/0022-1694(95)02748-E

Mays, P. A., & Edwards, G. S. (2001). *Comparison of Heavy Metal Accumulation in a Natural Wetland and Constructed Wetlands Receiving Acid Mine Drainage.* Ecol. Eng. 16, 487–500. doi 10.1016/S0925-8574(00)00112-9

McCall, G. J. H. (1967). *Geology of the Nakuru-Thomson's Falls-Lake Hannington Area* (No. 78; p. 122). Geological Survey of Kenya-Minsitry of Natural Resources.

McCartney, M.P. (2000). *The water budget of a headwater catchment containing a dambo.* Phys. Chem. Earth Part B Hydrol. Oceans Atmosphere 25(7): 611–616, doi 10.1016/S1464-1909(00)00073-3

McFarlane, M. J. (1992). *Groundwater movement and water chemistry associated with weathering profiles of the African surface in parts of Malawi.* In Hydrogeology of Crystalline Basement Aquifers in Africa from Wright, E.P. & Burgess W. G. Geol. Soc. London Spec. Publ. 66, 101–129

McLean, W., Jankowsk, J., & Lavitt, N. (2000). *Groundwater Quality and Sustainability in an Alluvial Aquifer, Australia.* In Sililo et al (Eds.) proc. XXX IAH congress on Groundwater: Past Achievements and Future Challenges. Cape Town South Africa 26th November-1st December. A.A. Balkema, Rotterdam, Brookfield. p 567–57

McLennan, S. M. (1993). *Weathering and Global Denudation.* J. Geol. 101(2), 295–303. doi 10.1086/648222

MEMR (Ministry of Environment and Natural Resources) (2012). *Kenya wetlands atlas.*

MEMR (Ministry of Environment and Natural Resources) (1987). *Baringo-Laikipia geological map, Degree square 35* [Map].

Mertes, L. A. K. (1997). *Documentation and significance of the perirheic zone on inundated floodplains.* Water Resour. Res. 33(7), 1749–1762. doi 10.1029/97WR00658

Meunier, A., Caner, L., Hubert, F., Albani, A. E., & Prêt, D. (2013). *The weathering intensity scale (WIS): An alternative approach of the Chemical Index of Alteration (CIA).* Am. J. Sci. 313(2), 113–143. doi 10.2475/02.2013.03

Meybeck, M. (1987). *Global chemical weathering of surficial rocks estimated from river dissolved loads.* Am. J. Sci. 287(5), 401–428. doi 10.2475/ajs.287.5.401

Middelburg, J. J., van der Weijden, C. H., & Woittiez, J. R. W. (1988). *Chemical processes affecting the mobility of major, minor and trace elements during weathering of granitic rocks.* Chem. Geol. 68(3–4), 253–273. doi 10.1016/0009-2541(88)90025-3

Ministry of Agriculture (1983). *Arid And Semi-Arid Lands Branch Laikipia District- A Pre-Investment Study of Human and Natural Resources.* Chapter 6—Soil and Water Management, Vol. 3. Isric Library. Wageningen Netherlands.

Mitsch, W. J., & Gosselink, J. G. (2000). *Wetlands*, 3rd edn. Jogn Wiley & Sons.

Mjengera, H. J., Mosha, H. J., & Mtalo, F. W. (1997). *Method of .excessive fluoride removal from potable water: A fluorosis preventive measure.* Tanzania Dent. J. 8.

MoEF (Ministry of Environment and Forestry) (2019). *Public notice of intention to declare Ewaso Narok Swamp in Laikipia County as a protected area.* Retrieved June 2019, from http://www.environment.go.ke/?p=5814

Montcoudiol, N., Molson, J., & Lemieux, J.-M. (2015). *Groundwater geochemistry of the Outaouais Region (Québec, Canada): A regional-scale study.* Hydrogeol. J. 23(2), 377–396. doi 10.1007/s10040-014-1190-5

Moore, D. M., & Reynolds, R. C. (1997). *X-Ray Diffraction and the Identification and Analysis of Clay Minerals.* Oxford University Press, 2nd edn.

Moore, D. S. (2008). *The basic practice of statistics*, 5th edn. Freeman.

Morgan, C. O., & Winner, M. D. Jr. (1962). *Hydrogeochemical facies in the "400-foot" and "600—Foot" sands of the Baton Rouge area, Louisiana* [US Geol. Surv. Prof. Paper 450–B].

Morris, D.A., and Johnson A.I., (1967). Summary of hydrologic and physical properties of rock and soil materials, as analyzed by the hydrologic laboratory of the U.S. Geological Survey, 1948-60 Water Supply Paper 1839-D. USGS Water Supply Paper: 1839-D.

Moser, H. (1998). *Environmental isotopes.* In Käss, W. Tracing Technique in Geohydrology. Balkema, Rotterdam.

Moser, H., & Stichler, W. (1970). *Deuterium Measurements on Snow Samples from the Alps.* Isotope Hydrology, IAEA, Vienna, 43–57.

Moya, C. E., Raiber, M., Taulis, M., & Cox, M. E. (2015). *Hydrochemical evolution and groundwater flow processes in the Galilee and Eromanga basins, Great Artesian Basin, Australia: A multivariate statistical approach.* Sci. Total Environ.508, 411–426. doi 10.1016/j.scitotenv.2014.11.099

Mungai, D. N., Ong, C. K., Kiteme, B., Elkaduwa, W., & Sakthivadivel, R. (2004). *Lessons from two long-term hydrological studies in Kenya and Sri Lanka.* Agric. Ecosyst. Environ 104(1), 135–143. doi 10.1016/j.agee.2004.01.011

Muriuki K, M. (2016). *Effects of human activities on wetland hydrology in Ewaso Narok Wetland, Laikipia County, Kenya* [Master's Thesis, unpublished]. Kenyatta University, Kenya.

Mutiga, J. K., Mavengano, S. T., Zhongbo, S., Woldai, T., & Becht, R. (2010). Water Allocation as a Planning Tool to Minimise Water Use Conflicts in the Upper Ewaso Ng'iro North Basin, Kenya. 24(14), 3939–3959. doi 10.1007/s11269-010-9641-9

Mwita, E., Menz, G., Misana, S., Becker, M., Kisanga, D., & Boehme, B. (2013). *Mapping small wetlands of Kenya and Tanzania using remote sensing techniques.* Int. J. Appl. Earth Obs. Geoinf. 21, 173–183. doi 10.1016/j.jag.2012.08.010

Nadew, G. A., & Tefera, Z. L. (2013). *Understanding the groundwater dynamics in the Southern Rift Valley Lakes Basin (Ethiopia): Multivariate statistical analysis method, oxygen ($\delta^{18}O$) and deuterium ($\delta^{2}H$).* J. Radioanal. Nucl. Chem. 297(3), 357–364. doi 10.1007/s10967-012-2357-y

Nahlik, A., & Mitsch, W. (2006). *Tropical Treatment Wetlands Dominated by Free-Floating Macrophytes for Water Quality Improvement in Costa Rica.* Ecol. Eng. 28, 246–257. doi10.1016/j.ecoleng.2006.07.006

Naiman, R. J., & Décamps, H. (1997). *The Ecology of Interfaces: Riparian Zones*. Annu. Rev. Ecol. Evol. Syst. 28(1), 621–658. doi 10.1146/annurev.ecolsys.28.1.621

Nair, K. R., & Manji, F. (1984). *The occurrence and distribution of fluoride in groundwaters of Kenya.* In proceedings of the Harare Symposium, Challenges in African Hydrology and Water Resources. 1AHS, 144, 12.

Naylor, D. V., & Overstreet, R. (1969). *Sodium-Calcium Exchange Behavior in Organic Soils 1*. Soil Sci. Soc. Am. J. 33(6), 848–851. doi 10.2136/sssaj1969.03615995003300060016x

Nesbitt, H. W., & Young, G. M. (1982). *Early Proterozoic climates and plate motions inferred from major element chemistry of lutites. Nature* 299(5885), 715–717. doi 10.1038/299715a0

Nesbitt, H. W., & Young, G. M. (1989). *Formation and Diagenesis of Weathering Profiles.* J. Geol. 97(2), 129–147. doi 10.1086/629290

Nesbitt, H. Wayne, Markovics, G., & price, R. C. (1980). *Chemical processes affecting alkalis and alkaline earths during continental weathering.* Geochim. Cosmochim. Acta. 44(11), 1659–1666. doi 10.1016/0016-7037(80)90218-5

Ngolo, P., Mildred, N., Machocho, A., & Oyieke, H. (2018). *Pesticides Use in Pest Management: A Case Study of Ewaso Narok Wetland Small-scale Vegetable Farmers, Laikipia County, Kenya.* J. Agric. Ecol. Res. Int. 14(2), 1–8. doi 10.9734/JAERI/2018/40143

Nichols, G. (2009). *Sedimentology and stratigraphy*, 2nd edn. Wiley-Blackwell.

Nilsson, C., & Berggren, K. (2000). *Alterations of Riparian Ecosystems Caused by River Regulation Dam operations have caused global-scale ecological changes in riparian ecosystems. How to protect river environments and human needs of rivers remains one of the most important questions of our time.* Biosci. J. 50(9), 783–792. doi 10.1641/0006-3568(2000)050[0783:AORECB]2.0.CO;2

Notter, B. (2003). *Rainfall-Runoff Modelling of Meso-Scale Catchments in the Upper Ewaso Ng'iro Basin, Kenya* [Diplomarbeit]. University of Bonn.

Nyarko, B. K., Essumang, D., Eghan, M. J., Reichert, B., van de Giesen, N., & Vlek, P. (2010). *Use of isotopes to study floodplain wetland and river flow interaction in the White Volta River basin, Ghana.* Isot. Environ. Health Stud. 46, 91–106. doi 10.1080/10256010903388543

Ó Dochartajgh, & Brighid, E. (2019). User Guide: Africa Groundwater Atlas Country Hydrogeology Maps [Open Report OR/19/035; Version 1, p. 21]. British Geological Survey. https://www.bgs.ac.uk/research/groundwater/international/africaGwAtlas.html

O'Connor, J. M., Jokat, W., Regelous, M., Kuiper, K. F., Miggins, D. P., & Koppers, A. P. (2019). Superplume mantle tracked isotopically the length of Africa from the Indian Ocean to the Red Sea. Nature Communications, *10*(1), 5493. https://doi.org/10.1038/s41467-019-13181-7

Omenda, P. A. (2007). *The Geothermal activity of the East African Rift.* Paper presented at Short Course II on surface Exploration for Geothermal Resources, organized by UNU-GTP and KenGen, at Lake Naivasha, Kenya, 2–17 November, 2007, 12.

Parker, A. (1970). *An Index of Weathering for Silicate Rocks*. In Geological Magazine, Vol. 107 (pp. 501–504). Cambridge University Press.

Paron, P., Olago, D. O., & Omuto, C. T. (2013). *Kenya: A Natural Outlook: Geo-Environmental Resources and Hazards*, Vol. 16. Newnes.

Patrick, W. H., & Khalid, R. (1974). *Phosphate Release and Sorption by Soils and Sediments: Effect of Aerobic and Anaerobic Conditions.* Science 186(4158), 53–55. doi 10.1126/science.186.4158.53

Pester, M., Knorr, K.-H., Friedrich, M. W., Wagner, M., & Loy, A. (2012). *Sulfate-Reducing Microorganisms in Wetlands – Fameless Actors in Carbon Cycling and Climate Change. Front Microbiol*. 3. doi 10.3389/fmicb.2012.00072

Petters, S. W. (1991). *Regional Geology of Africa*, Vol. 40. Springer-Verlag.

Pezeshki, S. R., & DeLaune, R. D. (2012). *Soil Oxidation-Reduction in Wetlands and Its Impact on Plant Functioning.* J. Biol. 1(2), 196–221. doi 10.3390/biology1020196

Pinder, G., & Gray, W. (1977). *Finite Element Simulation in Surface and Subsurface Hydrology*, 1st edn. Academic Press.

Piper, A.M. (1944). *A graphic procedure in the geochemical interpretation of water-analyses.* Papers, Hydrology, Transaction, AGU. 914-928

Price, J. R., & Velbel, M. A. (2003). *Chemical weathering indices applied to weathering profiles developed on heterogeneous felsic metamorphic parent rocks.* Chem. Geol. 202(3), 397–416. doi 10.1016/j.chemgeo.2002.11.001

Ransom, C., Rippberger, S., & Ritzenthaler, A. (2012). *Water Resource Management at the Mpala Conservancy, Laikipia District, Kenya* [Master's thesis]. University of Michigan.

Rassam, D. W., Pickett, T., & Knight, J. H. (2009). *Incorporating floodplain groundwater interactions in river modeling.* In: 18th World IMACS/MODSIM Congress, Cairns, Australia, 3-17 July, 3116–3122.

Reddy, K. R., & DeLaune, R. D. (2008). *Biogeochemistry of Wetlands: Science and Applications.* CRC Press.

Renaut, R. W., & Jones, B. (1997). *Controls on aragonite and calcite precipitation in hot spring travertines at Chemurkeu, Lake Bogoria, Kenya.* Can. J. Earth Sci. 34(6), 801–818. doi 10.1139/e17-066

Republic of Kenya Ministry of Water Development (1987). *Water Resources Assessment Study in Laikipia District.*

Richards, P. (1985). *Indigenous agricultural revolution: Ecology and food production in West Africa.* Westview Press.

Richardson, J. L., & Vepraskas, M. J. (2001). *Wetland soils: Genesis, hydrology, landscapes, and classification,* 1st edn. CRC Press, Taylor & Francis Group. doi 10.1201/9781420026238

Rietti-Shati, M., Yam, R., Karlen, W., & Shemesh, A. (2000). *Stable isotope composition of tropical high-altitude fresh-waters on Mt. Kenya, Equatorial East Africa.* Chem. Geol. 166(3–4), 341–350. doi 10.1016/S0009-2541(99)00233-8

Ronov, A. B. (1945). *Hydrogeology of the oarboniferons deposits of the Volga area.* Dokl. Acud. Sci. 48(5).

Rooney, T. O. (2017). *The Cenozoic magmatism of East-Africa: Part I — Flood basalts and pulsed magmatism*. Lithos, 286–287, 264–301. doi 10.1016/j.lithos.2017.05.014

Rossi, A. M., & Graham, R. C. (2010). *Weathering and Porosity Formation in Subsoil Granitic Clasts, Bishop Creek Moraines, California.* Soil Sci. Soc. Am. J. 74(1), 172–185. doi 10.2136/sssaj2009.0146

Rothfuss, Y., Merz, S., Vanderborght, J., Hermes, N., Weuthen, A., Pohlmeier, A., Vereecken, H., & Brüggemann, N. (2015). *Long-term and high-frequency non-destructive monitoring of water stable isotope profiles in an evaporating soil column.* Hydrol. Earth Syst. Sci. 19(10), 4067–4080. doi 10.5194/hess-19-4067-2015

Rovero, F., & Jones, T. (2012). *Wildlife Corridors in the Udzungwa Mountains of Tanzania*. Ecological Restoration, 30(4), 282–285. doi 10.3368/er.30.4.282

Rozanski, K., Araguás-Araguás, L., & Gonfiantini, R. (1993). *Isotopic Patterns in Modern Global Precipitation.* In P. K. Swart, K. C. Lohmann, J. McKenzie, & S. Savin (Eds.), Geophysical Monograph Series (pp. 1–36). https://agupubs.onlinelibrary.wiley.com/doi/pdf/10.1029/GM078p0001

Rozanski, L., Araguas-Araguas, L., & Gonfiantini, R. (1996). Isotope patterns of precipitation in the East African Region. In T. Johnson & E. Odada (Eds.), The Limnology, Climatology and Paleoclimatology of the East African Lakes (pp. 79–93). CRC Press.

Russi, D., Ten Brink, P., Farmer, A., Badura, T., Coates, D., Förster, J., Kumar, R. and Davidson, N. (2013). *The Economics of Ecosystems and Biodiversity for Water and Wetlands.* Final Consultation Draft.

Sabine, P. A., Harrison, R. K., & Lawson, R. I. (1986). *Classification of Volcanic Rocks of the British Isles on the Total Alkali Oxide-Silica Diagram and the Significance of Alteration.* Stationery Office Books.

SAHRA (2005). Isotopes & Hydrology- Sustainability of semi-Arid Hydrology and Riparian Areas SAHRA. http://web.sahra.arizona.edu/programs/isotopes/oxygen.html

Saiz-Rubio, V.& Rovira-Más, F. (2020). *From Smart Farming towards Agriculture 5.0: A Review on Crop Data Management*. Agron. J. 10(2), 207, doi 10.3390/agronomy10020207

Sakané, N,. Alvarez, M., Becker, M., Böhme, B., Handa, C., Kamiri, H.W., Langensiepen,. M., Menz, G., Misana, S., Mogha, N.G., Möseler, B.M., Mwita, E.J., Oyieke, H.A., van Wijk, M.T. (2011). *Classification, Characterisation, and Use of Small Wetlands in East Africa.* Wetl. Ecol. Manag. 31(6), 1103–1116, doi 10.1007/s13157-011-0221-4

Samoka, O. (2010). Groundwater recharge of confined aquifers in the Upper Ewaso Ng'iro North River Basin, Kenya. University of Nairobi.

Sarin, M. M., Krishnaswami, S., Dilli, K., Somayajulu, B. L. K., & Moore, W. S. (1989). *Major ion chemistry of the Ganga-Brahmaputra river system: Weathering processes and fluxes to the Bay of Bengal.* Geochim. Cosmochim. Acta. 53(5), 997–1009. doi10.1016/0016-7037(89)90205-6

Schiff, J. A., & Fankhauser, H. (1981). *Assimilatory Sulfate Reduction.* In H. Bothe & A. Trebst (Eds.), Biology of Inorganic Nitrogen and Sulfur (pp. 153–168). Springer Berlin Heidelberg.

Schlüter, T. (1997). *Geology of East Africa.* Gebrüder Borntraeger.

Schlüter, T., & Trauth, M. H. (2006). *Geological atlas of Africa: With notes on stratigraphy, tectonics, economic geology, geohazards and geosites of each country*. Springer.

Schoeller, H. (1955): *Geochemie des eaux souterraines.* Revue de l'Institute Français du petrole, 10, 230-44.

Schoeller, H. (1977). *Geochemistry of groundwater.* In Groundwater Studies—An international guide for research and practice, Ch. 15 (pp. 1–18). UNESCO, Paris.

Sciortino, J. A., Ravikumar, R., BOBP & FAO. (1999). *Fishery Harbour Manual on the Prevention of Pollution—Bay of Bengal Programme* (BOBP/MAG/22). BOBP for Fisheries Management.

Semeniuk, C. A., & Semeniuk, V. (1995). *A geomorphic approach to global classification for inland wetlands.* In C. Max Finlayson & A. G. van der Valk (Eds.), Classification and Inventory of the World's Wetlands (pp. 103–124). Springer Netherlands. doi 10.1007/978-94-011-0427-2_9

Shackleton, R.M. (1978). *Structural development of the East African Rift system.* Geol. Soc. Spec. Publ. London 6, 19–28.

Shankar, S., Shanker, U., & Shikha. (2014). *Arsenic Contamination of Groundwater: A Review of Sources, Prevalence, Health Risks, and Strategies for Mitigation.* Sci. World J. 2014, 1–18. doi 10.1155/2014/304524

Shedlock, R. J., Wilcox, D. A., Thompson, T. A., & Cohen, D. A. (1993). *Interactions between groundwater and wetlands, southern shore of Lake Michigan, USA.* J. Hydrol. 141(1), 127–155. doi 10.1016/0022-1694(93)90047-D

Sheoran, A. S., & Sheoran, V. (2006). *Heavy metal removal mechanism of acid mine drainage in wetlands: A critical review.* Miner. Eng. 19(2), 105–116. doi 10.1016/j.mineng.2005.08.006

Shotterer, U., & Muller, I. (1985). *A Hydrogeological Investigation in the Semi-arid Region of Northwest Mount Kenya.* In Bull. De Centre de Hydrogeologie, Vol. 6.

Sikes H.L. (1934). *The underground water resources of Kenya colony and records of the results of drilling for water during the years 1926-1932.* Westminsterm the Crown Agents… on behalf of the Government of the Kenya Colony and protectorate. 40:5. [CR. The geographical Journal p.529].

Sigg, L., & Stumm, W. (1996). *Aquatische Chemie Eine Einführung in die Chemie wässriger Lösungen und natürlicher Gewässer.* B. G. Teubner.

Simpson, H. J., & Herczeg, A. L. (1991). *Salinity and evaporation in the River Murray Basin, Australia.* J. Hydrol. 124(1), 1–27. doi 10.1016/0022-1694(91)90003-Z

Singh, A. K., Mondal, G. C., Singh, P. K., Singh, S., Singh, T. B., & Tewary, B. K. (2005). *Hydrochemistry of reservoirs of Damodar River basin, India: Weathering processes and water quality assessment.* Environ. Geol. 48(8), 1014–1028. doi 10.1007/s00254-005-1302-6

Sklash, M. G., & Mwangi, M. P. (1991). An isotopic study of groundwater supplies in the Eastern Province of Kenya. J. Hydrol. 128(1), 257–275. doi 10.1016/0022-1694(91)90141-4

Smith, M., & Mosley, P. (1993). *Correction to "Crustal heterogeneity and basement influence on the development of the Kenya Rift, East Africa*." Tectonics, 12(3). doi 10.1029/93TC01133

Smith, R. L., Howes, B. L., & Duff, J. H. (1991). *Denitrification in nitrate-contaminated groundwater: Occurrence in steep vertical geochemical gradients.* Tectonics 55(7), 1815–1825. doi 10.1016/0016-7037(91)90026-2

Solution- Mineral Equilibria Part 1: Carbonates. In: Introduction to Geochemistry. http://geoweb.uwyo.edu/geol2100/CarbonateChemistry.pdf

Sonntag, C., Muennich, K. O., Junghans, C., Klitzsch, E., Thorweihe, U., Weistroffer, K., Loehnert, E. P., El-Shazly, E. M., & Swailem, F. M. (1979). *Palaeoclimatic information from deuterium and oxygen-18 in carbon-14-dated north Saharian groundwaters. Groundwater formation in the past.* In Isotope Hydrology 1978, Int. At. Energy Agency (I.A.E.A.), Vienna (pp. 569–581).

Spieles, D. J., & Mitsch, W. J. (2000). *The effects of season and hydrologic and chemical loading on nitrate retention in constructed wetlands: A comparison of low- and high-nutrient riverine systems.* Ecol. Eng. 14(1/2), 77–91.

Sprecher, S. (2008). *Installing monitoring wells in soils (Version 1.0).* National Soil Survey Center, Natural Resources Conservation Service, USDA, Lincoln, NE.

Sracek, O., & Zeman, J. (2004). *Introduction to environmental hydrogeochemistry.* Masaryk University.

Srodon, J., & Eberl, D. D. (1984). *Illite.* In Micas, S. W. Bailey, ed., Reviews in Mineralogy 13, Mineralogical Society of America (pp. 495–544).

Stanford, J. A., & Ward, J. V. (1993). *An Ecosystem Perspective of Alluvial Rivers: Connectivity and the Hyporheic Corridor.* J. North. Am. Benthol. Soc. 12(1), 48–60. doi 10.2307/1467685

StatSoft, Inc. (1997) *Electronic statistics textbook.* StatSoft, Inc. Tulsa, OK. http://www.statsoft.com/textbook/stathome.html

Stober, I., Bucher, K. (2007). *Hydraulic properties of the crystalline basement*. Hydrogeol. J. 15, 213–224. https://doi.org/10.1007/s10040-006-0094-4

Stoch, L., & Sikora, W. (1976). *Transformations of Micas in the Process of Kaolinitization of Granites and Gneisses.* Clays and Clay Miner. 24(4), 156–162. doi 10.1346/CCMN.1976.0240402

Sturman, P. J., Stein, O. R., Vymazal, J., & Kröpfelová, L. (2008). *Sulfur Cycling in Constructed Wetlands.* In J. Vymazal (Ed.), Wastewater Treatment, Plant Dynamics and Management in Constructed and Natural Wetlands (pp. 329–344). Springer Netherlands. doi 10.1007/978-1-4020-8235-1_29

Subramani, T., Rajmohan, N., & Elango, L. (2010). *Groundwater geochemistry and identification of hydrogeochemical processes in a hard rock region, Southern India.* Environ. Monit. Assess. 162(1–4), 123–137. doi 10.1007/s10661-009-0781-4

Summerfield, M. A. (1991). *Sub-aerial denudation of passive margins: Regional elevation versus local relief models.* Earth Planet. Sci. Lett. 102(3), 460–469. doi 10.1016/0012-821X(91)90036-H

Tardy, Y. (1971). *Characterization of the principal weathering types by the geochemistry of waters from some European and African crystalline massifs.* Chem. Geol. 7(4), 253–271. doi 10.1016/0009-2541(71)90011-8

Tardy, Y., Bocquier, G., Paquet, H., & Millot, G. (1973). *Formation of clay from granite and its distribution in relation to climate and topography.* Geoderma 10(4), 271–284. doi 10.1016/0016-7061(73)90002-5

The Open University. (2006). *Earth's physical resources: Origin, use and environmental impact. Course S278*.

Thenya, T. (2001). *Challenges of conservation of dryland shallow waters, Ewaso Narok swamp, Laikipia District, Kenya.* Hydrobiol. J. 458(1), 107–119. doi 10.1023/A:1013196500456

Thenya, T., Kahiu, N., Karanja, F., Onjwang', D., Ouko, C., Wambugu, G., & Njuguna, E. C. (2011). *Assessment of Ecological Status and Socio-Economic Dynamics of Upper Ewaso Ng'iro Basin Wetlands.* CETRAD. http://docrepo.wlrc-ken.org/xmlui/handle/123456789/70

Thompson, M. L., & Ukrainczyk, L. (2002). *Micas*. In D. Dixon & D. Schulze (Eds.), Soil Mineralogy with Environmental Applications, Vol. 7 (pp. 431–466). Soil Science Society of America, Inc.

Thorpe, R. S., & Smith, K. (1974). *Distribution of Cenozoic volcanism in Africa.* Earth Planet. Sci. Lett. 22(1), 91–95. doi 10.1016/0012-821X(74)90068-5

Tiwari, A. K., & Singh, A. K. (2014). *Hydrogeochemical investigation and groundwater quality assessment of Pratapgarh district, Uttar Pradesh.* J. Geol. Soc. India 83(3), 329–343. doi 10.1007/s12594-014-0045-y

Tockner, K., & Stanford, J. (2002). *Review of: Riverine Flood Plains: Present State and Future Trends.* Environ. Conserv. 29(3), 308–330. doi 10.1017/S037689290200022X

Todd, D. K. (1959). *Annotated Bibliography on Artificial Recharge of Groundwater Through 1954* (Geological survey water-supply paper 1477). U.S. Government Printing Office.

UN (United Nations) (2019). *World Population Prospects 2019—Population Division*. https://population.un.org/wpp/

UNDP (United Nations Development Programme)(2018). *Unlocking the Potential of Arid and Semi Arid Lands of Kenya.* http://www.ke.undp.org/content/kenya/en/home/presscenter/pressreleases/2018/unlocking-the-potential-of-arid-and-semi-arid-lands-of-kenya-.html

UNESCO-WWAP (United Nations Education, Scientific, and Cultural Organization-World Water Assessment Program) (2006). *Kenya National Water Development Report prepared for 2nd UN World Water Development Report 'Water: A shared responsibility'* (No. 12). UNESCO and Berghahn.

UCCC (University of California Committee of Consultant) (1974). *Guidelines for Interpretations of water Quality for Irrigation.* Technical Bulletin, University of California Committee of Consultants, California, USA. 20–28.

Uusi-Kämppä, J., Braskerud, B., Jansson, H., Syversen, N., & Uusitalo, R. (2000). *Buffer Zones and Constructed Wetland as Filters for Agricultural Phosphorus.* J. Environ. Qual. 29(1), 151–158. doi 10.2134/jeq2000.00472425002900010019x

Van Bladel, R., & Gheyi, H. R. (1980). *Thermodynamic Study of Calcium-Sodium and Calcium-Magnesium Exchange in Calcareous Soils.* Soil Sci. Soc. Am. J. 44(5), 938–942. doi 10.2136/sssaj1980.03615995004400050012x

Van der Weijden, C.H. & Pacheco, F. L. (2007). *From hydrochemistry to chemical weathering: models and problems.* Congress Report, Geochimica XV Semana, 27-32.

Van der Weijden, C. H., & Pacheco, F. A. L. (2003). *Hydrochemistry, weathering and weathering rates on Madeira island.* J. Hydrol. 283(1), 122–145. doi 10.1016/S0022-1694(03)00245-2

Van Oostrom, A. J., & Russell, J. M. (1994). *Denitrification in Constructed Wastewater Wetlands Receiving High Concentrations of Nitrate.* Water Sci. Technol. 29(4), 7–14. doi 10.2166/wst.1994.0146

Verhoeven, J. T. A., Arheimer, B., Yin, C., & Hefting, M. M. (2006). *Regional and global concerns over wetlands and water quality.* Trends Ecol. Evol. 21(2), 96–103. doi 10.1016/j.tree.2005.11.015

Viviroli, D., Dürr, H. H., Messerli, B., Meybeck, M., & Weingartner, R. (2007). *Mountains of the world, water towers for humanity: Typology, mapping, and global significance.* Water Resour. Res., 43(7). doi 10.1029/2006WR005653

Wachira, G. G. (2014). *Shiva Farm Limited- Rumuruti Sector—Farm A/ Farm B*.

Walter, B., Géraud, Y., Bartier, D., Kluska, J.-M., Diraison, M., Morlot, C., & Raisson, F. (2018). *Petrophysical and mineralogical evolution of weathered crystalline basement in western Uganda: Implications for fluid transfer and storage. AAPG Bulletin*, *102*(06), 1035–1065. doi 10.1306/0810171610917171

Ward, D. (2003). *Water Wars: Drought, Flood, Folly, and the Politics of Thirst.* Penguin.

Ward, J. (1963). *Hierarchical Grouping to Optimize an Objective Function.* J. Am. Stat. Assoc. 58(301), 236–244. doi 10.1080/01621459.1963.10500845

Ward, J., Tockner, K., & Schiemer, F. (1999). *Biodiversity of floodplain river ecosystems: Ecotones and connectivity*. Regul. Rivers: Res. Manage 15(1–3), 15.

Ward, M., Jones, R. R., Brender, J. D., de Kok, T. M., Weyer, P. J., Nolan, B. T., Villanueva, C. M., & van Breda, S. G. (2018). *Drinking Water Nitrate and Human Health: An Updated Review. Int. J. Environ. Res. Public Health* 15(7). doi 10.3390/ijerph15071557

WB (The World Bank) (2017). *Water in Agriculture.* Understanding Poverty, Water in Agriculture. http://www.worldbank.org/en/topic/water-in-agriculture

Weiss, J. (1995). *Ion chromatography* (2nd ed.). Wiley- VCH.

Welz, B. (1976). *Atomic absorption spectroscopy*, 2nd edn. Verlag Chemie GmbH.

Westerhof, A., Härmä, P., Isabirye, E., Katto, E., Koistinen, T., Kuosmanen, E., Lehto, T., I. Lehtonen, M., Mäkitie, H., Manninen, T., Mänttäri, I., Pekkala, Y., Pokki, J., Saalmann, K., & Virransalo, P. (2014). *Geology and Geodynamic Development of Uganda With Explanation of the 1:1,000,000 Scale Geological Map*. Geol Surv Final.

Whigham, D. F., Chitterling, C., & Palmer, B. (1988). *Impacts of freshwater wetlands on water quality: A landscape perspective.* J. Environ. Manage. 12(5), 663–671. doi 10.1007/BF01867544

White, Arthur F., & Brantley, S. L. (2018). *Chemical Weathering Rates of Silicate Minerals*, Vol. 31. Walter de Gruyter GmbH & Co KG.

WHO (World Health Organization) (2016). Nitrate and Nitrite in Drinking-water Background document for development of WHO Guidelines for Drinking-water Quality.

WHO (World Health Organization) (2015). Basic and safely managed drinking water services—Data by country. Global Health Observatory Data Repository. http://apps.who.int/gho/data/view.main.WSHWATERv?lang=en

WHO (World Health Organization) (2011). Guidelines for drinking-water quality, 4th edn.

Wieder, R. K., & Lang, G. E. (1988). *Cycling of inorganic and organic sulfur in peat from Big Run Bog, West Virginia.* Biogeochemistry 5(2), 221–242. doi 10.1007/BF02180229

Wiklander, L. (1964). *Cation and anion exchange phenomena.* In F. Bear (Ed.), Chemistry of the Soil (pp. 162–205). Chapman & Hall.

Wilford, J. (2012). *A weathering intensity index for the Australian continent using airborne gamma-ray spectrometry and digital terrain analysis.* Geoderma 183–184, 124–142. doi 10.1016/j.geoderma.2010.12.022

Wilkinson, A. F. (1983). *Bulletin notes for the Pesi Swamp, Sheet (No. 106/3)* (unpublished). Mines & Geol. Dept. Kenya.

Williams, J. B. (2002). *Phytoremediation in Wetland Ecosystems: Progress, Problems, and Potential.* Crit. Rev. Plant Sci. 21(6), 607–635. doi 10.1080/0735-260291044386

Winter, T. C. (1999). *Relation of streams, lakes, and wetlands to groundwater flow systems.* Hydrogeol. J. 7(1), 28–45. doi 10.1007/s100400050178

Woessner, W. (2000). *Stream and Fluvial Plain Groundwater Interactions: Rescaling Hydrogeologic Thought.* Groundwater, 38, 423–429. doi 10.1111/j.1745-6584.2000.tb00228.x

WoldeGabriel, G., Olago, D., Dindi, E., & Owor, M. (2016). *Genesis of the East African Rift System.* In Schagerl M. (Ed.), Soda Lakes of East Africa (pp. 25–59). Springer, Cham. doi 10.1007/978-3-319-28622-8_2

Wolf, P., (1967). Methods of non-linear programming. In: I*nterscience, J.* 6: 97-131. Wiley, New York.

Wood, A. (1985). *A century of development measures and population redistribution along the Upper Zambezi (Zambia).* In: Clarke JI, Khogali M, Kosinski LA (Eds) Population and development projects in Africa (pp. 163–175). Cambridge University Press.

Wood, A., Dixon, A., & McCartney, M. (2013). *Wetland Management and Sustainable Livelihoods in Africa*, 1st edn. Routledge.

WRA (Water Resource Authority). *Ewaso Ng'iro North Basin Area (ENNBA).* Retrieved August 14, 2020, from https://wra.go.ke/ewaso-ngiro-north-basin-area-ennba/

WRAP (Wetlands Regulatory Assistance Program). (2000). Installing Monitoring Wells/Piezometers in Wetlands (ERDC TN-WRAP-00-02; p. 17). US Army Engineer Research and Development Center. http://hdl.handle.net/11681/3541

WRI (Water Resource Institute) (2005). *Millennium Ecosystem Assessment.* Ecosystems and human well-being [Synthesis report]. Washington DC, USA.

Wright, E. P. (1992). *The hydrogeology of crystalline basement aquifers in Africa.* Geol. Soc. Spec. Publ. London 66(1), 1–27. doi 10.1144/GSL.SP.1992.066.01.01

WRMA (Water Resource Management Authority) and LWF (Lutheran World Federation)(2013). Lower Ewaso Narok WRUA sub-catchment management plan. Rumuruti Town

WRMA (Water Resource Management Authority). (2007). *Ol Maisor- Borehole No. WRMA/ENNCA/CW/026.* Form: WRMA 009A [Borehole Completion Record].

WRMA (Water Resource Management Authority). (2013a). *WRMA data* (Unpublished data).

WRMA (Water Resource Management Authority) . (2013b). *Kifuku—Borehole No. WRMa/50/RUM/5AB/10076/G* [Borehole Completion Record].

WRMA (Water Resource Management Authority). (2013c). *Shiva Farm BH2 -Borehole No. C-20860. WRMA/ENVA/GW/10073* [Borehole Completion Record].

WRMA (Water Resource Management Authority). (2016). *WRMA data*, cited with permission (Unpublished).

WTW (2009). *SenTIX ORP 900 Operating Manual* (p. 39). WTW GmbH, Weilheim.

Wu, S., Kuschk, P., Brix, H., Vymazal, J., & Dong, R. (2014). *Development of constructed wetlands in performance intensifications for wastewater treatment: A nitrogen and organic matter targeted review.* Water Res. 57, 40–55. doi 10.1016/j.watres.2014.03.020

Xue, Y., Kovacic, D. A., David, M. B., Gentry, L. E., Mulvaney, R. L., & Lindau, C. W. (1999). *In Situ Measurements of Denitrification in Constructed Wetlands.* J. Environ. Qual. 28(1), 263–269. doi 10.2134/jeq1999.00472425002800010032x

Yeh, T. Y. (2008). *Removal of Metals in Constructed Wetlands: Review. Pract. Period. Hazard. Toxic Radioact.* Waste Manage. 12(2), 96–101. doi 10.1061/(ASCE)1090-025X(2008)12:2(96)

Zhu, T., & Sikora, F. J. (1995). *Ammonium and nitrate removal in vegetated and unvegetated gravel bed microcosm wetlands.* Water Sci. Technol. 32(3), 219–228. doi 10.1016/0273-1223(95)00623-0

Appendices

App. 1: In-situ water sampling data (2016).

UID	Coordinates		Elevation	EC	T_W	pH	Redox	DO	Titration HCl	Titration NaOH	Acid capacity	Base capacity
	X	Y	[m a.s.l.]	[µS/cm)	[°C]	[-]	[mV]	[%]	[ml]	[ml]	[mmol/l]	[mmol/l]
GW1	0.18692	36.44387	1896	272	24.8	7.17	265.8	82.4	8.5	0.4	2.52	0.08
GW4	0.18042	36.58539	1829	934	21.9	7.65	241.9	133.6	22.2	0.6	5.41	0.12
GW5	0.20376	36.5568	1715	4470	24.4	7.21	-152.8	39.2	21	2.2	11.74	0.44
GW7	0.26253	36.62199		1010	25.5	7.68	160.6	85.1	31.5	0.2	6.3	0.04
GW9	0.2563	36.54589		1515	25.3	7.58	186.8	88.8	55.8	0.4	11.01	0.08
GW10	0.2563	36.54589		1342	22.2	7.42	193.4	68.8	56.4	0.6	10.99	0.12
GW11	0.25741	36.54734		513	29	6.78	280.5	161.7	7.2	0.7	1.44	0.14
GW14	0.2624	36.53628		1418	20.3	8.40	110	44.3	55.5	0	11.1	0
GW17	0.26881	36.54007	1845	1583	21.5	9.14	141.2	90.1	38.5	0	7.7	0
GW18	0.26882	36.54007	1835	966	25.2	9.22	125	72.7	30.5	0	6.1	0
GW19	0.2752	36.54715		1229	27.5	9.32	98.8	94.1	50	0	7.38	0
GW23	0.27125	36.50795	1894	961	24.5	8.76	160.4	93	27.1	0	5.91	0
GW24	0.26799	36.45367	1959	574	23.2	8.10	163.6	71.1	26.5	0.1	5.3	0.02
GW27	0.29423	36.60807		1212	27.8	8.04	171	56.1	42	0.1	8.4	0.02
GW30	0.32485	36.57368		1934	26.5	8.65	99.6	86.4	33	0	6.6	0
GW31	0.32713	36.58896		285	26.6	5.62	91.2	1.1	5	0	1	0
GW32	0.32713	36.58896	1690	365	17.4	7.25	197.1	43	6.6	0.9	1.32	0.18
GW41	0.3271	36.65176		464	23.2	7.27	265.8	174.4	13.5	0.4	3.19	0.08
GW44	0.40824	36.62259	1831	1345	26.3	8.68	157.3	25.3	30	0	5.00	0
GW45	0.4147	36.65713	1816	1986	27.7	9.46	99.2	61.9	59.5	0	11.9	0
GW46	0.43124	36.68181	1744	2050	23.3	7.17	170.2	50.6	41.7	1.2	8.34	0.24
GW47	0.41246	36.74078		1594	27.8	9.35	109.7	66.6	51.1	0	8.58	0
GW49	0.44089	36.6146	1842	2006	22.9	8.35	153.5	36.5	31.7	0	6.34	0
GW50	0.51082	36.60472		1863	22	7.61	214.8	99.6	47.8	2	11.40	0.4
GW52	0.55529	36.62372	1766	1447	25.9	6.97	182	29.8	44	1.7	7.16	0.34
SF2	0.21701	36.46278	1826	290	23.3	8.14	191.7	103.4	10.4	0.2	2.08	0.04
SF3	0.22109	36.47068	1857	121.5	19.9	7.93	188.8	100.4	5.3	0.3	1.06	0.06
SF6	0.25237	36.59776	1750	114.9	17.1	6.86	214.2	97.6	4.6	0.6	0.92	0.12
SF8	0.25626	36.54587		288	25.4	6.93	233.6	81.7	8.6	0.6	1.72	0.12
SF12	0.26129	36.56282	1779	242	27.8	7.06	207.3	83.3	6.8	0.9	1.72	0.18
SF13	0.26029	36.56343	1746	217	20.4	7.75	167.3	105.4	6.8	0.3	1.46	0.06
SF15	0.2624	36.53628	1680	146.1	23.3	7.5-	194.4	106.1	3.1	0.3	0.95	0.06
SF16	0.26439	36.54733	1700	123.2	21.3	7.86	178.7	99.7	5.6	0.5	1.12	0.1
SF20	0.2751	36.54921	1694	216	18.8	6.80	192	98.2	6.9	0.8	1.38	0.16
SF21	0.27383	36.54768		1697	25.9	9.2	81.7	85.2	66	0	9.92	0
SF22	0.27472	36.55468	1769	203	19.9	7.46	195.1	91.4	6.8	0.4	1.36	0.08
SF25	0.29701	36.59643	1726	218	25	7.42	250	102.9	3.5	0.2	0.7	0.04
SF26	0.29701	36.59643	1726	570	26.5	7.47	237.1	105.4	4	0.2	1.11	0.04
SF28	0.316	36.57698		185	22.3	7.14	180.4	68	6.3	2.5	1.26	0.5
SF29	0.3206	36.57247		316	24.7	7.78	194.9	101.8	12.5	0.4	2.5	0.08
SF33	0.32152	36.61446	1741	137.1	21.6	7.55	289.9	20.1	4	0.4	1.12	0.08
SF34	0.32239	36.61217	1675	117.8	19.9	6.71	286.8	52.6	5	3.5	0.84	0.7
SF35	0.32235	36.61148		94.3	19	7.26	262.1	85.6	3.4	0.5	0.84	0.1
SF36	0.32953	36.6048	1667	196.6	20.4	7.72	171.5	110.3	7.9	0.2	1.58	0.04
SF37	0.3297	36.60507		193.2	20.7	7.41	228	82.3	6.9	0.4	1.38	0.08
SF38	0.33041	36.60877		164	23.1	7.48	224.7	96.9	5.2	0.3	1.04	0.06
SF39	0.33848	36.61311	1809	203	24.8	7.33	754.7	85.3	4.7	0.4	1.27	0.08
SF40	0.33577	36.62542	1799	105.4	23.1	7.23	264.9	85.1	3.1	0.3	1.15	0.06
SF42	0.35374	36.63301	1790	165.1	22.4	6.85	204.2	98.2	7	1.5	1.4	0.3
SF43	0.3743	36.65301	1687	133.1	19.2	7.08	210.4	99.5	7.8	0.3	1.41	0.06
SF48	0.4342	36.7114		163.8	20.8	7.5	241.9	103.5	4	0.2	1.13	0.04
SF51	0.53252	36.61396		395	21.9	7.8	213.5	87	0.1	12	1.64	2.4
SF53	0.53064	36.57457		128.8	23.8	7.67	248.4	107.8	0.4	0.7	1.33	0.14

App. 2: Hydrochemistry of water samples.

UID	Fe^{2+} [mg/l]	Mn^{2+} [mg/l]	Mg^{+} [mg/l]	Na^{+} [mg/l]	K^{+} [mg/l]	Ca^{2+} [mg/l]	Al^{3+} [mg/l]	As^{3+} [mg/l]	Cd^{2+} [mg/l]	Cr^{3+} [mg/l]	Cu^{2+} [mg/l]	Sr^{2+} [mg/l]	Ni^{2+} [mg/l]	Pb^{2+} [mg/l]	Zn^{2+} [mg/l]
GW1	0.40	0.30	3.00	30.00	14.40	19.50	1.00	0.01	0.01	0.01	0.01	0.50	0.01	0.01	0.01
GW4	0.01	0.06	21.80	123.00	15.50	46.50	0.02	0.01	0.01	0.01	0.01	0.50	0.01	0.01	0.20
GW5	0.10	2.30	42.90	439.00	30.80	540.00	0.09	0.01	0.01	0.01	0.01	4.00	0.01	0.01	0.01
GW7	0.01	0.08	6.00	185.00	14.40	19.00	0.01	0.01	0.01	0.01	0.01	0.50	0.01	0.01	0.01
GW9	0.01	0.05	8.80	269.00	8.30	37.00	0.02	0.01	0.01	0.01	0.90	0.50	0.01	0.01	1.00
GW10	0.01	0.06	16.20	215.00	20.10	44.00	0.02	0.01	0.01	0.01	0.01	0.50	0.01	0.01	0.06
GW11	0.01	0.80	7.10	42.00	15.80	27.00	0.04	0.01	0.01	0.01	0.01	0.50	0.01	0.01	0.02
GW14	0.70	0.07	6.30	314.00	10.20	26.50	1.60	0.01	0.01	0.01	0.01	0.50	0.01	0.01	0.01
GW17	0.01	0.02	1.30	310.00	5.00	2.70	0.03	0.01	0.01	0.01	0.01	0.50	0.01	0.01	0.01
GW18	0.01	0.03	1.20	210.00	5.40	5.40	0.04	0.01	0.01	0.01	0.01	0.50	0.01	0.01	0.01
GW19	0.01	0.05	0.30	251.00	4.00	1.80	0.04	0.01	0.01	0.01	0.01	0.50	0.01	0.01	0.01
GW23	0.01	0.03	1.10	210.00	7.20	5.40	0.01	0.01	0.01	0.01	0.01	0.50	0.01	0.01	0.01
GW24	0.17	0.04	0.80	145.00	8.00	3.80	0.03	0.01	0.01	0.01	0.01	0.50	0.01	0.01	0.06
GW27	0.01	0.07	0.90	241.00	11.30	4.10	0.01	0.01	0.01	0.01	0.01	0.50	0.01	0.01	0.01
GW30	0.01	0.02	1.00	364.00	8.20	6.10	0.03	0.01	0.01	0.01	0.01	0.50	0.01	0.01	0.01
GW31	0.36	1.80	2.60	42.00	8.90	13.30	0.80	0.01	0.01	0.01	0.01	0.50	0.01	0.01	0.10
GW32	0.16	0.30	4.10	21.00	16.20	25.40	1.30	0.01	0.01	0.01	0.01	0.50	0.01	0.01	0.07
GW41	0.03	0.05	5.00	57.00	22.10	18.60	0.06	0.01	0.01	0.01	0.01	0.50	0.01	0.01	0.08
GW44	0.01	0.01	0.90	228.00	5.80	4.20	0.01	0.01	0.01	0.01	0.01	0.50	0.01	0.01	0.01
GW45	0.01	0.05	1.00	412.00	14.60	2.80	0.04	0.01	0.01	0.01	0.01	0.50	0.01	0.01	0.01
GW46	0.01	0.02	33.50	241.00	18.60	94.00	0.01	0.01	0.01	0.01	0.01	1.00	0.01	0.01	0.07
GW47	0.01	0.01	0.80	304.00	7.50	3.30	0.02	0.01	0.01	0.01	0.01	0.50	0.01	0.01	0.01
GW49	0.10	0.08	0.30	398.00	19.90	2.80	0.15	0.01	0.01	0.01	0.01	0.50	0.01	0.01	0.01
GW50	0.01	0.08	23.00	210.00	30.30	121.00	0.02	0.01	0.01	0.01	0.01	1.50	0.01	0.01	1.30
GW52	0.01	0.02	18.20	213.00	22.60	49.00	0.02	0.01	0.01	0.01	0.01	0.80	0.01	0.01	0.05
SF2	0.37	0.16	3.10	38.00	8.50	13.00	1.00	0.01	0.01	0.01	0.01	0.50	0.01	0.01	0.01
SF3	0.78	0.07	1.30	15.80	6.00	5.60	0.60	0.01	0.01	0.01	0.01	0.50	0.01	0.01	0.01
SF6	0.68	0.23	2.10	14.20	3.80	8.20	1.00	0.01	0.01	0.01	0.01	0.50	0.01	0.01	0.01
SF8	4.40	1.20	2.50	33.00	10.60	11.00	1.30	0.01	0.01	0.01	0.01	0.50	0.01	0.01	0.02
SF12	1.20	0.90	3.50	30.00	4.20	17.50	2.70	0.01	0.01	0.01	0.01	0.50	0.01	0.01	0.06
SF13	0.80	0.23	3.30	24.00	3.50	12.00	1.30	0.01	0.01	0.01	0.01	0.50	0.01	0.01	0.02
SF15	0.80	0.14	1.40	17.40	16.90	6.70	0.48	0.01	0.01	0.01	0.01	0.50	0.01	0.01	0.02
SF16	0.50	0.08	1.20	16.20	6.50	5.60	0.56	0.01	0.01	0.01	0.01	0.50	0.01	0.01	0.01
SF20	0.90	0.12	2.20	26.70	10.50	0.90	0.90	0.01	0.01	0.01	0.01	0.50	0.01	0.01	0.01
SF21	0.40	0.55	2.70	316.00	20.10	15.00	0.50	0.01	0.01	0.01	0.01	0.50	0.01	0.01	0.01
SF22	0.92	0.43	2.10	26.70	9.10	9.70	0.80	0.01	0.01	0.01	0.01	0.50	0.01	0.01	0.08
SF25	1.30	0.50	2.30	18.20	8.20	9.80	1.50	0.01	0.01	0.01	0.01	0.50	0.01	0.01	0.10
SF26	0.90	0.30	2.50	15.10	8.60	10.40	1.20	0.01	0.01	0.01	0.01	0.50	0.01	0.01	0.01
SF28	1.80	0.14	1.70	23.30	6.00	8.00	0.70	0.01	0.01	0.01	0.01	0.50	0.01	0.01	0.04
SF29	0.84	0.46	3.00	42.00	21.30	15.50	1.50	0.01	0.01	0.01	0.01	0.50	0.01	0.01	0.01
SF33	0.85	0.19	2.10	16.10	8.40	9.10	1.00	0.01	0.01	0.01	0.01	0.50	0.01	0.01	0.01
SF34	0.92	0.30	1.80	8.50	5.80	8.20	1.90	0.01	0.01	0.01	0.01	0.50	0.01	0.01	0.07
SF35	1.10	0.35	2.00	9.20	7.50	8.50	1.90	0.01	0.01	0.01	0.01	0.50	0.01	0.01	0.05
SF36	1.40	0.22	2.20	30.00	20.40	9.70	0.80	0.01	0.01	0.01	0.01	0.50	0.01	0.01	0.02
SF37	1.00	0.40	2.50	23.00	12.80	12.50	1.40	0.01	0.01	0.01	0.01	0.50	0.01	0.01	0.05
SF38	1.10	0.30	2.40	22.00	11.70	11.70	1.30	0.01	0.01	0.01	0.01	0.50	0.01	0.01	0.02
SF39	0.90	0.35	2.30	17.30	9.10	11.10	1.60	0.01	0.01	0.01	0.01	0.50	0.01	0.01	0.07
SF40	1.00	0.40	2.20	14.30	7.80	10.20	1.70	0.01	0.01	0.01	0.01	0.50	0.01	0.01	0.10
SF42	1.30	0.18	2.00	21.00	6.20	8.40	0.70	0.01	0.01	0.01	0.01	0.50	0.01	0.01	0.01
SF43	1.10	0.10	2.00	18.20	8.40	8.10	0.80	0.01	0.01	0.01	0.01	0.50	0.01	0.01	0.01
SF48	1.10	0.13	1.90	16.20	5.70	8.60	0.90	0.01	0.01	0.01	0.01	0.50	0.01	0.01	0.02
SF51	1.90	0.60	4.30	11.80	8.70	24.00	1.60	0.01	0.01	0.01	0.01	0.50	0.01	0.01	0.12
SF53	0.70	1.00	2.90	12.10	8.00	17.00	2.50	0.01	0.01	0.01	0.01	0.50	0.01	0.01	0.02

App. 2: Hydrohemistry of water samples (continued).

UID	Cl^- [mg/l]	NO_3^- [mg/l]	SO_4^{2-} [mg/l]	NO_2^- [mg/l]	NH_4^+ [mg/l]	F^- [mg/l]	Br^- [mg/l]	PO_4^{3-} [mg/l]	Bo_3^{3-} [mg/l]	SiO_2 [mg/l]	NH_4^+ [mg/l]	HCO_3^- [mg/l]
GW1	7.40	1.80	4.10	0.20	3.52	0.90	0.00	0.16	0.02	23.96	3.52	153.73
GW4	76.20	34.20	45.50	0.00	5.28	1.00	0.40	0.01	0.01	40.86	5.28	329.93
GW5	695.40	0.00	380.80	0.00	19.36	1.90	2.40	0.48	0.01	25.46	19.36	716.28
GW7	107.70	9.10	54.90	0.00	1.76	1.60	0.40	0.16	0.01	33.80	1.76	384.43
GW9	139.50	21.20	72.00	0.00	3.52	1.80	0.80	0.16	0.01	34.87	3.52	671.98
GW10	91.00	23.10	53.20	0.00	5.28	1.70	0.50	0.07	0.01	41.93	5.28	670.31
GW11	82.90	6.40	26.00	0.00	6.16	0.00	0.40	0.00	0.01	22.46	6.16	87.87
GW14	32.30	2.30	79.10	0.30	0.00	15.20	0.50	0.99	0.05	27.39	0.00	677.32
GW17	144.60	0.00	49.70	0.30	0.00	19.01	0.70	0.78	0.01	6.93	0.00	469.85
GW18	72.60	0.00	32.80	0.00	0.00	4.30	0.40	0.46	0.01	9.07	0.00	372.22
GW19	80.30	0.00	27.90	0.00	0.00	7.82	0.40	0.79	0.01	6.63	0.00	450.20
GW23	48.80	65.00	17.20	0.00	0.00	1.70	0.30	0.36	0.01	21.14	0.00	360.73
GW24	18.20	10.00	7.00	0.00	0.88	1.30	0.00	0.39	0.01	13.65	0.88	323.41
GW27	80.30	3.50	27.90	0.40	0.88	2.60	0.70	1.10	0.01	34.87	0.88	512.57
GW30	223.50	2.60	98.60	0.00	0.00	9.12	1.30	0.38	0.02	9.20	0.00	402.73
GW31	24.80	0.90	41.50	0.00	0.00	0.30	0.00	0.42	0.02	9.50	0.00	61.02
GW32	43.50	1.60	7.20	0.00	7.92	13.30	0.00	0.78	0.02	9.58	7.92	80.55
GW41	11.50	19.40	6.90	0.00	3.52	0.80	0.00	0.02	0.00	66.43	3.52	194.75
GW44	163.80	21.10	76.10	0.00	0.00	8.70	1.00	0.25	0.01	21.91	0.00	305.12
GW45	192.00	7.70	83.40	0.80	0.00	10.90	1.60	0.34	0.01	8.60	0.00	726.14
GW46	248.30	193.40	98.90	0.00	10.56	1.30	1.00	0.02	0.01	28.78	10.56	508.91
GW47	137.70	0.00	65.20	0.00	0.00	10.00	0.80	0.38	0.02	9.58	0.00	523.62
GW49	253.00	67.20	128.80	0.60	0.00	3.30	2.30	0.07	0.02	5.22	0.00	386.87
GW50	132.10	33.40	20.60	0.00	17.60	0.50	0.40	0.09	0.01	35.52	17.60	695.35
GW52	119.30	73.20	52.00	0.00	14.96	3.00	0.70	0.05	0.01	50.06	14.96	436.98
SF2	20.60	0.90	6.30	0.00	1.76	0.20	0.00	0.64	0.04	23.23	1.76	126.92
SF3	7.80	2.10	3.70	0.00	2.64	0.00	0.00	0.40	0.03	16.13	2.64	64.68
SF6	9.50	0.00	5.70	0.00	5.28	0.30	0.00	0.55	0.03	18.78	5.28	56.14
SF8	23.20	0.00	5.60	0.00	5.28	0.30	0.00	0.72	0.09	12.45	5.28	104.95
SF12	18.10	0.00	11.40	0.00	7.92	0.40	0.00	0.98	0.07	34.45	7.92	105.10
SF13	11.40	0.00	4.50	0.00	2.64	0.30	0.00	0.52	0.06	15.49	2.64	88.99
SF15	9.20	3.90	3.80	0.00	2.64	6.60	0.00	0.49	0.03	13.56	2.64	57.83
SF16	11.20	2.10	5.10	0.00	4.40	0.20	0.00	0.34	0.04	17.24	4.40	68.34
SF20	16.20	0.00	4.70	0.00	7.04	0.30	0.00	0.52	0.05	13.86	7.04	84.21
SF21	123.20	0.00	39.10	0.00	0.00	9.00	0.50	1.90	0.06	17.93	0.00	605.46
SF22	30.00	0.00	5.20	0.00	3.52	0.30	0.10	0.68	0.05	15.10	3.52	82.99
SF25	8.40	1.70	26.90	0.00	1.76	0.40	0.00	1.50	0.04	20.37	1.76	42.71
SF26	11.10	0.00	9.30	0.00	1.76	1.10	0.00	1.30	0.04	13.18	1.76	67.82
SF28	8.90	0.00	3.40	0.00	22.01	0.30	0.00	0.26	0.06	15.79	22.01	76.89
SF29	21.40	1.10	5.40	0.00	3.52	0.90	0.00	0.40	0.03	15.66	3.52	152.55
SF33	9.10	0.20	4.30	0.00	3.52	0.30	0.00	0.60	0.07	17.20	3.52	68.82
SF34	5.20	0.20	5.00	0.60	30.81	0.40	0.00	1.20	0.05	17.20	30.81	51.02
SF35	4.90	0.30	3.10	0.60	4.40	0.30	0.00	1.82	0.24	19.77	4.40	51.49
SF36	22.20	0.00	4.30	0.00	1.76	0.30	0.00	0.45	0.06	15.23	1.76	96.41
SF37	30.20	0.80	5.70	0.00	3.52	0.60	0.00	0.06	0.05	24.65	3.52	84.21
SF38	28.20	0.50	4.30	0.00	2.64	0.60	0.00	0.08	0.04	18.27	2.64	63.46
SF39	12.90	1.30	5.10	0.00	3.52	0.50	0.00	0.08	0.06	13.99	3.52	77.36
SF40	6.40	1.40	4.40	0.40	2.64	0.40	0.00	0.50	0.11	19.73	2.64	70.00
SF42	9.70	0.50	3.20	0.00	13.20	0.40	0.00	0.51	0.03	13.74	13.20	85.43
SF43	13.50	0.40	3.10	0.00	2.64	0.40	0.00	0.42	0.04	18.40	2.64	86.19
SF48	8.30	0.90	3.50	0.00	1.76	0.30	0.00	0.72	0.04	12.32	1.76	68.82
SF51	7.80	1.60	2.40	0.00	105.62	8.20	0.00	0.17	0.04	12.75	105.62	100.22
SF53	7.20	1.40	4.00	0.00	6.16	0.90	0.00	1.24	0.06	30.12	6.16	80.88

App. 3: Stable water isotopes of surface water and groundwater samples.

UID	^{18}O [‰ VSMOW]	STDEV	^{2}H [‰ VSMOW]	STDEV
GW1	-1.67	0.35	-1.2	0.5
GW4	-2.88	0.14	-12.9	0.7
GW5	0.53	0.14	6.9	0.6
GW7	-3.37	0.21	-18.7	0.9
GW9	-2.57	0.10	-10.4	0.5
GW10	-2.50	0.21	-12.8	0.5
GW11	-2.10	0.14	-6.3	0.7
GW14	-1.67	0.12	-3.5	0.8
GW17	-3.72	0.15	-15.0	0.8
GW18	-3.76	0.19	-16.1	0.7
GW19	-3.16	0.16	-13.6	0.8
GW23	-2.82	0.19	-15.4	0.7
GW24	-3.52	0.18	-12.9	0.9
GW27	-3.22	0.23	-16.2	0.9
GW30	-3.15	0.15	-15.2	0.7
GW31	-0.39	0.19	6.2	1.1
GW32	-1.41	0.02	3.0	0.1
GW41	-2.05	0.21	-9.0	0.3
GW44	-3.14	0.16	-14.6	0.9
GW45	-3.66	0.19	-18.1	0.6
GW46	-3.63	0.21	-15.0	0.6
GW47	-3.52	0.15	-17.3	0.8
GW49	-2.89	0.12	-16.6	0.9
GW50	-2.48	0.12	-11.8	0.7
GW52	-1.96	0.21	-6.6	0.9
SF2	-2.40	0.21	-4.4	0.4
SF3	-1.43	0.21	-2.7	0.9
SF6	-3.28	0.13	-7.6	0.8
SF8	-0.28	0.19	8.3	0.6
SF12	0.85	0.18	11.0	0.9
SF13	-0.75	0.13	5.6	0.9
SF15	-1.53	0.10	2.0	0.6
SF16	-2.22	0.19	-4.7	0.8
SF20	-0.48	0.18	3.5	0.4
SF21	-1.14	0.19	-2.7	0.4
SF22	-1.08	0.16	3.6	0.7
SF25	-1.51	0.21	-1.9	0.7
SF26	-1.40	0.22	0.8	1.0
SF28	-1.80	0.12	-1.5	0.6
SF29	1.14	0.19	10.7	0.8
SF33	-1.82	0.13	0.9	0.7
SF34	-0.73	0.20	11.6	1.0
SF35	-1.25	0.16	11.6	0.9
SF36	-0.72	0.12	4.2	0.8
SF37	0.01	0.16	10.7	0.8
SF38	-0.04	0.09	10.5	0.7
SF39	-0.57	0.16	7.5	0.7
SF40	-0.83	0.17	10.7	0.5
SF42	-1.96	0.19	-0.7	0.7
SF43	-2.08	0.18	-2.1	0.2
SF48	-1.37	0.15	1.2	0.5
SF51	1.24	0.15	9.7	0.4
SF53	0.89	0.20	14.7	0.7

App. 4: Average precipitation (mm/month) at four weather stations across Ewaso Narok.

		Average precipitation (mm/month)											
	Year/Month	Jan	Feb	Mar	Apr	May	Jun	Jul	Aug	Sept	Oct	Nov	Dec
63717101 OL MAISOR FARM	Aver (65-16)	23.01	15.26	40.91	120.92	82.59	47.36	71.59	68.67	29.46	47.44	68.20	29.03
8936064 RUMURUTI MINISTRY OF WORK	Aver (64-16)	30.64	27.93	47.32	107.70	66.29	59.03	85.83	86.33	34.58	52.03	76.50	40.32
9036134 NDARAGWA FOREST STATION	Aver (73-13)	36.50	34.53	52.49	93.60	62.56	77.88	106.24	116.08	52.31	50.24	85.58	61.86
8903068 AMS NYAHURURU	Aver (79-14)	24.52	23.19	38.41	104.88	75.22	82.52	103.35	97.16	48.96	45.63	57.92	43.45

App. 5: Piezometer installation (after Sprecher, 2008).

1. Auger a hole in the ground with a bucket auger ~5 cm wider than the well stock to a depth approximately 2 cm deeper than the bottom of the piezometer. Be sure the auger hole is vertical.
2. Scarify the sides of the auger hole over the area to be screened if smeared during augering.
3. Place ~2 cm of clean sand at the bottom of the hole.
4. Insert the piezometer into the hole but not through the sand.
5. Pour and gently tamp more of the same sand in the annular space around the screen and 2 to 4 cm above. Be careful not to overfill with sand. The depth of tamping for each well can be marked on the side of the tamping tool with a piece of tape.
6. Pour and gently tamp bentonite chips above the sand to the ground surface.
7. Make a mound of soil and dry bentonite around the riser at the ground surface, shaped to prevent puddling around the base of the riser. Moisten before leaving.
8. Check for clogging. Reinstall and recheck if necessary.
9. Mark the side of the riser with paint at the top of the mounded soil/bentonite mixture and label the well.
10. Record the height of well above the ground surface and document installation.
11. Install and calibrate any water-level recording instruments.

App. 6: DHWQ of the samples exceeded, how many times, and which constituent was exceeded.

Sample	Number of guidelines exceeded	Constituent that was exceeded
GW1	1	Al^{3+}
GW4	0	
GW5	2	F^-, Mn^{2+}
GW7	1	F^-
GW9	1	F^-
GW10	1	F^-
GW11	1	Mn^{2+}
GW14	3	Fe^{2+}, F^-, Al^{3+}
GW17	2	F^-, As
GW18	1	F^-
GW19	1	F^-
GW23	2	F^-, NO_3^-
GW24	0	
GW27	1	F^-
GW30	1	F^-
GW31	2	Fe^{2+}, Mn^{2+}
GW32	2	F^-, Al^{3+}
GW41	0	
GW44	2	F^-, As
GW45	1	F^-
GW46	1	NO_3^-
GW47	1	F-
GW49	2	F^-, NO_3^-
GW50	0	
GW52	2	F^-, NO_3^-
SF2	2	Fe^{2+}, Al^{3+}
SF3	1	Fe^{2+}
SF6	2	Fe^{2+}, Al^{3+}
SF8	3	Fe^{2+}, Mn^{2+}, Al^{3+}
SF12	3	Fe^{2+}, Mn^{2+}, Al^{3+}
SF13	2	Fe^{2+}, Al^{3+}
SF15	2	Fe^{2+}, F^-
SF16	1	Fe^{2+}
SF20	2	Fe^{2+}, Al^{3+}
SF21	3	Fe^{2+}, F^-, Mn^{2+}
SF22	2	Fe^{2+}, Mn^{2+}
SF25	3	Fe^{2+}, Mn^{2+}, Al^{3+}
SF26	2	Fe^{2+}, Al^{3+}
SF28	1	Fe^{2+}
SF29	3	Fe^{2+}, Mn^{2+}, Al^{3+}
SF33	2	Fe^{2+}, Al^{3+}
SF34	2	Fe^{2+}, Al^{3+}
SF35	2	Fe^{2+}, Al^{3+}
SF36	1	Fe^{2+}
SF37	3	Fe^{2+}, Mn^{2+}, Al^{3+}
SF38	2	Fe^{2+}, Al^{3+}
SF39	1	Al^{3+}
SF40	3	Fe^{2+}, Mn^{2+}, Al^{3+}
SF42	1	Fe^{2+}
SF43	1	Fe^{2+}
SF48	2	Fe^{2+}, Al^{3+}
SF51	4	Fe^{2+}, F^-, Mn^{2+}, Al^{3+}
SF53	3	Fe^{2+}, Mn^{2+}, Al^{3+}

App. 7: Mineral identification and quantification of soil and rock samples.

Sample	Quartz [%]	Calcite [%]	K feldspar [%]	Plagioclase [%]	Illite/Muscovite [%]	Goethite [%]	Kaolinite group [%]
R1	1.81	21.03	29.19	11.22	32.16	4.59	0.00
R2	1.49	15.51	29.54	12.43	36.90	4.13	0.00
R3	8.65	0	39.23	14.77	30.76	6.59	0.00
R4	1.32	0	22.29	7.48	35.95	5.55	27.41
R5	1.73	4.55	41.49	5.61	24.58	3.46	18.58
R6	2.25	21.77	33.30	7.67	29.68	5.33	0.00
R7	7.70	0	39.20	20.89	27.55	4.66	0.00
R8	5.47	0	33.81	12.71	43.24	4.77	0.00
R9	10.64	0	31.36	16.11	37.35	4.54	0.00
R10	7.91	0.00	29.68	13.08	45.25	4.08	0.00
R11	6.86	16.32	34.20	0.00	38.00	4.62	0.00
R12	1.94	0.00	10.33	23.57	58.80	0.49	4.87
R13	2.83	0	9.08	16.29	70.76	1.04	0.00
R14	2.25	1.91	20.99	0.00	74.50	0.35	0.00
R15	1.13	0.00	51.51	5.90	7.41	8.68	25.37
R16	0.00	0	55.57	3.57	20.84	1.96	18.06
R17	0.00	0	67.34	0.00	9.47	5.41	17.78
S1	2.40	0	25.03	11.83	39.53	1.91	19.30
S2	4.98	10.08	35.97	15.67	25.88	7.42	0.00
S3	1.84	0.00	8.93	0.00	85.04	0.00	4.19
S4	1.05	0.00	10.49	0.00	82.41	0.00	6.05
S5	0.83	0.00	4.13	0.00	89.54	0.00	5.50

Note: Quantification was done with Rietveld method (Program Profex 3.14.0)

App. 8: Main elements and loss of ignition (LOI) of soil and rock samples (Total sum = sum of oxides and LOI; MP = melted pill; IQ+ = evaluation with powered press pills).

Sample	Total sum [%]	LOI [%]	Sum_{oxides} [%]	SiO_2 [%]	Al_2O_3 [%]	Fe_2O_3 [%]	MnO [%]	MgO [%]	CaO [%]	Na_2O [%]	K_2O [%]	TiO_2 [%]	P_2O_5 [%]	SO_3 [%]	Measured by
R1	100.51	14.30	86.21	43.92	19.12	7.82	0.20	1.23	9.34	1.26	2.14	0.69	0.03	0.25	MP
R2	100.11	11.48	88.63	48.04	19.89	8.43	0.25	1.26	5.66	1.53	2.45	0.74	0.03	0.14	MP
R3	100.76	9.24	91.52	51.62	20.89	11.32	0.35	0.66	0.60	1.37	3.28	0.85	0.06	0.26	MP
R4	101.27	9.75	91.52	49.40	23.19	11.82	0.28	0.90	0.78	1.31	2.43	0.83	0.04	0.28	MP
R5	101.41	9.03	92.38	49.99	21.08	10.22	0.33	1.13	2.58	1.70	4.12	0.72	0.04	0.21	MP
R6	101.22	13.61	87.61	43.04	18.47	11.11	0.62	1.11	8.11	1.13	2.86	0.63	0.03	0.22	MP
R7	100.70	6.97	93.73	56.49	18.02	10.41	0.48	0.60	0.84	2.34	2.87	1.07	0.06	0.28	MP
R8	99.28	7.63	91.65	55.61	19.53	8.62	0.27	0.54	0.70	1.84	2.84	1.26	0.05	0.17	MP
R9	100.56	10.14	90.42	52.92	18.82	10.26	0.38	1.22	1.24	1.28	2.92	0.81	0.05	0.28	MP
R10	100.44	10.00	90.44	52.47	19.35	10.41	0.36	1.28	1.20	1.23	2.80	0.83	0.04	0.22	MP
R11	99.62	12.81	86.81	47.24	16.99	9.19	0.34	1.38	6.71	1.17	2.56	0.74	0.03	0.22	MP
R12	100.33	7.80	92.53	53.15	20.42	10.53	0.17	0.72	0.85	1.85	2.22	1.90	0.14	0.29	MP
R13	100.69	8.63	92.06	52.89	21.91	9.98	0.28	0.92	0.73	1.12	2.92	0.86	0.04	0.18	MP
R14	100.04	9.46	90.58	51.27	20.62	9.30	0.21	1.16	2.61	1.16	3.02	0.82	0.04	0.16	MP
R15	99.24	8.38	90.86	41.08	18.58	21.62	2.97	0.20	0.25	1.11	4.08	0.85	0.09	0.03	IQ+
R16	100.37	6.14	94.23	53.17	23.80	6.49	0.25	0.50	0.34	2.72	5.80	0.77	0.03	0.16	MP
R17	99.33	7.81	91.52	43.48	19.26	19.57	1.83	0.16	0.29	1.79	4.21	0.82	0.09	0.02	IQ+
S1	101.68	9.19	92.49	53.99	22.53	8.94	0.30	0.81	0.66	1.06	2.63	0.98	0.04	0.28	MP
S2	100.15	14.54	85.61	42.80	19.12	8.67	0.35	1.04	9.05	1.20	2.29	0.69	0.04	0.16	MP
S3	99.31	15.21	84.10	48.34	19.57	11.09	0.12	0.46	0.91	0.38	1.36	1.50	0.18	0.19	IQ+
S4	99.69	14.57	85.12	49.32	20.88	10.32	0.15	0.45	0.81	0.28	1.13	1.28	0.34	0.16	IQ+
S5	99.44	18.70	80.74	49.43	17.24	9.83	0.15	0.41	0.92	0.26	1.00	1.01	0.27	0.22	IQ+

App. 9: Carbon, nitrogen, and sulfur in the soil and rock samples (LOD = limit of detection).

Samples	TN [%]	TC [%]	TS [%]
R1	<0.05	2.09	<0.10
R2	<0.05	1.25	<0.10
R3	0.09	1.03	<0.10
R4	0.05	0.58	<0.10
R5	<0.05	0.68	<0.10
R6	<0.05	1.86	<0.10
R7	0.05	0.66	<0.10
R8	<0.05	0.62	<0.10
R9	0.13	1.72	<0.10
R10	0.11	1.47	<0.10
R11	0.07	2.24	<0.10
R12	<0.05	0.57	<0.10
R13	<0.05	0.60	<0.10
R14	<0.05	0.83	<0.10
R15	<0.05	<0.23	<0.10
R16	<0.05	<0.23	<0.10
R17	<0.05	<0.23	<0.10
S1	0.07	0.90	<0.10
S2	<0.05	2.26	<0.10
S3	0.34	3.99	<0.10
S4	0.34	3.18	0.10
S5	0.56	6.34	0.12
LOD	**0.05**	**0.23**	**0.10**

App. 10: Trace elements in the soil and rock samples.

Sample	Sc [mg/kg]	V [mg/kg]	C [mg/kgr]	Mn [mg/kg]	*Co* [mg/kg]	Ni [mg/kg]	Cu [mg/kg]	Zn [mg/kg]	Ga [mg/kg]	As [mg/kg]	Rb [mg/kg]	Sr [mg/kg]	Y [mg/kg]	Zr [mg/kg]
R1	9	44	38	1533	11	20	11	138	28	4.6	119	160	91	624
R2	10	44	37	1832	10	20	12	148	30	2.8	124	148	104	681
R3	11	66	50	2591	15	27	11	143	31	7.9	137	86	65	726
R4	13	64	47	2177	12	30	10	165	35	3.6	147	111	67	766
R5	9	49	24	2469	15	31	11	131	28	6.1	125	147	85	566
R6	8	61	31	4747	16	27	13	144	27	7.5	115	167	96	585
R7	11	68	51	3971	18	21	10	130	27	8.7	103	124	71	718
R8	11	70	54	2160	14	22	10	143	30	8	119	95	79	811
R9	12	69	54	2861	16	27	12	138	29	7.7	140	115	75	719
R10	12	67	52	2735	15	29	12	144	30	6.9	146	116	75	741
R11	10	64	49	2626	15	25	10	129	27	6.1	129	167	76	652
R12	15	98	58	1244	19	26	16	178	33	7.7	102	147	96	845
R13	12	58	47	2216	14	28	11	163	32	5.6	151	71	62	729
R14	10	61	45	1656	14	27	12	159	31	7.2	144	95	74	704
R15	10	109	46	19671	43	80	15	118	28	11.6	125	68	30	654
R16	7	24	5	1986	14	12	3	104	27	3	108	81	26	479
R17	8	80	34	11630	39	53	9	97	24	9	105	76	23	502
S1	11	60	50	2059	12	28	12	167	32	7.3	143	64	76	790
S2	8	51	38	2652	13	25	10	142	27	6.6	118	165	87	591
S3	12	68	48	774	13	32	17	187	36	3.4	114	78	57	848
S4	12	64	46	719	14	37	20	196	38	5.5	118	61	50	889
S5	11	59	40	863	13	33	16	181	32	5.3	102	55	65	756

App. 10: Trace elements in the soil and rock samples (LOD =limit of detection) (continued)

Sample	Nb [mg/kg]	Mo [mg/kg]	Cs [mg/kg]	Ba [mg/kg]	La [mg/kg]	Ce [mg/kg]	Nd [mg/kg]	Sm [mg/kg]	Hf [mg/kg]	W [mg/kg]	Pb [mg/kg]	Th [mg/kg]	U [mg/kg]
R1	161	**1**	**<LOD**	309	201	208	105	14	7	*39*	30	20	7.1
R2	177	**2**	**4**	306	243	236	132	21	8	*33*	32	21	8.2
R3	184	**3**	**5**	384	184	292	90	7	9	*43*	35	22	4.7
R4	190	**3**	**4**	305	178	285	95	9	16	*45*	34	22	6.1
R5	174	**1**	**8**	600	323	390	151	18	9	*35*	31	21	3.4
R6	160	**2**	**7**	735	242	545	138	14	11	*35*	32	18	4.3
R7	169	**2**	**4**	502	205	346	105	10	9	*52*	36	22	5.7
R8	207	**2**	**7**	345	208	324	119	16	14	*47*	37	26	6.2
R9	167	**1**	**8**	432	189	308	103	11	11	*34*	35	22	4.8
R10	172	**<LOD**	**4**	401	183	288	97	11	11	*35*	34	23	3.8
R11	152	**1**	**3**	432	171	270	97	12	8	*33*	32	20	5.1
R12	204	**2**	**7**	419	283	379	153	22	11	*35*	37	24	6.3
R13	183	**2**	**5**	316	152	263	78	12	13	*31*	35	21	4.7
R14	183	**2**	**4**	235	192	318	100	11	12	*31*	37	22	4.1
R15	191	**9**	**35**	2341	171	1181	63	2	12	*67*	58	22	5.1
R16	186	**<LOD**	**2**	754	105	116	34	3	7	*26*	34	20	2.2
R17	169	**8**	**8**	1467	121	685	44	3	6	*56*	51	19	4.2
S1	206	**2**	**7**	323	193	305	102	13	10	*28*	36	24	5.4
S2	156	**1**	**7**	351	197	251	101	14	10	*29*	32	18	5.3
S3	211	**3**	**3**	343	160	207	81	13	14	*26*	34	23	4.4
S4	219	**3**	**2**	300	144	175	71	9	15	*26*	33	24	5.3
S5	183	**3**	**5**	273	153	219	92	9	11	*22*	31	20	5.2

App. 11: Secondary data of surface water and groundwater, location, coordinates, source, depth, static water level, and altitude.

UID	Name and code	Location	X	Y	Source	Depth [m]	SWL [m]	Altitude [m]
EGW1	C38		0.39997	36.5332	WRMA	186	23	1890
EGW2	R. Catholix Mission CDN D139	Catholic Mission	0.27	36.53694	Well Drilling			
EGW3	C40Sosian	Sosian Ranch	0.216686	36.6332	WRMA	152	57	1859
EGW4	C101		0.183287	36.5167	WRMA	112	55	1935
EGW5	C342Narok Ranch	Narok Ranch	0.433271	36.5667	WRMA			
EGW6	C515		0.116692	36.7500	WRMA			
EGW7	C913Sipili		0.410765	36.3745	WRMA			
EGW8	C932		0.033294	36.7167	WRMA			
EGW9	C876		0.116694	36.7833	WRMA			
EGW10	C1143		0.08329	36.6333	WRMA			
EGW11	C-1646Narok Ranch	Narok Ranch	0.549968	36.6167	WRMA			
EGW12	C-1663		0.549961	36.6000	WRMA	132	47	1853
EGW13	Dip 1819	Ol Maisor	0.44089	36.6146	Well drilling			
EGW14	C1008		0.116691	36.6333	WRMA	203	40	1920
EGW15	C1684		0.33328	36.7167	WRMA	123	123	1795
EGW16	C1698		0.299978	36.6000	WRMA	76	6	1830
EGW17	C1705		0.299977	36.6333	WRMA	62	39	1830
EGW18	C1767		0.149993	36.6333	WRMA	127	24	1951
EGW19	C1792		0.19999	36.6333	WRMA	101	56	1913
EGW20	C1832		0.516665	36.5667	WRMA	250	31	1935
EGW21	C1845		0.483267	36.7000	WRMA	177	50	1830
EGW22	C-1957		0.366674	36.7167	WRMA	136	49	1768
EGW23	C2027		0.49992866	36.76638	WRMA			
EGW24	Sosian Ranch C 12677	Sosian Ranch	0.55529	36.62372	Well Drilling			
EGW25	C-2381		0.133293	36.4167	WRMA	159.4	23.8	2134
EGW26	C-1921		0.349975	36.5666	WRMA	220	28	1844
EGW27	C2676KirumunSosian		0.666656	36.8666	WRMA			
EGW29	C2727Kirumun	Kirumun	0.34998	36.5167	Well Drilling	179	60	2118
EGW30	C-1663		0.549961	36.6000	WRMA			
EGW31	2805NarokRanch	Narok Ranch	0.483272	36.5832	WRMA			
EGW32	C2858Tfalls	Thomsan Falls	0.133291	36.3999	WRMA	106.1	12.2	2133
EGW33	2889KifukuEstate	Kifuku Estate	0.216685	36.56667	Well Drilling			1829
EGW34	2895Mawe	Ol Maisor	0.40824	36.62259	Well Drilling	121.9	74.2	1829
EGW35	C3054		0.199991	36.4000	WRMA	91.4	21	570
EGW36	C-3057		0.583264	36.5833	WRMA	193.6	64	1860
EGW37	C-3098		0.433272	36.5167	WRMA	243	56	1951
EGW38	C-3200		0.566666	36.6667	WRMA	138	35	1853
EGW39	C-3201		0.533268	36.7500	WRMA	160	45.7	1831
EGW40	C3215		0.483273	36.7167	WRMA	198	3 then 9	1829
EGW41	C-3761		0.433276	36.5000	WRMA	247	115.2	1981
EGW42	C-9373		0.199357	37.7789	WRMA	140	48.71	2021
EGW43	C-9372		0.019411	37.77833	WRMA	200	43.64	2020
EGW44	ShivaBH2	Shiva Farm	0.22991666	36.46672	Well Drilling			
EGW45	KiharaC2895	Ol Maisor	0.40824	36.62259	Well Drilling			
EGW46	NyingamaOlMaisorC2280	Ol Maisor	0.51082	36.60472	Well Drilling	110.3	48.8	1856
EGW47	Kifuku 009A	Kifuku Estate	0.20006472	36.5835	Well Drilling			
EGW48	C39		0.199984	36.6499	WRMA	69	56	1859
EGW49	Manhouse	Ol Maisor	0.4147	36.65713	Well Drilling			
EGW50	familia Takatifu TREATED	Tafitku	0.26866	36.54019	WRMA			
EGW51	familia Takatifu Raw	Tafitku	0.26866	36.54019	WRMA			
EGW52	C-3098		0.433272	36.5167	Well Drilling			
EGW53	Farm A (2014) report		0.221477	36.4715				
EGW54	Farm A (2014) report		0.227416	36.4805				
EGW55	NAROK2805	Narok Ranch	0.483272	36.5833	WRMA	194	49	1890
EGW56	Narok Ranch1646	Narok Ranch	0.549968	36.616677	WRMA			
EGW57	1699		0.299978	36.6000	WRMA	85	7	1830
EGW58	Mpala GW-978	Mpala	0.334507	36.8654	Mpala report			
EGW62	296Mutara Farm	Mutara Farm	0.099994	36.7500				
EGW63	297Mutara Farm	Mutara Farm	0.199984	36.7167				
EGW66	SouthAiyamSpring		0.433272	36.5167				

App. 11: Secondary data of surface water or groundwater, location, coordinates, source, depth, static water level, and altitude (continued).

UID	Name and code	Location	X	Y	Source	Depth [m]	SWL [m]	Altitude [m]
EGW67	MutangaSpring		0.40138888	36.47833				
EGW68	RumurutiParishosmosis	Rumuruti Parish	0.43124	36.68181	Well Drilling			
EGW69	C2259Sosian	Sosian Ranch	0.616659	36.8000				
EGW70	UnderRAAAGrowers	AAA Growers	0.18692	36.44387	Well Drilling			
EGW71	BHoleAAAG15	AAA Growers	0.18692	36.44387	Well Drilling			
EGW74	C932MutaraFarm	Mutara Farm	0.033294	36.7167				
EGW75	HouseOlMaisor07	Ol Maisor	0.4147	36.65713	Well Drilling			
EGW76	AroundOlMaisor07	Ol Maisor	0.4147	36.65713	Well Drilling			
EGW77	C337Rumuruti		0.604007	36.6832				
EGW78	C3413		0.699953	36.7500				
EGW79	C20860Shiva	Shiva Farm	0.227415	36.80465				
EGW80	C1819OlMaisor	Ol Maisor	0.449973	36.6167		180	76	1905
ESF1	familia Takatifu Raw	Tafitku	0.26866	36.54019	WRMA			
ESF2	familia Takatifu Treate	Tafitku	0.26866	36.54019	WRMA			
ESF3	5AC15 Ewaso Narok SW		0.25853	36.53815	WRMA			
ESF4	5AC10 Ewaso Narok SW		0.4375	36.7239	WRMA			
ESF5	Jessel Surguroi		0.243199	36.8482				
ESF6	Nyanja source		0.336211	36.8851				
ESF7	RiverWaterAAA	AAA Growers	0.18692	36.44387	Well Drilling			
ESF8	DamwaterAAAG13	AAA Growers	0.18692	36.44387	Well Drilling			
ESF9	5AA17 Ewaso Narok SW	NYAHURURU NEAR HIPPO POOL	0.26866	36.54019	WRMA			

App. 12: Water quality data from secondary sources.

Well Name	Date sampling	Well Code	EC [µS/cm]	pH [-]	DO [%]	Fe^{2+} [mg/l]	Mn^{2+} [mg/l]	Mg^{2+} [mg/l]	Na^{+} [mg/l]	K^{+} [mg/l]	Ca^{2+} [mg/l]	PO_4^{3-} [mg/l]	SiO_2 [mg/l]	NH_4^{+} [mg/l]
Sosian Rumuruti	2004	C-12677	136	9.4		0.1	0.1	0.3	299	8	1		41	
Sosian Rumuruti	1996	C-12677		8.5		0.03	0.01	2.5	166	12	6,5		55	
Sosian Nyeri	1999	CDN D192	132	8.6		0.4	0.1	7.9	300	10.7	33		25	
Ol Maisor	2007	House	1781	9.38		0.7	0.03	0.32	281.5		0.94			
Ol Maisor	2007	Around	176	9.3				2	287		4		50	
Ol Maisor	2008	House	1661.6	9.6		197	20		398.4	8.7	0.7			
Ol Maisor	2008	Around	1805.4	8.9		212.6	8		405.3	5.9	1.8			
Shiva Farm BH2	2013	C-20860	420	7.2		0.04		0.97	78.8	2	0.8			
Kifuku	2013	Warma 009A	749	7.19		0.04	0.2	24.28	23.9	32	40.04	0.24	77	
Kifuku Estate		2889		7.5		15							260	
AAA Growers	2012	Under R.	260	7.27		0.78	1.43	4.07	31	11.4	17.8	0.03	15	0.01
AAA Growers	2015	B Hole	820	8.58		0.08		0.29	146	4.4	1,72	0.13	9.23	0.01
AAA Growers	2012	B Hole	690	8.27		0.11		0.34	174	5.44	1,87	0.14	5.01	0.022
AAA Growers	2013	Dam water	190	7.64		3.14	0.13	1.96	30.2	6.21	7.86	0.01	19.7	0.01
AAA Growers	2014	Dam water	210	8.76		0.93	0.24	5.7	41.7	7.7	24.5	0.068	15.8	0.067
AAA Growers	2015	Dam water	160	7.52		1.35	0.24	1.88	23.6	6.44	7.5	0.07		0.01
AAA Growers	2012	River Water	160	8.08		1.09	0.016	1.41	21.9	5.87	5.58	0.05	9.49	0.01
AAA Growers	2011	River Water	200	7.34		2.93	0.01	1.77	23.46	5.45	7.14	0.33	23.19	1.5
Rumuruti Mission	2000	CDN D139	72	9,3		3.3		0.1	208	3,1	1.3		18,1	
Rumuruti Mission	1998	CDN D139	620	8,6		0.3		1.2	223.2	7,5	10		10	
Rumuruti Parish	2014	Rumuruti Parish	158	9.1				1	268					
Nyingama- Ol Maisor	1969	Nyingama- Ol Maisor		7.8		0.1			148	14	20		40	
Kihara	1995	Kihara		7.7		0.1		3	192	15	13		35	
Sosian Armstrong		C 40												
Sosian LTD		C 3413												
CURRY B.H.	11/1/1985	C 296 Mutara Ranch	860	7.9		0.1	0.01	22			28			
Curry B.H.	11/1/1985	C297 Mutara Ranch	700	8.3		0.49	0.01	15			28			
Capt. Mills	3/25/1986	C342 Narok Ranch	799	8.3		0.3	0.02	1.7	160	13	0.02			
Edwards W.G.	1/11/1986	C 1646 Narok Ranch	560	8		0.1	0.1	2.5	130	17	5.9			
Ol Mzsor C Rumuruti LR. 2440	3/25/1986	C 1819 Ol Maisor	1960	9		0.3	0.01	0.1	370	13	1.1			
Edwards W.G.	3/26/1986	C 2259 Sosian	747	8.6		1	0.05	0.2	159	2.2	0.5			
Narok Estate LTD	3/26/1986	C2805 Narok Ranch	890	8.9		0.2	0.01	0.2	180	5	0.9			
Ol Myson	7/20/1986	C2895 Ol Maisor	1355	7.4		0.6	0.02	2.5	200	15	4.3		40	
Ol Mysor Rumuruti	before 86	2280	730	8.6		0.1	0	1.9	164	9.2	12.8		25	
Meyler RE ESQ	before 86	2858		7.3		0.7							50	
Meyler RE ESQ	after 86	C2858 Sironi	235	7,7		0.7	0,23	1,6	67	11.4	2.5			
Meyler RE ESQ	after 86	C2858 Sironi	230	7,9		0.5	0,01	1,4	59	8.4	2.6			
Meyler RE ESQ	after 86	C 2889 Kieni Farm	860	8,3		0.4	0,01	1,9	190	15.6	4.4			
Lerematesо LTD	before	3761	645	9		6		0	36	11	4			
C913	before	C913	650			0.1	0.1	1.1			4.6			
C913 Sipili	after 85	C913 Sipili	800	8.8		0.2	0.01	1			2.4			
C 337 Rumuruti	after 85	C 337 Rumuruti	500	8.5		0.1	0.01	10.7			25			
C 2676 Kirumun	after 86	C 2676 Kirumun	1220	7.6		0,4	0.01	8.3	170	24	14			
C932 Kiboke Farm	after 85	C932 Kiboke Farm	670	8.9		0,18	0.01	14.8			21			
C 2259 Sosian	after 86	C 2259 Sosian	747	8.6		1	0.05	0.2	159	2.2	0.5			
South Aiyam Spring	after 85	South Aiyam Spring	335	8.7		0.4	0.01	8			0.4			
Mutanga Spring	after 85	200		7.2		0.5	0.01	3.9			5.6			

App. 12: Secondary data water quality (continued).

Well Name	UID	Date sampling	EC [µS/cm]	T. [°C]	pH [-]	DO [%]	Fe^{2+} [mg/l]	Mn^{2+} [mg/l]	Mg^{2+} [mg/l]	Na^{+} [mg/l]	K^{+} [mg/l]	Ca^{2+} [mg/l]	PO_4^{3-} [mg/l]	SiO_2 [mg/l]	NH_4^{+} [mg/l]
Familia Takatifu (TREATED) GW	EGW50	11/18/2010	65		6.8		0.01	0							
		8/23/2011	30.8	16.1	8.2				10.20			1.6032	1.4		
		11/16/2011	67.9	21.3	7.5				5.3			0			
		6/18/2012	126.4	19.8	8.56				0.5			0			
		9/11/2012	34.4	21.2	8.81										
		14/11/2012	31.3	21.4	6.9				0.97			0.8			
		13/6/2013	56	20.1	7.0										
		14/11/2013	166	19.2	8.2	4.3			0			0.0			
		11/03/14	161	19.9	8.3	4.7			1.9			0			
		11/06/14	47.0	16.6	9.0				0.96			0			0.01
familia Takatifu (RAW) GW	EGW51	11/18/2010	756		8.7		0.1	0.001							0.01
		6/20/2011	908	17.1	9.1				4.4			8			0.022
		8/23/2011	948	16.2	9.2				13.60			3.2064			0.01
		11/16/2011	887	21.3	8.8				1.5			1.6			0.067
		6/18/2012	890	19.6	8.9				1			1.6			0.01
		9/11/2012	851	21	8.79										0.01
		14/11/2012	886	21.4	8.96				0.49			1.6			1.5
		13/6/2013	798	20	8.9										
		14/11/2013	828	19.3	8.7	5			2.4			1.6			
		11/03/14	786	19.8	8.2	4.6			3.9			0			
		11/06/14	866.0	16.4	9.1				0.96			0			
5AC15 Ewaso Narok SW	ESF3	11/08/2010													
		3/29/2011							5.34			13.6			
		6/20/2011							5.832			10.42			
		8/23/2011							16.03			7.214			
		3/26/2012													
		5/11/2012							4.4			4			
		9/11/2012													
		14/11/2012							1.9			10.4			
		14/11/2013							6.8			12.0			
		24/11/2013							6.3			13.6			
		26/02/2014							5.8			11.2			
		11/06/2014							1.46			10.42			
5AA17 Ewaso Narok SW	ESF9														
familia Takatifu (TREATED)	EGW50	2014	104	16.6	9.0	4.7	0.01		1.9			1.2	1.4		
familia Takatifu (RAW)	EGW51	2014	866	16.4	9.1	4.8	0.1	0.001	3.53			2.93			
5AC15 Ewaso Narok SW		2014	173	21.7	7.6	5.2	0.01	0.01	5.8			10.42			
5AC10 Ewaso Narok SW	ESF4	2014	203.3	16.4	7.6				3.4			16.83			
5AA17 Ewaso Narok SW		2014	200.6	20.4	7.4	5.1			4.665			17			
Mpala GW-978		2010	1710		8.4		0.4	0.1	8	266	7.20	4			
Jessel Surguroi		2010	1432		8.5		0.01	0.01	1.46	324	1.2	0.8			
Ewaso Ngiro Road Bridge		2010	170		7.74		1.44	0.03	4.31	17.1	3.98	12.02			
Nyanja source		2010	110		8.54		10.22	0.08	2.44	16	5.8	5.01			
Nanya Dam		2012	350		6.5										

App. 12: Secondary data water quality (continued).

Well Name	UID	HCO_3^- [mg/l]	Cl^- [mg/l]	NO_3^- [mg/l]	SO_4^{2-} [mg/l]	F^- [mg/l]	Br^- [mg/l]	NO_2^- [mg/l]	Al^{3+} [mg/l]	Cu^{2+} [mg/l]	TDS [mg/l]
Sosian Rumuruti		455	112		62	12					990
Sosian Rumuruti			33.00		18	0.8					287
Sosian Nyeri			185		61	5					628
Ol Maisor			180	0.72	69	10					1104
Ol Maisor		591	242		39	14					1229
Ol Maisor			195	13	82	10.5		0.33	109.1	4	9
Ol Maisor			309	84	158	3		1.61	12.3	4.70	624
Shiva Farm BH2			20	3		5					110
Kifuku			45.41	1,5		1.18		0.00		0.01	244
Kifuku Estate		3650	580		280	2.5					6150
AAA Growers		147	9.33	0.08	3.37			0.37			227
AAA Growers		285	73	1.35	47	1.39		5.98			565
AAA Growers		332	49	0.14	28	1.49		0.64			591
AAA Growers		97	10	0.21	1.76			0.94			160
AAA Growers		138	11	0.01	4			0.01			233
AAA Growers		91	6.75	0.09	2.69			0.38			142
AAA Growers		99	7.38	0.01	0.54			0.01			143
AAA Growers		83	6	0.15							132
Rumuruti Mission			62		31	5.08					310
Rumuruti Mission			65		70	4					374
Rumuruti Parish		679				8					956
Nyingama- Ol Maisor		330	74	2	25	2					655
Kihara		404	92	1.30	30	1					786
Sosian Armstrong											0
Sosian LTD											0
CURRY B.H.		380	76		37	1.2					516
Curry B.H.		374	48		15.7	1.4					420
Capt. Mills		326	38	0.07	19	2.1					479
Edwards W.G.		192	35	0.63	11	0.4					336
Ol Mysor C Rumuruti LR.		200	324	0.07	166	3.6					1176
Edwards W.G.		258	59	0.02	20	1.6					448
Narok Estate LTD	C2805 Narok	290	79	0.08	32	0.55					534
Ol Myson	C2895 Ol Maisor	414	27	0.9	25	1.2					813
Ol Mysor Rumuruti LR.	2280	314	30		12.5	1.5					500
Meyler RE ESQ	2858		13		0	0.2					250
Meyler RE ESQ	C2858 Sironi	157	12	0,02	2,3	0,29					200
Meyler RE ESQ	C2858 Sironi	154	12	0,03	1,7	0,27					200
Meyler RE ESQ	C 2889 Kieni Farm	368	53	0,08	23	2.6					516
Lerematesо LTD		285	29		25	4.3					326
C913			1								397
C913 Sipili		330	11		5.6	0,4					480

App. 12: Secondary data water quality (continued).

Well Name	UID	HCO_3^- [mg/l]	Cl^- [mg/l]	NO_3^- [mg/l]	SO_4^{2-} [mg/l]	F^- [mg/l]	Br^- [mg/l]	NO_2^- [mg/l]	Al^{3+} [mg/l]	Cu^{2+} [mg/l]	TDS [mg/l]
C 337 Rumuruti		260	18		11	1,8					300
C 2676 Kirumun		216	95	0.1	69	0.85					732
C932 Kiboke		304	33		20	1.3					402
C 2259 Sosian		258	59	0,02	20	1.6					448
South Aiyam Spring		200	12		1,8	0,25					201
Mutanga Spring		94	19		9,3	0,47					120
Familia Takatifu (TREATED) GW	EGW50		18		3	0.95		0.09			40
			13								20
			6								4
			24		4						82
			7								34
			4		4						20
			7		2						36
			17		5						108
			10		3						105
			6		2						31
	RUMURUTI ON		19	9.2	14.1	0.50		0.22			112
	AT SOSIAN		18		14.7						132
Familia Takatifu (RAW) GW	EGW51				18	10		42			468
			72	1	0						589
			84		7						616
			66								577
			136		25						579
			21								553
			60		31						576
			9		28						519
			64		22						538
			65		23						511
			70		35						563
5AC15 Ewaso Narok SW	ESF3		40		3			0.43			144
			10	4	1	0.50		0.01			149
			15	1	1						126
			19								70
			12								128
			14		2						137
			6								97
			18		1						158
			2		6						63

App. 12: Secondary data water quality (continued).

Well Name	UID	HCO_3^- [mg/l]	Cl^- [mg/l]	NO_3^- [mg/l]	SO_4^{2-} [mg/l]	F^- [mg/l]	Br^- [mg/l]	NO_2^- [mg/l]	Al^{3+} [mg/l]	Cu^{2+} [mg/l]	TDS [mg/l]
5AC15 Ewaso Narok SW	ESF3		17		10						120
			15		9						104
			19		2						132
			15		16						118
Familia Takatifu (TREATED) GW	EGW50		8		2.4	0.95		0.09			68
Familia Takatifu (RAW) GW	EGW51		70	1.0	35.4	10		0.42			563
	NYAHURURU NEAR HIPPO POOL		16		36.5						131
	Mpala GW-978	492	222	1.2	117	29		0.01			112
	Jessel Surguroi	181	235	2.5	134	18		0.01			1242
	Ewaso Ngiro Road	79	6.3	0.1	3.0	0.34		0.03			72
	Nyanja source	54	5.2	0.0	3.0	0.11		0.01			48
	Nanya Dam										990

App. 13: Elaboration on the use of data.

Regarding EGW50 and EGW 51: Information of quality was available from 2010-2014, the most recent was used. There was no significant difference with the previous read.

For 1GW, 49GW, 50GW, and 44GW, the following averages were used:

	Well 1	Well 49	Well 50	Well 44
Sampled	GW1	GW49	GW50	GW44
Literature	EGW70	EGW13	EGW27	EGW34
Average of both sampled and literate is used in MCM and is donated as	1XGW	49XGW	50XGW	44XGW

App. 14: Mixing cell model (MCM) input data.

Location	EC [µs/cm]	Fe^{2+} [mg/l]	Mn^{2} [mg/l]	Mg^{2+} [mg/l]	Na^{+} [mg/l]	K^{+} [mg/l]	Ca^{2+} [mg/l]	PO_4^{3-} [mg/l]	SiO_2 [mg/l]	NH_4^{+} [mg/l]	HCO_3^{-} [mg/l]	Cl^{-} [mg/l]	NO_3^{-} [mg/l]
GW1	272	0.4	0.3	3	30	14.4	19.5	0.16	11.2	3.5	153.7	7.4	1.8
GW4	934	0.005	0.06	21.8	123	15.5	46.5	0.01	19.1	5.3	329.9	76.2	34.2
GW7	1010	0.005	0.08	6	185	14.4	19	0.16	15.8	1.8	384.4	107.7	9.1
GW9	1515	0.005	0.05	8.8	269	8.3	37	0.16	16.3	3.5	671.9	139.5	21.2
GW10	1342	0.005	0.06	16.2	215	20.1	44	0.07	19.6	5.3	670.3	91	23.1
GW14	1418	0.7	0.07	6.3	314	10.2	26.5	0.99	12.8	0	677.3	32.3	2.3
GW17	1583	0.005	0.02	1.3	310	5	2.7	0.78	3.2	0	469.9	144.6	0
GW18	966	0.005	0.03	1.2	210	5.4	5.4	0.46	4.2	0	372.2	72.6	0
GW19	1229	0.005	0.05	0.3	251	4	1.8	0.79	3.1	0	450.2	80.3	0
GW23	961	0.005	0.03	1.1	210	7.2	5.4	0.36	9.9	0	360.7	48.8	65
GW24	574	0.17	0.04	0.8	145	8	3.8	0.39	6.4	0.9	323.4	18.2	10
GW27	1212	0.005	0.07	0.9	241	11.3	4.1	1.1	16.3	0.9	512.6	80.3	3.5
GW30	1934	0.005	0.02	1	364	8.2	6.1	0.38	4.3	0	402.7	223.5	2.6
GW31	285	0.36	1.8	2.6	42	8.9	13.3	0.42	4.4	0	61.1	24.8	0.9
GW32	365	0.16	0.3	4.1	21	16.2	25.4	0.78	4.5	7.9	80.6	43.5	1.6
SF2	290	0.37	0.16	3.1	38	8.5	13	0.64	10.9	1.8	126.9	20.6	0.9
SF3	121.5	0.78	0.07	1.3	15.8	6	5.6	0.4	7.5	2.6	64.7	7.8	2.1
SF6	114.9	0.68	0.23	2.1	14.2	3.8	8.2	0.55	8.78	5.3	56.1	9.5	0
SF8	288	4.4	1.2	2.5	33	10.6	11	0.72	5.82	5.3	104.9	23.2	0
SF12	242	1.2	0.9	3.5	30	4.2	17.5	0.98	16.1	7.9	105.1	18.1	0
SF13	217	0.8	0.23	3.3	24	3.5	12	0.52	7.24	2.6	88.9	11.4	0
SF15	146.1	0.8	0.14	1.4	17.4	16.9	6.7	0.49	6.34	2.7	57.8	9.2	3.9
SF16	123.2	0.5	0.08	1.2	16.2	6.5	5.6	0.34	8.1	4.4	68.3	11.2	2.1
SF20	216	0.9	0.12	2.2	26.7	10.5	0.9	0.52	6.5	7.1	84.2	16.2	0
SF21	1697	0.4	0.55	2.7	316	20.1	15	1.9	8.4	0	605.5	123.2	0
SF22	203	0.92	0.43	2.1	26.7	9.1	9.7	0.68	7.1	3.5	82.9	30	0
SF25	218	1.3	0.5	2.3	18.2	8.2	9.8	1.5	9.5	1.8	42.7	8.4	1.7
SF26	570	0.9	0.3	2.5	15.1	8.6	10.4	1.3	6.2	1.8	67.8	11.1	0
SF28	185	1.8	0.14	1.7	23.3	6	8	0.26	7.4	22	76.9	8.9	0
SF29	316	0.84	0.46	3	42	21.3	15.5	0.4	7.3	3.5	152.6	21.4	1.1
SF33	137.1	0.85	0.19	2.1	16.1	8.4	9.1	0.6	8.1	3.5	68.8	9.1	0.2
SF34	117.8	0.92	0.3	1.8	8.5	5.8	8.2	1.2	8.1	30.8	51.1	5.2	0.2
SF35	94.3	1.1	0.35	2	9.2	7.5	8.5	1.82	9.2	4.4	51.5	4.9	0.3
SF36	196.6	1.4	0.22	2.2	30	20.4	9.7	0.45	7.1	1.8	96.4	22.2	0
SF37	193.2	1	0.4	2.5	23	12.8	12.5	0.06	11.5	3.5	84.2	30.2	0.8
SFS11	513	0.013	0.8	7.1	42	15.8	27	0	10.5	6.2	87.9	82.9	6.4

App. 14: Mixing cell model (MCM) input data (continued).

Location	EC [µs/cm]	Fe^{2+} [mg/l]	Mn^{2} [mg/l]	Mg^{2+} [mg/l]	Na^{+} [mg/l]	K^{+} [mg/l]	Ca^{2+} [mg/l]	PO_4^{3-} [mg/l]	NH_4^{+} [mg/l]	HCO_3^{-} [mg/l]	Cl^{-} [mg/l]	NO_3^{-} [mg/l]
Cell1	264.91	0.96	0.28	2.58	24	10.72	6.06	0.69	4.58	79.66	23.35	2.31
Cell1_1	160.88	0.52	0.16	2.43	21.75	10.75	5.75	0.69	4.40	73.34	12.72	3.04
Cell1_2	180.73	0.77	0.21	1.83	23.2	8.7	5.4	0.51	4.99	78.51	13.7	0.7
Cell1_3	219.5	0.96	0.42	2.78	26.85	6.83	10.03	0.68	5.28	90.32	18.93	0
Cell2	151.43	1.03	0.31	2.19	17.55	10.44	10.13	0.60	6.60	64.70	14.89	0.59
Cell2_1	151.43	1.03	0.31	2.19	15.77	9.01	10.13	0.30	3.14	64.70	7.7	0.33
Cell2_2	113.65	0.97	0.31	2.03	12.03	7.38	9	1.03	10.34	60.33	6.4	0.53
Cell2_NF	150.5	1.06	0.24	2.03	18.2	11.53	9	0.75	12.03	72.08	12.17	0.133
Cell3	149.1	1.2	0.14	2	19.6	7.3	8.25	0.47	7.92	85.81	11.6	0.45
Cell4	163.8	1.1	0.13	1.9	16.2	5.7	8.6	0.72	1.76	68.81	8.3	0.9
Cell4_NF	183.55	1.1	0.13	2.65	16.2	5.7	12.72	0.72	1.76	68.81	13.15	0.9
EGW50	104	0.01		1.9			1.2	1.4			8	
EGW51	866	0.1	0.001	3.53			2.93				70	1
ESF3	173	0.01	0.01	5.8			10.42				19	9.2
GW41	464	0.03	0.05	5	57	22.1	18.6	0.02	3.52	194.75	11.5	19.4
GW44	1345	0.01	0.01	0.9	228	5.8	4.2	0.25	0	305.12	163.8	21.1
GW45	1986	0.005	0.05	1	412	14.6	2.8	0.34	0	726.13	192	7.7
GW46	2050	0.005	0.02	33.5	241	18.6	94	0.02	10.56	508.91	248.3	193.4
GW47	1594	0.005	0.01	0.8	304	7.5	3.3	0.38	0	523.62	137.7	0
GW49	2006	0.1	0.08	0.3	398	19.9	2.8	0.07	0	386.87	253	67.2
GW50	1863	0.005	0.08	23	210	30.3	121	0.09	17.60	695.35	132.1	33.4
GW52	1447	0.007	0.02	18.2	213	22.6	49	0.05	14.96	436.98	119.3	73.2
SF38	164	1.1	0.3	2.4	22	11.7	11.7	0.08	2.64	63.46	28.2	0.5
SF39	203	0.9	0.35	2.3	17.3	9.1	11.1	0.08	3.52	77.35	12.9	1.3
SF40	105.4	1	0.4	2.2	14.3	7.8	10.2	0.5	2.64	70	6.4	1.4
SF42	165.1	1.3	0.18	2	21	6.2	8.4	0.51	13.20	85.43	9.7	0.5
SF43	133.1	1.1	0.1	2	18.2	8.4	8.1	0.42	2.64	86.19	13.5	0.4
SF48	163.8	1.1	0.13	1.9	16.2	5.7	8.6	0.72	1.76	68.81	8.3	0.9
SF51	395	1.9	0.6	4.3	11.8	8.7	24	0.17	105.62	100.22	7.8	1.6
SF53	128.8	0.7	1	2.9	12.1	8	17	1.24	6.16	80.88	7.2	1.4

App. 14: Mixing cell model (MCM) input data (continued).

Location	SO_4^{2-} [mg/l]	F^- [mg/l]	Al^{3+} [mg/l]	Cu^{2+} [mg/l]	Zn^{2+} [mg/l]	SiO_2 [mg/l]	TDS [mg/l]	^{18}O [‰ VSMOW]	^{2}H [‰ VSMOW]	Sr^{2+} [mg/l]	T [°C]	pH [-]	Redox [mV]	As^{3+} [mg/l]
GW1	4.1	0.9	1	0.005	0.011	2.14	201.14	-1.67	-1.17	0.5	24.8	7.2	265.8	0.005
GW4	45.5	1	0.019	0.005	0.2	0.04	659.99	-2.88	-12.93	0.5	21.9	7.7	241.9	0.005
GW7	54.9	1.6	0.008	0.005	0.01	0.02	800.84	-3.37	-18.71	0.5	25.5	7.7	160.6	0.005
GW9	72	1.8	0.018	0.9	1	0.04	1259.93	-2.57	-10.40	0.5	25.3	7.6	186.8	0.005
GW10	53.2	1.7	0.018	0.005	0.062	0.04	1178.63	-2.50	-12.85	0.5	22.2	7.4	193.4	0.005
GW14	79.1	15.2	1.6	0.005	0.008	3.42	1179.13	-1.67	-3.52	0.5	20.3	8.4	110	0.005
GW17	49.7	19.01	0.029	0.005	0.005	0.06	1007.72	-3.72	-15.01	0.5	21.5	9.1	141.2	0.01
GW18	32.8	4.3	0.036	0.005	0.005	0.08	709.57	-3.76	-16.10	0.5	25.2	9.2	125	0.005
GW19	27.9	7.82	0.04	0.005	0.008	0.09	988.18	-3.16	-13.59	0.5	27.5	9.3	98.8	0.007
GW23	17.2	1.7	0.012	0.005	0.005	0.03	698.21	-2.82	-15.37	0.5	24.5	8.8	160.4	0.005
GW24	7	1.3	0.03	0.005	0.063	0.06	525.88	-3.52	-12.95	0.5	23.2	8.1	163.6	0.005
GW27	27.9	2.6	0.014	0.005	0.005	0.03	904.13	-3.22	-16.23	0.5	27.8	8	171	0.005
GW30	98.6	9.12	0.028	0.005	0.005	0.06	1122.38	-3.15	-15.24	0.5	26.5	8.7	99.6	0.007
GW31	41.5	0.3	0.8	0.005	0.1	1.71	202.86	-0.39	6.25	0.5	26.6	5.6	91.2	0.005
GW32	7.2	13.3	1.3	0.005	0.07	2.78	227.01	-1.41	2.95	0.5	17.4	7.3	197.1	0.005
SF2	6.3	0.2	1	0.005	0.009	2.14	231.85	-2.40	-4.43	0.5	23.3	8.1	191.7	0.005
SF3	3.7	0	0.6	0.005	0.01	1.28	118.94	-1.43	-2.66	0.5	19.9	7.9	188.8	0.005
SF6	5.7	0.3	1	0.005	0.01	2.14	115.99	-3.28	-7.60	0.5	17.1	6.9	214.2	0.005
SF8	5.6	0.3	1.3	0.006	0.02	0.64	209.17	-0.28	8.34	0.5	25.4	6.9	233.6	0.005
SF12	11.4	0.4	2.7	0.006	0.06	5.78	195.76	0.85	10.99	0.5	27.8	7.1	207.3	0.005
SF13	4.5	0.3	1.3	0.005	0.017	0.64	153.98	-0.75	5.62	0.5	20.4	7.8	167.3	0.005
SF15	3.8	6.6	0.48	0.005	0.019	1.03	114.67	-1.53	1.97	0.5	23.3	7.5	194.4	0.005
SF16	5.1	0.2	0.56	0.005	0.014	0.43	130.36	-2.22	-4.69	0.5	21.3	7.9	178.7	0.005
SF20	4.7	0.3	0.9	0.005	0.009	0.64	161.32	-0.48	3.49	0.5	18.8	6.8	192	0.005
SF21	39.1	9	0.5	0.005	0.012	1.07	1342.85	-1.14	-2.66	0.5	25.9	9.2	81.7	0.005
SF22	5.2	0.3	0.8	0.005	0.08	0.64	179.35	-1.08	3.60	0.5	19.9	7.5	195.1	0.005
SF25	26.9	0.4	1.5	0.006	0.1	3.21	133.73	-1.51	-1.93	0.5	25	7.5	250	0.005
SF26	9.3	1.1	1.2	0.005	0.009	2.57	117.88	-1.40	0.85	0.5	26.5	7.5	237.1	0.005
SF28	3.4	0.3	0.7	0.007	0.04	1.5	160.63	-1.80	-1.52	0.5	22.3	7.1	180.4	0.005
SF29	5.4	0.9	1.5	0.009	0.01	3.21	276.22	1.14	10.69	0.5	24.7	7.8	194.9	0.005
SF33	4.3	0.3	1	0.005	0.011	2.14	112.19	-1.82	0.87	0.5	21.6	7.6	289.9	0.005
SF34	5	0.4	1.9	0.005	0.07	4.07	138.54	-0.73	11.58	0.5	19.9	6.7	286.8	0.005
SF35	3.1	0.3	1.9	0.006	0.05	4.07	95.55	-1.25	11.55	0.5	19	7.3	262.1	0.005
SFS11	26	0	0.035	0.005	0.017	0.08	313.45	-2.10	-6.34	0.5	29	6.8	280.5	0.005

App. 14: Mixing cell model (MCM) input data (continued).

Location	SO_4^{2-} [mg/l]	F^- [mg/l]	Al^{3+} [mg/l]	Cu^{2+} [mg/l]	Zn^{2+} [mg/l]	SiO_2 [mg/l]	TDS [mg/l]	^{18}O [‰ VSMOW]	^{2}H [‰ VSMOW]	Sr^{2+} [mg/l]	T [°C]	pH [-]	Redox [mV]	As^{3+} [mg/l]
Cell1	9.53	2.39375	0.808	0.005	0.028	0.67	192.18	-1.12	2.55	0.5	20.425	7.78	198.76	0.005
Cell1_1	5.88	0.45	0.685	0.005	0.03	0.69	127.55	-1.33	3.02	0.5	20.26667	7.70	190.05	0.005
Cell1_2	5	0.266667	0.75	0.005	0.03	0.57	157.01	-1.26	3.55	0.5	20	7.371	188.6	0.005
Cell1_3	6.45	0.325	1.425	0.005	0.041	1.93	172.601	-0.36	5.93	0.5	21.725	7.27	190.42	0.005
Cell2	4.53	0.425	1.45	0.006	0.049	3.10	139.92	-0.74	8.45	0.5	21.575	7.34	310.33	0.005
Cell2_1	4.53	0.425	1.45	0.006	0.049	3.10	154.01	-0.85	9.53	0.5	21.575	7.34	246.84	0.005
Cell2_2	4.2	0.35	1.625	0.007	0.058	3.48	111.49	-1.16	8.66	0.5	20.9	7.19	275.92	0.005
Cell2_NF	4.53	0.33	1.23	0.005	0.034	2.64	149.25	-1.09	5.53	0.5	20.63333	7.33	249.4	0.005
Cell3	3.15	0.4	0.75	0.005	0.008	1.18	160.83	-2.02	-1.43	0.5	20.8	6.97	207.3	0.005
Cell4	3.5	0.3	0.9	0.005	0.017	1.93	104.23	-1.37	1.15	0.5	20.8	7.5	241.9	0.005
Cell4_NF	9.1	0.3	0.9	0.005	0.017	1.93	118.21	-1.37	1.15	0.5	18.6	7.55	241.9	0.005
EGW50	2.35	0.95					67.6				16.6	9		
EGW51	35.35	10					563				16.4	9.1		
ESF3	14.1	0.5					112				21.7	7.6		
GW41	6.9	0.8	0.058	0.01	0.084	0.12	341.22	-2.05	-8.96	0.5	23.2	7.27	265.8	0.005
GW44	76.1	8.7	0.008	0.005	0.005	18.61	886.74	-3.14	-14.64	0.5	26.3	8.68	157.3	0.012
GW45	83.4	10.9	0.038	0.005	0.006	0.08	1457.86	-3.66	-18.14	0.5	27.7	9.46	99.2	0.006
GW46	98.9	1.3	0.014	0.005	0.07	0.03	1463.97	-3.63	-14.96	1	23.3	7.17	170.2	0.005
GW47	65.2	10	0.02	0.005	0.005	0.04	1158.31	-3.52	-17.29	0.5	27.8	9.35	109.7	0.005
GW49	128.8	3.3	0.15	0.005	0.009	0.32	1266.28	-2.89	-16.58	0.5	22.9	8.35	153.5	0.005
GW50	20.6	0.5	0.015	0.005	1.3	0.03	1190.54	-2.48	-11.82	1.5	22	7.61	214.8	0.005
GW52	52	3	0.021	0.005	0.05	0.05	1127.23	-1.96	-6.59	0.8	25.9	6.97	182	0.005
SF36	4.3	0.3	0.8	0.005	0.02	1.71	197.022	-0.72	4.15	0.5	20.4	7.72	171.5	0.005
SF37	5.7	0.6	1.4	0.005	0.048	2.99	189.36	0.01	10.74	0.5	20.7	7.41	228	0.005
SF38	4.3	0.6	1.3	0.005	0.02	2.78	158.06	-0.04	10.51	0.5	23.1	7.48	224.7	0.005
SF38	3.5	0.3	0.9	0.005	0.017	1.93	104.22	-1.37	1.15	0.5	20.8	7.5	241.9	0.005
SF39	5.1	0.5	1.6	0.005	0.07	3.42	128.91	-0.57	7.52	0.5	24.8	7.33	754.7	0.005
SF40	4.4	0.4	1.7	0.012	0.1	3.64	99.70	-0.83	10.65	0.5	23.1	7.23	264.9	0.005
SF42	3.2	0.4	0.7	0.005	0.008	1.49	158.97	-1.96	-0.71	0.5	22.4	6.85	204.2	0.005
SF43	3.1	0.4	0.8	0.005	0.008	0.86	162.69	-2.08	-2.14	0.5	19.2	7.08	210.4	0.005
SF51	2.4	8.2	1.6	0.005	0.12	3.42	184.81	1.24	9.65	0.5	21.9	7.8	213.5	0.005
SF53	4	0.9	2.5	0.005	0.022	5.35	82.123	0.89	14.66	0.5	23.8	7.67	248.4	0.005